# APPLICATION OF MAGNETIC TECHNIQUES IN ALBERTAN OIL SANDS CORES FOR IMPROVED RESERVOIR CHARACTERIZATION

by

Toan Huu To

A thesis submitted in partial fulfillment of the requirements for the degree of

Doctor of Philosophy

in

Geophysics

Department of Physics
University of Alberta

# ABSTRACT

The purpose of this study was to assess some novel techniques to improve oil sand reservoir characterization. The main focus of the study was on high resolution, non-destructive, low field probe volume magnetic susceptibility measurements on slabbed core from 3 oil sands wells in northern Alberta. The results demonstrated that this technique was able to distinguish the main lithologies (clean sands, inclined heterolithic stratification – IHS – beds comprising interbedded sand and clay, and clay/shale) better than traditional borehole logging methods such as gamma ray and spontaneous potential. The magnetic data also allowed estimates of the paramagnetic clay mineral illite to be determined. High resolution X-ray fluorescence (XRF) measurements were taken at the same points as the magnetic susceptibility in order to provide supplementary compositional information. The magnetically derived illite contents correlated with the elemental contents of iron, potassium and aluminium (all components of illite) from the XRF. Correlations between the magnetic susceptibility and XRF were even better for small ext-++racted core samples compared to the measurements on the slabbed core. The magnetically derived illite contents also correlated with available fluid permeability measurements, and provided a tool for identifying anomalous mineralogies (where the "illite" content exceeded 100%).

Isothermal remanent magnetization (IRM) measurements on core samples were able to identify and quantify extremely small amounts of remanence carrying particles (in this case ferrimagnetic magnetite) in representative core samples. An independent method involving low field versus high field magnetic susceptibility gave consistent results (similar to those from the IRM method) for the magnetite content for a key muddy sand sample. The low field versus high field magnetic

susceptibility method also provided strong evidence for a paramagnetic iron carbonate mineral (siderite) as a significant component of one of the “anomalous minerals”.

Temperature dependent magnetic susceptibility measurements on core samples provided an improved method to identify and quantify the paramagnetic mineral contents. The illite content results from this method corresponded well with the illite contents derived from the room temperature probe volume magnetic susceptibility measurements on the slabbed core. The temperature dependent curves are more time consuming, but intrinsically better, than single room temperature measurements, since they are able to improve the identification of specific minerals or mineral mixtures as they follow separate curves, whereas single room temperature measurements may result from more than one possible mineral mixture.

The probe magnetic results on the slabbed core indicated the potential for in situ borehole applications of magnetic susceptibility in oil sands reservoirs. The temperature dependence of magnetic susceptibility is important in this respect, since temperature generally increases with depth in a borehole, and therefore will affect the magnetic susceptibility of paramagnetic minerals. Model template curves for volume magnetic susceptibility with temperature and depth were therefore constructed for in situ borehole magnetic susceptibility applications in oil sands reservoirs.

# PREFACE

This thesis is the original work by Toan Huu To. Any use of work conducted by other authors within this thesis is given a proper acknowledgement at the point of their use.

The high field magnetic susceptibility measurements in **Chapter 5** were done by the company Advanced Downhole Petrophysics (ADP) in the UK.

# PUBLICATION ARISING FROM THIS THESIS

Part of **Chapter 3** of this thesis has been published as:
To, T.H., Potter, D.K., Abiola, A., and Ebufegha, V.T., 2018. Probe magnetics as a rapid, non-destructive screening tool for consolidated and unconsolidated core in conventional and unconventional reservoirs. *Proceedings of the 2018 International Symposium of the Society of Core Analysts, 27-30 August 2018, Trondheim, Norway. Paper SCA 2018-057 (9 pages)*.

# PAPER IN PREPARATION

To, T. H. and Potter, D. K., 2021. Comparison of high resolution probe magnetic, X-ray fluorescence and permeability on core with borehole spectral gamma ray and spontaneous potential in an oil sand well. *Submitted and currently in peer review for the 2021 International Symposium of the Society of Core Analysts, September 2021, Austin, Texas, USA*.
(The Abstract for this paper was accepted as a Poster with Accompanied Manuscript. The manuscript was submitted on 2 November 2020 for peer review, and was provisionally accepted on 7 December 2020 subject to some minor revisions).

# DEDICATION

This thesis is dedicated to my parents, to my sister and brother in-law, to my nephew and niece, and to my wife, my son and my daughter.

# ACKNOWLEDGEMENTS

Foremost, I would like to express my sincere appreciation to my supervisor, Dr. David K. Potter, for giving me the opportunity to pursue this degree and for his continuous support since the first days I came to the university. His invaluable advice, guidance and suggestions, as well as his encouragement and financial support, helped me so much during the time of my study and research.

I would like to express my thanks for a scholarship from the 911 program, funded by the Vietnamese Ministry of Education and Training. I thank Cenovus FCCL Ltd. for providing the oil sand slabbed cores and the available downhole log and conventional core data, as well as providing a research grant to Dr. Potter. I thank Innotech Alberta for the heavy oil sample from the Albertan oil sands. I also extend my thanks to Dr. Nicholas Harris and Dr. Murray Gingras for the use of the XRF equipment, and to Maya LaGrange Rao for her guidance in using the XRF analysis system. I thank Dr. Petar Petrov for his guidance in using the temperature dependent magnetic susceptibility measurement system, and to Martyn Greensmith of Advanced Downhole Petrophysics for the high field magnetic susceptibility measurements on extracted samples.

I would like to thank to the other members of my supervisory committee, Dr. Jeffrey Gu and Dr. Moritz Heimpel, as well as other members of my candidacy and PhD thesis defence examining committee, Dr. Hassan Dehghanpour and Dr. Jeffrey Kavanaugh, for their insightful comments, questions and suggestions regarding my research and thesis. I thank Dr. Lesley James of Memorial University of Newfoundland for being my external PhD defence examiner and for her questions and very helpful suggestions.

Last but not least, I would like to express my appreciation to my parents, and other family members in Vietnam, who always loved and supported me unconditionally. More importantly, I would like to thank my beloved wife and son for always being by my side and encouraging me over the years.

**TABLE OF CONTENTS**

# LIST OF TABLES

# LIST OF FIGURES

## Chapter 1: Introduction

**Chapter 2: Magnetic susceptibility of common reservoir minerals and fluids and the magnetic susceptibility sensor techniques used in this study**

**Chapter 4: A comparison between high resolution X-Ray fluorescence, probe magnetic susceptibility and traditional downhole log data**

**Chapter 5: Special core analysis on selected extracted samples: (i) volume and mass magnetic susceptibilities versus X-ray fluorescence, (ii) isothermal remanent magnetization, (iii) low field versus high field magnetic susceptibility, and (iv) temperature dependent magnetic susceptibility**

**Appendices**

# NOMENCLATURE

## LIST OF SYMBOLS

| | |
|---|---|
| B | Magnetic induction |
| $E_L$ | Liquid junction potential |
| $E_s$ | Membrane potential |
| $F_I$ | Fraction of illite |
| $F_Q$ | Fraction of quartz |
| FW | Formation water |
| g | Acceleration due to gravity |
| H | Applied magnetic field |
| k | Volume magnetic susceptibility |
| $k_I$ | Volume magnetic susceptibility of illite |
| $k_m$ | Volume magnetic susceptibility of magnetite |
| $k_Q$ | Volume magnetic susceptibility of quartz |
| $k_T$ | Total volume magnetic susceptibility of the sample |
| $m_o$ | Orbital magnetic moment of an electron |
| $m_s$ | Spin magnetic moment of an electron |
| M | Magnetization per unit mass |
| Ma | Million years |
| $M_r$ | Remanent magnetization |
| $M_s$ | Saturation magnetization |
| $\mu$ | Magnetic permeability |
| $\mu_0$ | Magnetic permeability of free space |
| $\mu_r$ | Relative magnetic permeability |
| $\rho$ | Density of the material |
| $Q_v$ | Cation exchange capacity per unit pore volume |
| $S_o$ | Stock tank oil specific gravity |
| $R^2$ | Regression coefficient |
| $T_c$ | Curie Temperature |
| $\chi$ | Mass magnetic susceptibility |
| $\chi_I$ | Mass magnetic susceptibility of illite |

| | |
|---|---|
| $\chi_m$ | Mass magnetic susceptibility of magnetite in the sample |
| $\chi_Q$ | Mass magnetic susceptibility of quartz |
| $\chi_T$ | Total mass magnetic susceptibility of the sample |

**LIST OF UNITS**

| | |
|---|---|
| $^oAPI$ | American Petroleum Institute gravity |
| $^oC$ | Degree Celsius |
| A | Amperes |
| $Am^{-1}$ | Amperes per metre |
| $Am^2kg^{-1}$ | Amperes metre squared per kilogram |
| cm | centimetre |
| cP | centipoise |
| D | Darcy |
| emu | Electromagnetic unit |
| emu $cm^{-1}$ | Electromagnetic unit per centimetre |
| emu $g^{-1}$ | Electromagnetic unit per gram |
| eV | Electronvolt |
| G | Gauss |
| GAPI | Gamma API |
| H | Henry |
| $Hm^{-1}$ | Henry per metre |
| Hz | Hertz |
| K | Kelvin |
| kg | Kilogram |
| $kgm^{-3}$ | Kilogram per cubic metre |
| kHz | Kilohertz |
| m | metre |
| $m^2$ | squared metre |
| mD | Millidarcy |
| mg | Milligram |
| ms | Millisecond |

| | |
|---|---|
| $ms^{-2}$ | metre per squared second |
| mT | Millitesla |
| mV | Millivolt |
| MeV | Megaelectronvolt |
| μm | Micrometre |
| Oe | Oersted |
| s | Second |
| ppm | Parts per million |
| T | Tesla |
| V | Volt |

## GLOSSARY OF TERMS

| | |
|---|---|
| AC | Alternating current |
| ADP | Advanced Downhole Petrophysics |
| AMS | Anisotropy of magnetic susceptibility |
| API | American Petroleum Institute |
| CAD | Canadian dollar |
| CGS | Centimetre-Gram-Second System of units |
| DC | Direct current |
| DF | Direct field |
| FW | Formation water |
| FZI | Flow zone indicator |
| GR | Gamma ray |
| IHS | Inclined Heterolithic Stratigraphy |
| IRM | Isothermal remanent magnetization |
| NGS | Natural gamma ray spectroscopy |
| SAB | Student Association Building |
| SI | International System of Units |
| SP | Spontaneous potential |
| SQUID | Super conducting quantum interference device |
| W01 | Well 01 |

| | |
|---|---|
| W02 | Well 02 |
| W03 | Well 03 |
| WCSB | Western Canada sedimentary basin |
| XRD | X-ray diffraction |
| XRF | X-ray fluorescence |

# Chapter 1

# Introduction

## 1.1. General introduction

This study primarily introduces the application of a novel, quantitative, high resolution probe magnetic technique for reservoir characterization of slabbed cores from 3 different oil sands wells located in Northern Alberta, Canada. The purpose of this research was to produce an additional tool that complements, yet has significant advantages over, other traditional core and log based methods of oil sands reservoir characterization. Various additional measurements, such as X-ray fluorescence (XRF), were also undertaken in order to support the interpretations provided by the magnetic technique.

Reservoir characterization studies provide critical information on reservoir heterogeneity and petrophysical properties, which are key for constructing reservoir models (Lucia et al., 2013). Reservoir characteristics and petrophysical properties are determined by various traditional methods using well logging, core analysis and well production data. Well logging allows in-situ estimation of properties, whereas core analysis allows ground truthing using actual recovered samples (rock and fluid) from the reservoir. Well production data give generally large scale information after a reservoir is economic production. These traditional methods, however, have certain limitations. For example:

1. Borehole gamma ray and core gamma ray can be influenced not only by permeability controlling clay minerals, but also by uranium in organic matter or small amounts of gamma

ray emitting heavy minerals. Borehole gamma ray data can also be influenced by high gamma ray emitting drilling mud components, such as potassium chloride (KCl).

2. The spontaneous potential (SP) log is usually used to detect permeable beds based on the difference in salinity between the borehole fluids and the formation fluids, and causes a voltage deflection (generally measured in millivolts) from the shale baseline. However, if the salinities are equal there will be no deflection and the SP log will not be able to pick out the permeable zones in this situation.
3. Certain core analysis techniques are not always applicable in unconsolidated oil sands reservoirs. Often it is not possible to cut core plugs in such unconsolidated oil sands cores. In addition some measurement techniques on slabbed cores might damage the cores. For example, standard probe permeability measurements require the probe tip to be sealed to the rock surface, and the procedure can lead to the probe tip puncturing and therefore damaging the core, and resulting in overestimated permeability values. Other core measurement techniques, such as X-ray diffraction, can be time consuming, costly, and therefore tend to be limited to a small number (and small size) of samples.
4. For oil sands slabbed cores it is often difficult to visually recognize and quantify lithological changes in the cores when they are saturated with black heavy oil or bitumen. This thesis will demonstrate how useful the probe magnetic method is in identifying lithological changes and quantifying mineralogy in these situations.
5. Well production data can be useful for large scale interpretations, but not so useful for small scale high resolution heterogeneities.

In contrast, the novel, quantitative probe magnetic technique and the XRF method used in this study, are rapid and non-destructive. These techniques are particularly suitable for unconsolidated oil sands slabbed cores, unlike some other core analysis techniques that can potentially damage the cores (such as industry standard probe permeability methods as mentioned above, where the probe tip can puncture the unconsolidated core). Moreover, the probe magnetic sensor and recording meter are relatively inexpensive pieces of kit (totalling around $6,000 CAD for both items). The main applications of these techniques in this study were to identify the different lithologies and help quantify the mineralogy of the slabbed cores at high resolution, as additional techniques to complement existing traditional tools.

This study focused on slabbed cores from 3 different oil sands wells (denoted in this thesis as Wells 01, 02 and 03) in Northern Alberta provided by Cenovus FCCL Ltd. Standard well log and some core permeability measurements were provided by the company. The study mainly applied high resolution, low field, novel probe volume magnetic susceptibility measurements on the slabbed cores, supported by high resolution XRF measurements to determine elemental contents. The results were compared with the traditional log data (gamma ray and spontaneous potential) and core permeability. The comparisons helped to evaluate the effectiveness of the probe magnetic and XRF techniques and demonstrate the advantages of these techniques for oil sands reservoir characterization.

Some additional more complex magnetic measurements, not previously undertaken on oil sands cores as far as I know, were performed on small extracted samples of the core. These measurements were undertaken in order to further characterize the cores, and also to provide

potential additional means of accurately interpreting borehole magnetic susceptibility data for in-situ application of the technique. These measurements included the following:

1. Temperature dependent magnetic susceptibility measurements. Paramagnetic minerals, such as permeability controlling clays like illite, exhibit a temperature dependent magnetic susceptibility (as will be discussed in **Chapter 5**). Theoretically modelling and measuring this temperature dependence allows one to: (i) accurately determine the paramagnetic mineral content in a rock sample, and (ii) model the depth dependence of magnetic susceptibility (knowing the local geothermal gradient or using borehole temperature measurements) in order to accurately interpret in-situ magnetic susceptibility data from borehole measurements.
2. Magnetic remanence measurements. This provides a means of identifying minerals that can acquire a magnetic remanence (e.g., ferrimagnetic minerals such as magnetite, or canted antiferromagnetic minerals such as hematite). More detailed information regarding magnetic classes and magnetic remanence will be given later in **Chapter 1**, and some magnetic remanence measurements will be presented in **Chapter 5**.
3. High field magnetic susceptibility. A comparison between the low field magnetic susceptibility measurements from the probe device with high field measurements from another sensitive instrument provides another independent method of identifying minerals that can acquire a magnetic remanence. The magnetic susceptibility of such minerals tends to saturate in high fields and thus in most cases contributes little or nothing to the high field magnetic susceptibility. This will be further discussed in **Chapter 5**.

## 1.2. Magnetic susceptibility

Since this study mainly focuses on the use of magnetic susceptibility for characterizing cores, an understanding of basic magnetic properties and magnetic susceptibility is crucial. The following sections will introduce fundamental magnetic properties related to magnetic susceptibility and laboratory methods for susceptibility measurements, as well as the classification of magnetic materials.

A magnetic field is a vector field around a magnetic material, a permanent magnet for example, or a motion of an electric charge or electric current. The magnetic field is conventionally denoted by the symbol H ($Am^{-1}$). When a material is subjected to a magnetic field, the response of this material associated with the field is called magnetic induction or magnetic flux density and is denoted by the symbol B (units: Tesla). The magnetic induction B is related to the magnetic field H by the following equation:

$$B = \mu H \qquad \textbf{(1.1)}$$

where $\mu$ is the magnetic permeability of the material. Thus, the magnetic permeability of a material is the ability of a material to support the formation of a magnetic field inside itself. In free space (i.e., a vacuum):

$$B = \mu_0 H \qquad \textbf{(1.2)}$$

where $\mu_0$ is the magnetic permeability of free space and until recently was considered a constant equal to $4\pi \times 10^{-7}$ $NA^{-2}$ (or Henry $m^{-1}$). Since May 2019 it is now thought of as a parameter to be measured rather than a constant.

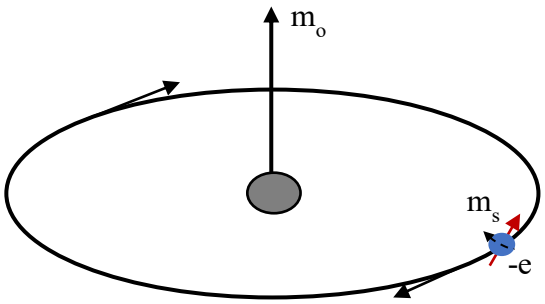


**Figure 1.1:** Schematic of the orbital magnetic moment ($m_o$) and spin magnetic moment ($m_s$) of an electron.

In order to understand the magnetic susceptibility of a material, the source of the susceptibility needs to be addressed. The magnetism in a material is associated with the motion of electrons in their orbits and, in particular, to the spin of the electrons (**Figure 1.1**). These two motions of electrons each generate their own magnetic dipole moments: the orbital magnetic moment ($m_o$) and spin magnetic moment ($m_s$). Once a material is subjected to an applied external magnetic field, the magnetic dipole moments precess in the direction of the field and generate an internal magnetic field within the sample. This internal magnetic field causes an induced magnetization, whose strength and direction depends on the electron structure of the material. Magnetization is related to the applied external magnetic field by the magnetic susceptibility of the material. Thus, magnetic susceptibility is a magnetic property of material that expresses the ability of a material to be magnetized by an applied field. Magnetic susceptibility is usually expressed in terms of magnetic susceptibility per unit volume k as:

$$k = J/H \qquad \textbf{(1.3)}$$

or in terms of magnetic susceptibility per unit mass $\chi$ as:

$$\chi = M/H = k/\rho \qquad \textbf{(1.4)}$$

where J is the magnetization per unit volume and determined as the magnetic moment divided by the volume of the material, M is the magnetization per unit mass and determined as the magnetic

moment divided by the mass of the material, H is the applied external magnetic field, and ρ is the density of the material. Since both magnetic susceptibility and magnetic permeability represent the response of the material to the external applied field, they also relate to each other by the following equation in terms of volume magnetic susceptibility:

$$\mu = \mu_0 \, \mu_r = \mu_0 \, (1 + k) \qquad \textbf{(1.5)}$$

or in terms of mass magnetic susceptibility:

$$\mu = \mu_0 \, \mu_r = \mu_0 \, (1 + \chi\rho) \qquad \textbf{(1.6)}$$

where $\mu_r$ is the relative magnetic permeability. This means that the magnetic induction or magnetic flux density (B) of a material can be written in terms of volume magnetic susceptibility as:

$$B = \mu_0 \, (1 + k) \, H = \mu_0 \, (J + H) \qquad \textbf{(1.7)}$$

or in terms of mass magnetic susceptibility as:

$$B = \mu_0 \, (1 + \chi\rho) \, H = \mu_0 \, (M\rho + H) \qquad \textbf{(1.8)}$$

In the study of magnetism, there are two main systems of units: SI and CGS. These are used to define and quantify magnetic parameters, and **Table 1.1** summarizes the conversion factors between the two systems of units for different magnetic parameters. This thesis study uses the SI unit system.

**Table 1.1:** Magnetism unit systems and conversion factors. T is Tesla, A is Ampere, m is meter, cm is centimeter, kg is kilogram, g is gram, emu is electromagnet unit, G is Gauss, Oe is Oersted, and Dim.less is dimensionless.

| Magnetic Quantity | Symbol | SI Unit | CGS Unit | Conversion Factor |
|---|---|---|---|---|
| Magnetic induction | B | T | G | $1\ T = 10^4\ G$ |
| Magnetic field | H | $Am^{-1}$ | Oe | $1\ Am^{-1} = 4\pi 10^{-3}\ Oe$ |
| Volume magnetization | J | $Am^{-1}$ | emu $cm^{-1}$ | $1\ Am^{-1} = 10^{-3}$ emu $cm^{-1}$ |
| Mass magnetization | M | $Am^2kg^{-1}$ | emu $g^{-1}$ | $1\ Am^2kg^{-1} = 1$ emu $g^{-1}$ |
| Volume susceptibility | k | Dim.less | Dim.less | $4\pi$ (SI) = 1 (CGS) |
| Mass susceptibility | $\chi$ | $m^3kg^{-1}$ | emu $Oe^{-1}g^{-1}$ | $1\ m^3kg^{-1} = 10^3(4\pi)^{-1}$ emu $Oe^{-1}g^{-1}$ |
| Magnetic permeability | $\mu$ | $Hm^{-1}$ | Dim.less | $4\pi.10^{-7}\ Hm^{-1} = 1$ (CGS) |

## 1.3. Standard conventional magnetic susceptibility measurement systems

There are different methods for measuring the magnetic susceptibility of a material. The following section will describe the basic principles of each method.

### 1.3.1. The force balance methods

The force magnetic susceptibility measurement was initially proposed by Louis Georges Gouy, a French physicist, in 1889 and is also known as the Gouy balance method. Gouy derived a mathematical expression showing that force is proportional to magnetic susceptibility for the interaction of a material in a uniform magnetic field. He stated that measurements can be made by measuring weight differences of a tube containing material suspended inside a magnetic field using a balance (**Figure 1.2**). An initial balance reading is performed when there is no applied field on the sample, and a subsequence reading is taken with an applied field. The difference between the two readings is due to the magnetic force on the sample expressed by the following equation (Brubacher and Stafford, 1962):

$$\text{Force} = (m_2 - m_1)\, g = 1/2\, (k_2 - k_1)\, AH^2 \qquad \textbf{(1.9)}$$

where $m_2$ is the second mass reading (in kg), $m_1$ is the initial mass reading (in kg), g is gravitational acceleration (in $ms^{-2}$), $k_1$ is the volume susceptibility of the medium (unitless), which is usually air of negligible value, $k_2$ is the volume susceptibility of the sample (unitless), H is the applied field (in $Am^{-1}$), and A is the area of the sample tube (in $m^2$). In initial measurements, an inhomogeneous magnetic field is generated by two flat poles of a permanent magnet or an electromagnet. A powder or liquid sample in a cylindrical tube needs to be placed in the centre of the field. Since magnetic induction arises when a sample is subjected to a magnetic field, the sample can be attracted or repelled from the field. A sample with positive magnetic susceptibility will be attracted (and pulled downward) by the magnetic field and result in a positive difference in apparent mass. A sample with negative magnetic susceptibility, in contrast, will be slightly repelled by the magnetic field and result in a negative difference in apparent mass. The force exerted on the sample is measured by an analytical balance. Errors due to inhomogeneous packing in the sample tube are difficult to eliminate.

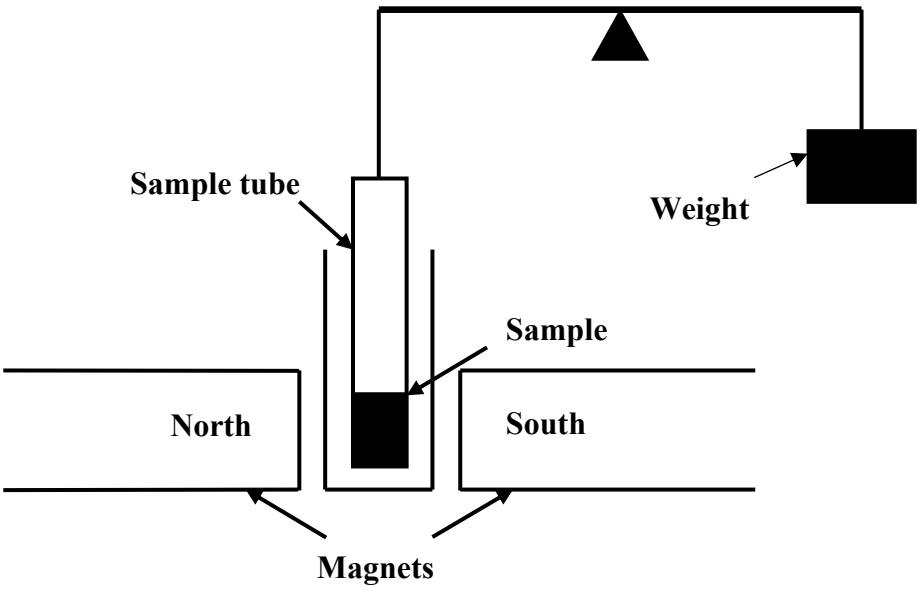


**Figure 1.2:** A schematic of the Gouy balance method for magnetic susceptibility measurement.

Along with the Gouy balance method, there are some other balance methods that have been developed for measuring susceptibility, such as the Faraday balance and Evans balance (also known as the Johnson-Matthey balance). In the Faraday balance, the shape of the pole magnets was redesigned to create a homogeneous magnetic field with the field strength constant over the sample. The magnetic force acting on the sample is in this case independent of any slight inhomogeneous packing of the sample and depends only on the total mass of the material present. The force is also measured as the weight changes by using a torsion balance. This method is sensitive and can be applied to a single crystal (Carlin,1986).

In the Evans (1974) balance system, two pairs of magnets are placed back-to-back on a suspension strip, making a balanced system with a magnetic field at each end. When a sample fixed in a glass holder is placed into the gap between one of the pairs of magnets, a torsional force is generated and deflects the beam. The torsional force is restored by the current passed through the coil, which is placed at the gap between the second pair of magnets, giving a reading on a display. The Evans balance system is more convenient than the Gouy and Faraday balances since it is less time-consuming. One reason for the time-consuming nature of the latter balances is that the sample needs to be suspended in between two magnet poles and to stay in the same place during the measurements. With the Evans balance system, a reading takes just a few seconds, although sensitivity and accuracy is a little less compared to the other two methods. The Evans method can measure the susceptibility of liquids, solids, and gases.

### 1.3.2. The direct current (DC) methods

As per its definition, the magnetic susceptibility of a material is the result of magnetization divided by the applied field. The DC method directly measures the induced magnetization of a sample that is generated by the application of a direct field (i.e., a constant unidirectional field). The susceptibility is then given by the ratio of the induced magnetization to the applied field. One can use ballistic, astatic, and superconducting magnetometers for measuring susceptibility with this method.

#### a) Ballistic method

This method is based on the principle that the magnetic moments within a sample subjected to an applied field will change the magnetic flux through a search coil positioned near the sample, which will give rise to an electric current. The induced electric current can be measured with a ballistic galvanometer and is a function of the magnetic susceptibility. The applied magnetic field is generated by a coil or a solenoid, and the magnetic flux through the search coil is changed either by altering the geometrical relationship between the applied field coil and the sample or by reversing the polarity of the current through the applied field coil.

An improved ballistic magnetometer was developed by West and Dunlop (1971). The basic instrument could be used to determine magnetic properties including the magnetic susceptibility of natural samples with a wide variation of temperatures (up to 750 $^{o}$C). However, the measurements with this instrument were mainly applied for igneous rocks rather than sedimentary rocks due to its limited sensitivity.

**b) Astatic method**

In this method magnetic susceptibility is measured by using an astatic magnetometer, which is a very simple and reliable instrument. The instrument can also be used for measuring magnetization and anisotropy of magnetic susceptibility (AMS). This magnetometer works on the principle that the torque on a suspended magnet depends on the applied magnetic field. Therefore, when a sample is close to a suspended magnet, the field associated with the magnetized sample will twist the magnet. In the astatic magnetometer there are two similar magnets aligned antiparallel to each other (Thompson and Oldfield, 1986).

**c) Superconducting magnetometer method**

A much more sensitive technique for magnetic susceptibility measurement is the use of a superconducting magnetometer. This system consists of one or more superconducting pick-up coils, a field-transferring coil, and a super conducting quantum interference device (SQUID) sensor. When a sample is introduced into the system, the pick-up coil configuration initiates an induced direct current, which will change the magnetic flux and is detected by a SQUID sensor. A superconducting magnetometer can also utilize an alternating current (AC) for magnetic measurements. The main advantages of the superconducting magnetometer are its high sensitivity and fast response time.

### 1.3.3. The alternating current (AC) induction method

The alternating current (AC) induction method measures induced magnetization, which is produced by the presence of a sample in an alternating magnetic field. This method has different approaches for measuring magnetic susceptibility. One approach involves the use of a balanced

AC bridge circuit (Mooney, 1952). In a susceptibility bridge system, the magnetic field is generated by a current carrying solenoid, flat coil, or Helmholtz coil. An induced magnetization is detected by a balanced coaxial pick-up coil. When a sample is introduced into the magnetic field, its induced magnetization affects the inductive balance and produces an out-of-balance signal in the pick-up coil that is proportional to the magnetic susceptibility of the sample. Alternative approaches have been used for susceptibility measurement, such as the use of a double coaxial pick-up and Helmholtz pair (Bruckshaw and Robertson, 1948) or measuring at different frequencies (Likhite et al., 1965; Radhakrishnamutry et al., 1968). A further approach is to detect the frequency change that is caused in a sharply tuned "metal detector" oscillator circuit by the introduction of a sample (Lancaster, 1966).

There are two different types of instrument for measuring magnetic susceptibility of samples based on the AC induction method. The first type uses a stationary instrument, where measurement is made by inserting a sample into the system. The other type is the use of portable equipment with a sensing head in different shapes and sizes that can be used for measuring the susceptibility of samples in the laboratory or in-situ in outcrop (Thompson and Oldfield, 1986). In general, the AC method is widely used due to its accuracy and sensitivity.

The novel techniques used for magnetic susceptibility measurements on rock samples in this study operate on the principle of the AC induction method. The equipment includes a susceptibility meter pairing with a novel sensor. In this thesis two novel sensors were used: one probe sensor was specially adapted for low field magnetic susceptibility measurements on slabbed core, and another sensor was used for low field measurements on small powdered

samples or core plugs. More details regarding the sensors and the measurements are given in **Chapter 2**.

## 1.4. Magnetic classification of materials and their associated magnetic susceptibilities

When a material is subjected to a magnetic field, the magnetic moments of atoms are affected. The response of the material to the applied field depends on several factors, such as the atomic structure and the net magnetic field associated with the atoms. Based on this response the material can be magnetically classified into five main magnetic classes: diamagnetic, paramagnetic, ferromagnetic, ferrimagnetic, and anti-ferromagnetic, with canted anti-ferromagnetic as a subclass of the latter. The following sections will describe these different magnetic classes and their magnetic susceptibilities.

### 1.4.1. Diamagnetic materials

In a diamagnetic material, the atomic shells are filled with an even number of electrons being paired so that the opposite spins cause their magnetic fields to cancel each other. Therefore, there is no permanent net magnetic moment per atom, resulting in no net magnetization when no external magnetic field is applied (**Figure 1.3 (A)**). When a material is subjected to a magnetic field, the electrons revolving in the orbits of an atom will accelerate or decelerate in order to create an opposing magnetic moment (induced magnetization). This is a result of Lenz's law, which causes a change in the motion of the electrons, resulting in the magnetic moments opposing the external field (**Figure 1.3 (B)**). The external magnetic field in the material is weakened by the induced magnetization, resulting in a small negative magnetic susceptibility of the material. Therefore, the magnetization of a diamagnetic mineral decreases with increasing

magnetic field strength (**Figure 1.3 (C)**). The main reservoir minerals, such as quartz in clastic reservoirs and calcite in carbonate reservoirs (Dunlop and Özdemir, 1997; Thompson and Oldfield, 1986), and reservoir fluids such as crude oil and formation water (Ivakhnenko and Potter, 2004), are diamagnetic.

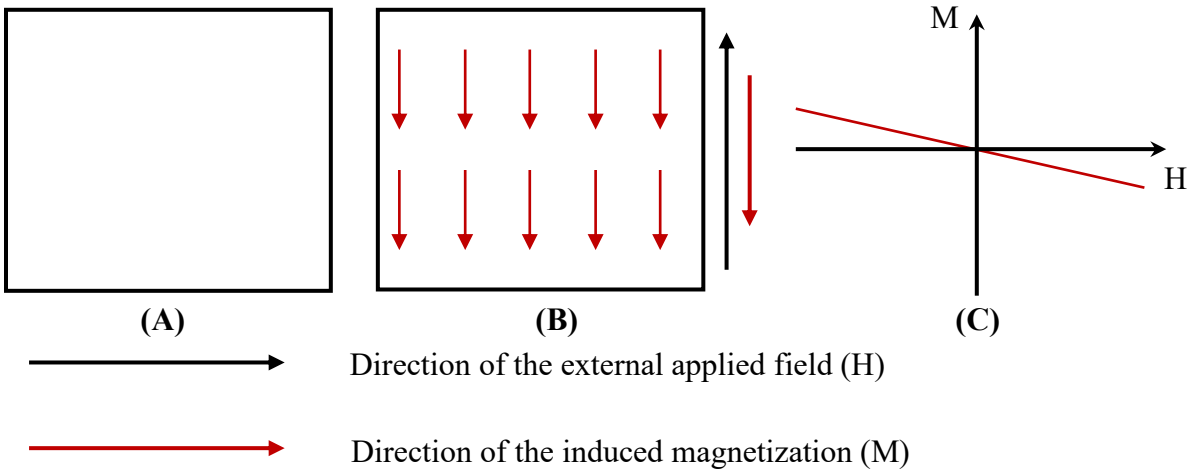


**Figure 1.3:** Behaviour of the magnetic moments of a diamagnetic material in **(A)** the absence and **(B)** the presence of an external magnetic field. Smaller red arrows in the boxes represent the magnetic moments. **(C)** shows the decreasing of magnetization with increasing magnetic field strength, and the negative slope is the negative susceptibility of a diamagnetic material (mineral or fluid).

### 1.4.2. Paramagnetic materials

In a paramagnetic material, there are partially filled electron shells resulting in unpaired electrons. Due to the unpaired electrons, some of the atoms in paramagnetic materials will have net magnetic moments. These atoms do not magnetically interact with each other. Thus, their magnetic moments are random in direction, resulting in no net magnetization in zero magnetic field (**Figure 1.4 (A)**). When an external field is applied, the atomic magnetic moments precess and produce an induced magnetization in the same direction as the applied field (**Figure 1.4 (B)**). The magnetic field within the material is strengthened by the magnetization, resulting in a positive magnetic susceptibility of the paramagnetic material. Since magnetic flux density within

paramagnetic material is directly proportional to the strength of the applied field, the magnetic susceptibility is constant with applied field strength. Therefore, the magnetization of a paramagnetic mineral increases with increasing magnetic field strength (**Figure 1.4 (C)**). Upon removal of the applied field, the thermal motion of the atoms randomizes the magnetic moments, resulting in zero net magnetization. Some typical reservoir paramagnetic minerals are the clays illite, chlorite, and the iron carbonate siderite (Hunt et al., 1995). Paramagnetic minerals have positive magnetic susceptibility values compared to the negative values of diamagnetic minerals. Also, the absolute magnitudes (if one takes the moduli of the values) are generally significantly higher for paramagnetic minerals. Detailed comparisons of susceptibility between common reservoir diamagnetic and paramagnetic minerals and fluids will be described in **Chapter 2**.

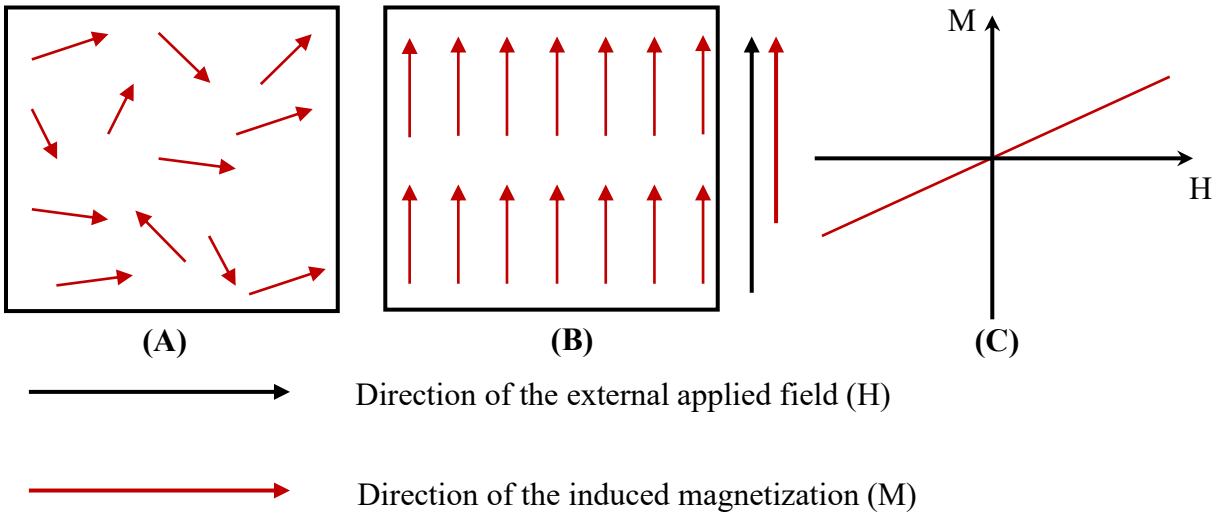


**Figure 1.4:** Behaviour of the magnetic moments of a paramagnetic mineral in **(A)** the absence and **(B)** the presence of an external magnetic field. Smaller red arrows in the boxes represent magnetic moments. **(C)** shows the increasing of magnetization with increasing magnetic field strength, and the positive slope is the magnetic susceptibility of a paramagnetic material (this generally means paramagnetic minerals in reservoirs since most reservoir fluids are diamagnetic).

### 1.4.3. Ferromagnetic materials

In a ferromagnetic material, strong interactions of neighbouring electrons result in parallel alignment of magnetic moments that produces a self-magnetization even without the application of an external magnetic field (**Figure 1.5 (A)**). Once an external field is applied, all the magnetic moments are enhanced and align parallel with the field producing a strong induced magnetization in the material (**Figure 1.5 (B)**). The electron spins of adjacent cations are directly coupled. An exchange force operates so that the magnetic vectors all point in the same direction. However, when the strength of the magnetic field reaches a critical point, the magnetization saturates at a maximum value. This point is called the saturation magnetization ($M_s$) and results in zero magnetic susceptibility beyond this point (**Figure 1.5 (C)** which is a typical magnetic hysteresis plot) since the slope of the magnetization versus applied field curve is zero. After the applied field is removed, the material retains part of the magnetization, which is defined as the remanent magnetization ($M_r$). In a ferromagnetic material, the magnetic moments occupy small regions called magnetic domains. All atomic magnetic moments in a domain are aligned in the same direction. The size of the magnetic domains depends on the ferromagnetic material. The response of magnetic domains to the applied magnetic field determines the magnetic susceptibility of the material. Ferromagnetic susceptibility is positive and much higher than that of paramagnetic susceptibility. Examples of ferromagnetic materials are the pure metals iron and nickel.

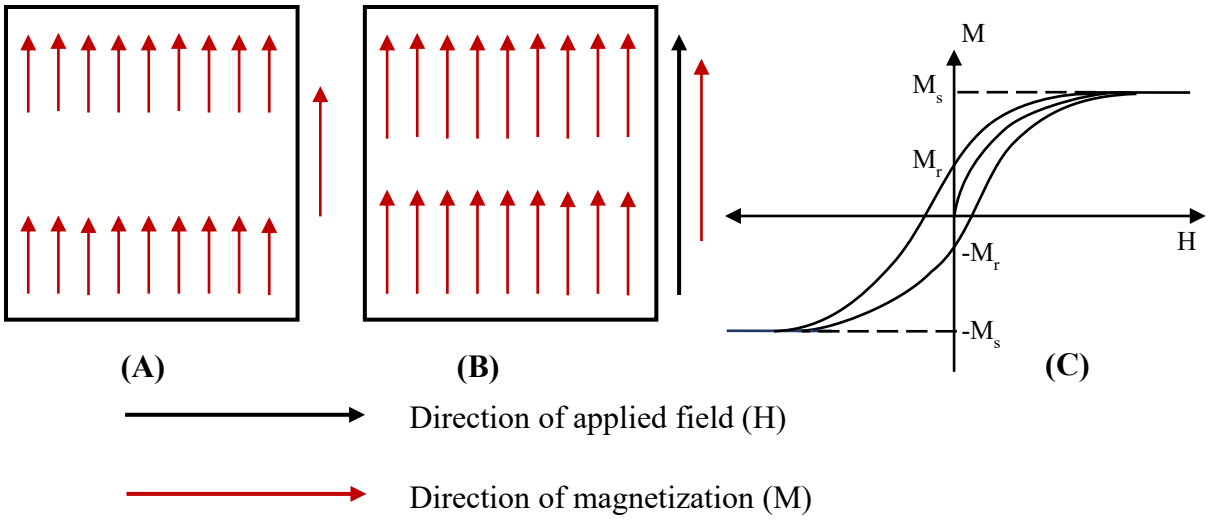


**Figure 1.5:** Behaviour of the magnetic moments of a ferromagnetic material in **(A)** the absence and **(B)** the presence of an external magnetic field. Smaller arrows in the boxes represent magnetic moments. **(C)** is a typical magnetic hysteresis curve of a ferromagnetic material, showing the saturation magnetization ($M_s$) at a high applied magnetic field and the remanent magnetization ($M_r$) after removal of the field (H = 0).

### 1.4.4. Ferrimagnetic materials

Similar to ferromagnetic material, there are strong interactions of magnetic moments within ferrimagnetic material. The electron spins of the cations are shared via the electron shell of an intermediate anion (in the case of oxides this is oxygen). The interaction results in a coupling force known as the super-exchange force. The direction of the electron spins in the adjacent cations are reversed, which results in two oppositely magnetized lattices of magnetic moments within the material (**Figure 1.6 (A)**). These two lattices are not equal in magnitude due to the differences in ionic populations or crystallographic structure. This results in a net magnetization even when the applied field is removed. When an external magnetic field is applied the magnetic moments in the direction of the applied field are enhanced, while the magnetic moments in the opposite direction are diminished, producing a strong induced magnetization (**Figure 1.6 (B)**). This magnetization is also saturated at a high field ($M_s$), like that of a ferromagnetic material,

and retains a remanent magnetization ($M_r$) after removal of the applied magnetic field (**Figure 1.6 (C)**). A ferrimagnetic material behaves similarly to a ferromagnetic material at high magnetic field. Ferrimagnetism is observed more in compounds with complex crystal structures than in pure elements, and the magnetic susceptibility of a ferrimagnetic material is positive and much higher than diamagnetic and paramagnetic minerals, though generally slightly lower than for ferromagnetic materials. Magnetite is an example of a ferrimagnetic mineral that is present in small amounts some reservoir rocks. This will be discussed in more detail in **Chapter 5**.

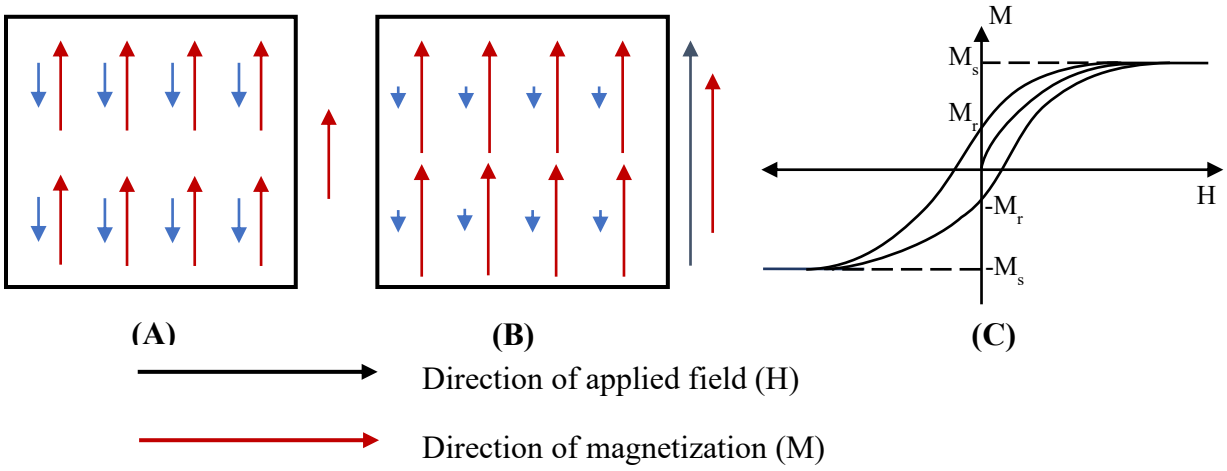


**Figure 1.6**: Behaviour of the magnetic moments of a ferrimagnetic material in **(A)** the absence and **(B)** the presence of an applied magnetic field. Red and blue small arrows in the boxes show two lattices of magnetic moments. **(C)** is a typical hysteresis curve of a ferrimagnetic mineral showing the saturation magnetization ($M_s$) at a high applied magnetic field and the remanent magnetization ($M_r$) after removal of the field (H = 0).

### 1.4.5. Anti-ferromagnetic materials

Similar to ferrimagnetic materials, there are two oppositely magnetized lattices of magnetic moments due to the super-exchange interactions of cations in an anti-ferromagnetic material. In zero applied magnetic field, the opposing lattices of magnetic moments are equal in magnitude (unlike the ferrimagnetic case), which results in no net magnetization of the material (**Figure 1.7 (A)**). When the material is subjected to an external magnetic field it acquires an induced

magnetization in the same direction as the field (**Figure 1.7 (B)**). Once the external field is removed, the magnetic moments relax back to their original state, and the material retains no remanent magnetization. Beyond a certain temperature, called the Néel temperature, an anti-ferromagnetic material behaves like a paramagnetic material since the thermal agitation overcomes interaction effects, and the magnetic susceptibility varies with temperature. An example of an antiferromagnetic material is nickel oxide, and an example of an antiferromagnetic mineral is ilmenite.

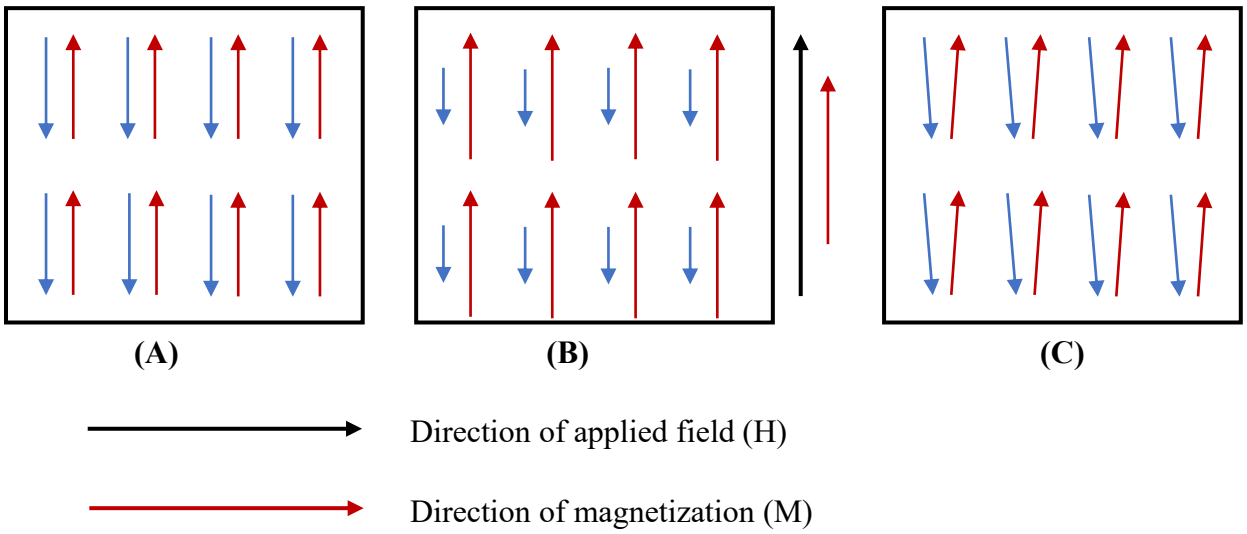


**Figure 1.7**: Behaviour of the magnetic moments of an anti-ferromagnetic material in **(A)** the absence and **(B)** the presence of magnetic field. Small arrows in red and blue in the boxes show two opposite lattices of the magnetic moments. The hysteresis curve of a typical antiferromagnetic substance would go through the origin (there would be no hysteresis loop since no remanence is acquired) and saturate at high fields. **(C)** presents the slightly inclined magnetic moments of a canted anti-ferromagnetic material. The hysteresis curve of a typical canted antiferromagnetic mineral such as hematite would generally exhibit a wide hysteresis loop, and may not saturate in a field of 1 Tesla.

When two lattices of opposing magnetic moments in a material are at a slight angle instead of being exactly anti-parallel (this is termed "canted"), the material is called canted antiferromagnetic (**Figure 1.7 (C)**). This will create a small remanent magnetization oriented to

the right in **Figure 1.7 (C)** even when there is no applied magnetic field. An example of a canted antiferromagnetic mineral is hematite.

## 1.5. Previously published works on the application of magnetic susceptibility for hydrocarbon reservoir characterization

In the past, the application of diamagnetic and paramagnetic material to the study of rock magnetism was believed to be limited, due to both of their mineral susceptibility signals being small compared to those of minerals in other magnetic classes such as ferrimagnetic and anti-ferromagnetic (Nagata, 1961; Dunlop and Özdemir, 1997). Most previous magnetic susceptibility studies have concentrated on ferrimagnetic (e.g., magnetite) and canted anti-ferromagnetic (e.g., hematite) minerals and their applications in palaeomagnetism and magnetostratigraphy. However, some recent works as detailed below have proved the usefulness of diamagnetic and paramagnetic susceptibility for reservoir studies. This section will summarize previously published results showing the application of magnetic susceptibility measurement for characterizing different reservoir properties.

An early study by Ergin and Yarulin (1979) presented results of susceptibility measurements on crude oil samples from different oil field provinces of the former USSR. This study showed that the mass susceptibility of the crude oil was diamagnetic with low and negative magnetic susceptibility that varied from -0.942 to -1.042 x $10^{-8}$ $m^3kg^{-1}$. The authors also analyzed components of the crude oil and found that the most diamagnetic hydrocarbon compounds were alkanes, cyclo-pentanes, and cyclo-hexanes. They also found some correlations between susceptibility and certain physical and chemical properties. The results clearly indicated the

variation of magnetic susceptibility values with different oil field regions. Therefore, the authors suggested that one could potentially use magnetic susceptibility for distinguishing crude oil from different oil field reservoirs.

An extensive study by Ivakhnenko and Potter (2004) introduced the application of magnetic susceptibility measurements to different reservoir fluids including crude oils, refined oil fractions, and formation waters. The crude oil samples were collected from worldwide oil regions such as the Middle East, North America, the Far East, and Russia, while the refined oil and formation waters came from the Forties oil field in the North Sea. The results showed that all fluid samples in this study were diamagnetic, and there was a significant difference between the mass susceptibility of crude oil and formation water. The authors also found correlations between the magnetic susceptibility of crude oils and their densities and other physical properties (such as residue content, stock tank oil gravity, and viscosity), and with chemical properties (such as the content of sulphur, vanadium, cadmium, nickel, and iron). The magnetic susceptibility of formation waters depended on their chemical composition. Based on the results, the authors suggested that magnetic susceptibility could potentially be used to characterize the physical differences between various reservoir fluids, and could distinguish crude oils from various oil provinces. A further study by Ivakhnenko (2012) has extended this work to more worldwide localities.

Magnetic susceptibility measurements were first applied for characterizing rock core plug samples from a vertical North Sea oil well, and the results showed the potential use of magnetic susceptibility for quantifying mineral contents (Potter et al., 2004). In this study, core plugs of 1

inch in diameter and 1.5 inches long were cut from selected depths from two wells (a 24 foot long interval in PEGASUS Well 2, and a 120 ft interval in PEGASUS Well 2a). Core plugs were then hot soxhlet cleaned before measuring their mass magnetic susceptibility, and X-ray diffraction (XRD) measurements were made on small powder samples from the cleaned cores. The mineral contents of illite and quartz quantified by magnetic susceptibility and XRD had generally similar trends with depth, and the absolute values were close within the uncertainties of each technique. There were some differences due to the limitations of each technique, for example XRD did not identify fine amorphous illite. An extended study of a much larger interval of PEGASUS Well 2 by Potter (2007) also indicated the usefulness of magnetic susceptibility in identifying the main lithologies of a clastic shoreface reservoir and predicting permeability. In this study, low field magnetic susceptibility measurements were undertaken on nearly 300 core plugs from this well. The results of the raw magnetic susceptibilities and magnetically derived illite contents showed strong correlations with core plug permeability, the depth-matched downhole gamma ray signal, the flow zone indicator (FZI), and the cation exchange capacity per unit pore volume ($Q_v$).

The above studies examined the low field mass magnetic susceptibility of fluids or core plug samples. In these studies the total magnetic susceptibility signal represents the sum of all the mineral or fluid susceptibility components in the sample, including any ferrimagnetic mineral components. Since the magnetic susceptibility of ferrimagnetic minerals is extremely high compared to the main diamagnetic and paramagnetic minerals comprising a rock, the presence of any ferrimagnetic components can potentially affect reservoir properties predicted from low field magnetic susceptibility measurements (such a clay content and fluid permeability). Fortunately,

the susceptibility signal of a ferrimagnetic mineral can be eliminated by the application of high field magnetic susceptibility measurements. Studies comparing the low and high field magnetic susceptibilities of some core plugs showed that the high field susceptibility had a slightly higher correlation with permeability in a shoreface North Sea oil reservoir (Potter and Ivakhnenko, 2008), and a much higher correlation with permeability and porosity in an Arab-D carbonate reservoir (Potter et al., 2011) compared to low field susceptibility. The high field measurements effectively removed the contribution of the ferrimagnetic components to the magnetic susceptibility signal (since the ferrimagnetic signal saturates in high fields), and allowed the strong relationships between the paramagnetic clays and the petrophysical properties to be observed.

A few studies on anisotropy of magnetic susceptibility (AMS) have shown the potential application of AMS for reservoir core characterization. These studies found that the amount of paramagnetic clay was directly related to the degree of anisotropy in different types of rock samples such as shoreface sandstones (Potter and Ivakhnenko, 2008), carbonates (Potter et al., 2011), and shales (Ebufegha and Potter, 2015).

Whilst magnetic susceptibility has shown good results for characterizing petrophysical properties in different types of reservoirs such as clastic shorefaces (North Sea; Potter, 2007), carbonate reservoirs (Arab-D; Potter et al., 2011), or shales (North America; Ebufegha and Potter, 2015), its application still needs to be tested in other types of reservoir. In addition, most previous susceptibility measurements were performed on discrete core plugs, which generally limited the results to one data point per foot. Therefore, the study presented in this thesis focuses on

evaluating the application of magnetic susceptibility measurements for characterizing slabbed cores from oil sands reservoirs. The rapid, non-destructive probe magnetic susceptibility measurements presented in this thesis have the following advantages:

(1) They allow a much larger number of high resolution data points to be collected at shorter spacings compared to the industry standard of one core plug per foot. This allows small changes (potentially even at the lamina scale) to be identified.

(2) The probe magnetic technique does not require core plugs to be cut and cleaned, thus saving time and expense.

(3) The probe magnetic technique is especially useful for the unconsolidated slabbed oil sands core, since the probe is completely non-destructive to the core. Some other probe techniques (such as probe permeability devices that require a seal between the probe tip and the slabbed core) can be destructive to the core since the probe tip can often puncture unconsolidated core.

### 1.6. Geological background and distribution of Albertan oil sands

In this research, the application of the magnetic susceptibility measurement focused on 3 oil sands reservoirs in northern Alberta. Slabbed cores covering several hundred metres were made available to us from each of these 3 wells. This section will briefly introduce the historic geological background of the Western Canada Sedimentary Basin, where Alberta's oil sands were deposited, and detail the distribution of the oil sands.

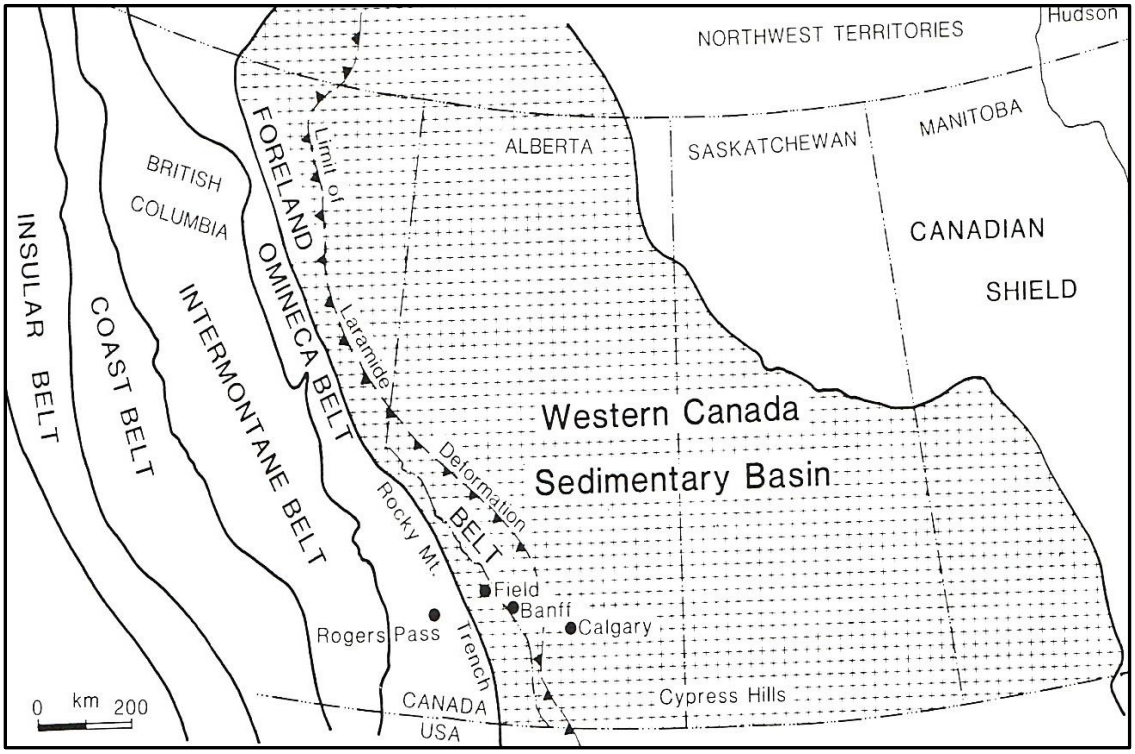


**Figure 1.8**: Outline geological map of the Western Canada Sedimentary Basin (Ricketts, 1989).

### 1.6.1. Western Canada sedimentary basin

The Western Canada sedimentary basin (WCSB) is a wedge of sedimentary rocks overlying 1,400,000 $m^2$ of Western Canada including southwestern Manitoba, southern Saskatchewan, Alberta, northeastern British Columbia, and the southwest corner of the Northwest Territories (**Figure 1.8**). The basin consists of massive Phanerozoic sediments that were deposited thickening southwestward from the Canadian Shield to the Foreland Belt of the eastern Canadian Cordillera. The basin developed from the Early Paleozoic to Early Tertiary periods on a stable crystallized foundation of the North American craton. In terms of current plate tectonic theory, the WCSB can be divided into two distinct depositions: the miogeocline platform deposited from the Cambrian to the mid-Jurassic, and the Foreland basin deposited from the mid-Jurassic to about the Oligocene (Mossop and Shetsen, 1994). The platform deposited on a stable craton due

to extensional tectonics of the supercontinent Rodinia. In the early Cambrian, rifting of the old Neoproterozoic continent led to the opening of the new ocean basin and formed a continent-ocean margin reserved within the eastern Canadian Cordillera (Monger and Price, 2002). The overlying foreland basin succession was formed as consequence of plate convergence between the North American craton and the oceanic plate . Beginning in the mid-Jurassic, North America began to drift westward and collided with oceanic terranes that accreted along its western margin. Consequently, sedimentary rocks deposited outboard of the ancient margin were compressed and displaced eastward over the continental margin. During compressive deformation, loading of the North American craton caused the depression and flexure of the craton and formed the Foreland basin (Price, 1973). The basin was then filled with sediments that eroded from the newly uplifted western source. The uplift of the Rocky Mountains tilted the basin to the west and assumed the geometry of an asymmetrical foreland basin with a gently dipping eastern margin and a thrust-bounded western margin. The Foreland basin wedge is characterized by upward-coarsening progradational cycles capped by extensive non-marine deposits (Mossop and Shetsen, 1994).

### 1.6.2. Alberta oil sands: origins and depositions

Along with conventional hydrocarbon resources, the Alberta oil sands are known as the largest oil reserves of the WCSB and are mainly deposited in the northern Alberta region. The oil sands depositions occur mostly in the Mannville group of the basin, which accounts for more than 70% of the total oil sands reserves in Alberta (Hay, 1994). The Mannville group comprises the early Cretaceous sedimentary rocks of most of the Foreland basin that was the result of subsidence and sedimentation from a long period of uplift, exposure, and erosion of older strata (Hayes et al.,

1994). During the early Cretaceous period, the accretion of terranes in the western Cordillera compressed older miogeoclinal rocks and thrust them onto the continental margin. The loading of the thrust sheets on the craton edge caused its subsidence and formed an accommodation for huge sediments that eroded from the west (Smith et al., 1994). The deposition took place over an unconformity surface ranging from the lowermost Cretaceous in the foothills to the lower Paleozoic at the eastern margin of the sediment basin.

Studies based on biomarker characteristics have suggested that all the bitumen and heavy oil in Alberta have similar source rocks from the Devonian – Mississipian Exshaw formation (Fowler et al., 2001). This marine source rock is thin, about 10 meters, but extremely rich in organic content (up to 20%). The duration of hydrocarbon generation was from 110 to 80 Ma in the vicinity of the Alberta – British Columbia border and 60 to 56 Ma in the Peace River area of Alberta (Riediger et al., 1999; Riediger et al., 2000). This genesis ended in the Early Tertiary due to the Laramide Orogeny, which also brought the hydrocarbon (light oil) reservoir close to the surface. The oil from the source rock then migrated northeastward by at least 360 kilometers for the Athabasca deposit and by at least 80 kilometers for the Peace River deposits (Anfort et al., 2001; Adam et al., 2004). During this migration, the light oil was subjected to a complex series of subsequent compositional modifications and tranformed into heavy, high-viscosity oil sands (Tissot and Welte, 1984; Hunt, 1996).

There are three major oil sands deposits in the Western Canada Sedimentary Basin—Athabasca, Cold Lake, and Peace River—and they are all located within Alberta. The Athabasca oil sands region is known as one of the single largest hydrocarbon reservoirs in the world. This huge oil

sands deposition is located in northeastern Alberta and covers an area of approximately 75,000 $km^2$. The Athabasca oil sands hold the most accessible reserves of bitumen, which are mainly in the McMurray formation of the Lower Cretaceous Mannville group. The depth of the Athabasca oil sand deposition varies from 0 m in outcrop at the Athabasca River, up to more than 450 m at the southwest of the deposit, and its interval thickness can be up to 110 m (Ranger and Gingras, 2003). The McMurray formation deposited directly on top of the Devonian evaporites and carbonates with the sharp contact of an unconformity surface. The McMurray sub-basin, a broad northwesterly trending valley, was created by the erosion of Devonian carbonates and surrounded by the Precambrian Shield at the west (Stewart and MacCallum, 1978). In general, the McMurray formation displays sedimentary environments from fluvial in the lower parts, to estuarine in the middle, to marine shoreface near the top (Gingras and Korosh, 2004). One of the wells studied in this thesis (Well 03) is situated in the Athabasca oil sands.

The Cold Lake oil sands cover approximately 22,000 $km^2$ in the east-central region of Alberta, with oil sands deposited in multiple beds in the Lower Cretaceous Mannville Group at a depth of 985-1970 m below the ground surface (Shuquing et al., 2008). The Clearwater shales in Athabasca change facies southward to a near-shore deltaic and shoreface complex (Gingras and Korosh, 2004), which form the main reservoir beds of the Cold Lake oil sands. The hydrocarbon in much of the Cold Lake oil sands is less viscous (often up to around 20,000 cP and frequently termed “heavy oil”) than the bitumen of the Athabasca oil sands (which can be around 100,000 cP). Two of the wells studied in this thesis (Wells 01 and 02) are situated close to the northern edge of the Cold Lake oil sands.

Peace River is the smallest oil sands deposition in Alberta with about 8,000 $km^2$ covering the area along the axis of the Peace River Arch (Hubbard et al., 1999). The Peace River deposit comprises bitumen-rich sands from the Gething formation, Ostracod zone, and Bluesky formation, all of which overlie Paleozoic and older Mesozoic strata. These sediments were deposited when the Boreal Sea inundated the area from the north. The depositional framework shows a transgressive evolution from a fluvial, non-marine system of the Gething formation to the brackish bay system of the Ostracod zone and the marginal marine estuarine complex of the Bluesky formation (Hubbard et al., 1999). Oil accumulation in Peace River was sealed by overlying Wilrich Member shales of the Spirit River Formation. Mississippian-saturated carbonates underlie the target depositions and provide a bottom seal to the reservoir.

### 1.7. Research main objectives

The main objectives of this study were as follows:

1. To undertake novel low field probe volume magnetic susceptibility measurements at high resolution on slabbed core intervals from 3 different Albertan oil sands wells. The results allow an independent means of identifying the main lithologies and their boundaries in each of the wells. One aim was to compare the magnetic results with conventional downhole log data, principally gamma ray and spontaneous potential (SP) logs, which are traditionally used to identify different lithologies. Comparisons were also made between the magnetic results and some limited core permeability data. The purpose of all these comparisons was to determine whether the magnetic measurements improve the identification of the main lithologies compared to the traditional methods, and to evaluate the magnetic technique as an

additional complementary (rapid, cheap, non-destructive) tool for oil sand reservoir characterization.

2. To quantitatively estimate mineral content from the volume magnetic susceptibility measurements. The technique potentially allows the content of key clay minerals (such as illite) to be estimated, which in turn is useful for predicting permeable zones (where the best oil sands intervals are likely to be located), since illite content has been shown in other reservoirs to influence fluid permeability (Potter, 2007). The results were compared with traditional spectral gamma ray log data (which is often used to estimate clay content), and spontaneous potential (SP) log data (which is traditionally used to identify permeable zones).
3. To undertake high resolution portable X-ray fluorescence (XRF) measurements on the slabbed core from the 3 oil sands wells at the same points where the probe magnetic measurements were taken. These XRF measurements provided elemental composition data to support and constrain the lithological and mineralogical conclusions generated from the magnetic data.
4. To undertake low applied field volume magnetic susceptibility, as well as mass magnetic susceptibility, measurements on some standard mineral samples using the novel probe and bridge sensors utilized in this thesis. The purpose was to test the accuracy and validity of the sensors by comparing the results with previously published data for those minerals. The minerals used for this purpose were typical of those expected in oil sands wells.
5. To compare the probe volume magnetic susceptibility results with visual observations of the slabbed core in some key sections. The purpose was to determine whether the quantitative magnetic measurements identified features that were not easily picked out by mere visual inspection in black bitumen or heavy oil saturated core sections.

6. To measure the volume and mass magnetic susceptibilities of small extracted samples of the unconsolidated rock from the slabbed core. The results could be converted to a mineral content (e.g., illite content) and then compared to X-ray fluorescence (XRF) measurements on identical samples. Mass magnetic susceptibility has the advantage of being less dependent upon porosity than volume magnetic susceptibility, and therefore potentially could allow further improved mineral content estimates. The magnetic susceptibility of a small representative sample of an oil sands reservoir hydrocarbon fluid (in this case a heavy oil sample) was also measured in order to evaluate its contribution to the overall magnetic susceptibility signals.
7. To measure the temperature dependence of magnetic susceptibility of small samples extracted from the slabbed core. This potentially provides an even better method of quantifying the paramagnetic mineral content (e.g., illite content), and could be compared with traditional measurements. Temperature dependent modelling and measurements for paramagnetic minerals was also undertaken in order to potentially apply the magnetic susceptibility technique for in-situ borehole magnetic susceptibility measurements where the temperature varies with depth.
8. To identify the presence of remanence carrying minerals (e.g., ferrimagnetic magnetite) in the slabbed core samples. This would enable us to extract out any contribution from a small amount of remanence carrying minerals that might be present and would further enable an improved paramagnetic clay content to be estimated. Two methods were employed to identify remanence carrying minerals: (i) acquisition of a magnetic remanence (in this case isothermal remanent magnetization, IRM), and (ii) a comparison of low field and high field magnetic susceptibility.

## 1.8. Thesis organization

The organization of this thesis is as follows:

**Chapter 1** gives the background of the research area and introduces the research objectives. The background gives an overview of the main magnetic classes, the magnetic susceptibility of materials and the common magnetic susceptibility measurement techniques. An overview of previous studies applying magnetic susceptibility to hydrocarbon reservoir characterization is presented, as well as a brief description of the geological background of the study area, the Alberta oil sands.

**Chapter 2** details the novel sensors used in the study, and gives results for a standard suite of typical reservoir minerals and fluids relevant to the oil sands. The purpose of these calibration measurements was to compare the results with previously published data in order to first evaluate the reliability of the novel sensors used in this study. Initial test results are then presented of low field probe magnetic susceptibility on representative sections of the slabbed cores from the 3 Albertan oil sands wells. These initial results were used to validate the usefulness of the probe magnetic technique in readiness for the extensive high resolution probe measurements presented in **Chapter 3**.

**Chapter 3** details the results of high resolution volume magnetic susceptibility measurements on large intervals of oil sands slabbed cores from the 3 Albertan oil sands wells using the novel probe magnetic susceptibility sensor technique. The magnetic results were used for identifying the different lithologies, estimating mineral contents, and for identifying the permeable zones (in which the best oil sands intervals were located). The results were compared with depth matched

downhole log data, as well as available core permeability data, to evaluate the magnetic susceptibility technique.

**Chapter 4** details the results of high resolution X-ray fluorescence (XRF) measurements for quantifying the content of different elements non-destructively on the slabbed cores from the 3 Albertan oil sands wells. The measurements were conducted at the same points on the slabbed cores as the probe magnetic susceptibility measurements for direct comparison. The XRF technique was used as an independent method for core characterization, and the data compared with the magnetic results to help evaluate the probe magnetic technique.

**Chapter 5** presents further magnetic measurements on small samples extracted from the same oil sands slabbed cores as in the previous chapters. The samples covered the range of different lithologies seen throughout the 3 wells. Magnetic remanence measurements (in this case isothermal remanent magnetization) were undertaken to determine the content of remanence carrying particles (e.g., ferrimagnetic magnetite, $Fe_3O_4$) in the samples. A comparison between low and high field magnetic susceptibility was also undertaken on the extracted samples. This comparison not only enables one to independently confirm the presence of remanence carrying particles, but also potentially enables one to determine the contribution of these particles to the magnetic susceptibility. XRF measurements were also made on the extracted samples for direct comparison with the magnetic susceptibility results.

This chapter also details temperature-dependent magnetic susceptibility measurements on the extracted samples. Such measurements have two main applications: (i) they enable one to

quantify the content of paramagnetic versus diamagnetic material in a sample (the magnetic susceptibility of paramagnetic substances is temperature dependent whereas that of diamagnetic substances is not), and (ii) they enable one to accurately determine the magnetic susceptibility with depth, and therefore are important for in-situ borehole applications of magnetic susceptibility.

**Chapter 6** summarizes the overall conclusions from the study. This chapter also presents some recommendations for further research arising from the results of this study.

## 1.9. References


Adams, J. J., Rostron, B. J., Mendoza, C. A, 2004. Coupled fluid flow, heat and mass transport, and erosion in the Alberta basin: implications for the origin of the Athabasca oil sands. *Canadian Journal of Earth Sciences*, **41**, 1077-1095.

Anfort, S. J., Bachu, S., Bentley, L. R., 2001. Regional-scale hydrogeology of the Upper Devonian-Lower Cretaceous sedimentary succession, south-central Alberta basin, Canada. AAPG Bulletin, **85**, 637-660.

Brubacher, L., Stafford, F, 1962. Magnetic susceptibility: A physical chemistry laboratory experiment. *Journal of Chemical Education*, **39**, 574-584.

Bruckshaw, J. M., Robertson, E. I., 1948. The measurement of the magnetic properties of rocks. *J. Sci. Instrument*., **25**, 444-449.

Carlin, R. L., 1986. *Magnetochemistry*. Springer 312 pp.

Dunlop, D. J. and Özdemir, Ö, 1997. *Rock Magnetism: Fundamentals and Frontiers*. Cambridge University Press, Cambridge, 573 pp.

Ebufegha, V. T and Potter, D. K., 2015. Low temperature magnetic anisotropy in shales and mudstones: application in modelling mineralogy and fabric in the Horn River Basin, British Columbia. *2015 GeoConvention: New Horizons*, Calgary, Alberta, Canada.

Ergin, Y. V., & Yarulin, K. S. (1979). *Magnetic Properties Of Oils*. Nauka., Moscow, USSR, 200 pp.

Evans, D. F., 1974. A new type of magnetic balance. *Journal of Physics E: Scientific Instruments*, **7**, 247-249.

Fowler, M. G., Stasiuk, L. D., Hearn M., et al, 2001. Devonian hydrocarbon source rocks and their derived oils in the Western Canada Sedimentary Basin. *Bulletin of Canadian Petroleum Geology*, **49**, 117-148.

Gingras, M. K. and Korosh, D., 2004. A brief overview of the geology of heavy oil, bitumen and oil sand deposits. 2004 *CSEG National Convention*, Calgary, Alberta, Canada.

Hay, P. W., 1994. Oil and Gas Resources of the Western Canada Sedimentary Basin. In: *Geological Atlas of the Western Canada Sedimentary Basin*, G. D. Mossop and I. Shetsen (comp.). Calgary, Canadian Society of Petroleum Geologists and Alberta Research Council, Chapter 32, 469-470.

Hayes, B. J. R., Christopher, J. E., Rosental, L., Los, G., Mc Kercher, B., Minken, D. F., Tremblay, Y. M., and Fennell, J. W., 1994. Cretaceous Mannville Group of the Western Canada Sedimentary Basin. In: *Geological Atlas of the Western Canada Sedimentary Basin*, G. D. Mossop and I. Shetsen (comp.). Calgary, Canadian Society of Petroleum Geologists and Alberta Research Council, Chapter 19, 317-335.

Hubbard S. M., Pemberton S. G., and Howard E. A., 1999. Regional geology and sedimentology of the basal Cretaceous Peace River Oil Sands deposit, north-central Alberta. *Bulletin of Canadian Petroleum Geology*, **47**, 270-297.

Hunt, C. P., Moskowitz, B. M. and Banerjee, S.K., 1995. Magnetic properties of rocks and minerals, In: *Rock Physics and Phase Relations: A Handbook of Physical Constants*, T. J. Ahrens, (Ed.): American Geophysical Union Reference Shelf 3, 189-204.

Hunt, J. M., 1996. *Petroleum Geology and Geochemistry (2nd)*. W. H. Freeman and Co., New York. 743 pp.

Ivakhnenko. O. P., 2012. Magnetic susceptibility of petroleum reservoir crude oils in petroleum engineering. In: *Crude Oil Exploration in the World*, Prof. Mohamed Younes (Ed.), Chapter 4, 71-88, InTech.

Ivakhnenko, O. P. and Potter, D. K., 2004. Magnetic susceptibility of petroleum reservoir fluids. *Physics and Chemistry of the Earth*, **29**, 899-907.

Lancaster, D. E., 1966. Electronic metal detection. *Electronic World*, (Dec.), 39-63.

Likhite, S. D., Radhakhrishnamurty, C. and Sahasrabudhe, P. W., 1965. Alternating current electromagnet-type hysteresis loop tracer for minerals and rocks. *Rev. Sci. Instrum*, **36**, 1558-1621.

Lucia, F. J., Kerans, C., Jenning, J. W., 2003. Carbonate reservoir characterization. *Journal of Petroleum Technology, Society of Petroleum Engineering*, **55**, (no. 6), 70-72. SPE-82071-PA. DOI: 10.2118/82071-MS.

Monger, J. and Price, R., 2002. The Canadian Cordillera: Geology and Tectonic Evolution. *Recorder of Canadian Society of Exploration Geophysics*, **27**, 17-36.

Mooney, H. M., 1952. *Geophysics*, **27**, (no. 3), 531-543.

Mossop, G. D. and Shetsen, I., 1994. Introduction to the Geological Atlas of the Western Canada Sedimentary Basin. In: *Geological Atlas of the Western Canada Sedimentary Basin*, G. D.

Mossop and I. Shetsen (comp.). Calgary, Canadian Society of Petroleum Geologists and Alberta Research Council, Chapter 1, 1-12.

Nagata, T., 1953. *Rock Magnetism*. Maruzen Co, Tokyo, 225 pp.

Potter, D. K., 2007. Magnetic susceptibility as a rapid, non-destructive technique for improved petrophysical parameter prediction. *Petrophysics*, **48** (issue 3), 191-201.

Potter, D. K., Al-Ghamdi, T. M., Ivakhnenko, O. P., 2011. Sensitive carbonate reservoir rock characterization from magnetic hysteresis curves and correlations with petrophysical properties. *Petrophysics*, **52** (issue 1), 50-57.

Potter, D. K., Corbett, P. W. M., Barclay, S. A., and Haszeldine, R. S., 2004. Quantification of illite content in sedimentary rocks using magnetic susceptibility—a rapid complement or alternative to X-ray diffraction. *Journal of Sedimentary Research*, *Research Methods Papers Section*, **74** (no. 5), 730-735.

Potter, D. K. and Ivakhnenko, O. P., 2008. Clay typing - sensitive quantification and anisotropy in synthetic and natural reservoir samples using low- and high-field magnetic susceptibility for improved petrophysical appraisals. *Petrophysics*, **49** (issue 1), 57-66.

Price, R.A., 1973. Large-scale gravitational flow of supracrustal rocks, southern Canadian Rockies. In: *Gravity and Tectonics*. K. A. De Jong and R. Scholten (eds.). New York, Wiley and Sons, 491-502.

Radhakrishnamurty, C., Likhite, S. D., Admin, B. S. and Somayajulu B. L. K., 1968. Magnetic susceptibility stratigraphy in ocean sediment cores. Earth Planet. Sci. Letters, **4**, 464-471.

Ranger, M. J., and Gingras, M. K., 2003. Geology of the Athabasca Oil Sands – Field guide and overview. *Canadian Society of Petroleum Geologists*, Calgary, 123 pp.

Ricketts, B. D, 1989. *Western Canada Sedimentary Basin – A Case History*. Calgary, Canadian Society of Petroleum Geologists, 320 pp.

Riediger, C. L, Fowler, M. G., Snowdon L. R. et al, 1999. Origin and alteration of Lower Cretaceous Mannville Group oils from the Provost oil field, east central Alberta, Canada. *Bulletin of Canadian Petroleum Geology*, **47**, 43-62.

Riediger, C. L., Ness S., Fowler M. G., Akpulat, T., 2000. Timing of oil migration, Palaeozoic and Cretaceous bitumen and heavy oil deposits, eastern Alberta. *Proceedings of GeoCanada 2000*, Calgary, Alberta, Paper 419, 4pp.

Smith, D. G., 1994. Paleogeographic Evolution of the Western Canada Foreland Basin. In: *Geological Atlas of the Western Canada Sedimentary Basin*, G. D. Mossop and I. Shetsen (comp.). Calgary, Canadian Society of Petroleum Geologists and Alberta Research Council, Chapter 17, 277-296.

Shuquing, Z., Haiping, H., and Yuming, L., 2008. Biodegradation and origin of oil sands in the Western Canada Sedimentary Basin. *Petroleum Science*, **5** (no. 2), 87-94.

Stewart, G.A., MacCallum, G.T., 1978. Athabasca Oil Sands Guide Book. *C.S.P.G. international conference, facts and principles of world oil occurrence*. Canadian Society of Petroleum Geologists, Calgary, Alberta, 33 pp.

Thompson, R., and Oldfield, F., 1986. *Environmental Magnetism*. Allen and Unwin, London, 243 pp.

Tissot, B. P. and Welte, D. H., 1984. *Petroleum Formation and Occurrence (2nd Ed.)*. Springer-Verlag Berlin Heidelberg, New York, 160-198.

West, G. F. and Dunlop, D. J., 1971. An improved ballistic magnetometer for rock magnetic experiments. *J. Phys. E: Sci*. Instrum., **4**, 37-40.

# Chapter 2

# Magnetic susceptibility of common reservoir minerals and fluids and the magnetic susceptibility sensor techniques used in this study

## 2.1. Introduction

Previous studies have demonstrated potential uses of magnetic susceptibility measurements on core plugs in order to estimate some key petrophysical parameters like clay content and fluid permeability in different reservoirs such as clastic shoreface (Potter et al., 2004; Potter and Ivakhnenko, 2008; Ali et al., 2014), carbonate (Potter et al., 2011) and shales (Ebufegha and Potter, 2015). However, in many reservoirs, it is not practical to cut core plugs, particularly in unconsolidated samples (such as sands) or in fissile samples (such as some shales) that might easily fracture. The present thesis therefore primarily introduces the application of a probe magnetic susceptibility tool on slabbed cores to provide a rapid, non-destructive technique for magnetic susceptibility measurements that can be used to characterize unconsolidated sand and shale samples from oil sands reservoirs in Northern Alberta.

This chapter will introduce the sensor techniques used in this study to measure magnetic susceptibility, and detail results of initial measurements using the sensors on a suite of standard typical reservoir minerals and fluids. The results will be compared to previous published data in order to evaluate the reliability of the sensor techniques. The chapter then concentrates on the application of the probe magnetic technique for measuring the volume magnetic susceptibility on the slabbed cores, and shows some test examples of how this technique has advantages over mere visual core observations. The probe magnetic technique can identify and quantify

differences in lithology (related to differences in mineralogy) that may not be obvious even from visual observations. This is especially important for some of the oil sands sections in this thesis, which are often saturated with black bitumen or heavy oil, and changes in the mineralogy and lithology may not be apparent even by visually looking at the core.

## 2.2. Magnetic susceptibility measurements and the novel sensors used in this study

As introduced in **Chapter 1**, magnetic susceptibility is a measurement of the magnetic response of a material to an external magnetic field; it can be expressed in either terms of volume magnetic susceptibility (dimensionless unit in SI) or mass magnetic susceptibility ($m^3kg^{-1}$). Reservoir minerals and fluids can be classified into four main groups with significantly differing values of magnetic susceptibility (diamagnetic, paramagnetic, ferrimagnetic and canted anti-ferromagnetic, whilst pure ferromagnetic substances are not expected to be encountered in terrestrial reservoirs due to the Earth's oxidising or reducing conditions). While the magnetic susceptibility of diamagnetic materials is negative, that of paramagnetic, ferrimagnetic and canted anti-ferromagnetic materials is positive.

The application of an external magnetic field affects all substances including solids and fluids. A reminder that the applied magnetic field creates a magnetic induction (B in Tesla) described by the following equation (in the SI system):

$$B = \mu_0 (J + H) \qquad \textbf{(2.1)}$$

where H (in $Am^{-1}$) is the magnetic field strength, $\mu_0$ (in $Hm^{-1}$) is the permeability of free space (generally given by the constant $4\pi \times 10^{-7}$ Henry $m^{-1}$ though since May 2019 is now thought of as a parameter to be measured) and J (in $Am^{-1}$) is the intensity of magnetization per unit volume. To

cancel the magnetic field strength dependence in **Equation (2.1)**, we divide both sides of the equation by H:

$$\mu = B/H = \mu_0 + \mu_0 (J/H) = \mu_0 + \mu_0 k = \mu_0 (1+k) \qquad \textbf{(2.2)}$$

where $\mu$ is the magnetic permeability of the substance and k is the dimensionless volume magnetic susceptibility ($k = J/H$). Magnetic susceptibility can also be expressed in terms of unit mass. The mass magnetic susceptibility, $\chi$, is given by the following equation:

$$\chi = M/H \qquad \textbf{(2.3)}$$

where M is the magnetization per unit mass. The units of $\chi$ are $m^3kg^{-1}$ in the SI system. Mass magnetic susceptibility can also be written as the volume magnetic susceptibility (k) divided by the density of the substance ($\rho$):

$$\chi = k/\rho \qquad \textbf{(2.4)}$$

Previous studies have published magnetic susceptibility data for different reservoir minerals (Thompson & Oldfield, 1986; Borradaile et al.,1990; Hunt et al., 1995; Ivakhnenko, 2006; Potter et al., 2011) and fluids (Ergin & Yarulin, 1979; Ivakhnenko & Potter, 2004; Ivakhnenko, 2006, 2012). These previous magnetic susceptibility data were measured with different instruments compared to the sensors used in the present study, and were based on some of the techniques described in **Chapter 1**. Therefore, it is important to measure the magnetic susceptibility of some standard samples of typical reservoir minerals and fluids (relevant to the oil sands) using our novel sensors, and compare the results with the previously published data in order to first evaluate the reliability of the novel sensor techniques. The magnetic susceptibility measurements of mineral and fluid samples, and the slabbed cores, were undertaken using two novel sensors. Small samples of material (minerals, fluids, and extracted powdered rock core) were measured

using a Bartington MS2W sensor, and the undisturbed slabbed cores were measured using a Bartington MS2E probe sensor. Each of these sensors is described in more detail below:

(i) MS2W sensor and MS2 meter for mass magnetic susceptibility measurements on small mineral, fluid and rock samples

The set-up consists of an MS2 meter (**Figure 2.1 (A)**), which gives a digital readout of the magnetic susceptibility connected to the MS2W sensor (**Figure 2.1 (B)**). The MS2W sensor operates on the principle of the AC induction method, though slightly modified from the standard AC induction methods described in **Chapter 1**. In the present study the MS2W sensor magnetic susceptibility measurement is based on the detection of a frequency change due to the presence of a sample. Power from the MS2 meter is supplied to an oscillator circuit within the sensor, and this generates a low intensity (approximately 80 $Am^{-1}$) alternating field with a frequency of 0.696 kHz. When a sample is placed within the influence of this field, it brings about a change in oscillator frequency. The frequency information is returned in pulse form to the meter where it is converted into a value to calculate mass magnetic susceptibility.

The initial calibration of the MS2W sensor was made using diamagnetic de-ionised water using a mass magnetic susceptibility value of $-0.9043 \times 10^{-8}$ $m^3kg^{-1}$ (Selwood, 1956). Repeat calibration measurements were regularly made throughout the measurement period in order to minimize any potential instrumental drift. The sensor was configured to be calibrated for a sample mass of 10g, and so a correction needed to be made after each measurement as follows:

$$\chi = \text{measured value} \times \text{calibration mass (10g)/sample mass} \quad \textbf{(2.5)}$$

Therefore, it was necessary to carefully weigh the sample prior to taking measurements. A Pioneer digital weighing balance was used to accurately weigh each sample. The accuracy of the balance was up to 0.0001 grams.

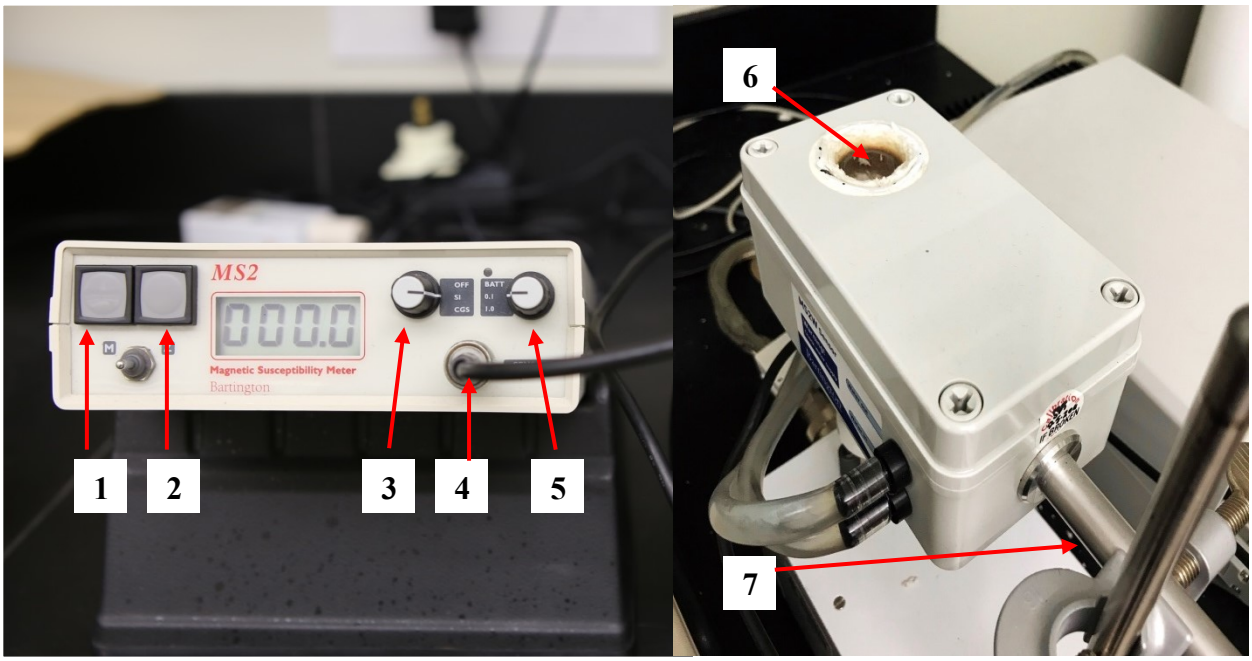


**Figure 2.1**: Bartington system used for mass magnetic susceptibility measurements of reservoir mineral and fluid samples. **(A)** is the MS2 meter where **1** is the measuring button, **2** is the zero-ing button, **3** is the magnetic unit (SI or CGS) system selector knob, **4** is the cable connecting the MS2 meter with the sensor, **5** is the sensitivity scale selector knob. **(B)** is the MS2W sensor where **6** is the sample chamber and **7** is the input for the cable **4** shown in **(A)** to connect with the meter.

(ii) MS2E probe sensor for magnetic susceptibility measurements on slabbed core

The MS2E sensor is designed to perform high resolution measurements of magnetic susceptibility along flat surfaces (in this research the surfaces of slabbed core) that have roughness less than 1mm. The sensor tip at the end of a ceramic tube (label **1** in **Figure 2.2 (A)** and label **4** in **Figure 2.2 (B)**) senses a rectangular surface area of 3.8 mm x 10.5 mm on the sample. This allows high resolution measurements to be made at the lamina scale. The sensor is calibrated to measure true volume magnetic susceptibility (k) when against a flat surface of a

sample greater than 10 mm in thickness. Most of the magnetic susceptibility signal is acquired within a penetration depth of up to about 5 mm into the sample. The ceramic tube is mounted on a metal enclosure that houses the electronic circuitry. The operating principle of the MS2E sensor is similar to that of the MS2W sensor detailed above. When the sensor is connected to the MS2 meter via a cable and the power is supplied, a low intensity alternating field (about 80 $Am^{-1}$ and about 2 kHz in frequency) is generated. This applied field penetrates a few mm into the sample when the tip of the sensor (label **4** in **Figure 2.2 (B)**) is placed on the flat surface of the slabbed core. A calibration sample is provided to check that sensor is working correctly.

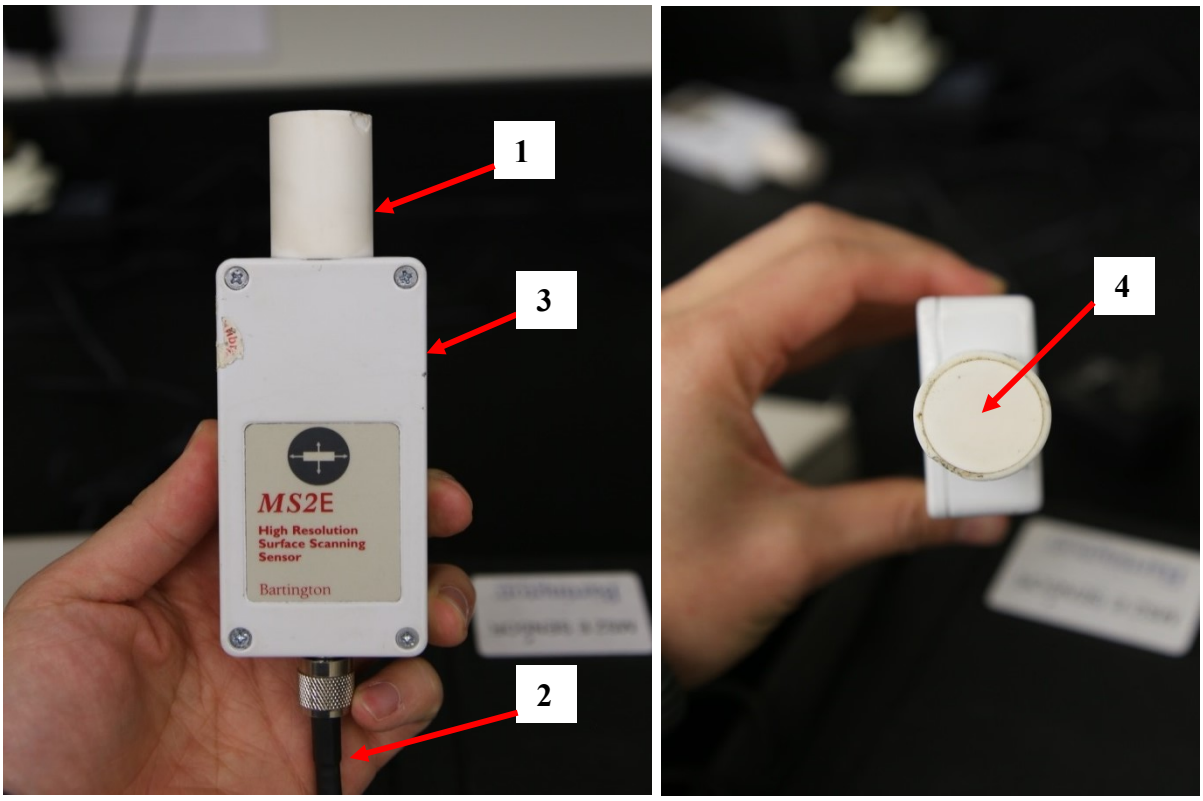


**(A)** **(B)**

**Figure 2.2**: MS2E probe sensor for surface magnetic susceptibility measurements on slabbed core. **1** is the probe tip with a ceramic guard and a sensor located at the end of the tube, **2** is the cable connected to the MS2 meter, **3** is a metal enclosure that houses the electronic circuity and **4** shows the cross section of the probe sensor tip that is gently applied to the surface of the slabbed cores.

## 2.3. Magnetic susceptibility of reservoir mineral and fluid samples

### 2.3.1. Measurements of mass magnetic susceptibility and volume magnetic susceptibility of a standard suite of typical reservoir mineral samples

A standard suite of typical oil sands reservoir minerals, including quartz, calcite, illite, kaolinite and chlorite, were selected for mass magnetic susceptibility and volume magnetic susceptibility measurements. The purpose was to compare the results with previously published data in order to evaluate the reliability of the novel sensors used in this study.

**Table 2.1**: A comparison of mass magnetic susceptibility values between a standard suite of typical reservoir minerals measured in the present study by the MS2W sensor (second column) and previously published results for the same minerals (third column) by Hunt et al. (1995), Borradaile et al (1990), Ivakhnenko (2006), Potter et al (2011) and Thompson and Oldfield (1986).

| **Minerals** | **Measured mass magnetic susceptibility using the MS2W sensor ($10^{-8}$ $m^3kg^{-1}$)** | **Previously published mass magnetic susceptibility ($10^{-8}$ $m^3kg^{-1}$)** |
|---|---|---|
| Illite | 13.50 | 15.0 |
| Chlorite | 22.38 | 12 to 52 |
| Quartz | -0.57 | -0.5 to -0.62 |
| Calcite | -0.40 | -0.3 to -1.4 |
| Kaolinite | -0.95 | -0.6 to -2.0 |

**Table 2.1** shows the results of mass magnetic susceptibility measurements of samples including diamagnetic quartz, calcite and kaolinite and paramagnetic illite and chlorite. The samples were supplied by Ward's Natural Science which is a supplier of science education materials with areas of focus including geology, earth science, biology, chemistry, environmental science and physical science. Most of the minerals were listed by the supplier as being free from contamination and high purity. However, the illite sample was listed as being 85% illite with the

remaining 15% being quartz. This would be consistent with the slightly lower magnetic susceptibility value using the MS2W sensor compared to previously published data. Overall the results obtained by the MS2W sensor were very close or within the ranges of the previously published data, indicating the reliability of the MS2W sensor. Chlorite has a larger range of previously published values, since the iron content will influence the magnetic susceptibility of chlorite, with higher iron content resulting in higher magnetic susceptibility (Borradaile et al., 1990).

**Table 2.2**: A comparison of volume magnetic susceptibility values between a standard suite of typical reservoir minerals measured in this study by the MS2E probe sensor (second column) and previously published results for the same minerals (third column) by Hunt et al. (1995), Borradaile et al (1990), Ivakhnenko (2006), Potter et al (2011) and Thompson and Oldfield (1986).

| **Minerals** | **Measured volume magnetic susceptibility using the MS2E sensor ($10^{-5}$ SI)** | **Previously published volume magnetic susceptibility ($10^{-5}$ SI)** |
|---|---|---|
| Illite | 37.1 | 41 |
| Chlorite | 66.1 | 34.8 to 150.8 |
| Quartz | -1.6 | -1.3 to -1.7 |
| Calcite | -1.1 | -0.75 to -3.9 |
| Kaolinite | -2.4 | -1.6 to -5.2 |

**Table 2.2** shows the results of volume magnetic susceptibility of the same samples measured by the MS2E probe sensor and a comparison with previous published results for similar minerals. The previously published data for illite, quartz and calcite were collated by Hunt et al (1995), and the other volume magnetic susceptibility values from previous work were converted from previously published mass susceptibility values using **Equation (2.4)**. Overall the results measured by the MS2E sensor are close or within the ranges of the previously published data,

indicating the reliability of the sensor. The measured result for the illite sample using the MS2E is again lower than the previously published value since the sample contains only 85% illite with the remainder being diamagnetic quartz.

### 2.3.2. Mass magnetic susceptibility of reservoir fluids

In addition to various minerals, a hydrocarbon reservoir also contains different natural fluids such as crude oil (light oil, heavy oil, bitumen or tar), gas condensates and formation waters. The magnetic susceptibility of crude oil can vary according to the specific reservoir where it is collected, and any magnetic differences between the crude oil in different regions may reflect specific features of the geological and geochemical history of the oil provenance (Ivakhnenko and Potter, 2004). In the present study, a heavy oil sample from the Albertan oil sands was available for mass magnetic susceptibility measurement. The sample was supplied by Innotech Alberta. This sample was chosen as being representative of the hydrocarbon in two of the wells (Wells 01 and 02) in this study that are situated in part of the Cold Lake deposit, where the hydrocarbon is often slightly less viscous than the bitumen in the Athabasca deposit further north. The heavy oil sample had a density of 0.95 x $10^3$ kg $m^{-3}$ and a viscosity of 20,000 cP at room temperature (20 ºC). The mass magnetic susceptibility of the heavy oil sample measured with the MS2W sensor was diamagnetic with a value of -0.9524 x $10^{-8}$ $m^3kg^{-1}$, which was slightly less diamagnetic than previously published results for crude oil samples by Ivakhnenko (2012) with values in the range -0.9592 to -0.9952 x $10^{-8}$ $m^3kg^{-1}$ (and a mean value of -0.9847 x $10^{-8}$ $m^3kg^{-1}$). Though there is no previously measured mass magnetic susceptibility of heavy oil (or bitumen) from the Albertan oil sands for comparison, the result for the heavy oil sample is consistent in that denser, more viscous crude oil samples tend to be less diamagnetic (less

negative magnetic susceptibility). The heavy oil samples in the Ivakhnenko (2012) study were from the Caucasian oil field, which might have different physical properties and chemical components compared to the Albertan oil sands heavy oil sample measured in this study. The heavy oil result from the present study is plotted for comparison with Ivakhnenko's (2012) mean value for the Caucasian heavy oil, along with other (non-heavy) crude oils, in **Figure 2.3**. Previous work (Ivakhnenko and Potter, 2004) showed that denser, more viscous crude oils have a higher residue content containing slightly higher amounts of trace metals. This would increase the magnetic susceptibility slightly.

The heavy oil result is also consistent with the trend of increasing mass magnetic susceptibility with decreasing API gravity of crude oils published by Ivakhnenko and Potter (2004) and Ivakhnenko (2012). The API gravity of the heavy sample is calculated by the equation:

$$^{o}\text{API} = [141.5/S_o] - 131.5 \qquad \textbf{(2.6)}$$

where $S_o$ is the stock tank oil specific gravity, or relative density, to water at 288 $^{0}$K. Therefore, using the above mentioned heavy oil density the API gravity of the heavy oil sample is 17.45 $^{o}$API.

For the present study there were unfortunately no easily accessible extracted samples of bitumen, which was the main hydrocarbon in Well 03 in the Athabasca oil sands. The typically higher viscosity (which can be in excess of 100,000 cP at room temperature), lower API gravity (<10 $^{o}$API) and expected slightly higher trace metal content of bitumen in the Athabasca oil sands might result in an even less negative (less diamagnetic) mass magnetic susceptibility signal than

that for the heavy oil sample studied here. Magnetic measurements on a relevant bitumen sample is one of the recommendations for further work listed in **Chapter 6**.

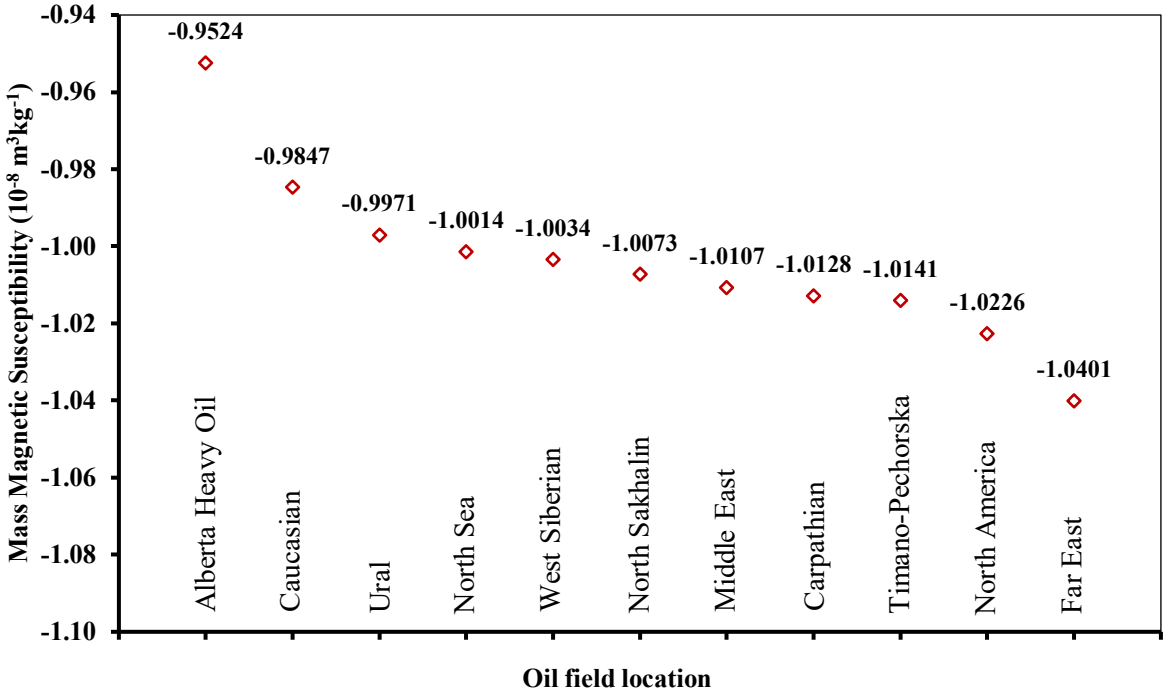


**Figure 2.3**: Mass magnetic susceptibility of crude oil from different oil field locations. The data for the Alberta heavy oil sample is from the present study, and the other data gives mean values of crude oils from other worldwide locations from Ivakhnenko (2012). The only other heavy oil in the list is the Caucasian crude oil.

In this study, there were unfortunately no formation water samples available for magnetic susceptibility measurements. However, studies by Ivakhnenko and Potter (2004) and Ivakhnenko (2012) showed that formation waters are diamagnetic, and differences in the mass magnetic susceptibility values for different water samples were related to the solutes they contained.

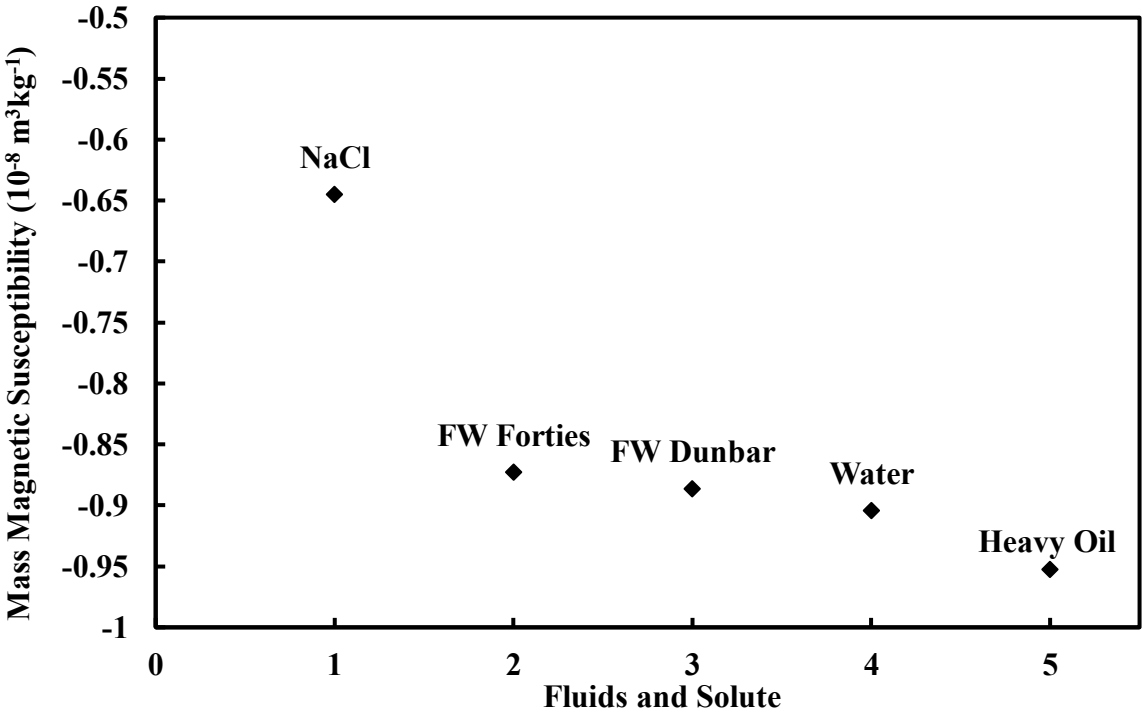


**Figure 2.4**: Comparison between the mass magnetic susceptibility of different fluids, as well as pure sodium chloride solute. Data includes reservoir formation water (FW) samples for the Forties and Dunbar fields in the North Sea (Ivakhnenko and Potter, 2004), pure solid sodium chloride NaCl (Ivakhnenko, 2012), de-ionized water (Selwood, 1956) and the heavy oil sample from the present study.

**Figure 2.4** clearly shows the differences in mass magnetic susceptibilities between heavy oil, de-ionized water and pure solid sodium chloride (NaCl), although they all have negative values. The de-ionized water, formation waters and solid NaCl are all less diamagnetic than the heavy oil sample, which in turn was less diamagnetic than other (generally less viscous) crude oil samples in **Figure 2.3**. The two formation water samples from the North Sea in **Figure 2.4** indicate that the presence of sodium chloride (the main dissolved salt in these samples) tends to decrease the diamagnetism of water, and is consistent with the result for pure solid sodium chloride being even less diamagnetic. The lower concentration of sodium chloride (34.13 kg $m^{-3}$) in the Dunbar formation water compared to that in the Forties formation water (79.50 kg $m^{-3}$) caused a more negative magnetic susceptibility in the Dunbar formation water (-0.8862 x $10^{-8}$ $m^3kg^{-1}$) than in the Forties formation water (-0.8729 x $10^{-8}$ $m^3kg^{-1}$) (Ivakhnenko and Potter, 2004).

### 2.3.3. Comparisons between the magnetic susceptibilities of reservoir minerals and fluids

Since the magnetic susceptibility of a substance can be expressed in terms of mass or volume, it may be useful to compare the mass and volume magnetic susceptibilities of typical reservoir diamagnetic minerals and fluids. The comparisons are shown in **Figure 2.5**. The mass and volume magnetic susceptibilities ($\chi$ and k) are related using the earlier **Equation (2.4)**. The numerical differences between the mass and volume susceptibilities (for the stated power of ten of each of these parameters) are greater for the minerals than for the fluids. This is merely due to the differences in their densities. The densities of quartz and calcite are 2.65 x $10^3$ $kgm^{-3}$ and 2.71 x $10^3$ $kgm^{-3}$ respectively, whilst the densities of the reservoir fluids were 1 x $10^3$ $kgm^{-3}$ for the de-ionized water, 1.01 x $10^3$ $kgm^{-3}$ for the Dunbar formation water, 1.05 x $10^3$ $kgm^{-3}$ for the Forties formation water (Ivakhnenko and Potter, 2004), and 0.95 x $10^3$ $kgm^{-3}$ for the heavy oil sample in the present study. An average formation water density from the Dunbar and Forties formation waters was used to plot typical formation water mass and volume magnetic susceptibilities in **Figure 2.5**.

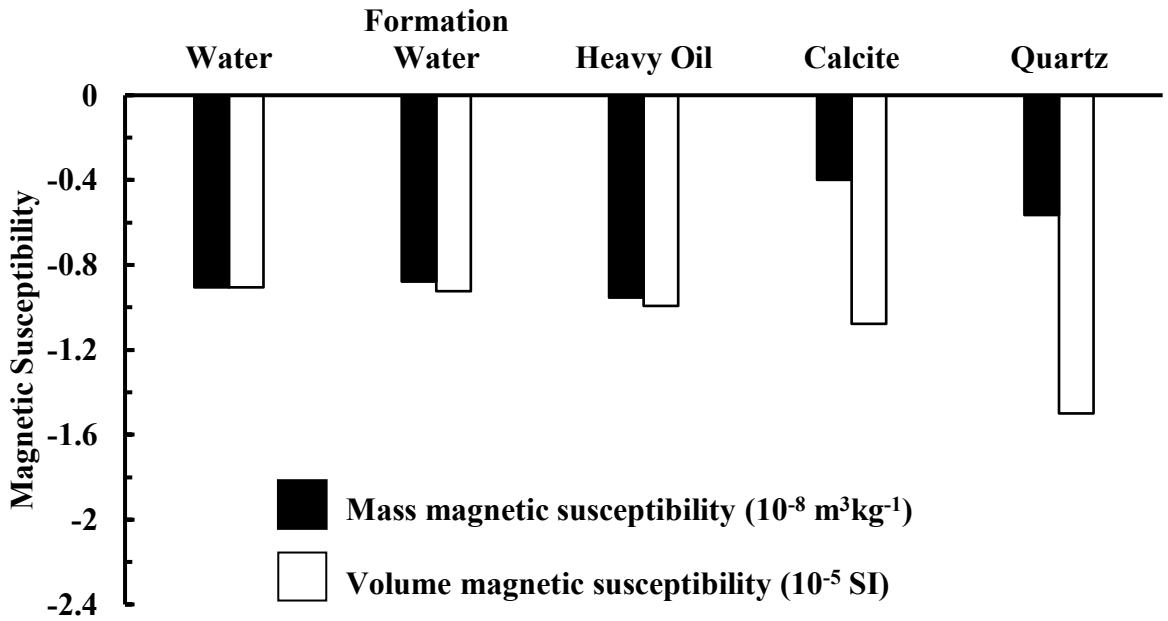


**Figure 2.5**: Comparisons between the mass and volume magnetic susceptibilities of common diamagnetic reservoir minerals and fluids. The susceptibilities of de-ionized water are from Selwood (1956), those of formation water (average of Dunbar and Forties formation waters) are from Ivakhnenko and Potter (2004), whilst the susceptibilities of heavy oil, quartz and calcite are results from the measurements of samples in the present study.

**Figure 2.6** shows a comparison of the probe volume magnetic susceptibilities between the common reservoir minerals and fluids that would be expected in Albertan oil sands reservoirs, using data generated in this project and detailed earlier in this chapter, and some previously published values. The minerals and fluids fall into two main magnetic classes. The diamagnetic class showing low negative magnetic susceptibility contains the main rock forming minerals quartz (forming the oil sands), calcite (a major component of some basal carbonates), and typical reservoir fluids. In contrast the paramagnetic class containing typical clay minerals such as illite and chlorite exhibit larger positive magnetic susceptibility. Small amounts of these clay minerals can dominate the magnetic susceptibility signal and can be a major control on the fluid permeability (especially illite). Therefore it is potentially very useful to use the probe magnetic susceptibility technique to identify small amounts of such paramagnetic clay even in the

presence of a much larger volume of the main rock forming minerals (such as quartz) and reservoir fluids.

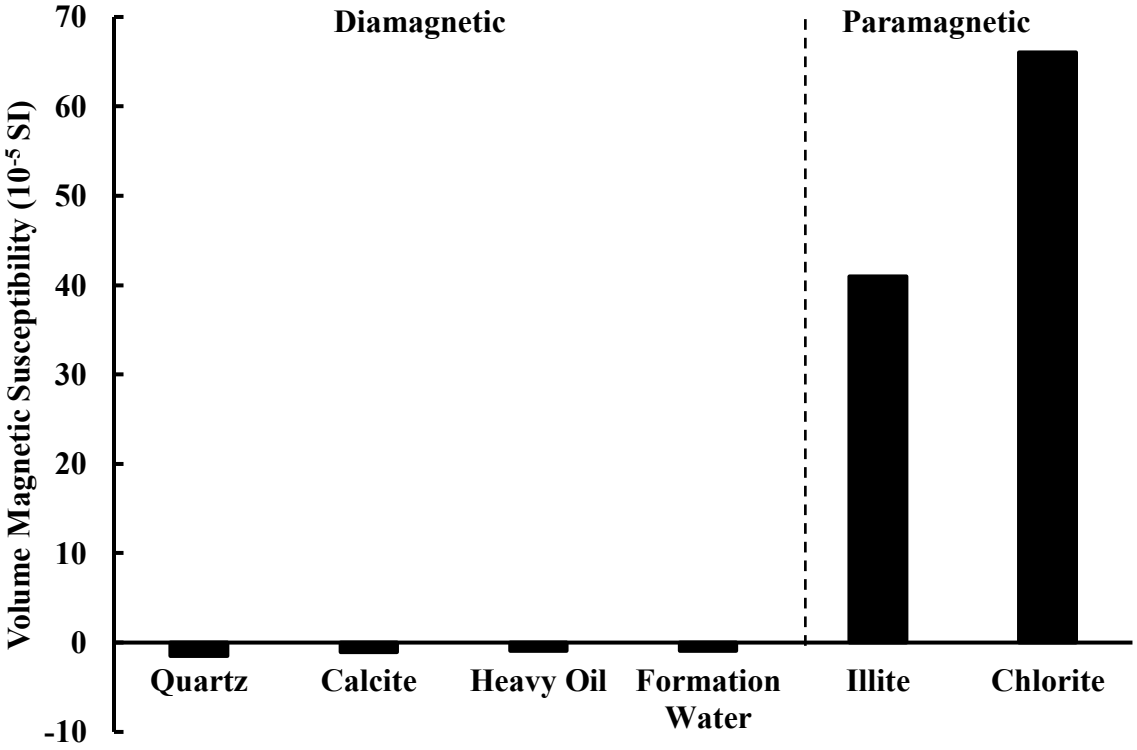


**Figure 2.6**: A comparison of the probe volume magnetic susceptibility values of the standard reservoir mineral samples (quartz, calcite, chlorite) and heavy oil from the present study with the values of formation water (average value from Dunbar and Forties formation waters from Ivakhnenko and Potter, 2004) and illite from Hunt et al (1995).

## 2.4. Test examples of volume magnetic susceptibility measurements on slabbed cores from the 3 wells in the Albertan oil sands using the MS2E probe sensor

As detailed in the previous section, typical minerals (such as quartz and calcite) and fluids (hydrocarbons and formation waters) in petroleum reservoirs are diamagnetic with small and negative volume magnetic susceptibility, while key permeability controlling clay minerals in muddy sandstones and shales are paramagnetic with high positive volume magnetic susceptibility. This section will show some test examples of volume magnetic susceptibility measured on different slabbed cores from the 3 oil sands wells using the Bartington MS2E probe

magnetic susceptibility sensor, to test the usefulness of the technique compared to visual observations. The MS2E probe sensor was connected to a MS2 meter to give a digital readout of the magnetic susceptibility as indicated previously in **Figure 2.1**. The magnetic susceptibility was directly measured by placing the probe tip gently on the surface of a slabbed core. The process is non-destructive, which is particularly useful for unconsolidated oil sands and fissile shales in the reservoir intervals studied, and no core preparation was needed. Measurements were made at high resolution every 2.5 cm down the core sections. The applied magnetic field of the probe sensor interrogates an area of about 3.8 x 10.5 mm and penetrates just a few mm into the core (most of the magnetic susceptibility signal comes from the first 5 mm into the core sample). The raw magnetic susceptibility values represent a reading on the core minus a background (in air) reading. The background and core readings at each depth take around 30 seconds in total (12 seconds for each reading plus a few second between readings) on the most sensitive measurement scale. This most sensitive scale was utilized since the magnetic susceptibility signal in certain intervals was low and negative (particularly in the best oil sands intervals), and the higher sensitivity allowed one to obtain the best results. A non-magnetic ruler was supported along the core to gauge the measurement intervals. The core and sensor needed to be at the same temperature before attempting measurements, and therefore the system ideally needed five to ten minutes of warm-up time before it was ready to take measurements.

**Figures 2.7**, **2.8**, **2.9** and **2.10** show some initial test results of the volume magnetic susceptibility measured by the probe technique, along with visual comparisons of the slabbed core images. These comparisons will demonstrate how magnetic susceptibility profiles can distinguish different lithologies and quantify the variation of mineralogy better than mere visual

observation of the cores. The selected test intervals covered a range of different lithologies in the 3 oil sands wells including clean sands with and without bitumen or heavy oil, and clay / shale.

**Figure 2.7** shows the probe volume magnetic susceptibility profile of a relatively clean sand (with thin interbedded clay layers) and a more paramagnetic clay rich interval (A) from Well 02, along with the core image. This core section was not significantly saturated with heavy oil. The magnetic susceptibility profile distinguishes the different mineralogical changes well. The significant positive magnetic susceptibility interval (A) correlates well with the thin paramagnetic clay interval seen in the core image. Elsewhere negative values of magnetic susceptibility correspond to quartz rich sand intervals, whilst positive values of magnetic susceptibility correspond to increased amounts of paramagnetic clay. The presence of this paramagnetic clay is not easily identified from the core observations alone, particularly at the top and bottom of the section, since the colour of the core is very similar and the variation of grain size is not obvious. However, a key advantage of the probe magnetic technique is that it can pin-point these subtle variations very readily.

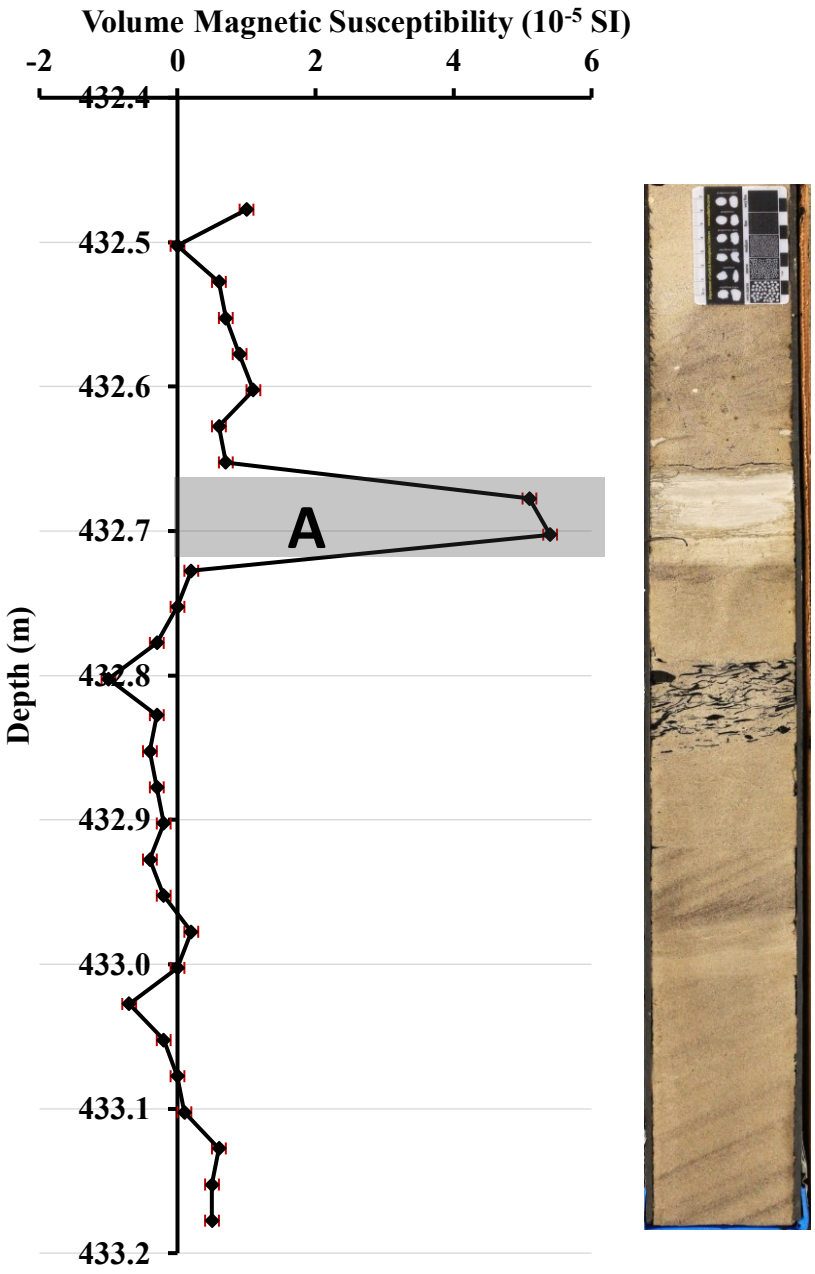


**Figure 2.7**: MS2E probe volume magnetic susceptibility profile of a relatively clean sand (with thin interbedded clay layers) and a more paramagnetic clay rich interval (A) without from Well 02, and the associated core image. This core was not significantly saturated with heavy oil. The magnetic susceptibility profile picks out the different mineralogical changes well. In particular, the significant positive magnetic susceptibility interval (A) correlates well with the thin paramagnetic clay interval seen in the core image. Elsewhere negative values of magnetic susceptibility correspond to the sand (quartz rich) intervals, and positive values of magnetic susceptibility correspond to increased amounts of paramagnetic clay. Measurement uncertainties, in relation to the plotted magnetic susceptibility scale, are shown and are close to the symbol sizes in this case.

**Figure 2.8** shows the probe volume magnetic susceptibility profile for an oil sands slabbed core section saturated with bitumen in Well 03. Since quartz sand is diamagnetic and bitumen is expected to be diamagnetic then it's not surprising that all the data points in this example exhibit negative magnetic susceptibility. The probe results show real quantitative variations greater than the measurement uncertainties shown. A major advantage of the quantitative probe magnetic measurements is that they reveal variations that one cannot see from mere visual observations, since the black bitumen obscures any small differences in the mineralogy. There are a number of possible reasons for the variations in magnetic susceptibility in **Figure 2.8**. They may include one or more of the following:

- The most likely explanation is due to the presence of small amounts of paramagnetic clay mixed with the sand. Note that, for example, just 4% of illite clay in a simple mixture of quartz + illite will cause the magnetic susceptibility to become positive. The simple mathematical equations detailing this will be given in **Chapter 3**.
- Another possibility is the presence of a very small amount of ferrimagnetic particles. This possibility is explored in more detail in **Chapter 5**.
- A further possible reason could be slight variations in the porosity and the bitumen saturation within the pore space. Note that the MS2E sensor probe volume magnetic susceptibility measurements are potentially more susceptible to variations in porosity (though the effect is likely to be very small) compared to the MS2W sensor mass magnetic susceptibility measurements. Mass magnetic susceptibility is less affected by porosity because changes in porosity lead to changes in both mass and magnetization, and these two parameters largely cancel one another out so that the mass magnetic susceptibility remains largely unaffected by porosity variations.

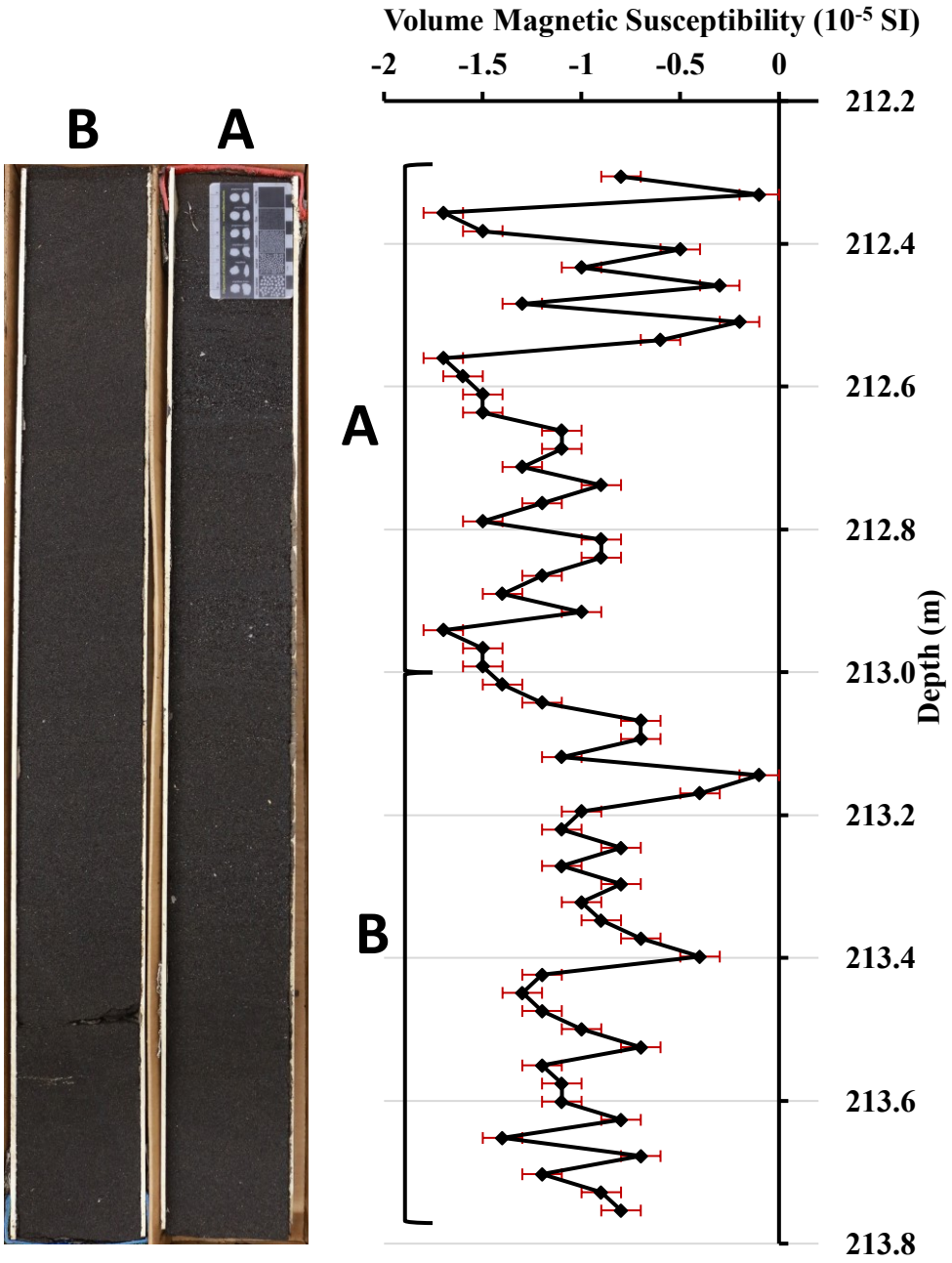


**Figure 2.8**: This example from Well 03 shows the results of the MS2E probe volume magnetic susceptibilities measured for an oil sands slabbed core saturated with bitumen. Since sand (quartz) is diamagnetic and bitumen is expected to be diamagnetic then this explains why all the values in this example exhibit negative magnetic susceptibility. The probe results show real quantitative variations (greater than the measurement uncertainties shown). The possible reasons for the variations are discussed in the text. A major advantage of the quantitative probe magnetic measurements is that they reveal variations that one cannot see from mere visual observations, since the black bitumen obscures any small variations in the mineralogy.

**Figure 2.9** shows the probe volume magnetic susceptibility profile for two distinct lithologies in Well 03: bitumen saturated sand at the top and shale at the base. The black bitumen saturated sand gives a diamagnetic negative magnetic susceptibility signal, whereas the brownish shale at the base contains paramagnetic clays (and possibly also an extremely small amount of ferrimagnetic minerals) which give a positive magnetic susceptibility.

**Figure 2.10** shows the probe volume magnetic susceptibility profile for two lithologies in Well 02 that are very difficult to distinguish from the core images alone, since the cores are saturated with heavy oil. This again demonstrates the usefulness of the probe magnetic technique. Section A is a heavy oil saturated sand resulting in net negative (diamagnetic) magnetic susceptibility values (due to the quartz + heavy oil), whereas Section B is a more shale rich interval containing paramagnetic clays. Note that some of the magnetic susceptibility values are greater than 75 x $10^{-5}$ SI, which immediately indicates that the mineralogy in this case cannot just be illite, since 100% illite would only give a signal of 41 x $10^{-5}$ SI. The results highlight another important advantage of the probe magnetic technique in being able to rapidly identify zones of anomalous mineralogy. In this case the possible mineralogy could include a combination of paramagnetic minerals (which may include illite), or one paramagnetic mineral with a higher magnetic susceptibility than illite, or a paramagnetic mineral or minerals with a small amount of a ferrimagnetic mineral (e.g., illite + magnetite). The presence of ferrimagnetic minerals will be explored quantitatively in more detail in **Chapter 5**.

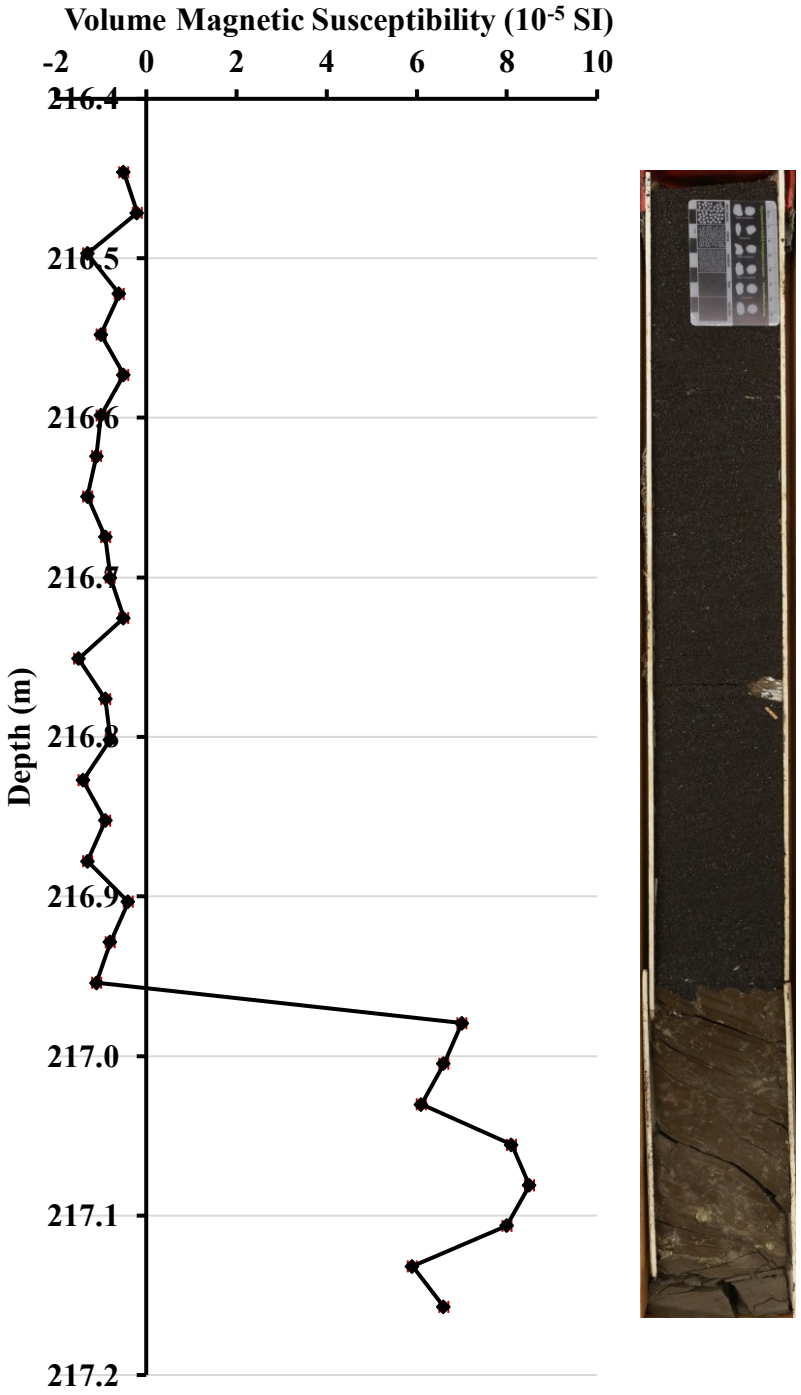


**Figure 2.9**: This example shows the results of the MS2E probe volume magnetic susceptibility measured for two distinct lithologies in Well 03: bitumen saturated sand at the top and shale at the base. The black bitumen saturated sand gives a diamagnetic negative magnetic susceptibility signal, whereas the brownish shale at the base contains paramagnetic clays (and possibly also an extremely small amount of ferrimagnetic minerals) which give a positive magnetic susceptibility.

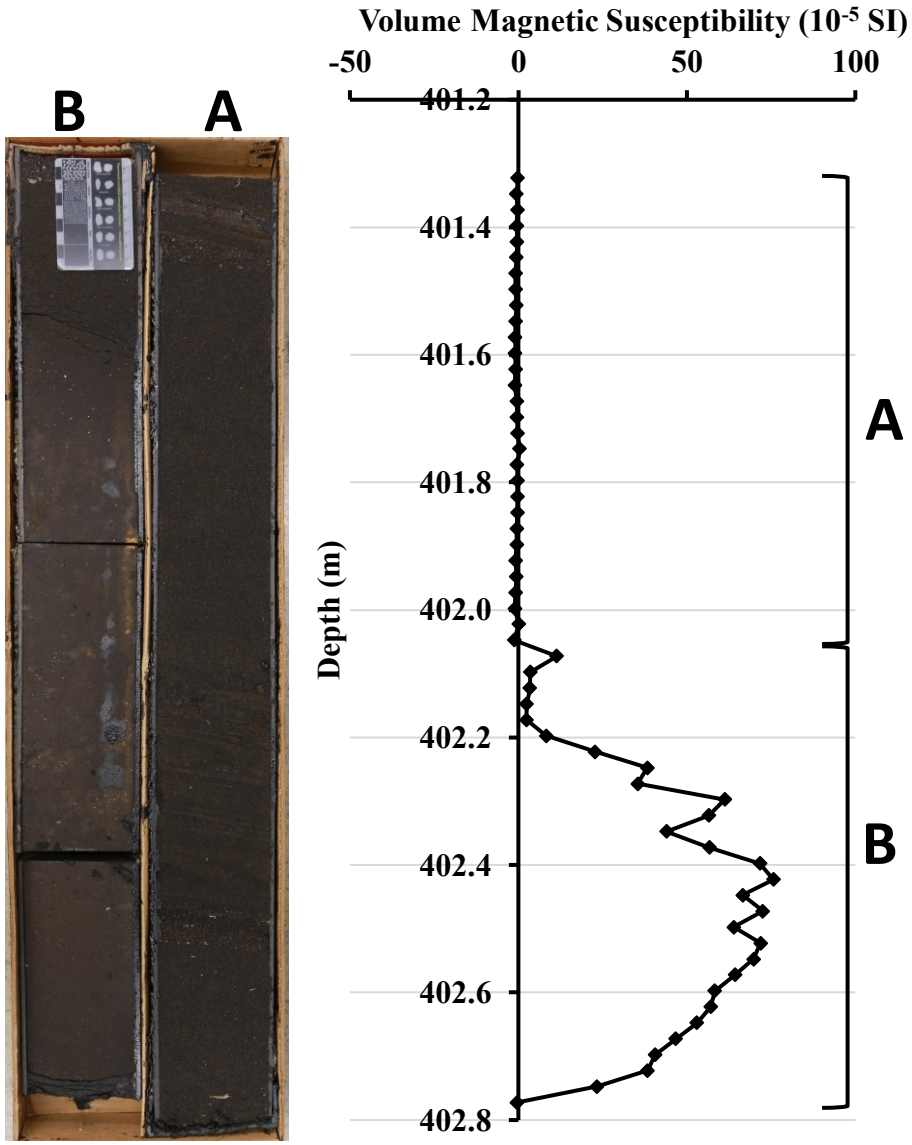


**Figure 2.10**: This example shows the results of the MS2E probe volume magnetic susceptibility for two lithologies from Well 02 that are difficult to distinguish from the core images alone, since the cores are saturated with heavy oil. This again demonstrates the usefulness of the probe magnetic technique. Section A is an oil sand giving net negative (diamagnetic) magnetic susceptibility values (due to the quartz + heavy oil), whereas Section B is a more shale rich interval containing paramagnetic clays. Note, however, that some of the values are greater than 75 x $10^{-5}$ SI, which immediately indicates that the mineralogy in this case cannot just be illite, since 100% illite would only give a signal of 41 x $10^{-5}$ SI. A discussion of the possible minerals present is given in the text. The results illustrate another important advantage of the probe magnetic technique in being able to rapidly identify zones of anomalous mineralogy.

## 2.5. Conclusions

The following conclusions can be drawn from the measurements on the standard suite of samples and the initial test results on the slabbed cores detailed in this chapter:

1. The mass magnetic susceptibilities of the standard suite of reservoir mineral samples using the MS2W sensor were very similar to those given in previously published data. This indicated the reliability of the MS2W sensor for making magnetic susceptibility measurements on such mineral samples, and gave confidence that this sensor would be capable of making meaningful measurements on small extracted samples from the oil sands slabbed core.
2. The volume magnetic susceptibilities of the standard suite of reservoir mineral samples using the MS2E probe sensor were also very similar to those given in previously published data. This indicated the reliability of the MS2E probe sensor for making meaningful magnetic susceptibility measurements on the oil sands slabbed core intervals.
3. Tests of probe magnetic susceptibility on some typical oil sands slabbed core demonstrated that the technique could pick out the different lithologies, and quantify changes in mineralogy. In addition to being rapid and non-destructive for these unconsolidated cores, the tests demonstrated that the probe magnetic technique was particularly useful for identifying different lithologies and quantifying variations in mineralogy in bitumen and heavy oil saturated cores, where the variations were not apparent by visual inspection of the cores since the black bitumen and heavy oil obscured the variations. This is a major advantage of the probe magnetic technique in oil sands core compare to mere visual observations.

4. The probe magnetic tests also demonstrate that the presence of any anomalous minerals (other than those that might be expected in these oil sands intervals) can be quickly pin-pointed by this technique (such as in Section B of **Figure 2.10**).
5. Magnetic susceptibility measurements on the heavy oil sample were consistent with previously published trends of crude oils (Ivakhnenko and Potter, 2004; Ivakhnenko, 2012), specifically its slightly increased mass magnetic susceptibility and decreased API gravity compared to other crude oils. The heavy oil sample had a less diamagnetic signal compared to the Ivakhnenko and Potter (2004) and Ivakhnenko (2012) data for heavy oils. Whilst no previously published data on the magnetic susceptibility data of bitumen or heavy oil in the Albertan oil sands was found, the results for the heavy oil sample in the present study are consistent with the Ivakhnenko and Potter (2004) study where heavier crude oils were less diamagnetic. Ivakhnenko and Potter (2004) also showed that these heavier oils contained slightly greater amounts of trace metals, which was the likely cause of the slightly increased magnetic susceptibility. The heavy oil sample in the present study also had a slightly more diamagnetic signal compared to formation waters, again consistent with previously published data comparing hydrocarbons with formation waters (Ivakhnenko and Potter, 2004).
6. The diamagnetic signal of the heavy oil sample means that it is unlikely to affect the ability of the probe magnetic sensor to distinguish between quartz rich oil sands and the increased amounts of paramagnetic clays in the IHS (inclined heterolithic stratification) beds and shales. Small differences in bitumen saturation (in Well 03) or heavy oil saturation (in Wells 01 and 02), however, may be one of the possible reasons for some of the small variations in the volume magnetic susceptibility profiles, for example in the bitumen saturated oil sands in Well 03 shown in **Figure 2.8**.

## 2.6. References

Ali, A., Potter, D. K. and Tugwell, A., 2014. Correlation between magnetic properties and permeability: results from a new case study in the North Sea. In *Proceedings of the 2014 International Symposium of the Society of Core Analysts*, 8-11 September 2014, Avignon, France. Paper SCA2014-077 (6 pages).

Borradaile, G. J., MacKenzie, A. and Jensen E., 1990. Silicate versus trace mineral susceptibility in metamorphic rocks. *Journal of Geophysical Research - Solid Earth*, **95**, 8447-8451.

Ebufegha, V. T and Potter, D. K., 2015. Low temperature magnetic anisotropy in shales and mudstones: application in modelling mineralogy and fabric in the Horn River Basin, British Columbia. *2015 GeoConvention: New Horizons*, Calgary, Alberta, Canada.

Ergin, Y. V. and Yarulin, K. S., 1979. Magnetic properties of oils. Nauka., Moscow, USSR, 200 pp.

Hunt, C. P., Moskowitz, B. M. and Banerjee, S.K., 1995. Magnetic properties of rocks and minerals, In: *Rock Physics and Phase Relations: A Handbook of Physical Constants*, T. J. Ahrens, (Ed.): American Geophysical Union Reference Shelf 3, 189-204.

Ivakhnenko, O. P., 2006. Magnetic analysis of petroleum reservoir fluids, matrix mineral assemblages and fluid-rock interactions. PhD Thesis, Heriot-Watt University, Edinburgh, UK, 210 pp.

Ivakhnenko. O. P., 2012. Magnetic susceptibility of petroleum reservoir crude oils in petroleum engineering. In: *Crude Oil Exploration in the World*, Prof. Mohamed Younes (Ed.), Chapter 4, 71-88, InTech.

Ivakhnenko, O. P. and Potter, D. K., 2004. Magnetic susceptibility of petroleum reservoir fluids. *Physics and Chemistry of the Earth*, **29**, 899-907.

Potter, D. K., AlGhamdi, T. M. and Ivakhnenko, O. P., 2011. Sensitive carbonate reservoir rock characterization from magnetic hysteresis curves and correlation with petrophysical properties. *Petrophysics*, **52** (issue 1), 50-57.

Potter, D. K., Corbett, P. W. M., Barclay, S. A., and Haszeldine, R. S., 2004. Quantification of illite content in sedimentary rocks using magnetic susceptibility—a rapid complement or alternative to X-ray diffraction. *Journal of Sedimentary Research*, *Research Methods Papers Section*, **74** (no. 5), 730-735.

Potter, D. K and Ivakhnenko, O. P., 2008. Clay typing - sensitive quantification and anisotropy in synthetic and natural reservoir samples using low- and high-field magnetic susceptibility for improved petrophysical appraisals. *Petrophysics*, **49** (issue 1), 57-66.

Selwood, P.W., 1956. Magnetochemistry, Second edition. Interscience Publishers, New York, 435 pp.

Thompson, R. and Oldfield, F., 1986. Environmental Magnetism. Allen & Unwin, London, 243 pp.

# Chapter 3

# Probe magnetic susceptibility as a non-destructive tool for characterizing oil sands slabbed cores: comparisons with traditional downhole gamma ray, spontaneous potential logs and core permeability

## 3.1. Introduction

As introduced in **Chapter 1** there are five main magnetic classes, whilst in **Chapter 2** terrestrial reservoir minerals and fluids can be classified into four of these classes (diamagnetic, paramagnetic, ferrimagnetic and canted antiferromagnetic) with distinct differences in magnetic susceptibility. While typical minerals and fluids in reservoirs of interest (like quartz, calcite, hydrocarbons and formation waters) are diamagnetic with small negative susceptibilities, permeability controlling clay minerals (such as illite and chlorite) are paramagnetic with significant positive susceptibilities. The comparisons between magnetic susceptibility results and core observations for the test slabbed core sections shown in **Chapter 2** demonstrated the potential usefulness of magnetic susceptibility for identifying different lithologies and quantifying the variation in mineralogy. Previous studies have indicated the potential use of magnetic susceptibility measurements on core plugs for estimating some key petrophysical properties (such as clay content, fluid permeability) in different reservoirs, such as clastic reservoirs (Potter, 2007; Potter and Ivakhnenko, 2008; Ali et al, 2014) and carbonate reservoirs (Potter et al, 2011). However, there have been limited applications so far to unconsolidated core samples, such as unconventional oil sands, in which the core is not practical to cut. This chapter will present the results of probe volume magnetic susceptibility measurements on the slabbed cores of 3 different oil sands wells for characterizing reservoir properties, such as distinguishing

the main lithology intervals, estimating illite content and identifying permeable zones. Magnetic susceptibility was directly measured on the surface of the slabbed cores without any core preparation by using the probe magnetic technique described in **Chapter 2**. The raw results were used to distinguish different lithologies, and were subsequently processed to provide quantitative magnetically derived estimates of paramagnetic clay mineral contents (illite in this case) to compare with other parameters and to help predict permeable zones. The magnetic results were compared with traditional reservoir characterization methods like downhole gamma ray (GR) and spontaneous potential (SP) logs. The comparisons assessed the effectiveness of the magnetic technique for reservoir characterization in the oil sands, and highlighted any advantages the magnetic technique had over the traditional methods.

## 3.2. Samples and methods

### 3.2.1. Samples

The samples were slabbed core intervals from 3 different oil sands wells, designated as Well 01, Well 02, and Well 03 in this study, that were provided by the company Cenovus FCCL Ltd. The wells were from different locations in Northern Alberta, and were drilled to the McMurray Formation in the Mannville Group of the Western Canada Sedimentary Basin. Two of the wells, Well 01 and Well 02, are located in the northern region of the Cold Lake oil sands, while Well 03 is located in the northeast region of the Athabasca oil sands (**Figure 3.1**). The available cores were recovered from depths of 467–517.5 m for Well 01, 354.78–433.5 m for Well 02, and 149.16–233.39 m for Well 03. All recovered cores were put in plastic (rather than metal) trays to ensure insignificant effect on the results of the magnetic measurements of the cores, since the plastic has extremely low volume magnetic susceptibility (averaging close to 0 x $10^{-5}$ SI).

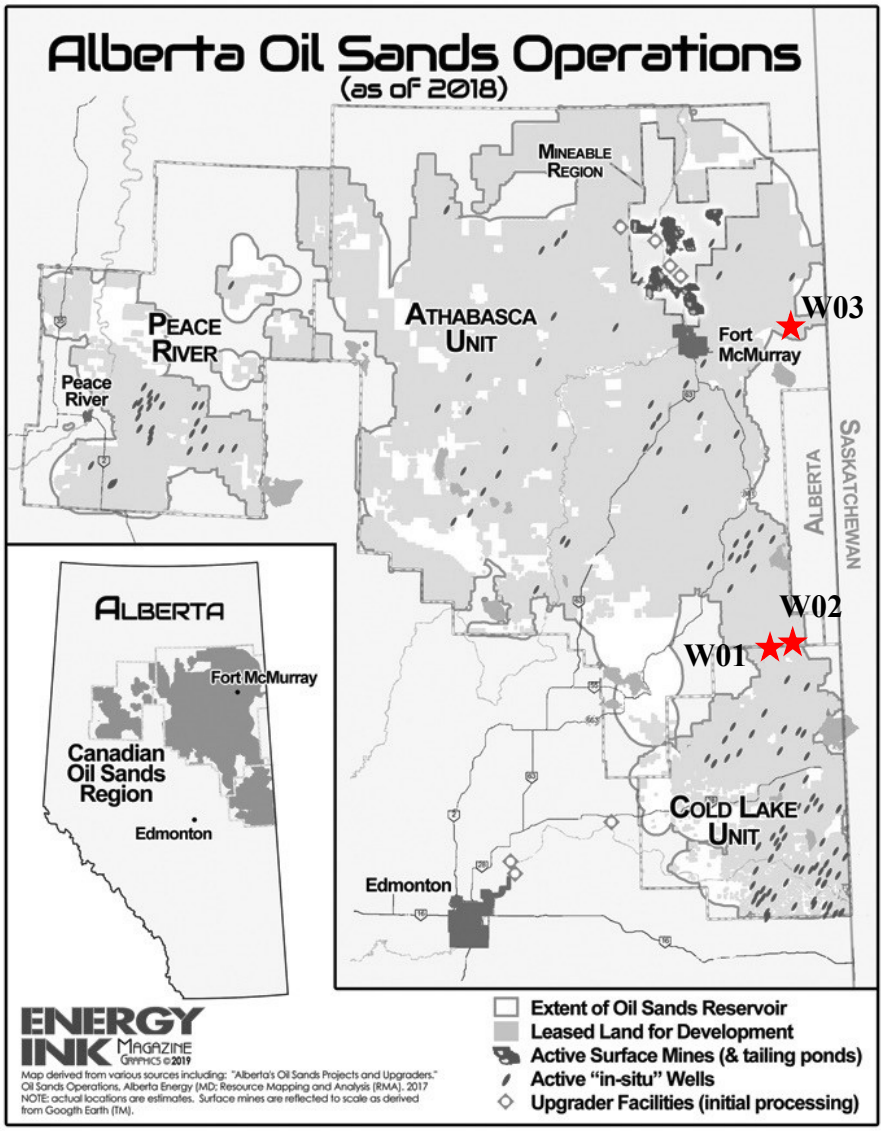


**Figure 3.1**: Map showing the approximate locations of the three oil sands wells in this study. **W01** is the location of Well 01, **W02** is the location of Well 02 and **W03** is the location of Well 03 (modified from Sharpe, 2019).

### 3.2.2. Probe volume magnetic susceptibility measurements

All measurements were undertaken in the core viewing room in the basement of the Student Association Building (SAB) at the University of Alberta where the cores were stored. The magnetic susceptibility measurements were taken using a portable Bartington high-resolution MS2E probe sensor connected to an MS2 meter (as described in **Chapter 2**) that allowed a

digital readout of the volume magnetic susceptibility. The sensor is designed to perform high-resolution measurements of magnetic susceptibility along flat surfaces that have a roughness of less than 1 mm. The sensing surface is at the end of a ceramic tube and has dimensions of 10.5 mm x 3.8 mm. A weak magnetic field (80 $Am^{-1}$) is generated by an alternating current with a frequency of 2 kHz, and penetrates just a few millimetres into the core. When a sample is introduced within the effected region of the magnetic field, the frequency is changed. The changing of the frequency is detected by the sensor and converted to a susceptibility value. The actual raw magnetic susceptibility value of a core sample is the result of a reading on the core minus a background (in air) reading. Since the rock samples in this study were weakly magnetic, the more sensitive range of x 0.1 was selected for the measurements, allowing background and core readings at each depth to take around 30 seconds in total (12 seconds for each reading plus a few seconds between readings). Magnetic susceptibility was measured at high resolution every 2.5 cm down the slabbed core for Well 01 and Well 02, and at every 1 inch for Well 03. This was because I wanted to compare the results with the downhole log data, which was acquired in metric depths for Wells 01 and 02, but acquired in imperial depths for Well 03. More than 2,500 measurements of raw volume magnetic susceptibility were made on the slabbed cores of each well. The cores were kept away from any strong magnetic material during the measurements.

## 3.3. Results of probe magnetic susceptibility for characterizing oil sands reservoir core

### 3.3.1. Probe volume magnetic susceptibility results for distinguishing lithologies

Each raw probe volume magnetic susceptibility value was carefully recorded with its depth. Since some core sections were not fully recovered, identifying the depths exactly was sometimes a challenge, but comparisons with the log data helped to quantify the core depths. The high

resolution raw probe volume magnetic susceptibility values were also subsequently averaged to give the same vertical interval averaging (about 30 cm or 1 foot) as for each measurement point of the downhole logs for direct comparisons with the log data. The magnetic data were averaged vertically over an interval of 30 cm for Wells 01 and 02, and vertically over an interval of 1 foot for Well 03 (since as mentioned above the logging depths for Wells 01 and 02 were taken by the service company in metric units, whilst the depths for Well 03 were taken in imperial units). **Figure 3.2** shows an example of the profiles of raw probe volume magnetic susceptibility (left hand figure) and the vertically running averaged values over intervals of 1 foot (right hand figure) from Well 03. One can use the raw magnetic susceptibility values or the averaged values to identify the lithology of the rock samples based on the distinct susceptibility differences principally between diamagnetic and paramagnetic minerals and fluids (**Figure 3.2**). The magnetic susceptibility signal recorded by the probe sensor is the sum of the values of all the component minerals and fluids in the sample. As detailed in **Chapter 2** any sample with a net negative magnetic susceptibility value will likely indicate a clean sand in the slabbed cores analysed (since quartz and reservoir fluids are diamagnetic), whereas a significant positive result will likely indicate increased amounts of paramagnetic clay minerals (such as illite).

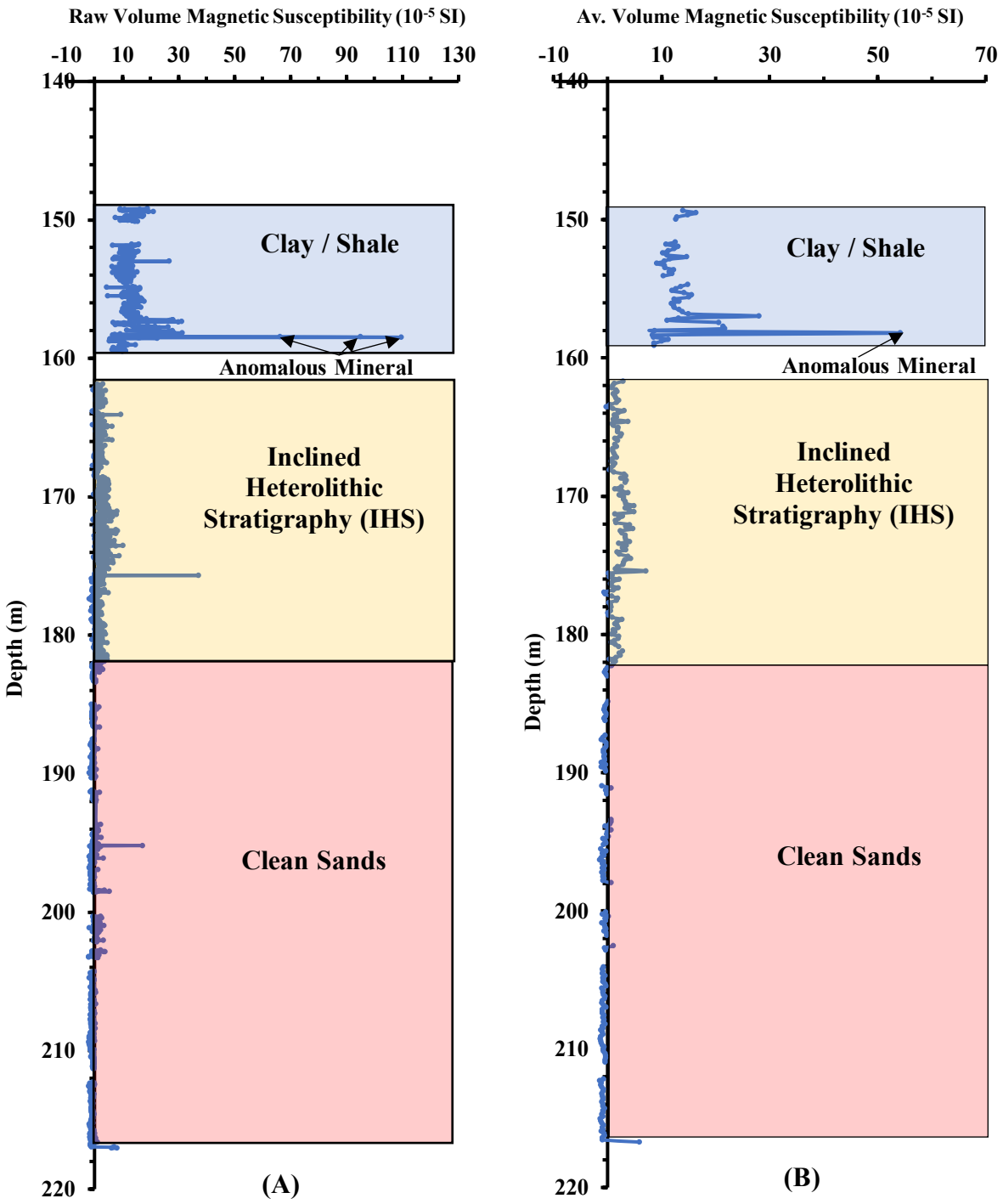


**Figure 3.2**: An example from Well 03 showing the profiles of **(A)** raw volume magnetic susceptibility values measured at high resolution (every 1 inch) down the slabbed core by the probe susceptibility system and **(B)** 1 foot vertically averaged volume magnetic susceptibility (so as to compare later with the downhole log data that averaged vertically over about 1 foot). The depth scale has been converted to metric units so as to compare later with the depth scales of Wells 01 and 02 (the downhole logging depths for Wells 01 and 02 were taken by the service company in metric units, whilst the logging depths for Well 03 were taken in imperial units).

### 3.3.2. Magnetically equivalent illite content for predicting permeable zones

Studies by Potter et al. (2004) and Potter (2007) have shown strong correlations between fluid permeability and the paramagnetic clay mineral components of rock samples in clastic reservoirs. Clean sand units containing primarily diamagnetic quartz exhibiting negative magnetic susceptibility were generally shown to have high fluid permeability (if there were no other natural cementing minerals present), whereas lower fluid permeability intervals were generally associated with muddy sands and shales, both of which contained an increased proportion of paramagnetic clay (mainly illite). Therefore, the estimation of permeability controlling paramagnetic clay content would seem potentially useful for predicting permeable zones in the oil sands, and thus indicating the best oil sands intervals. Following Potter et al. (2004) and Potter (2007) each magnetic susceptibility value can be converted to an estimate of mineral content in simple model systems. Assuming that a rock sample is a two-component system of diamagnetic quartz and paramagnetic illite clay and that the contribution of fluids in the pore space in the sample is negligible, the proportion of each mineral component can then be estimated. The total measured magnetic susceptibility signal per unit volume is:

$$k_T = \{(F_I)\,(k_I)\} + \{(1-F_I)\,(k_Q)\} \qquad \textbf{(3.1)}$$

where $k_T$ is the total measured susceptibility value measured by the probe magnetic technique, $F_I$ is the illite fraction per unit volume, $(1\text{-}F_I)$ is the quartz fraction per unit volume, and $k_I$ and $k_Q$ are the volume magnetic susceptibilities of illite and quartz, respectively. The illite fraction is then calculated as:

$$F_I = (k_T - k_Q) / (k_I - k_Q) \qquad \textbf{(3.2)}$$

Note that from Equation **(3.2)** any illite content of around 4% or higher in an illite + quartz mixture will mean that the net magnetic susceptibility of the sample is positive, whilst lower

values will mean the net magnetic susceptibility of the sample is negative. Furthermore there are two key advantages of converting the raw magnetic susceptibility signal into a mineral content as follows:

(i) The mineral contents can be plotted on logarithmic graphs (as long as the values are not zero), whereas raw negative magnetic susceptibility values cannot. It will be shown later in **Chapter 3** and in **Chapter 4** that there are good correlations between magnetically derived illite content and other parameters crossplotted on log-log graphs, which would not necessarily have been so apparent on crossplots of the raw magnetic susceptibility and the other parameters.

(ii) Any values greater than 100% illite content using **Equation (3.2)** immediately indicate the presence of an anomalous mineral or minerals with higher positive magnetic susceptibility than pure illite.

### 3.4. Volume magnetic susceptibility profiles and estimates of paramagnetic clay mineral content to identify lithologies and pin-point permeable zones

**Figure 3.3 (A)** shows the probe volume magnetic susceptibility results averaged over 30 cm vertical intervals on the slabbed core of Well 01. From the susceptibility profile one can see that negative magnetic susceptibilities and values close to zero exist from depths of 486.3–489.1 m and 503.3–505.8 m, indicating clean sand intervals (i.e., containing little or no paramagnetic clay) and thus potential oil sands reservoirs of interest where the lithology is mainly dominated by a diamagnetic mineral (quartz in this case). On the other hand, significant positive signals in the interval 474–476.9 m clearly indicate clay/shale intervals likely dominated by paramagnetic clays (especially illite). The small positive signals in between these two extremes appear to be

due to the inclined heterolithic stratification (IHS) beds where visual inspection of the cores also indicates thin layers of gently dipping interbedded sand and clay.

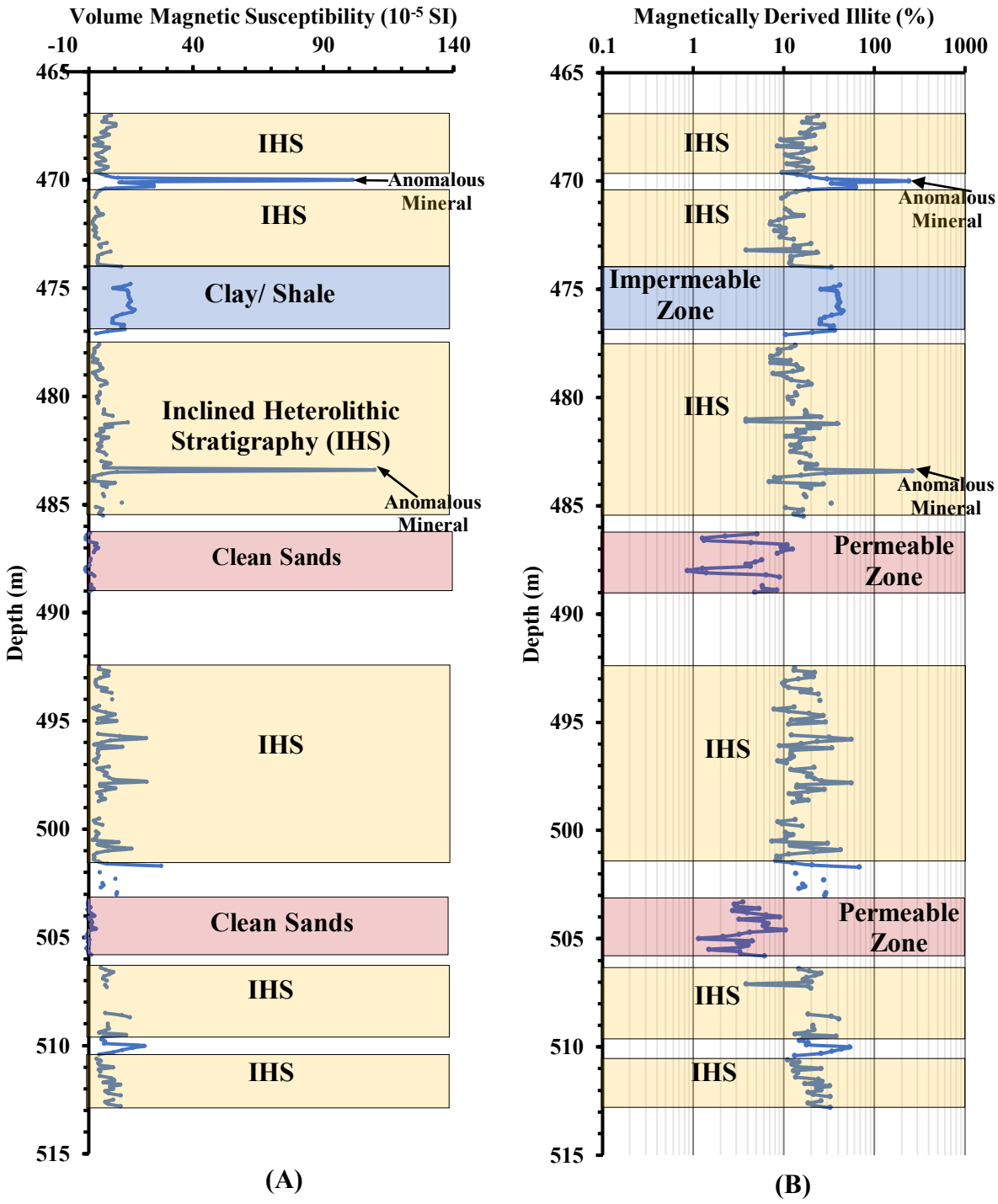


**Figure 3.3**: Probe magnetic results measured on the slabbed cores of Well 01. **(A)** is the profile of probe volume magnetic susceptibility values averaged over 30 cm intervals vertically, and **(B)** is the corresponding profile of magnetically estimated illite content using **Equation (3.2)**. The gaps in the curves represent intervals of unrecovered core.

**Figure 3.3 (B)** shows the magnetically derived illite content profile where the illite contents were calculated from the averaged susceptibility values using **Equation (3.2)**. The profile clearly shows two potential permeable zones where the illite contents are significantly lower than at other intervals in the well. In addition, at depths of 470.0 m and 483.4 m, the estimated "illite" contents are more than 100%, which indicates thin layers containing an anomalous mineral or minerals with a higher positive magnetic susceptibility than pure illite.

The averaged probe volume magnetic susceptibility profile of Well 02 is shown in **Figure 3.4 (A)**, and clearly distinguishes three different lithologies: two upper paramagnetic clay or shale intervals (354.9–364.4 m, and 369.8–380.6 m), a shaly sand interval (364.4–369.3 m), and a lower clean sand interval of diamagnetic quartz (389.3–425.1 m). The corresponding magnetically estimated illite profile (**Figure 3.4 (B)**) shows that the illite contents in the two clay/shale rich intervals are mainly in the range 20–100%, suggesting very low permeability or impermeable zones, while the illite contents in the shaly sand interval are mainly in the range 10–20%, suggesting a low permeability zone, but higher permeability than in the clay/shale intervals. In contrast, the illite contents in the clean sands are almost all in the 1–10% range (with most being less than 4% consistent with their negative magnetic susceptibilities), indicating a permeable zone. **Figure 3.4 (B)** also picks out thin layers of anomalous mineral(s) where the estimated "illite" values are more than 100%.

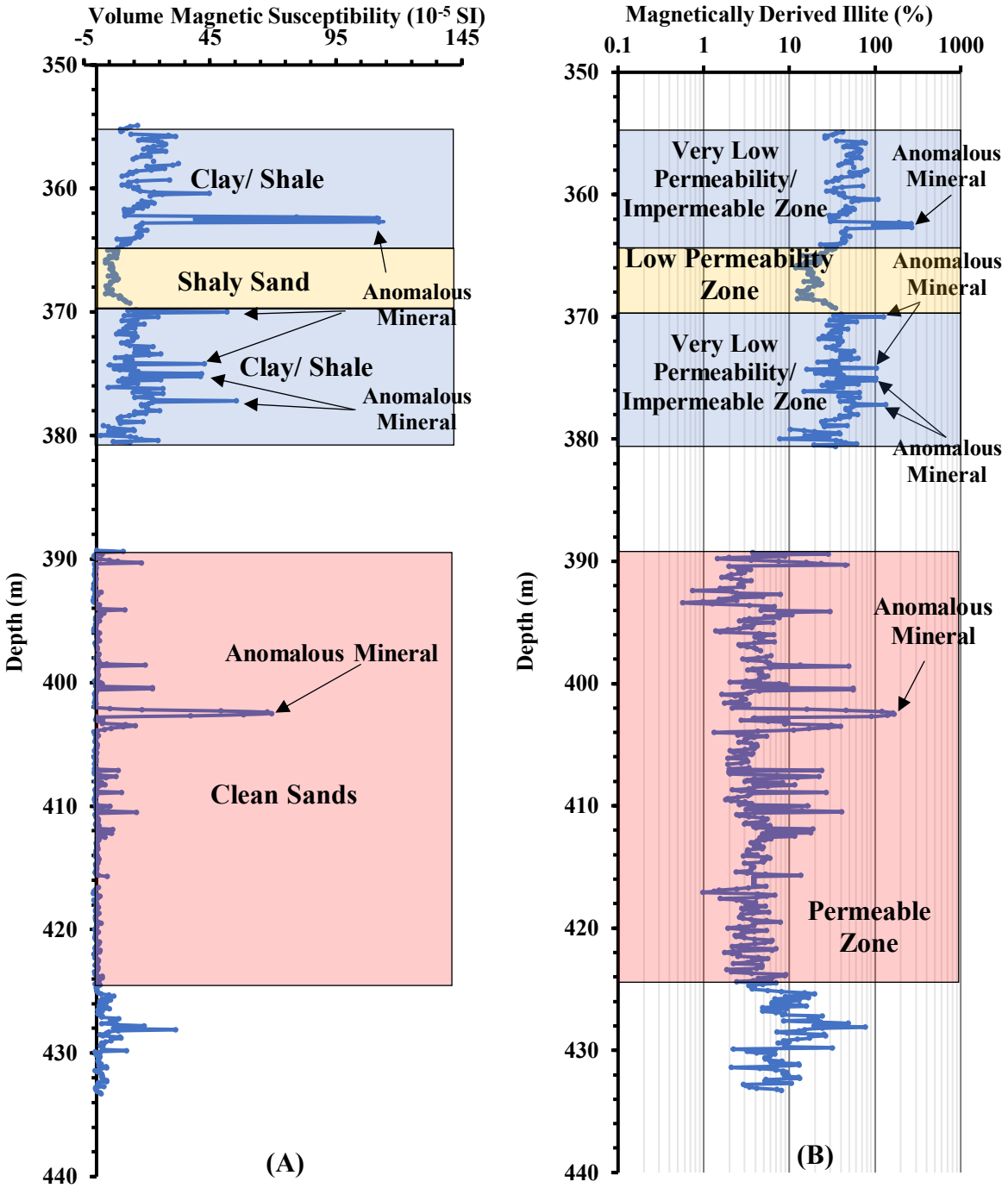


**Figure 3.4**: Probe magnetic results measured on the slabbed cores of Well 02. **(A)** is the profile of probe volume magnetic susceptibility values averaged over 30 cm vertically, and **(B)** is the corresponding profile of magnetically estimated illite content using **Equation (3.2)**. The gaps in the curves represent intervals of unrecovered core.

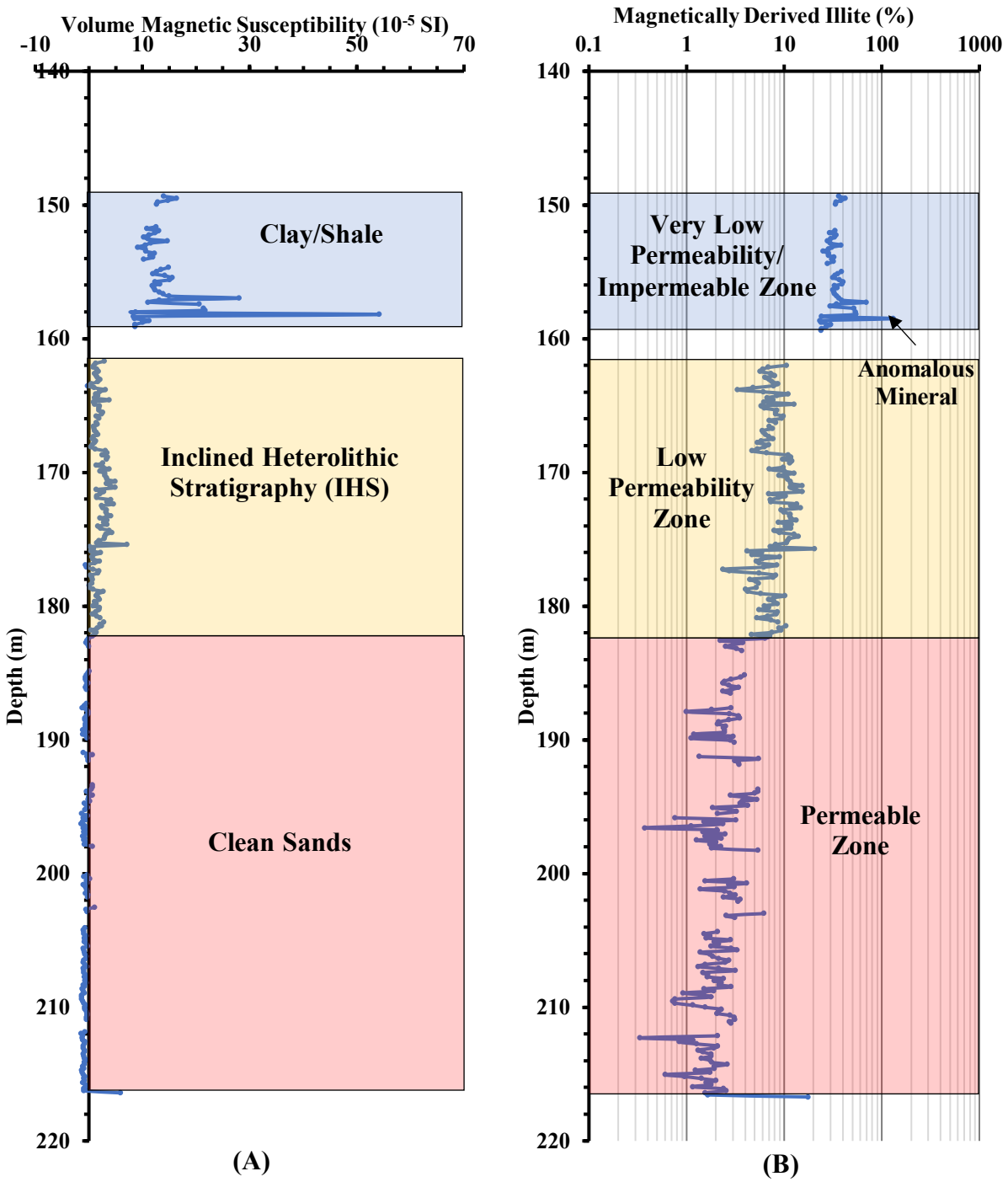


**Figure 3.5**: Probe magnetic results measured on the slabbed cores of Well 03. **(A)** is the profile of volume magnetic susceptibility values averaged over 1 foot vertically, and **(B)** is the corresponding profile of magnetically estimated illite content using **Equation (3.2)**. The gaps in the curves represent intervals of unrecovered core.

**Figure 3.5** shows the probe magnetic results measured on the slabbed cores of Well 03. The averaged probe volume magnetic susceptibility profile (**Figure 3.4 (A)**) clearly distinguishes three different lithologies. The significant positive susceptibilities between depths of 149–159 m indicate the dominance of paramagnetic clay minerals in this interval, while the negative susceptibility values between depths of 182.1–216.2 m clearly indicate a clean sand interval. In between these two intervals the slightly positive magnetic susceptibility values (up to about 5 x $10^{-5}$ SI) and their variation between the depths of 161.7–182.1 m indicate that the lithology consists of thin layers of interbedded sands (the lower values of magnetic susceptibility) and paramagnetic clays (the slightly higher values of magnetic susceptibility). This interval is likely to be part of the inclined heterolithic stratification (IHS) beds or a muddy sand interval.

The profile of magnetically estimated illite content (**Figure 3.5 (B)**) distinctly identifies the permeable zone between the depths of 182.1 – 216.2 m where the illite values are almost all less than 4%. In contrast, the illite contents in the upper clay/shale zone vary from about 20–70%. Within this clay/shale zone the estimated illite profile also points out a thin interval (at a depth of 158.5 m) of an anomalous mineral or minerals where the "illite" content is predicted to be more than 100%. In the labelled IHS zone the magnetically derived illite content is estimated to vary from about 2–20%.

The above cases for three different oil sands wells have shown how the probe magnetic technique is able to readily characterize unconsolidated slabbed cores from oil sands reservoirs. The magnetic susceptibility profile can distinguish the different lithologies, and the magnetically derived illite contents can potentially be used for identifying the permeable zones (the latter will

be confirmed in the next section by comparison with the spontaneous potential, SP, log). Moreover, any values of illite content over 100% immediately indicate the presence of an anomalous mineral or minerals.

### 3.5. Comparisons between the magnetic results and traditional downhole log data

In this section the above magnetic results will be compared with traditional borehole logging methods used for characterizing reservoirs, such as downhole total gamma ray (GR), spectral GR and spontaneous potential (SP) logs. The section will first briefly describe the fundamentals of GR and SP logs, and how they are usually used for formation evaluation. Then comparisons will be made between the magnetic results and the downhole log data for each well in this study. The comparisons will detail any correlations or differences, and also identify any advantages or disadvantages of the magnetic technique over the other methods.

#### 3.5.1. Downhole gamma ray

The downhole total gamma ray (GR) tool is a passive logging tool that records the naturally occurring radiation of gamma rays from a rock formation. Nearly all the gamma radiation encountered in the earth is emitted by radioactive potassium isotope ($K^{40}$), uranium ($U^{238}$) and thorium ($Th^{232}$). The energy of the emitted gamma rays is distinctive for each element. Potassium emits gamma rays of a single energy level at 1.46 MeV, while uranium and thorium emit gamma rays of at a number of different energy levels (though 1.76 MeV is characteristic of uranium and 2.62 MeV is characteristic of thorium). The measurements recorded by the total gamma ray logging tool (recorded in American Petroleum Institute, API, units) are proportional to the total radioactive material in the formation. The natural gamma ray spectroscopy (NGS) tool records

the number of gamma rays and energy levels of each, allowing the different contributions of radioactive potassium (in %), thorium (in parts per million, ppm), and uranium (in ppm) in a rock formation. The radioactive signal in a sedimentary formation generally ranges from a few gamma API (GAPI) in anhydrite or common salt (NaCl) to 150 GAPI or more in clay rich shale. In reservoir characterization, one usually uses a gamma ray log for distinguishing different lithologies, where a high gamma ray signal generally indicates a clay or shale interval, and a low gamma ray signal generally indicates a clean (i.e., low clay) sand or carbonate interval.

### 3.5.2. Spontaneous potential

The spontaneous potential (SP) tool is a passive tool that records the electrical potential (in terms of voltage) produced by the interaction of formation connate water, conducting drilling fluid, and certain ion-selective rocks (shale). The SP measurement is based on the principle that two conducting fluids of different salinities essentially create a battery, and current flows in the cell. This cell is very similar to the condition existing in a borehole where the drilling mud salinity is generally different from the formation water salinity. The SP is the voltage observed due to the natural currents flowing through the mud column and the formation rock. The voltage is mainly generated by two electrochemical components: the membrane potential and the liquid junction potential. For example, consider a permeable sand formation with thick shale beds above and below, and the system contains two electrolytes (drilling mud filtrate and formation water) of different salinities (**Figure 3.6**). Generally the main dissolved salt is sodium chloride (NaCl). The formation water generally has higher salinity than the mud filtrate in the borehole. The shale layers are only permeable to the $Na^+$ ions because of the negative charges on the clay lattice (due to oxygen atoms). Therefore, $Na^+$ cations are able to move through the shale from the more

concentrated to the less concentrated NaCl solution. The potential across the shale is called membrane potential. The other component of the electrochemical potential (the liquid junction potential) is generated at the edge of the invaded zone, where the mud filtrate and the formation water are in direct contact (the liquid junction). Here both $Na^+$ and $Cl^-$ ions can move either side of the junction, but the $Cl^-$ ions have greater ionic mobility than the $Na^+$ ions, so that there is preferential movement of $Cl^-$ ions from the more concentrated to the dilute side of the junction. This results in current flow in the opposite direction across the junction. The current flows due to the membrane potential and liquid junction potential are in the same direction and complete a circuit. If the salinity of the drilling mud filtrate in the borehole is greater than the salinity in the formation water then the current flow is in the opposite direction to that shown in **Figure 3.6**.

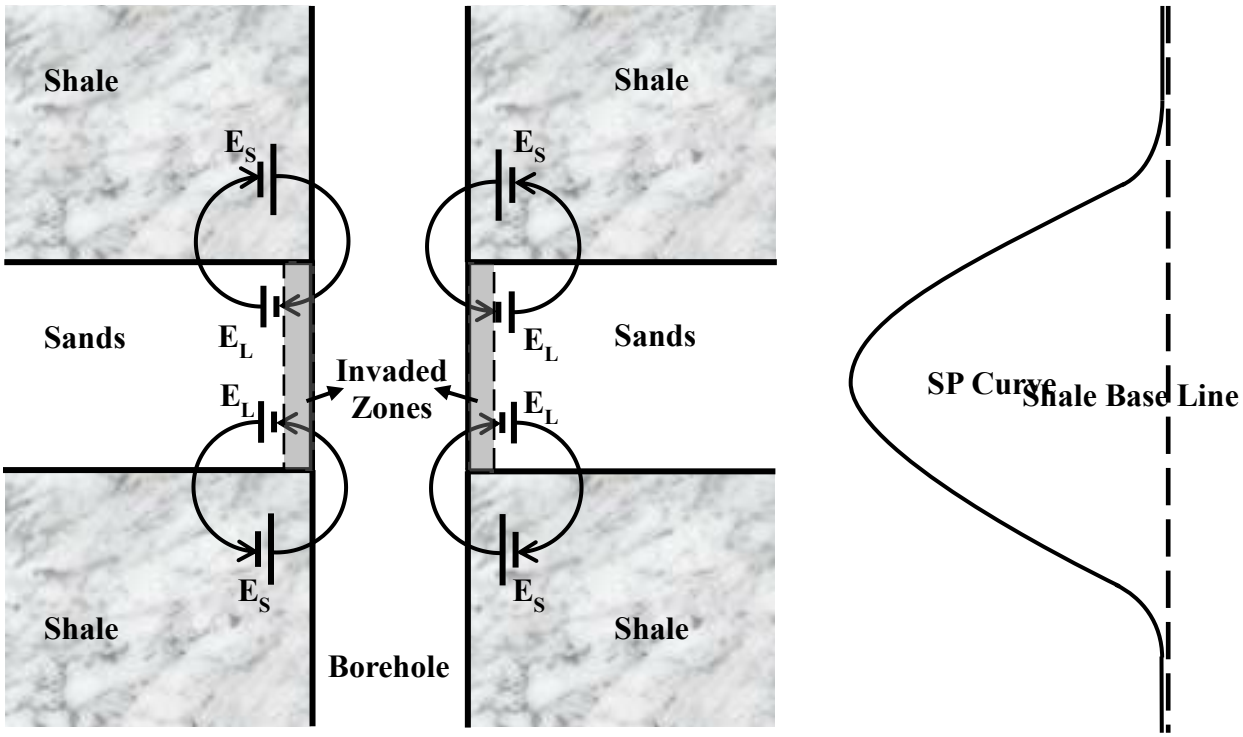


**Figure 3.6**: The schematic shows **(A)** the electrochemical potentials and current directions near a permeable bed and **(B)** the relevant SP curve. Note that in the case shown the formation water has a higher salinity than the mud filtrate in the borehole. $E_s$ is the membrane potential caused by the flow of $Na^+$ cations in a shale formation, and $E_L$ is the liquid junction potential caused by the flow of $Cl^-$ anions across the liquid junction between the mud filtrate and the formation water.

As shown in **Figure 3.6**, when the SP tool encounters a permeable bed, the SP curve is deflected away from the shale baseline, and the magnitude of the deflection depends on the salinity difference between the drilling mud filtrate and the formation water fluids, and the clay content of the formation.

### 3.5.3. Well 01: Comparisons between the magnetic results, depth-matched downhole logs and grain size profile

**Figure 3.7** shows the comparisons between the magnetic results and the downhole logs of Well 01. The left hand figure compares the averaged probe volume magnetic susceptibility and the total downhole gamma ray, and the right hand figure compares the corresponding magnetically derived illite content and the SP log. The raw magnetic susceptibility data points were averaged over vertical intervals of 30 cm to give direct comparisons with the same vertical intervals that each gamma ray log data point averages over. In general, there are good correspondences between the magnetic profiles and the logs in each comparison. In the left hand figure significant positive magnetic susceptibilities correlate with high gamma ray (GR) values in the main clay/shale interval (highlighted in the blue rectangle), whereas negative or close to zero susceptibilities correlate with low gamma ray values in the main clean sand intervals (highlighted in the pink rectangles). In the right hand figure low magnetically estimated illite contents correspond to large negative deflections to the left of the SP curve indicating the main permeable zones (highlighted in the pink rectangles), while the high percentages of magnetically estimated illite content correspond to the far right values of the SP curve along the shale baseline, indicating a very low permeability or impermeable zone (highlighted in the blue rectangle).

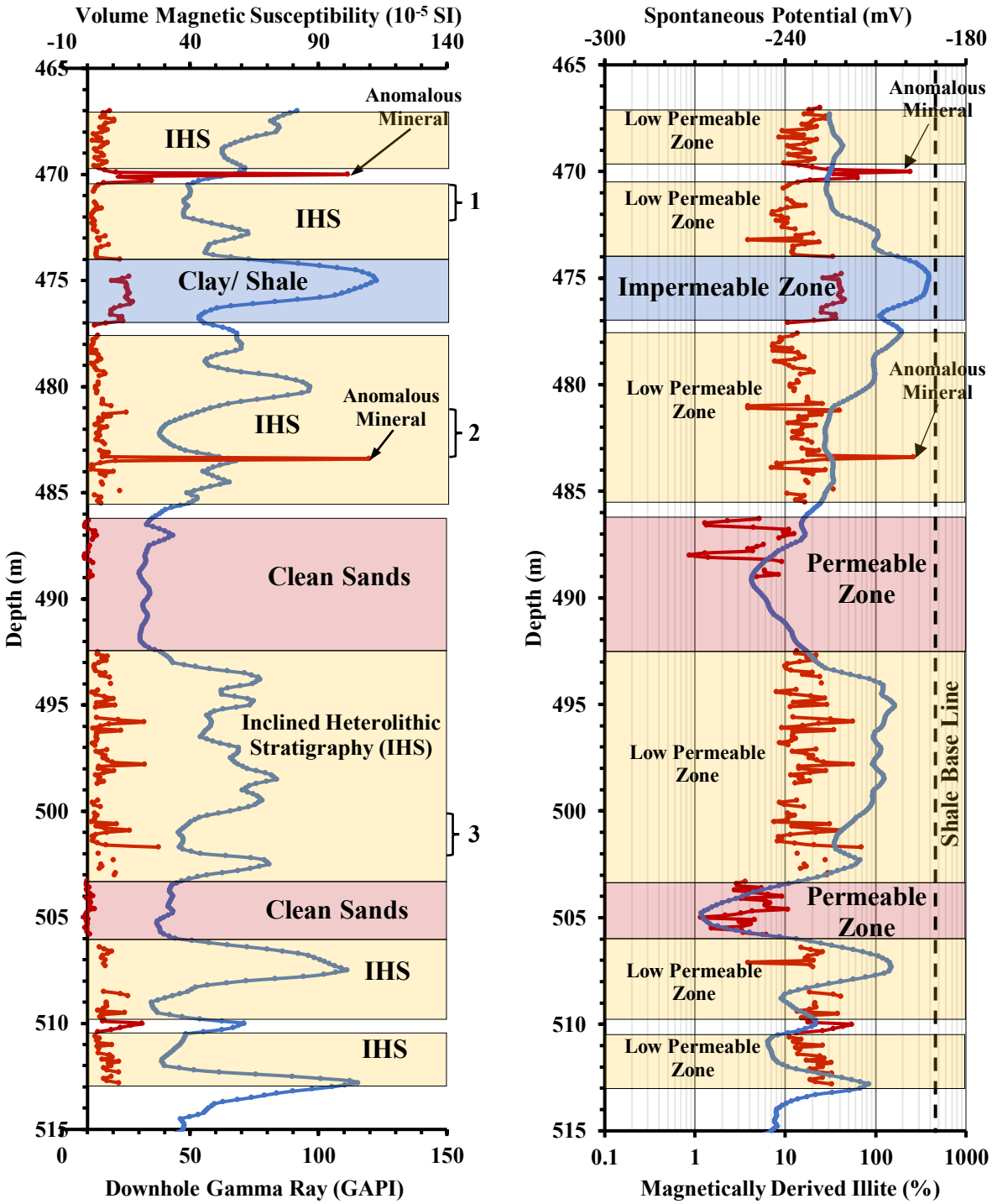


**Figure 3.7**: Comparisons between the averaged (30 cm vertically) magnetic results and depth-matched downhole logs for Well 01. The left hand figure is a comparison between the averaged (30 cm vertically) probe volume magnetic susceptibility profile (red curve) and the total downhole GR log (blue curve). The right hand figure is a comparison between the averaged (30 cm vertically) magnetically derived illite profile (red curve) and the SP log (blue curve).

**Figure 3.7** demonstrates that the magnetic susceptibility profile is more useful for identifying the clean sand intervals compared to the gamma ray (GR) log. Negative and close to zero volume magnetic susceptibility values (mostly less than 0.5 x $10^{-5}$ SI) clearly indicate clean sand intervals, whereas the variation of the GR signal might confuse one in deciding whether an interval is a clean sand or muddy sand interval. For example, one might think the low gamma ray signals at the intervals marked 1, 2, and 3 are the results of logging measurements at clean sands intervals, but positive magnetic susceptibilities clearly indicate that these are IHS beds or muddy sands containing paramagnetic clay minerals (between 7–40% magnetically derived illite content).

The two main clean sand intervals identified from the magnetic susceptibility results are confirmed by the SP log (**Figure 3.7**) and the grain size profile (**Figure 3.8**). The right hand plot of **Figure 3.7** shows that the largest negative deflections (to the left) of the SP signals, indicating the high permeability zones, correspond to the clean sand intervals identified by low magnetically derived illite content (shown by the pink rectangles). The deflections are negative since the salinity of the formation water is higher than the salinity of the borehole fluids. In the intervals marked 1, 2 and 3 (in the left hand plot of **Figure 3.7**) the SP deflections in the right hand plot are much less negative and suggest lower permeability zones, which are unlikely to be clean sand, and are consistent with the magnetic susceptibility and magnetically derived illite results. The comparisons in **Figure 3.8** also show the correlations between the magnetically derived illite contents (the left figure) with the grain size profile (the right figure). The grain size profile was generated by manual observations and the data input to Applecore$^{TM}$ software for presentation. The two main clean sand intervals (permeable zones) identified by the magnetic

results correlate with two main intervals of fine grain size sand, and the clay/shale interval identified from magnetic profile (impermeable or very low permeability zone) correlate with the main clay interval from the grain size log. The grain size profile also indicates that the rest of the core intervals are IHS beds with thin layers of very fine to fine sands interbedded with thin clay beds. In particular, the grain size profile provides support for the magnetic susceptibility results that suggested the intervals marked as 1, 2 and 3 were IHS beds (in the left hand plot of **Figure 3.8**).

Note that the magnetic results of **Figure 3.7 and 3.8** pick out thin layers of an anomalous mineral or minerals where the "illite" content is estimated to be more than 100%. These thin layers of an anomalous mineral or minerals were not detected by the gamma ray or spontaneous potential logs.

Comparisons between the magnetic results and the downhole log data also enabled one to fill in the gaps created by missing (unrecovered) core. For example, comparisons between the magnetic results and the log data in the clean sand interval between depths 486.3–489.1 m suggest that the immediate interval below between 489.1–492 m, where the core is missing, is also clean sand (top pink rectangles of **Figures 3.7** and **3.8**). Note that whilst there is some correspondence between the profiles of magnetically derived illite content and the downhole logs with depth, crossplots of the data do not give high correlation coefficients (**Figure A1.1** in **Appendix 1**). This is partly because the magnetic results distinguish the different lithologies better than the downhole logs in Well 01.

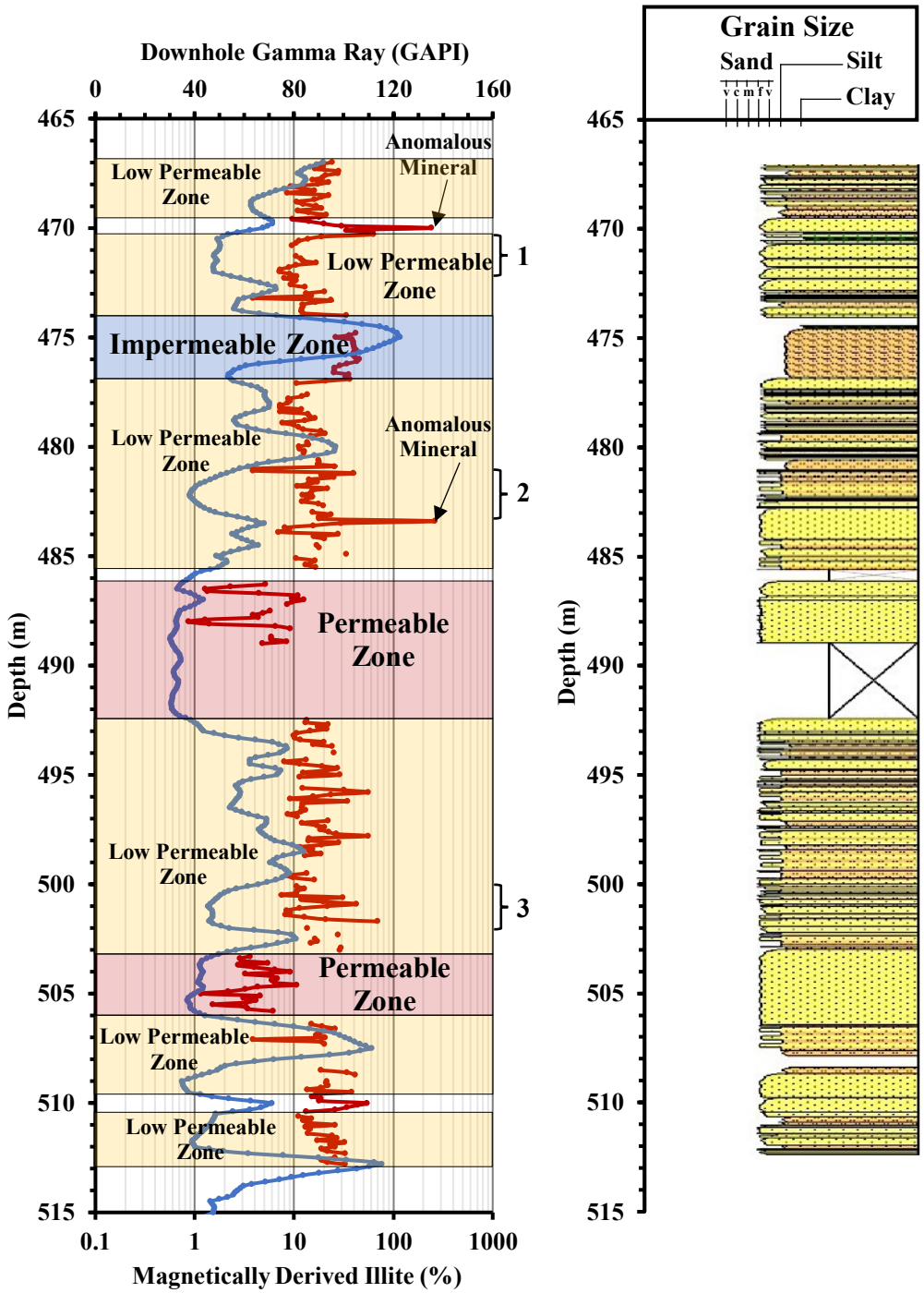


**Figure 3.8**: Comparisons between the averaged (30 cm vertically) magnetically derived illite results, depth-matched downhole gamma ray and grain size logs for Well 01. The left hand figure is a comparison between the averaged (30 cm vertically) magnetically derived illite (red curve) and the total downhole GR log (blue curve). The right hand figure is the grain size profile, which was determined from the slabbed core manually and displayed using Applecore™ software.

### 3.5.4. Well 02: Comparisons of magnetic results and downhole log data

#### a) Magnetic results versus depth-matched downhole logs and grain size profile

**Figure 3.9** shows the comparisons between the magnetic susceptibility results and the downhole logs of Well 02. The comparisons clearly illustrate correspondences between the average probe volume magnetic susceptibility profile and the total GR log data (left hand figure), and between the magnetically estimated illite content and the SP curve deflections (right hand figure). In the left hand figure the significant positive magnetic susceptibilities correlate with high GR values in the clay/shale intervals 354.9–364.4 m and 369.8–380.6 m, whereas in the interval 389.3–425.1 m the predominance of negative magnetic susceptibilities clearly indicate that this lithology is mainly clean sand. The total gamma ray, however, is very variable in this lower interval and ranges from about 15–65 API, which could be misinterpreted as being a muddy sandstone or IHS beds. In contrast, the SP log (right hand plot of **Figure 3.9**) is consistent with the magnetic results, where the largest deflections of the SP log to the left (indicating the most permeable zones) correspond to the lowest magnetically derived illite contents (generally less than 10%) in this mainly clean sand interval from 389.3–425.1 m. The high magnetically derived illite contents (20-100% illite) in the upper clay/shale intervals are associated with SP values closer to the shale baseline, indicating that the permeability is much lower.

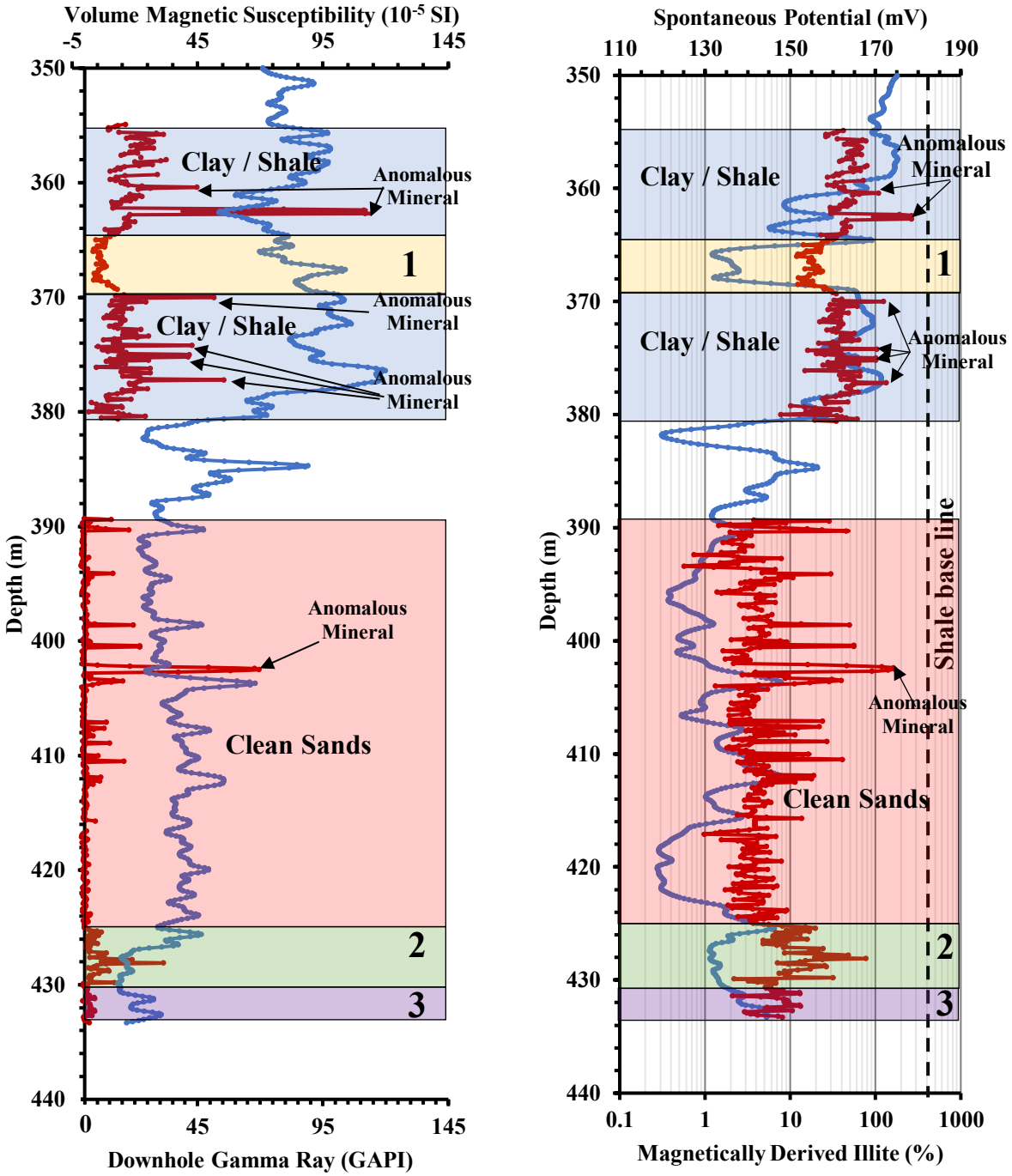


**Figure 3.9**: Comparisons between the magnetic results and downhole logs of Well 02. The left hand figure is a comparison of the averaged (30 cm vertically) probe volume magnetic susceptibility (red curve) and the total GR log (blue curve). The right hand figure is a comparison of the averaged (30 cm vertically) magnetically derived illite content (red curve) and the SP log (blue curve).

**Figure 3.10** shows the comparisons between the magnetically derived illite results, the depth-matched gamma ray log and the grain size profile of Well 02. The comparisons clearly show the correspondence between the illite contents (red curve of left hand figure) and the grain size (right figure). The two clay/shale intervals with high illite contents (20-100% illite) correlate with clay intervals identified by the grain size log, while the clean sand interval with low illite contents correlates with the sand interval from 389.3–425.1 m in the grain size log. Moreover, in the top section of the clean sand interval from 390–394 m the coarse grain size sand is associated with the lowest illite contents identified by the magnetic results.

Detailed comparisons between the magnetic profiles (**Figures 3.9** and **3.10**) and the total GR log data also indicate some small intervals with inverse trends. For example, in the shaly sand interval 1 (highlighted in yellow in) between depths 364.4-369.3 m decreasing magnetic susceptibilities (and decreasing magnetically derived illite contents) indicate that the lithology contains much less paramagnetic clay. In contrast, the increasing GR values suggest an increasing clay content in this interval. However, the deflection of the SP curve to the left correlates with the decreasing magnetic susceptibility and decreasing estimated illite content, indicating this interval is more permeable. Thus the SP log supports the magnetic results that suggest less permeability controlling clay in this interval. In addition, the grain size profile (the right figure of **Figure 3.10**) also illustrates that the lithology of interval 1 is more like shaly sand compared to the adjacent upper and lower clay/shale intervals. The supporting evidence of the SP log and the grain size profile therefore suggest that the magnetic susceptibility results are a better indicator of the permeability controlling clay content in this interval than the total GR.

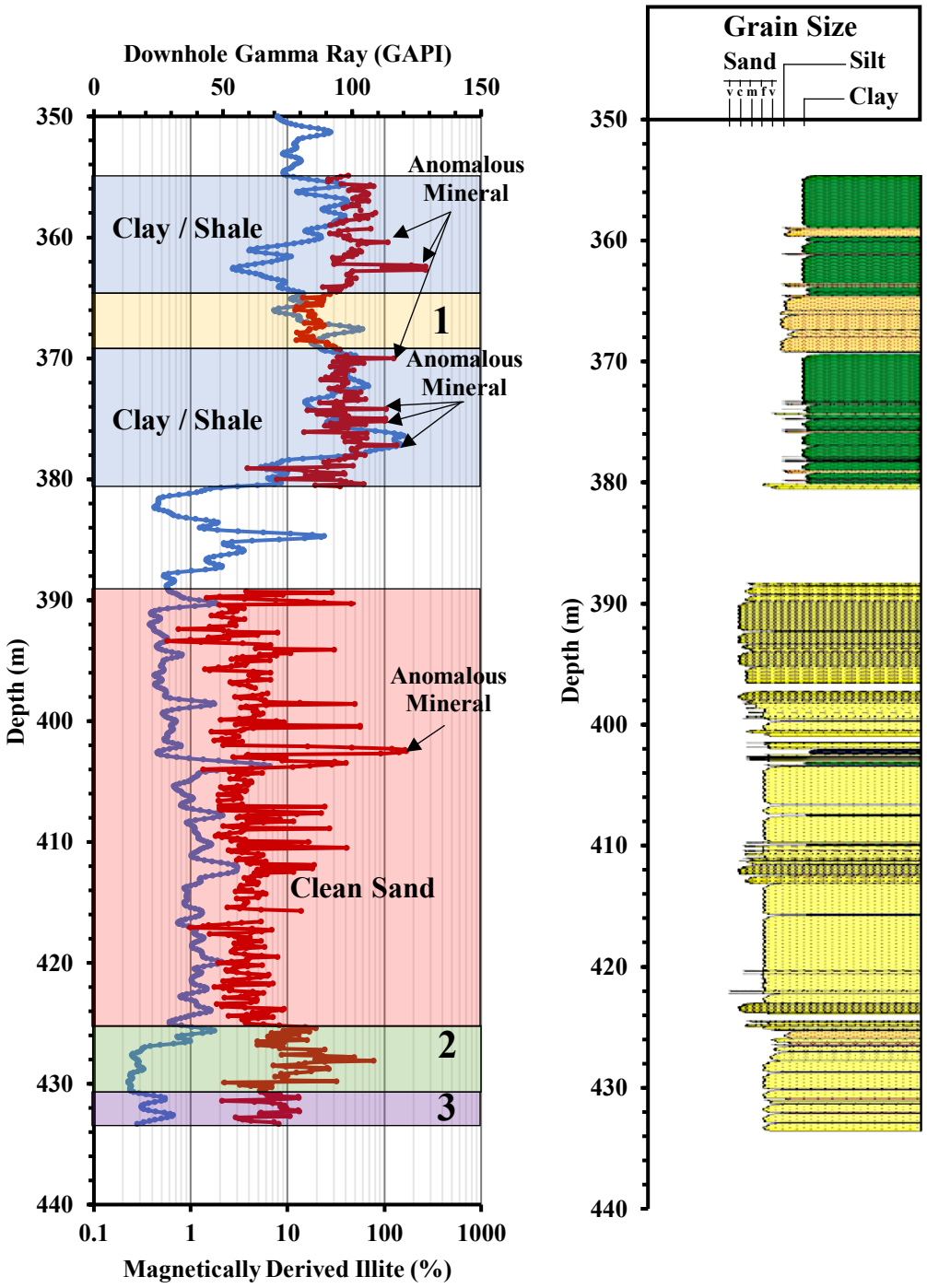


**Figure 3.10**: Comparisons between the averaged (30 cm vertically) magnetically derived illte results, depth-matched downhole gamma ray and grain size logs for Well 02. The left hand figure is a comparison between the averaged (30 cm vertically) magetically derived illite (red curve) and the total downhole GR log (blue curve). The right hand figure is the grain size profile, which was determined from the slabbed core manually and displayed using Applecore$^{TM}$ software.

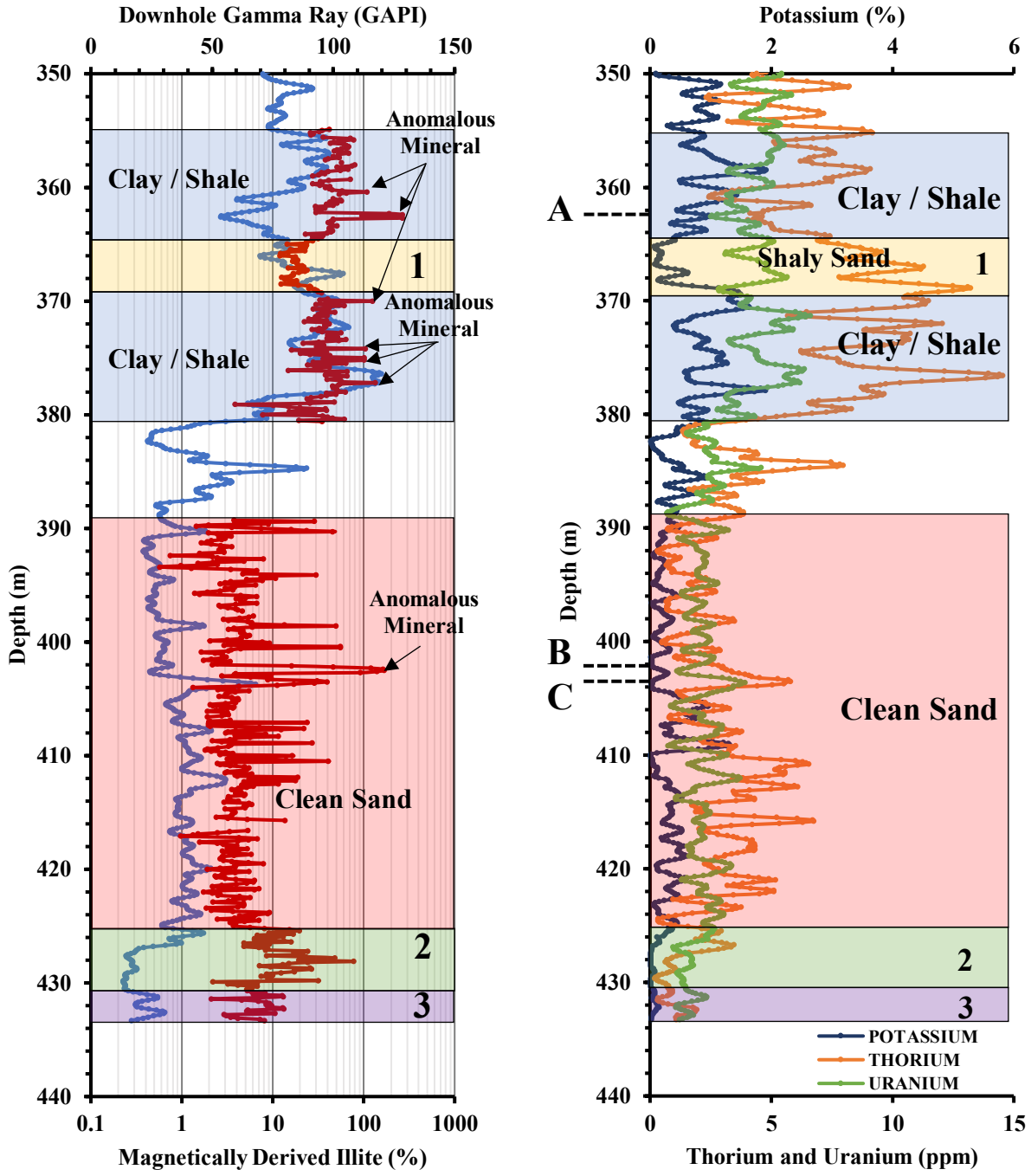


**Figure 3.11**: Comparisons between the averaged (30 cm vertically) magnetically derived illite content and the downhole total GR and spectral GR logs of Well 02. The left hand figure shows the profiles of the magnetically derived illite (red curve ) and the total GR (blue curve). The right hand figure shows the spectral GR logs of potassium, thorium, and uranium.

Moreover, the spectral gamma ray profiles (**Figure 3.11**) also indicate a correlation between the magnetic profiles and the potassium profile (potassium being an elemental component of illite), whereas the total GR signal appears to follow the trends of the thorium and uranium content profiles. Perhaps some organic matter in this interval is causing the observed increase in uranium content.

Other inverse trends between the magnetic results and total GR are observed in interval 2 (highlighted in green) and interval 3 (highlighted in purple) of **Figures 3.9**–**3.11**. Between depths of 425.1–430.6 m (green interval 2) the magnetic susceptibility (and magnetically derived illite) increases while the total GR decreases. The total GR values suggest clean sands with high permeability, whereas the magnetic results (higher susceptibility in **Figure 3.9** and higher illite content in **Figures 3.10** and **3.11**) suggest more clay rich sand with lower permeability. A lower deflection to the left of the SP curve (compared to the interval 416–422 m) also suggests a lower permeability in interval 2, which correlates with the increased magnetic susceptibility values of **Figure 3.9** and the higher illite contents of **Figures 3.10** and **3.11**. Between depths 430.6–434 m the magnetic susceptibility decreases, whereas the total GR increases. The magnetic results suggest clean sand, whereas the total GR suggests more muddy (increased clay) sand. In this interval, the SP log is slightly less to the left, suggesting that the permeability is slightly lower, which would be more consistent with the total GR in this case. However, the different trends of magnetic results and SP compared to the total GR data in interval 2 might also be due to the presence of another mineral rather than just quartz rich clean sands and clay. Further investigation into this will be described in **Chapter 4**.

The cores from Well 02 were not fully recovered (as was the case for Well 01), mainly because this oil sands and shale core is unconsolidated. Therefore, the magnetic susceptibility signal was useful for identifying the actual depths of the recovered cores, the depths of the missing core, and estimating the lithology, by the comparisons with the downhole log data. For example, **Figure 3.9** shows missing core in the depth interval 380.6–389.3 m. Negative or close to zero magnetic susceptibility together with low gamma ray and a deflection of the spontaneous potential to the left in other intervals generally means clean sand, whereas higher positive magnetic susceptibility together with higher gamma ray and less of a deflection to the left generally means a more clay rich lithology. Therefore one would expect clean sand in the interval 381.2–383.1 m, and a more clay rich lithology in intervals 380.5–381.2 m and 383.1–387.9 m.

The magnetic profiles for Well 02 again pick out thin layers of an anomalous mineral or minerals that were not detected by the GR and SP logs. For example, at depth 362.4 m in the right hand plot of **Figure 3.9** the estimated "illite" content is over 100%, while the GR shows a decrease, and the deflections of the SP log mainly detect permeable zones rather than anomalous minerals.

**b) Crossplots of magnetically derived illite content and depth-matched log data**

Magnetically derived illite content was crossplotted against depth-matched total GR (**Figure 3.12**) and against SP log data (**Figure 3.13**) in different cases. The crossplots clearly show the trend of a higher illite content with increasing GR and SP values. There are two distinct regions on each plot. The lower region contains the points of the clean sands with lower illite content (less than 10%), lower total GR signal (< 60 API) and lower SP (< 150 mV, which equates to a larger deflection to the left on the SP curve, indicating a more permeable formation). In contrast,

the upper region contains the points of clay/shale with higher illite content (> 10%), higher total GR signal (> 60 API) and higher SP (> 150 mV, which equates to a smaller deflection to the left from the shale baseline on the SP curve, indicating a less permeable formation).

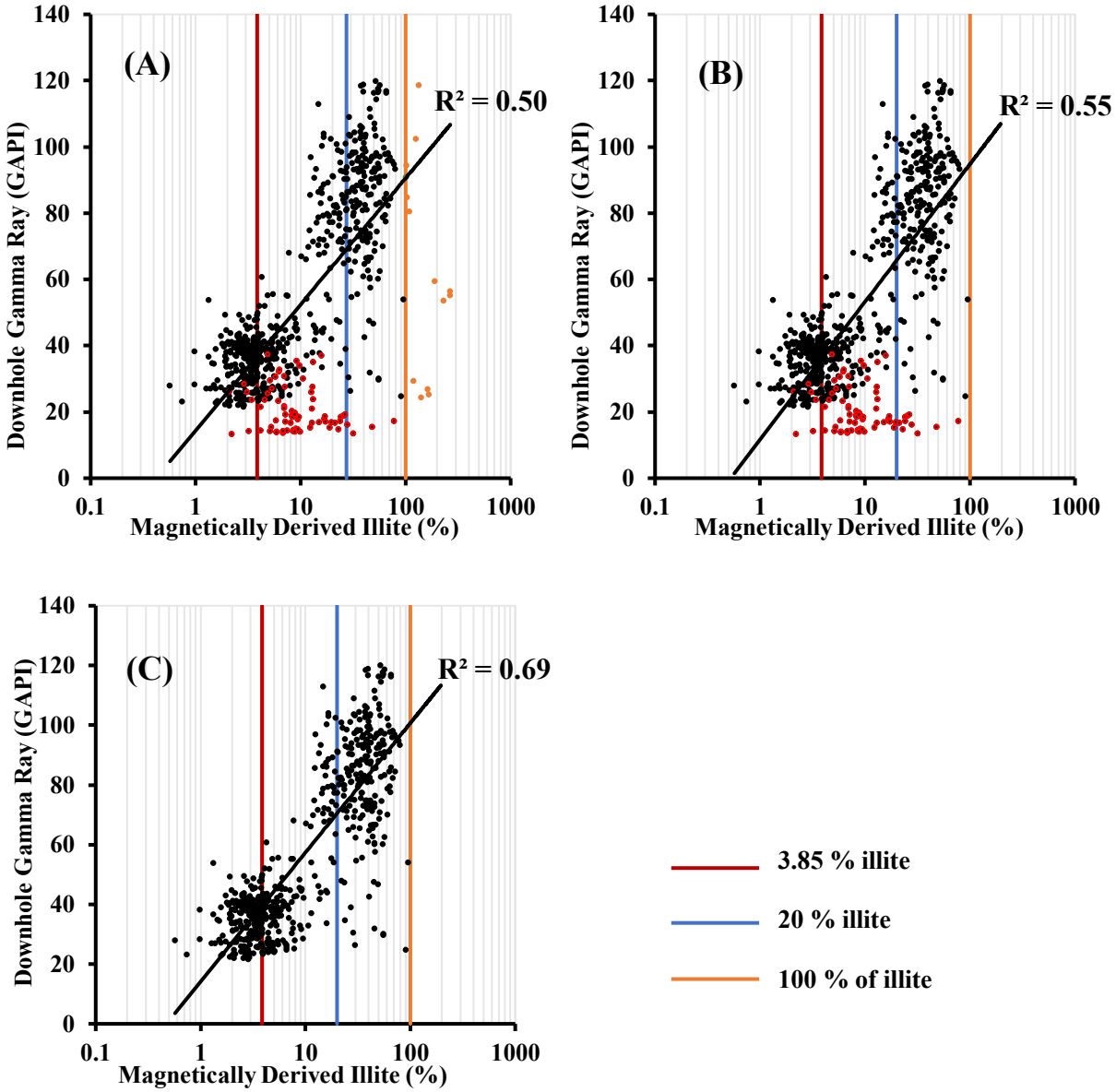


**Figure 3.12**: Crossplots of the averaged (30 cm vertically) magnetically derived illite content and depth-matched downhole total GR data in different cases for Well 02. **(A)** represents all the data points from the slabbed core intervals, **(B)** is **(A)** without the orange anomalous (>100% "illite") mineral points, and **(C)** is **(B)** without the red points in intervals 2 and 3 and (425.1–434 m) where there could be different lithologies from sand and clay. Note that the red 3.85% illite line represents the value below which the magnetic susceptibility is net negative, and above which it is net positive.

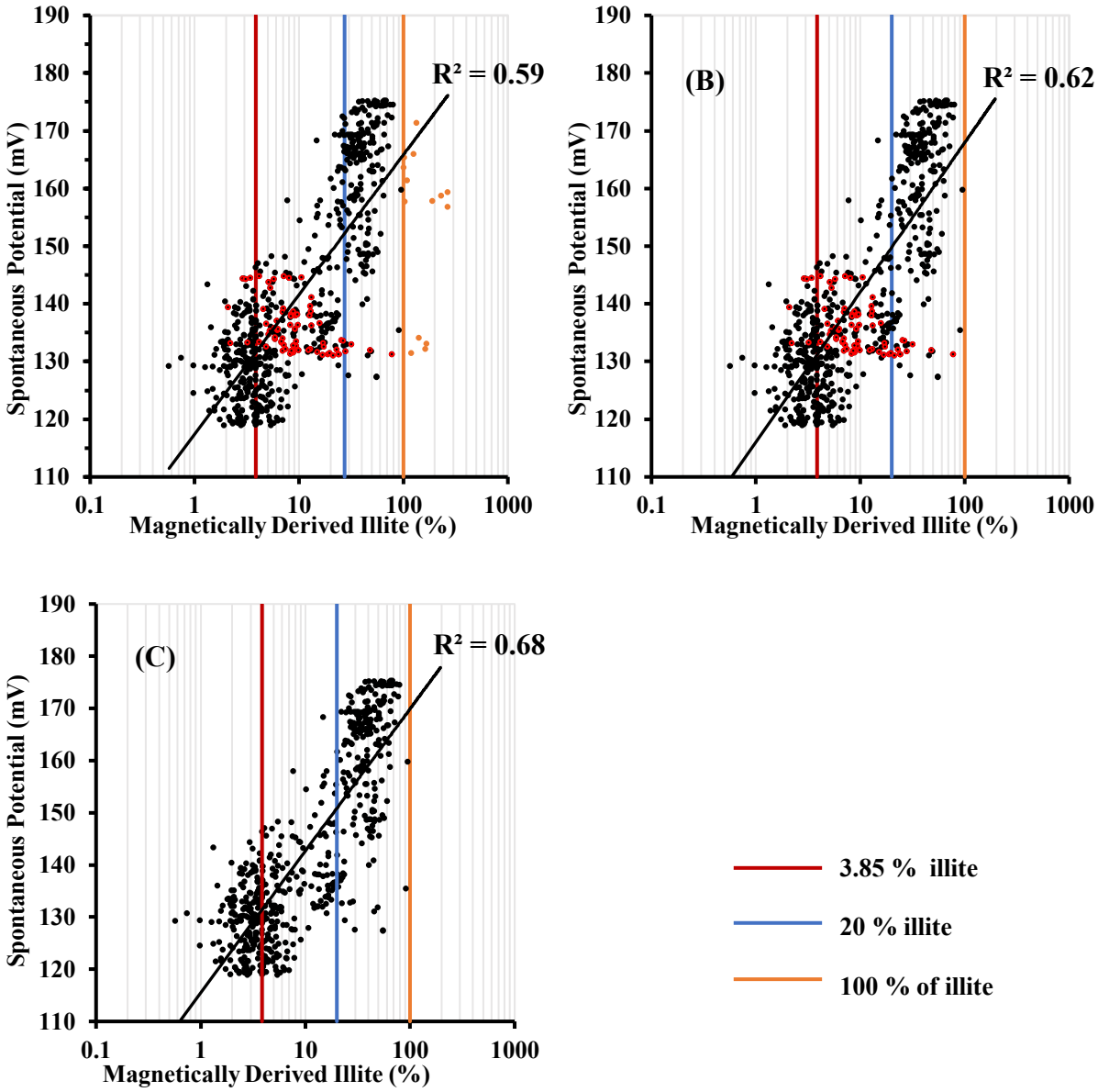


**Figure 3.13**: Crossplots of the averaged (30 cm vertically) magnetically derived illite content and depth-matched downhole SP data in different cases for Well 02. **(A)** represents all the data points from the slabbed core intervals, **(B)** is **(A)** without the orange anomalous (>100% "illite") mineral points, and **(C)** is **(B)** without the red points in intervals 2 and 3 (425.1–434 m) where there could be different lithologies from sand and clay. Note that the red 3.85% illite line represents the value below which the magnetic susceptibility is net negative, and above which it is net positive.

**Figures 3.12** and **3.13** each show the correlation between magnetically derived illite content and the log data for three different cases. Case **(A)** represents crossplots of illite content derived from all the (30 cm averaged) probe volume magnetic susceptibility measurements on the slabbed

cores against the depth-matched log data. As expected from the depth profile comparisons in the previous section, illite content and SP has a stronger relationship than illite content and total GR, with the $R^2$ values being 0.59 (**Figure 3.13 (A)**) and 0.50 (**Figure 3.12 (A)**) respectively. Case **(B)** is Case **(A)** without the points of estimated illite content that were greater than 100% (green points). The $R^2$ correlation coefficient increases to 0.55 for illite content versus total GR and to 0.62 for illite content vs SP. Case **(C)** is Case **(B)** with the removal of points between 425.1 – 434 m (intervals 2 and 3 on **Figures 3.9** – **3.11**), where the total GR shows inverse trends with the magnetic susceptibility profile throughout those intervals and to some extent with the SP logs in interval 2 (425.1–430.6 m). In Case **(C)** the $R^2$ correlation coefficient increases to 0.68 for illite content vs SP (**Figure 3.13 (C)**) and to 0.69 for illite content vs GR (**Figure 3.12 (C)**).

Whilst there is a general correspondence between the magnetic results and the total GR and SP log data it is important to point out that each technique is looking at slightly different properties, so one wouldn't necessarily expect high correlation coefficients between the different parameters. The magnetic susceptibility and total GR are both influenced by clay content, but the magnetic susceptibility has also been shown to pin-point the presence of anomalous minerals that the total GR did not detect, and therefore one wouldn't expect a direct correspondence between the two techniques for every data point. Equally the SP curve is mainly an indicator of permeable zones (via deflections from the shale baseline) and so some degree of correlation with the magnetic results might be expected, since clean sands will have low clay content and will generally be associated with low magnetic susceptibility and a large SP deflection from the shale baseline). More clay rich intervals (particularly paramagnetic clays such as illite) will generally have higher magnetic susceptibility and a smaller SP deflection from the shale baseline. The

results have shown that the magnetic susceptibility measurements enhance the characterization of oil sands reservoir intervals. They can differentiate the 3 main lithologies (clean sand, IHS beds and shale) better than the total GR and SP log data, whilst also pin-pointing the presence of anomalous minerals that the total GR and SP log data often do not.

### 3.5.5. Well 03: Comparison of magnetic results and downhole log data

#### a) Magnetic profiles with depth versus downhole log data and grain size profile

**Figure 3.14** (left hand plot) clearly shows how the probe volume magnetic susceptibility measurements (red curve) can differentiate the 3 main lithology types in Well 03. At the top of the profile (depths 149.4–159.1 m) the magnetic susceptibility values are highest and positive, indicating clay/shale. In the middle of the profile (depths 161.7–182.1 m) the magnetic susceptibility values are generally positive and relatively low, which generally means some clay mixed with sand in these oils sands wells, and is very likely to represent the IHS beds. At the bottom of the profile (depths 182.1–216.4 m) the magnetic susceptibility is generally negative, indicating clean sand (diamagnetic quartz), which is the best oil sands reservoir interval in Well 03.

The total GR curve (blue curve) generally follows the trend of the magnetic susceptibility profile (high GR in the shale, low GR in the clean sand), however the GR does not distinguish the different lithologies quite as well as the magnetic susceptibility. For example, between depths 162–168 m the total GR signal decreases, suggesting that this may be a clean sand interval. However, the magnetic susceptibility values indicate a significant paramagnetic clay content (about 3–15% magnetically derived illite shown in the right hand plot of **Figure 3.14**) suggesting

it is actually part of the IHS beds. The deflection of the SP curve in this interval (right hand plot of **Figure 3.14**) is not larger than in the rest of the presumed IHS bed interval shown in **Figure 3.14**, and so supports the magnetic susceptibility results by also suggesting this interval is part of the IHS beds with higher clay content and lower permeability than in the clean sands below depth 182.1 m. The largest defection of the SP curve to the left occurs at a depth interval of 196–198 m, which is consistent with the lowest magnetically derived illite content, and indicates a high permeability zone in the clean sand.

Comparisons between the magnetically derived illite contents and the total downhole GR (left hand plot of **Figure 3.15**) and the grain size profile (right hand plot of **Figure 3.15**) provide further evidence to support the lithologies identified by the magnetic results. The grain size profile clearly illustrates three different lithology intervals (clay/shale, IHS beds with interbedded clay and sand, and coarser grained clean sand) corresponding to those in the magnetic profile. In particular, the grain size profile clearly shows the IHS beds from 161.7 to 182.1 m with a number of thin layers of very fine sands interbedded with thin layers of clay, consistent with the IHS bed lithology identified by the magnetic results, but contrary to the "clean sand" lithology in part of this interval (162–168 m) that would have been mistakenly interpreted from the low GR log values.

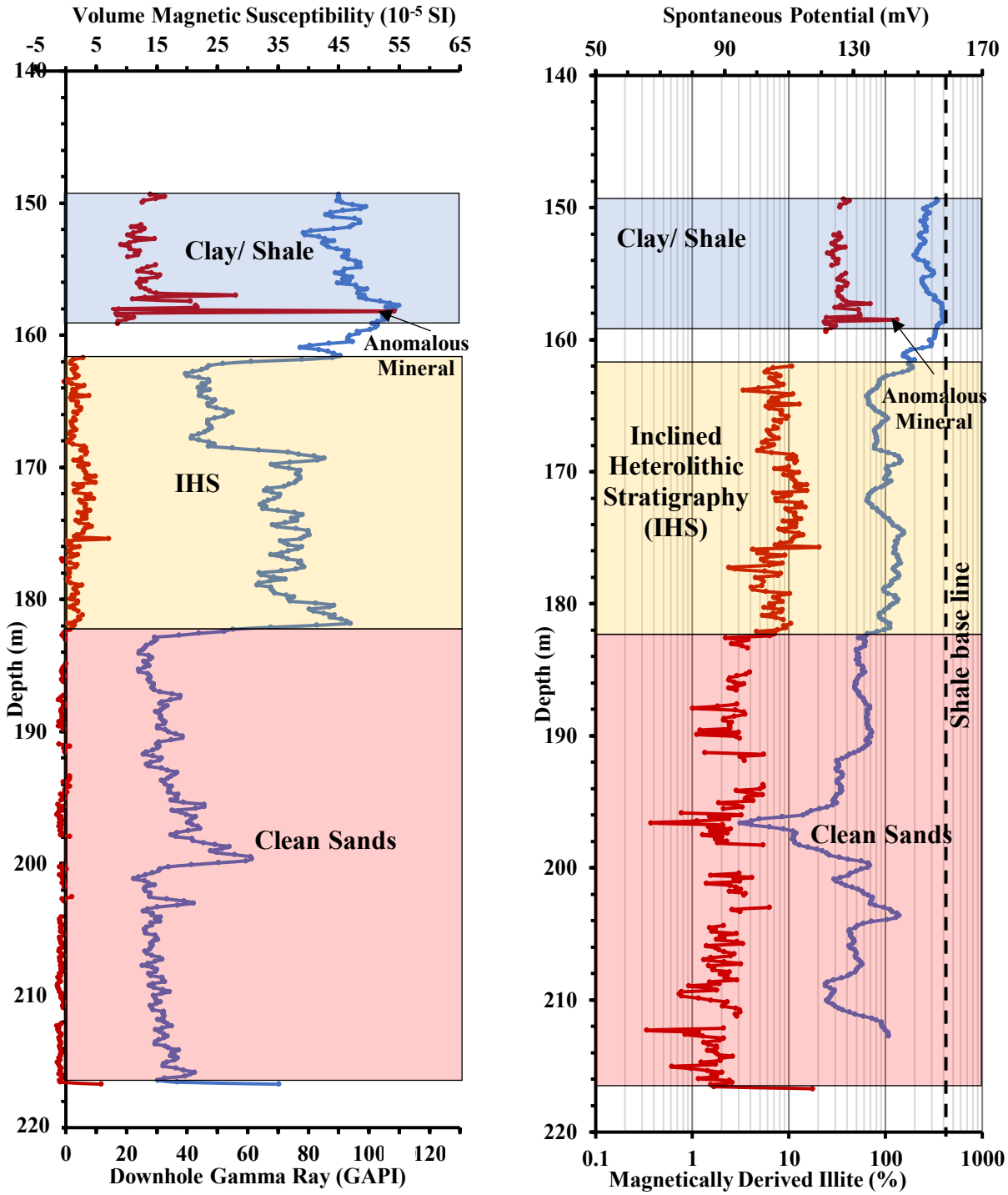


**Figure 3.14**: Comparisons between the magnetic results and downhole logs of Well 03. The left hand figure is a comparison of the averaged (1 foot vertically) probe volume magnetic susceptibility (red curve) and the total GR log (blue curve). The right hand figure is a comparison of the averaged (1 foot vertically) magnetically derived illite content (red curve) and the SP log (blue curve).

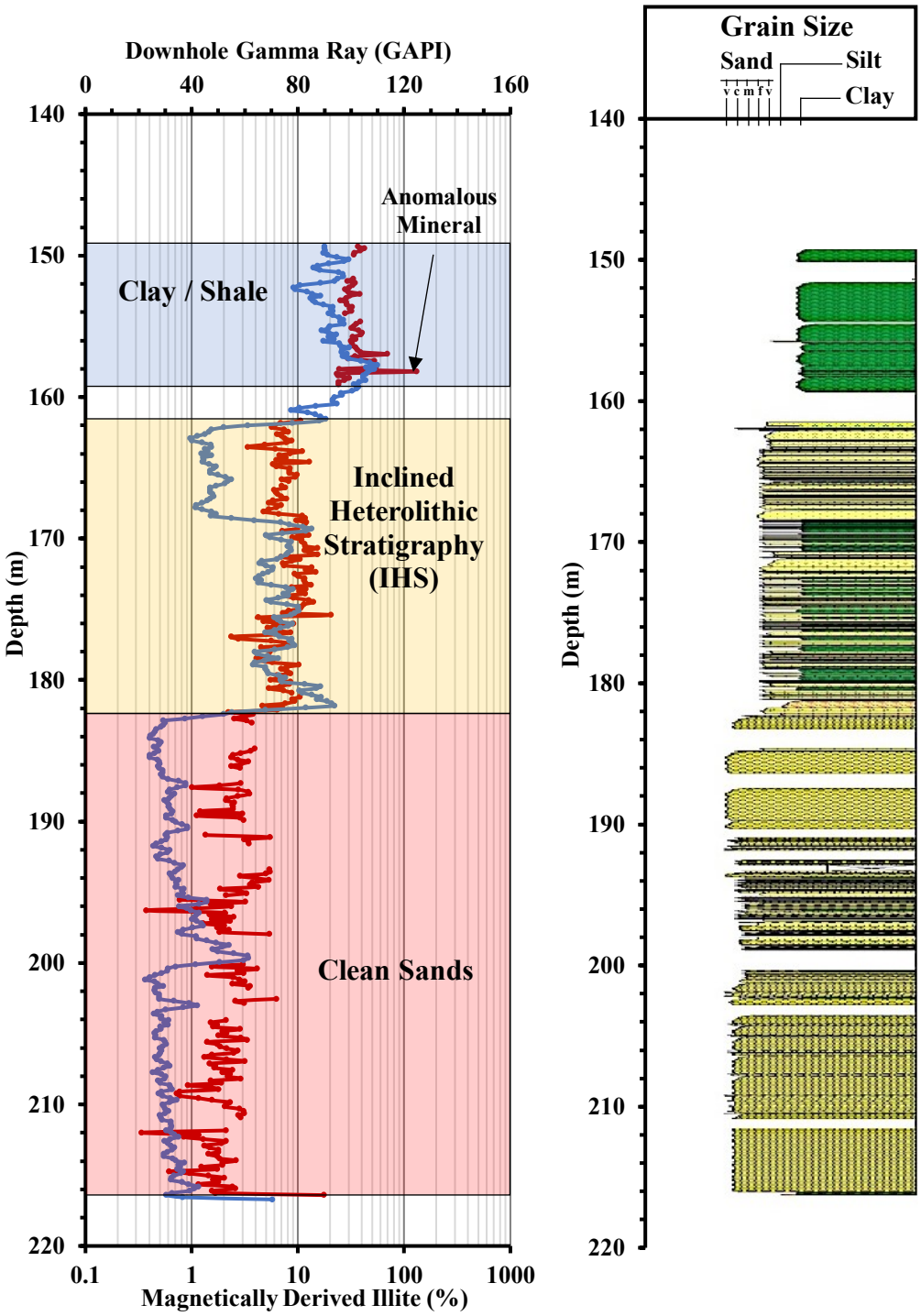


**Figure 3.15**: Comparisons between the averaged (1 foot vertically) magnetically derived illite results, depth-matched downhole gamma ray and grain size logs for Well 03. The left hand figure is a comparison between the averaged (1 foot vertically) magnetically derived illite (red curve) and the total downhole GR log (blue curve). The right hand figure is the grain size profile, which was determined from the slabbed core manually and displayed using Applecore™ software.

Another comparison between the magnetically derived illite content and the total GR (left hand plot of **Figure 3.16**) and the spectral GR signals (right hand plot of **Figure 3.16**) provide some insight into the low total GR signal in the IHS beds between depths 161.7–168.4 m. The potassium profile follows the trend of the magnetically derived illite content, however the thorium profile shows a marked decrease in the interval 161.7–168.4 m, and it is this that appears to influence the lower total GR signal within this interval. It is not clear at present why the thorium content is lower in this interval.

Like Well 01 and Well 02, **Figures 3.14**, **3.15 and 3.16** show small gaps in the magnetic data where some core from Well 03 is missing and therefore not fully recovered. Comparisons between the magnetic susceptibility results and the downhole log data again helped to identify the actual core depths, the missing core depths, and the lithology in those missing intervals.

The magnetic results again clearly pick out a thin bed of an anomalous mineral or minerals with a magnetically derived illite content greater than 100% at a depth of about 158 m (**Figure 3.15**). In this case, it does appear to coincide with the maximum total GR signal and the smallest deflection to the left in the SP curve, although the GR and SP curves don't pick out this thin bed quite so well as the magnetics does.

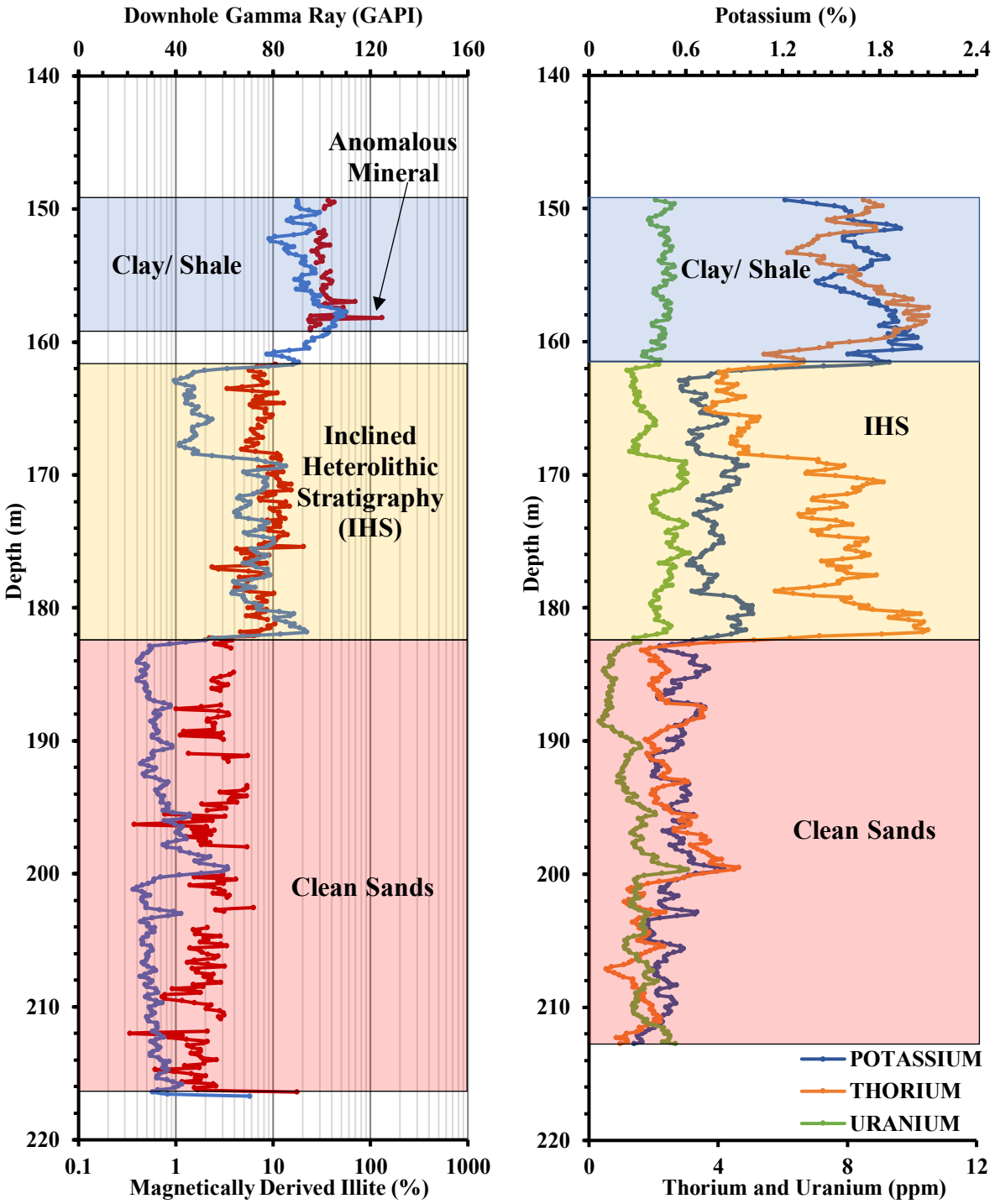


**Figure 3.16**: Comparisons between the averaged (1 foot vertically) magnetically derived illite content and the downhole total GR and spectral GR logs for Well 03. The left hand figure shows the profiles of the magnetically derived illite (red curve ) and the total GR (blue curve). The right hand figure shows the spectral GR logs of potassium, thorium and uranium.

**b) Crossplots of magnetically derived illite contents and downhole log data**

The results of the magnetically derived illite content for Well 03 are plotted against the depth-matched downhole total GR data (**Figure 3.17 (A)** and the SP log data (**Figure 3.17 (B)**). The trends show higher illite contents with increasing GR and SP signals as expected. These crossplots distinctly distinguish three different regions that represent 3 different lithologies. In general the clean sands region has less than 3.85% illite content, the IHS bed region has illite contents between 3.85% and 20%, and the clay/shale region has illite contents greater than 20%. In contrast, the crossplot of GR and SP (**Figure 3.17 (C)**) does not clearly differentiate these 3 different lithologies. This might be because the total GR does not clearly pick out the IHS beds in the depth interval 162–168 m as discussed in the last section.

One can use the crossplots of magnetically derived illite content and log data to identify the approximate values of the GR and SP signals at which there are significant changes in lithology or permeability. For example, from **Figure 3.17 (A)**, the clean sand interval could potentially be defined as having a total GR signal lower than 40 API, the IHS beds being between 40 and 80 API, and the shale interval being higher than 80 API, although these are just approximate values as there is some overlapping values between the different lithologies. From **Figure 3.17 (B)** the permeable zones are likely to occur at an SP signal of less than 150 mV. Lower SP values are likely to indicate higher permeability zones. Those critical values are difficult to determine from the GR versus SP crossplot (**Figure 3.17 (C)**), but could be estimated from the profiles with depth (**Figures 3.14** and **3.16**).

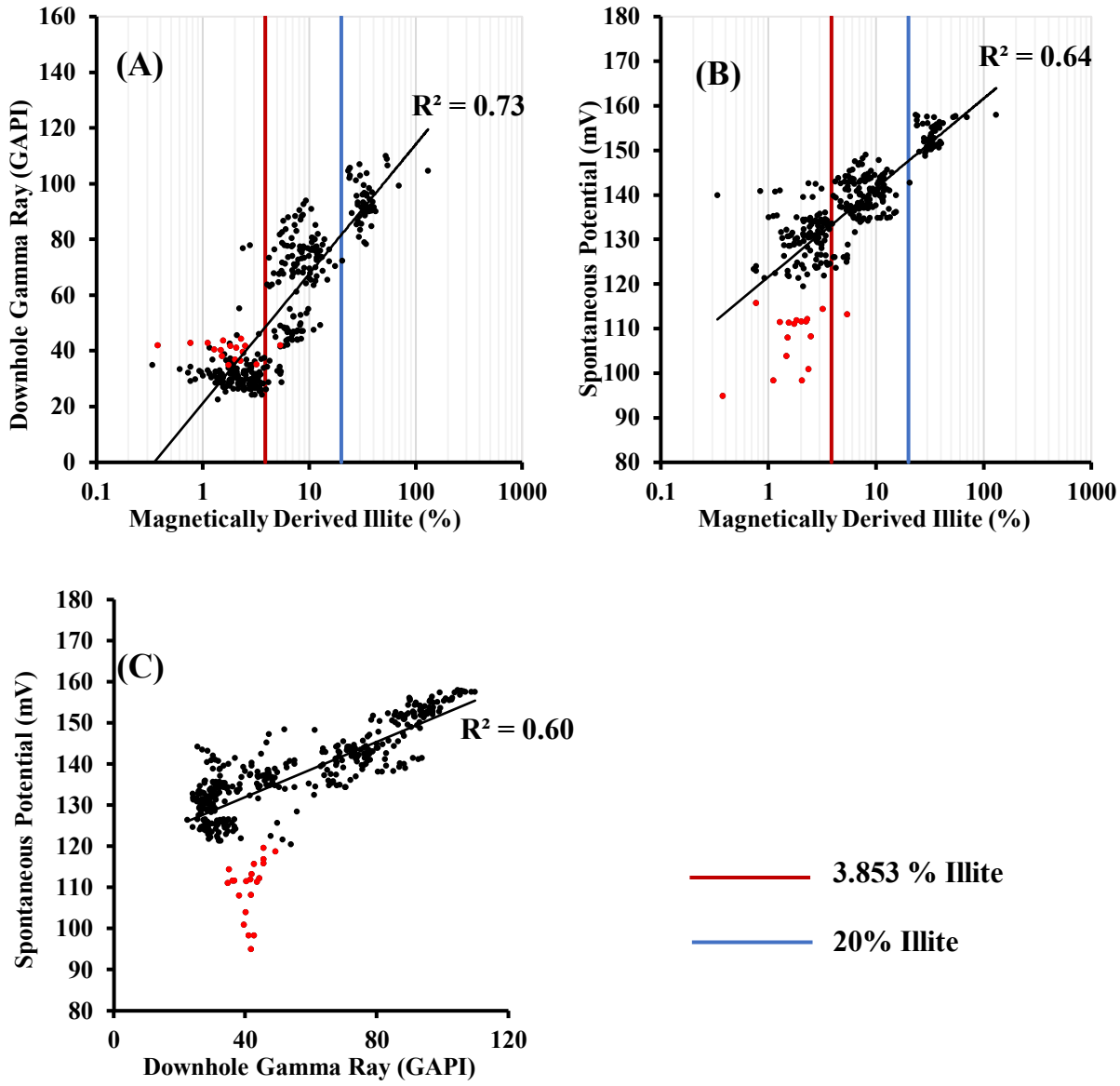


**Figure 3.17**: Crossplots for Well 03. **(A)** and **(B)** are crossplots of the averaged (1 foot vertically) magnetically derived illite contents with depth-matched downhole logs data and **(C)** is a crossplot of the downhole GR and SP log data.

The $R^2$ regression coefficients of crossplots **(A)** and **(B)** in **Figure 3.17** for the magnetically derived illite content against the total GR and SP log data are higher than that of crossplot **(C)** between the total GR and SP log data themselves. The $R^2$ value between illite content and total GR is 0.73, compared to 0.64 between illite content and the SP log data and 0.60 between the

total GR and SP log data. The lower $R^2$ of the GR – SP crossplot appears to be due to data points in the interval 196–198 m (**Figure 3.14**), which have low illite content and likely to have high permeability (due to the low illite and large negative SP deflection) and are shown in red in **Figure 3.17**. If these points are removed (**Figure 3.18**) all the $R^2$ values increase. In particular, the $R^2$ value of the total GR versus SP crossplot increases significantly to 0.75.

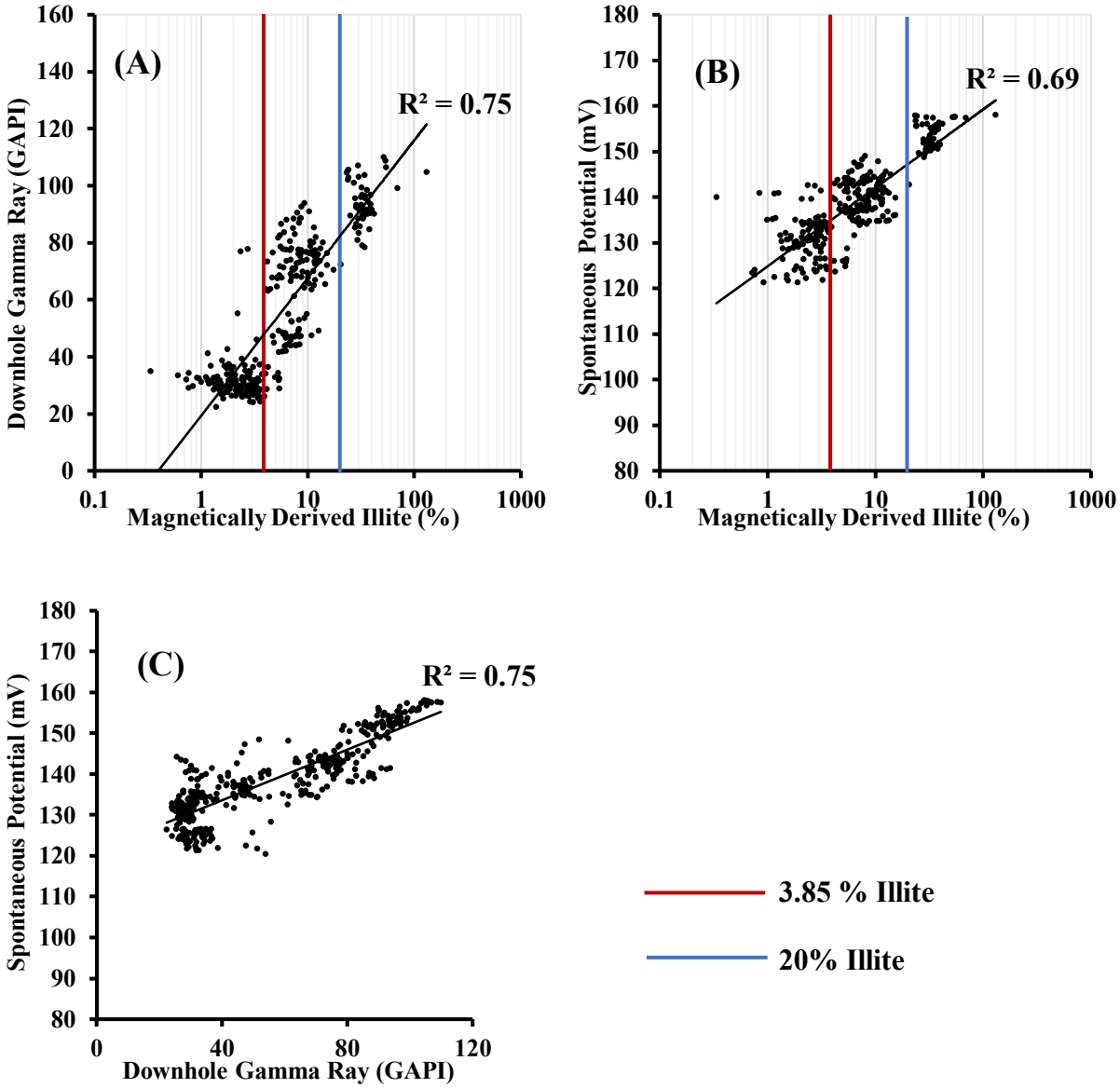


**Figure 3.18**: Crossplots for Well 03 similar to those in **Figure 3.17**, but without the low illite, expected high permeability, data points from the interval from depths 196–198 m.

### c) Crossplots of magnetically derived illite content, total downhole GR and spectral GR

**Figures 3.19** and **3.20** show crossplots of the spectral GR of potassium (K), thorium (Th) and uranium (U) against the depth-matched magnetically derived illite content and the total downhole GR log. The $R^2$ regression coefficient between magnetically derived illite content and spectral K (**Figure 3.19 (A)**) is 0.80 and higher than the $R^2$ values between magnetically derived illite content and spectral Th (**Figure 3.19 (B)**) and U (**Figure 3.19 (C)**) at 0.63 and 0.28 respectively. This is consistent with the assumption that illite is a key clay mineral in these oil sands, since potassium is a major elemental component of illite. On the other hand, the $R^2$ between total GR and spectral gamma ray K (**Figure 3.20 (A)**) at 0.76 is lower than the $R^2$ value between total GR and spectral gamma ray Th (**Figure 3.20 (B)**) at 0.88, and higher than the $R^2$ value between total GR and spectral gamma ray U (**Figure 3.20 (C)**) at 0.51. The stronger correlation between total GR and spectral gamma ray Th provides further evidence that the total GR signal is more influenced by thorium than potassium in this well, as was shown in the interval 162-168 m of the IHS beds in **Figure 3.16** as discussed earlier. This also means that the magnetic results are likely to better represent the illite contents in this well than the total GR signal.

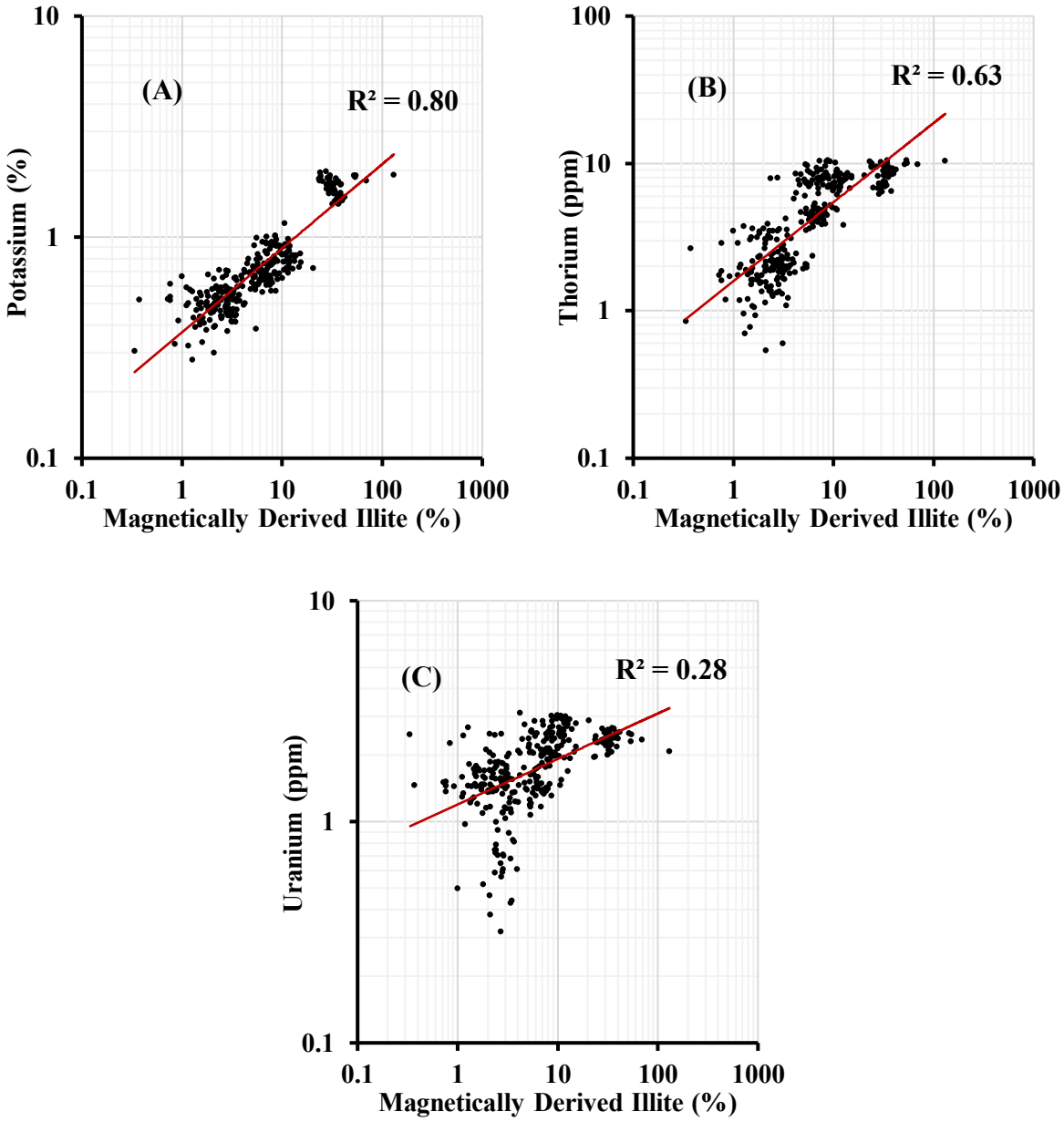


**Figure 3.19**: Crossplots for Well 03. **(A) (B)** and **(C)** are crossplots of the averaged (1 foot vertically) magnetically derived illite contents with the depth-matched spectral downhole logs data of potassium, thorium and uranium.
(A similar figure for Well 02 is given in **Appendix 2**, **Figure A2.1**, for completeness, but the correlation coefficients are lower, except for uranium, than for the Well 03 figures above. There was no spectral gamma ray data for Well 01 so no similar figure for Well 01 could be made).

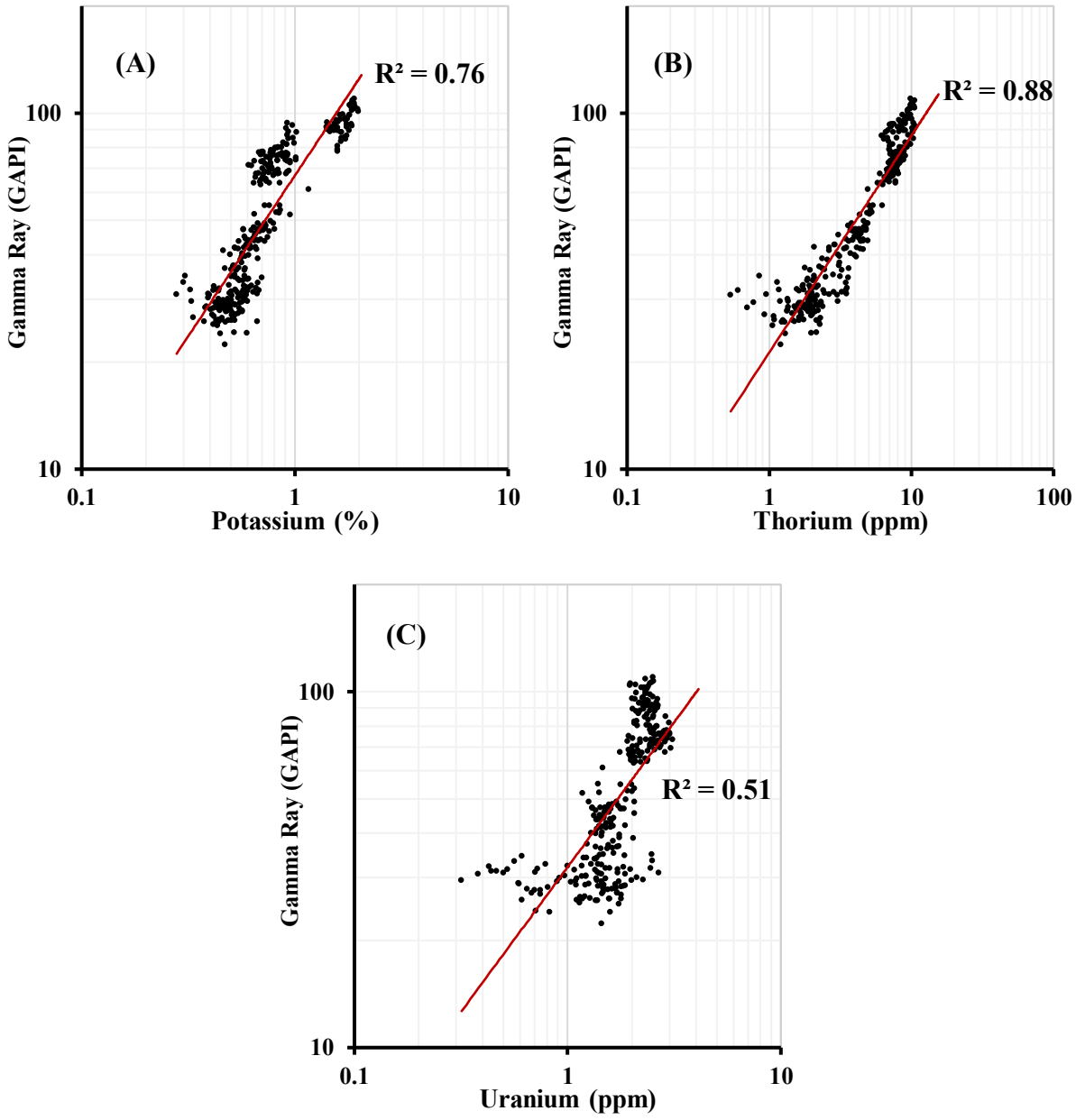


**Figure 3.20**: Crossplots for Well 03. **(A) (B)** and **(C)** are crossplots of the total downhole GR log data with the depth-matched spectral downhole log data of potassium, thorium and uranium.
(A similar figure for Well 02 is given in **Appendix 3**, **Figure A3.1**, for completeness. There was no spectral gamma ray data for Well 01 so no similar figure for Well 01 could be made).

**d) Comparisons between core permeability, magnetic results and downhole data**

Permeability is a measurement of the ability of a fluid to pass through a porous medium. In reservoir studies, it is an important parameter to determine how easily hydrocarbons can be extracted from a reservoir. Fortunately, around 20 core permeability measurements were available between the depths of 162–216 m in Well 03 in different lithologies, including IHS beds and clean sand intervals. **Figure 3.21** shows the comparisons between the core permeability and magnetically derived illite content (left hand plot) and SP log (right hand plot). The core permeability results generally correlate well with the trends of magnetically derived illite content and the SP curve, though there appears to be a better correspondence with the magnetically derived illite content (which will be confirmed in the crossplots of **Figure 3.22**). In the clean sand interval (185–216 m), the high permeability values (from 7.0 x $10^3$ mD to 12.5 x $10^3$ mD) correlate with low illite contents (less than 4%) and larger deflections to the left of the SP curve. In the IHS beds (161.7–183 m) the lower permeability values (from 0.4 x $10^3$ mD to 3.2 x $10^3$ mD) correlate with higher illite contents and less of a deflection to the left of the SP curve. However, the magnetically derived illite content appears to correlate with the core permeability better than the SP log in these IHS beds. Interval 2 in the IHS beds (**Figure 3.21**) has the lowest core permeability values and correlate with higher magnetically derived illite content, while the higher core permeability in intervals 1 and 3 (**Figure 3.21**) correlate with lower magnetically derived illite content. In contrast, the variation of the SP log does not clearly show the differences in permeability between these intervals. Therefore, the magnetic results appear to be more useful in predicting permeability trends in this case. Unfortunately, there was no available core permeability data in the top clay/shale interval for comparison.

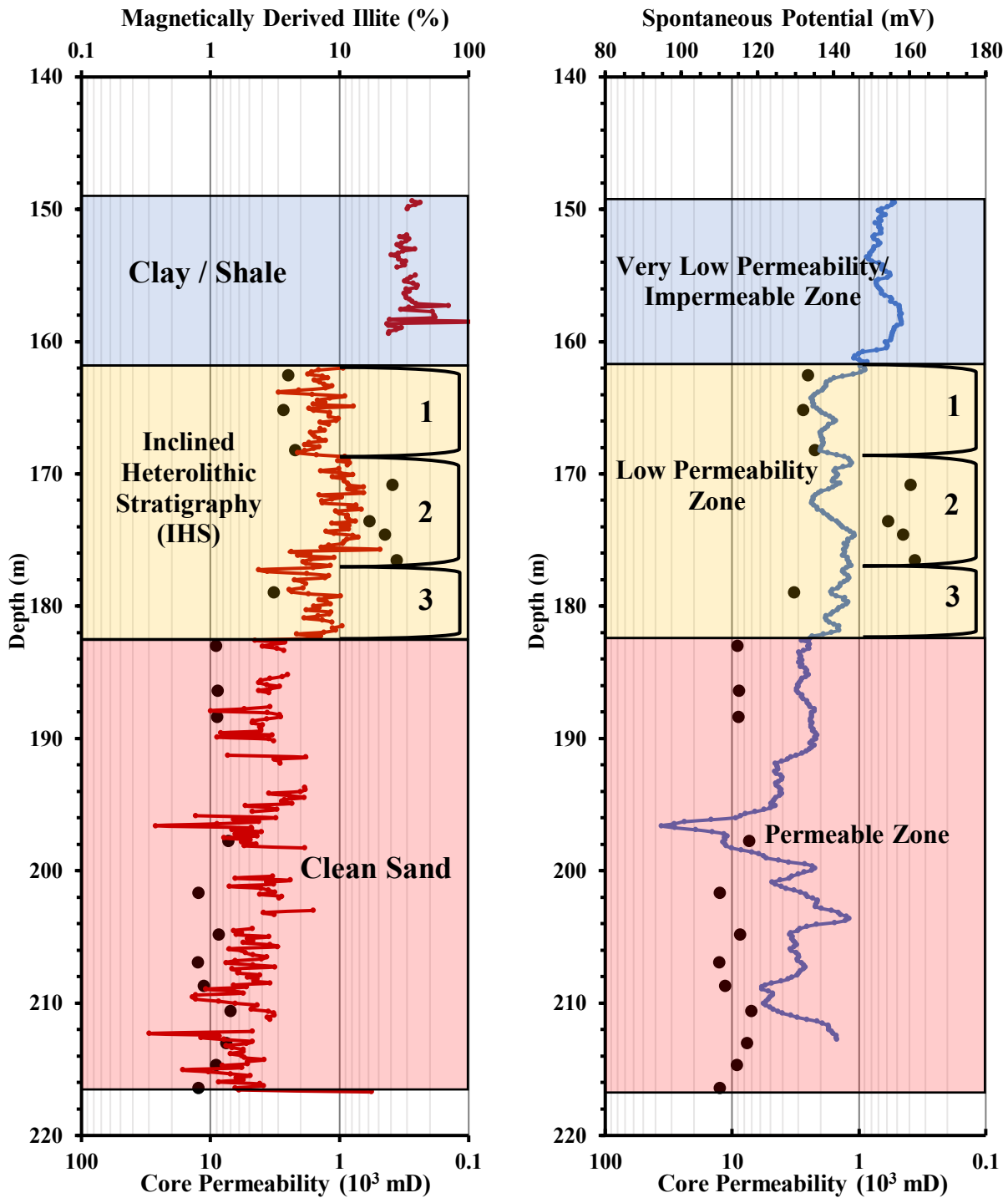


**Figure 3.21**: Comparisons between the core permeability values (black circles) and depth-matched magnetically derived illite contents (left hand plot, red curve) and downhole SP log (right hand plot, blue curve).

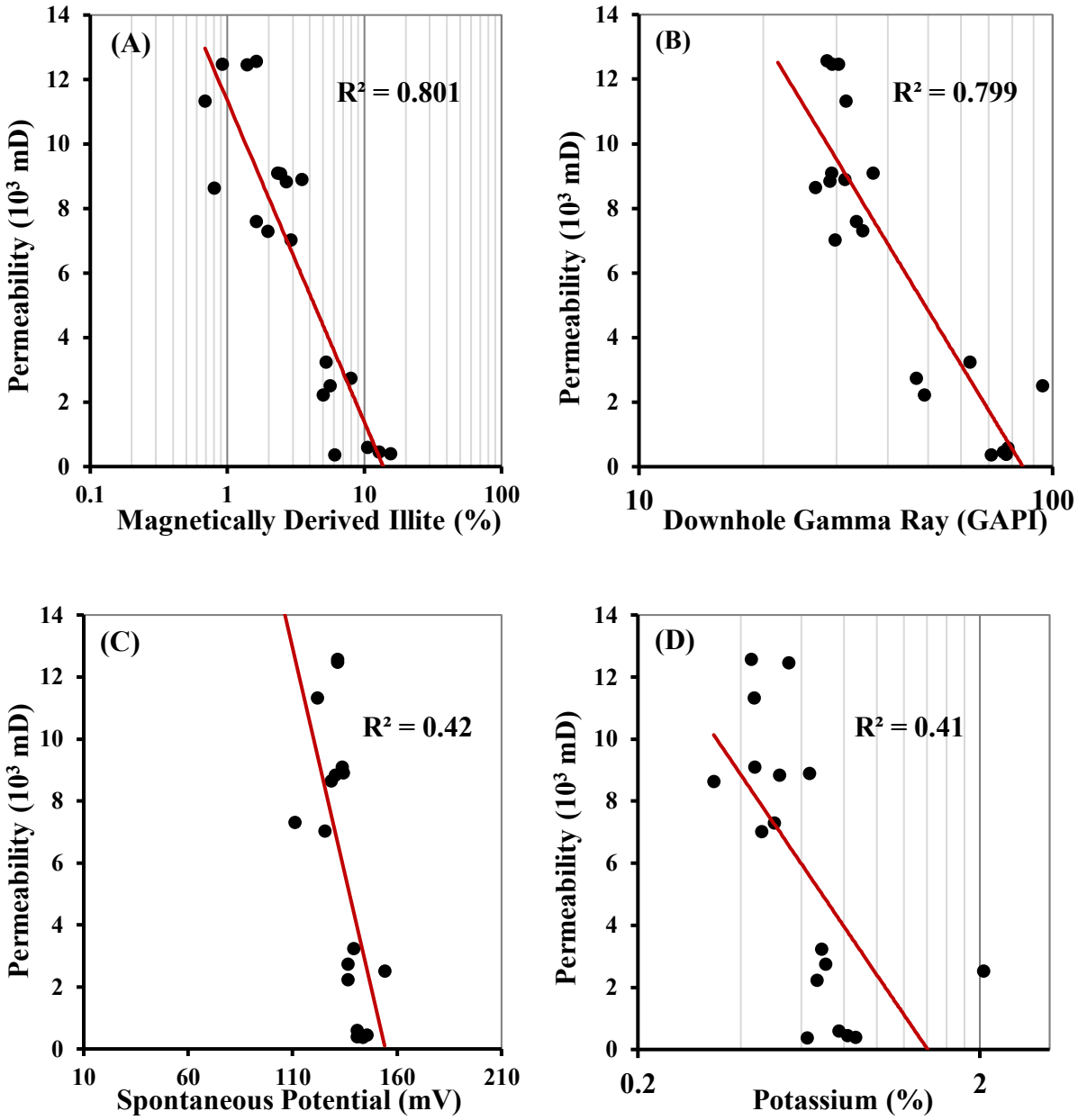


**Figure 3.22**: Crossplots between core permeability in Well 03 with **(A)** depth-matched magnetically derived illite contents, **(B)** downhole total gamma ray, **(C)** spontaneous potential, and **(D)** spectral gamma ray potassium contents.

**Figure 3.22** shows crossplots of the measured core permeability data with the depth-matched magnetically derived illite content results and the downhole log data. The plots clearly indicate strong relationships between the core permeabilities and both the magnetically estimated illite

content (**Figure 3.22 (A)**) and the total GR signal (**Figure 3.22 (B)**). In each case the $R^2$ value was close to 0.80, with that for the magnetic results being marginally better. The crossplots suggest a strong dependence of permeability on the paramagnetic clay content in the samples. In contrast, the relationships of the core permeabilities with the SP signal (**Figure 3.22 (C)**) and the potassium content from the spectral GR (**Figure 3.22 (D)**) are not particularly strong. Although there are differences in the $R^2$ values, all crossplots have similar trends that show a lower permeability with increasing magnetically derived illite content, GR, SP and spectral GR potassium content signals.

## 3.6. Conclusions

From the comparisons between the magnetic results, the depth-matched downhole log data and the core permeabilities from the three oil sands wells the following conclusions can be drawn:

1. Probe volume magnetic susceptilibility profiles (which can be generated rapidly and non-destructively on this unconsolidated core) were demonstrated to be capable of clearly distinguishing the 3 main lithologies in these oil sands wells. Negative and close to zero volume magnetic susceptibility values indicated clean sand intervals, small positive values (generally up to about $5 \times 10^{-5}$ SI) corresponded to IHS beds or muddy sands, and higher positive values (generally greater than $10 \times 10^{-5}$ SI) corresponded to shale.
2. Whilst there was a general correspondence between the magnetic and downhole total gamma ray (GR) data, the magnetic results were better at distinguishing the 3 main lithologies. In particular, the total GR did not clearly show a clean sand interval in Well 02, and incorrectly suggested clean sand instead of IHS beds in the interval 162 -168 m in

Well 03. In both these cases the magnetic results indicated the correct lithology, which was confirmed by visual observations and/or the quantitative grain size profiles.

3. The magnetic results that were acquired from slabbed core in this study indicate the potential for a magnetic susceptibility downhole tool for improved in-situ identification of oil sands lithologies. This will be further discussed in **Chapter 5**.
4. The magnetic results processed to a simple mineral percentage enabled one to identify thin layers of anomalous minerals, where values of magnetically derived illite content were greater than 100% from the simple model. The total GR, spectral GR and SP logs did not generally pick out these thin layers, especially in Wells 01 and 02. However, in Well 03 there was some suggestion that the anomalous mineral clearly identified by the magnetic results was also detected by the total GR (mainly the potassium and thorium in terms of spectral components) and SP, although the evidence from the GR and SP logs was far less convincing.
5. The magnetic technique appears to be better at estimating the paramagnetic clay content (in this case illite) profiles compared to the downhole total GR signal (for example in the interval 162–168 m in Well 03). Moreover, the correlation between the magnetic profiles and the spectral GR potassium content profiles is better than the correlation between the magnetic profiles and the total GR profiles. This might be expected since potassium is one of the elements comprising illite, and helps to confirm that the magnetic results are giving meaningful results for this paramagnetic clay. In contrast, the resulting total GR signal is the result of the combination of the thorium and uranium components in addition to the potassium component, and the thorium component in particular is influencing the total GR signal in Wells 02 and 03.

6. Strong correlations between magnetically derived illite content profiles and the downhole SP log data (in all three wells in this study) clearly show that the magnetic results are useful in identifying permeable zones. The larger deflections to the left on the SP log (which indicate permeable zones where the salinity of the formation water is greater than the salinity of the drilling mud filtrate) correlate with the lowest values of magnetically derived illite content. Note that the magnitude and direction of the deflection of the SP log depends on the difference in salinity between the formation water and drilling mud filtrate. The SP log would theoretically not show a deflection at a permeable zone if the salinities of the two fluids are equal. In contrast, the magnetic technique has an advantage in that it can potentially identify a permeable zone in this situation regardless of the salinity.
7. A strong correlation was observed between the magnetically derived illite content and core permeability in the one well (Well 03) where permeability data was available. This shows the potential of magnetic measurements for permeability prediction in oil sands reservoirs. The results were marginally better than the correlation between the core permeability and the total downhole GR signal, and substantially better than the correlations between the core permeability and either the SP log data or the spectral GR potassium data.
8. The relatively high $R^2$ correlation coefficient values of the crossplots between the magnetic results and depth-matched downhole log data (total GR and SP) in Wells 02 and 03 demonstrated a general correspondence between these parameters. Furthermore, crossplotting the magnetic results against the downhole log data helped to quantify the appropriate cut-offs for the total GR to improve its ability to distinguish the different

lithologies, and quantify the appropriate cut-offs for the SP log to improve its ability to identify permeable zones. Moreover, the crossplots of magnetically derived illite content against downhole total GR clearly showed separate regions for the main lithologies, and therefore has the potential to be used as a means of identifying these lithologies in these oil sands.

## 3.7. References


Ali, A., Potter, D. K. and Tugwell, A., 2014. Correlation between magnetic properties and permeability: results from a new case study in the North Sea. In *Proceedings of the 2014 International Symposium of the Society of Core Analysts*, 8-11 September 2014, Avignon, France. Paper SCA2014-077 (6 pages).

Potter, D. K., 2007. Magnetic susceptibility as a rapid, non-destructive technique for improved petrophysical parameter prediction. *Petrophysics*, **48** (issue 3), 191-201.

Potter, D. K., AlGhamdi, T. M. and Ivakhnenko, O. P., 2011. Sensitive carbonate reservoir rock characterization from magnetic hysteresis curves and correlation with petrophysical properties. *Petrophysics*, **52** (issue 1), 50-57.

Potter, D. K., Corbett, P. W. M., Barclay, S. A., and Haszeldine, R. S., 2004. Quantification of illite content in sedimentary rocks using magnetic susceptibility—a rapid complement or alternative to X-ray diffraction. *Journal of Sedimentary Research*, *Research Methods Papers Section*, **74**, no.5, 730-735.

Potter, D. K. and Ivakhnenko, O. P., 2008. Clay typing - sensitive quantification and anisotropy in synthetic and natural reservoir samples using low- and high-field magnetic susceptibility for improved petrophysical appraisals. *Petrophysics*, **49** (issue 1), 57-66.

Sharpe, E., 2019. Canada's Oil Sands – Familiar trouble. *Energy Ink Magazine*. July 2019.

# Chapter 4

# A comparison between high resolution X-Ray fluorescence, probe magnetic susceptibility and traditional downhole log data

## 4.1. Introduction

As presented in **Chapter 3**, the results of the probe magnetic susceptibility measurements on the slabbed cores of the three oil sands wells demonstrated the effectiveness of the technique as a non-destructive tool for characterizing oil sands reservoir properties. Whilst the comparisons of the magnetic results with traditional downhole logs such as gamma ray (GR) and spontaneous potential (SP) show a certain degree of correspondence, the magnetic results were shown to have certain advantages over the traditional methods. The profiles of average probe volume magnetic susceptibility clearly distinguished the different lithologies better than the GR in some intervals. The profiles of magnetically derived illite content were able to predict permeable zones, and identify thin layers of anomalous minerals that the GR and SP logs often did not. The crossplots of magnetically derived illite content and depth-matched downhole total GR log data showed a strong relationship between the magnetic results and the GR signals in sand and clay intervals. However, there are some intervals that require further investigation, for example where the magnetic results and downhole total GR log data did not show a strong correspondence. This chapter will introduce the application of X-ray fluorescence (XRF) as a further non-destructive characterization technique to quantify the elemental contents of the slabbed cores from the three oil sands wells. The results from the XRF measurements will be compared with the magnetic results and the downhole log data. The comparisons will determine whether the elemental contents can potentially be used for characterizing the lithology of these oil sands reservoirs. The

X-ray fluorescence technique is also an independent method to help evaluate the magnetically derived mineralogical data (e.g., the illite content in **Chapter 3** and ferrimagnetic content in **Chapter 5**) at similar high resolution.

## 4.2. X-Ray Fluorescence

X-ray fluorescence spectrometry is an elemental analysis technique that has a wide range of applications in science and industry. This section will briefly describe the fundamentals of XRF measurements and how the elemental contents of a sample are identified and quantified by the XRF technique.

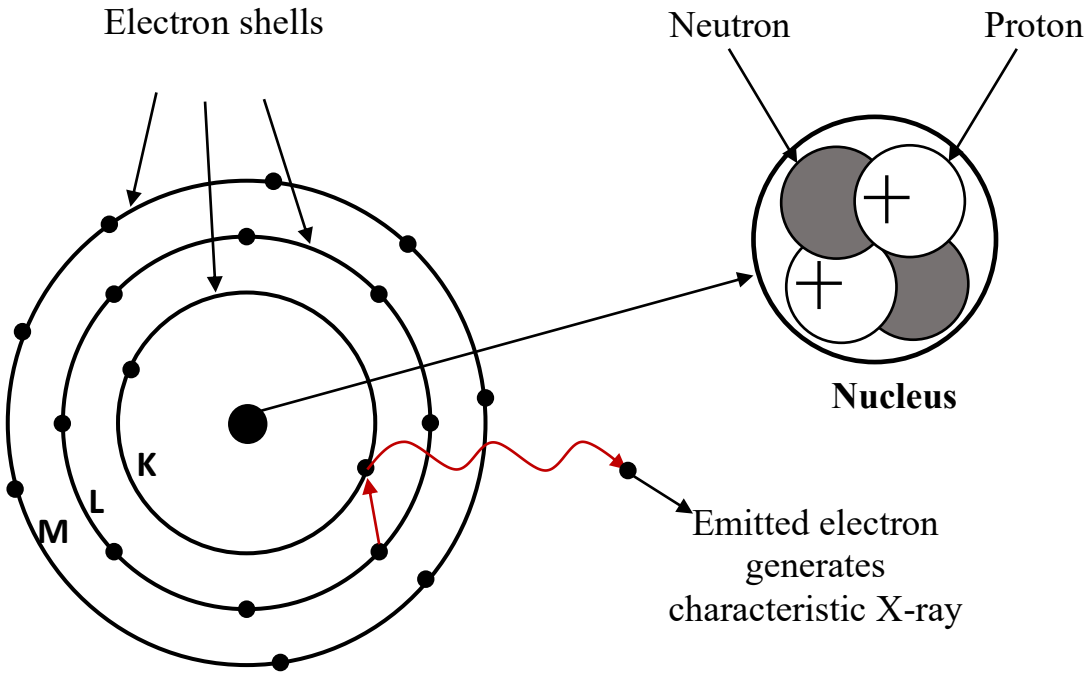


**Figure 4.1**: Schematic of an atomic structure of the Argon element including the nucleus and electrons shells (K, L, M) and the characteristic X-ray emitted from the electron during electron transfer.

A material is composed of various elements. An atom consists of two main parts: a central nucleus, including protons and neutrons, and electron shells with electrons orbiting around the nucleus. The distance between the shells is different for each element, and each shell has a maximum number of electrons that it can support. For the example shown in **Figure 4.1**, in an

atomic structure of the Argon element the K shell supports 2 electrons, the L shell 8, and the M shell 8. The energy of an electron varies inversely with its distance from the nucleus. Each element has a specific number of protons in its nucleus, which is called the atomic number of that element. The atomic number can be used to uniquely identify the element.

In an XRF measurement, two types of X-rays, Bremsstrahlung X-rays and characteristic X-rays, are created in two different processes. The process for the former is a continuous high energy spectrum generated by the X-ray source in an analyzer. The process for the latter is X-rays emitted from electrons during the electron shell transferring process, which happens when Bremsstrahlung X-rays eject electrons from the inner shells of atoms. Then, the vacancies left by the ejected electrons are quickly filled by other electrons dropping down from the outer shells as the atoms attempt to regain stability (**Figure 4.1**). The electrons that drop down to inner shell loss some energy. Since the distance between electron shells is different for each element, the energy level of each electron shell and the difference in energy between the shells are also different for each element. During the process, characteristic X-rays are emitted, and their precise energies are associated with the difference between the energy levels of the outer and inner electron shells of the atom.The emission of characteristic X-rays is the foundation of an X-ray fluorescence analysis.

### 4.3. Samples and Method

In this study elemental contents in the slabbed cores of the three oil sands wells were quantified by the application of a portable XRF analyzer, the Thermo Scientific Niton XL3t, supplied by Elemental Control Limited (in Toronto). The analyzer is designed to work either in a laboratory

or as a field operation device. The analyser can be positioned in a customized stand for accurate portable, non-destructive measurements in the laboratory or used as a handheld device in the field. The analyzer contains an X-ray tube that emits radiation only when the shutter is opened, and a detector to detect the characteristic X-rays of the elements in a sample (**Figure 4.2**). The radiation of the Bremsstrahlung X-rays is produced by the analyzer and emitted through the measurement window, and the radiation of the characteristic X-rays, which is generated by ejected electrons, also reaches the detector through the window. Therefore, during a measurement the sample should always be in contact with the window.

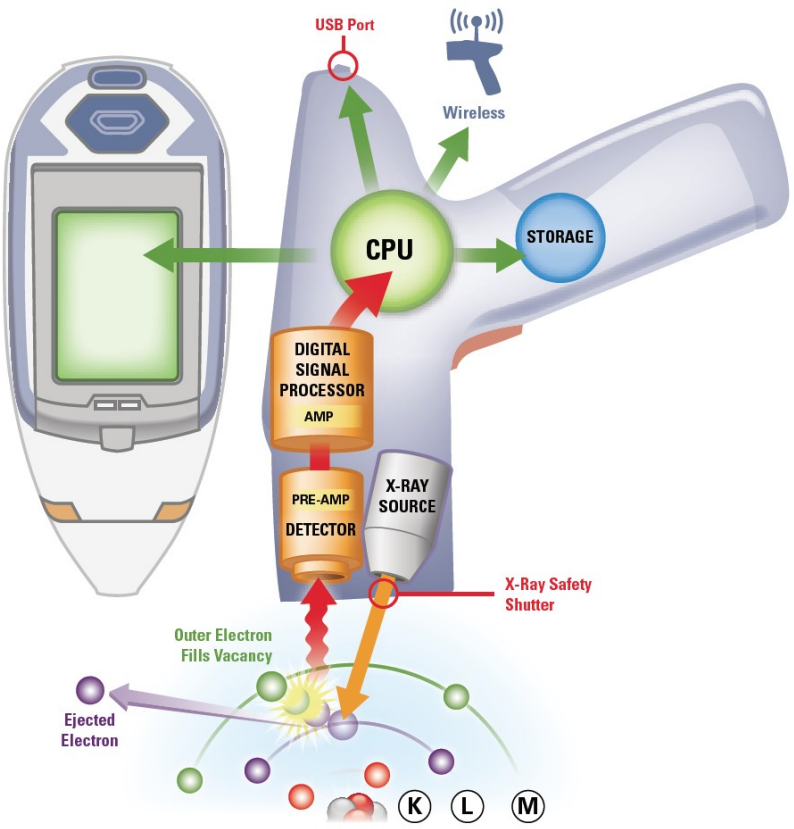


**Figure 4.2**: Schematic of the working principles of the Thermo Scientific Niton XL3t XRF analyzer (modified from Backman et al., 2016).

**Table 4.1**: Filter used, time of analysis, and elements analyzed by the portable XRF analyzer. Bal* stands for balance, which represents X-ray energy levels that the analyzer does not attribute to a particular element (modified from Fajber and Simandi, 2012).

| Filter | Analytical time interval | Elements analyzed |
|---|---|---|
| Main | 45 seconds | Ag, As, Au, Bal*, Bi, Cd, Co, Cu, Cr, Fe, Mn, Mo, Nb, Ni, Pb, Rb, Se, Sb, Sn, Sr, Th, Ti, U, V, W, Y, Zn, Zr |
| Low | 45 seconds | Ca, Cr, K, Ti, V |
| High | 45 seconds | Ag, Ba, Cd, Ce, La, Nd, Sb, Sn, Pr |
| Light | 45 seconds | Al, Cl, Mg, P, Si, S |

For sedimentary rock samples, it is recommended that the analyzer be used in "Mining Cu/Zn mode" for each measurement. The instrument operates with four different filters in order to obtain accurate results for a wide range of elements (**Table 4.1**). Each measurement takes a total of 3 minutes, with 45 seconds for each filter beam. In the laboratory, the cores are usually measured in the form of pressed powder, or are cut into small pieces for use with suitable portable stands. However, to measure the slabbed cores in the present study, the device needed to be kept in contact with the surface of the cores during the measurements. The measurement time was too long for one to hold the device by hand during the operation, so I fabricated a customized stand to ensure the accuracy of the results (**Figure 4.3**). The stand was simply comprised of two legs and a bridge that allowed the height of the analyzer to be suitably adjusted in relation to the surface of the slabbed cores. With the support of the stand, the analyzer was always stable, and therefore the measuring window was always in contact with the surface of the slabbed cores during the measurements. Each XRF measurement analyzes a small area of just 3 mm in diameter on the slabbed core. The analyzer was connected to a PC with an application that allowed one to control the XRF measurement from a safe distance. This helped to minimize the

dose of radiation I received during the measurements. In order to be qualified to operate the system, I needed to complete a training course and pass the exam to obtain the X-ray fluorescence analyzer operator personnel certification issued by Natural Resources Canada.

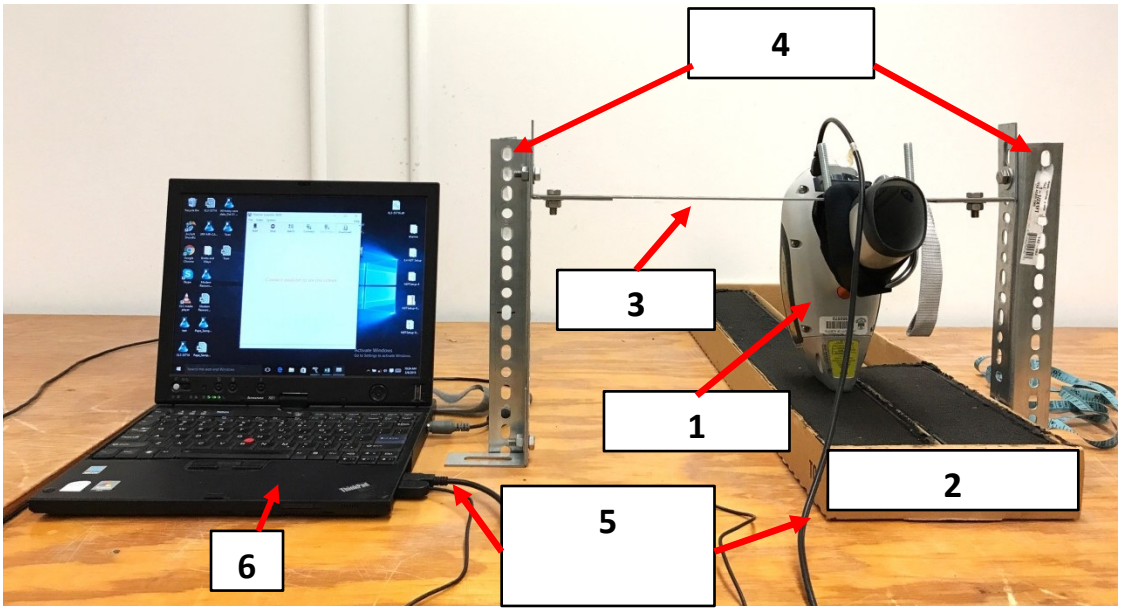


**Figure 4.3**: The custom-made system I constructed for XRF measurements on the oil sands slabbed cores. **1** is the XRF analyzer, **2** is the slabbed core, **3** is the bridge of the stand, **4** shows the legs of the stand, **5** is the cable connecting the analyzer and the computer, **6** is the laptop computer with an application to control the XRF analyzer from a distance.

## 4.4. Test example of X-ray fluorescence measurements on slabbed cores

A rock sample contains various minerals, and each mineral has different elemental components. **Table 4.2** summarizes common reservoir minerals in different magnetic classes with their chemical components and mass magnetic susceptibility values. As shown in the table, heavy elements like iron (Fe), aluminum (Al), and potassium (K) are present in paramagnetic illite clay and in iron-bearing minerals like siderite and magnetite. Therefore, the content of these elements, which are quantified by the XRF method, could potentially be used for identifying lithology and predicting the major minerals in a rock sample. This section will present some initial test results

of XRF measurements on a slabbed core sample and comparisons with the probe magnetic results and the core images.

**Table 4.2**: Chemical components and mass magnetic susceptibility of common reservoir minerals. D, P, and F refer to diamagnetic, paramagnetic, and ferrimagnetic classes, respectively. The values of all diamagnetic minerals were theoretically calculated by Ivakhnenko (2006) and Potter et al. (2011), and the values of illite, siderite, and magnetite are from Hunt et al. (1995).

| **Mineral** | **Mass Magnetic Susceptibility ($10^{-8}$ $m^3$ $kg^{-1}$)** | **Magnetic Class** |
|---|---|---|
| Quartz, $SiO_2$ | -0.62 | D |
| Calcite, $CaCO_3$ | -0.48 | D |
| Dolomite, $CaMg(CO_3)_2$ | -0.48 | D |
| Anhydrite, $CaSO_4$ | -0.45 | D |
| Gypsum, $CaSO_4 \cdot 2H_2O$ | -0.55 | D |
| Illite, $(K,H_3O)(Al,Mg,Fe)_2(Si,Al)_4O_{10}[(OH_2,(H_2O)]$ | 15 | P |
| Siderite, $FeCO_3$ | 122.57 | P |
| Magnetite, $Fe_3O_4$ | 20,000-to-110,000 | F |

**Figure 4.4** shows the profiles of the elemental contents of Fe and K measured by the XRF technique and their comparisons with the probe volume magnetic susceptibility profiles and the corresponding core images from an oil sands slabbed core from Well 02. The magnetic susceptibility profile clearly distinguishes two different mineralogical intervals: negative magnetic susceptibilities correlate with diamagnetic quartz at the top of the section, while significant positive magnetic susceptibilities indicate the presence of paramagnetic minerals and / or ferrimagnetic minerals in the lower part of the section. Certainly the region where the illite contents are estimated at over 100% suggest the presence of an anomalous mineral or minerals,

which could be a paramagnetic mineral with a higher magnetic susceptibility than illite or a small amount of a ferrimagnetic mineral or both. **Figure 4.4** clearly shows a good correspondence between the probe volume magnetic susceptibility and the XRF derived Fe profile. The top clean sands interval with negative magnetic susceptibilities (almost all less than 3.85% estimated illite contents) corresponds with the low Fe content interval (below 0.5% and mainly less than 0.1%). In contrast, below the depth of 402 m both the magnetic susceptibility and the Fe content increase significantly due to the increased paramagnetic and / or ferrimagnetic mineral content. The K profile (**Figure 4.4**), however, shows little increase in elemental content in this lower interval. The Al profile (**Figure 4.5)** from the XRF measurements does show some increase in elemental contents in this lower interval. However, one might expect that if this lower interval is dominated by paramagnetic clay then the elemental K and Al contents would be more pronounced. Significantly, the XRF results show increases in Ca and Ba elemental contents in the lower interval (**Figure 4.5**). The increased Ca suggests the lithology of the lower interval could contain carbonate minerals. Since the elemental Fe content and the magnetic susceptibility also increase significantly in this interval, it suggests an iron-bearing carbonate, such as siderite. Note from **Table 4.2** that the mass magnetic susceptibility of siderite is about 8 times more than that of illite. Therefore, the presence of a moderate amount of siderite could dominate the total magnetic susceptibility signal. The more sand rich upper interval is also shown by the increased Si content in that zone. The magnetic and elemental XRF profiles clearly distinguish the changing mineralogy in the core samples, while the core observation does not clearly show those differences since it is saturated by heavy oil.

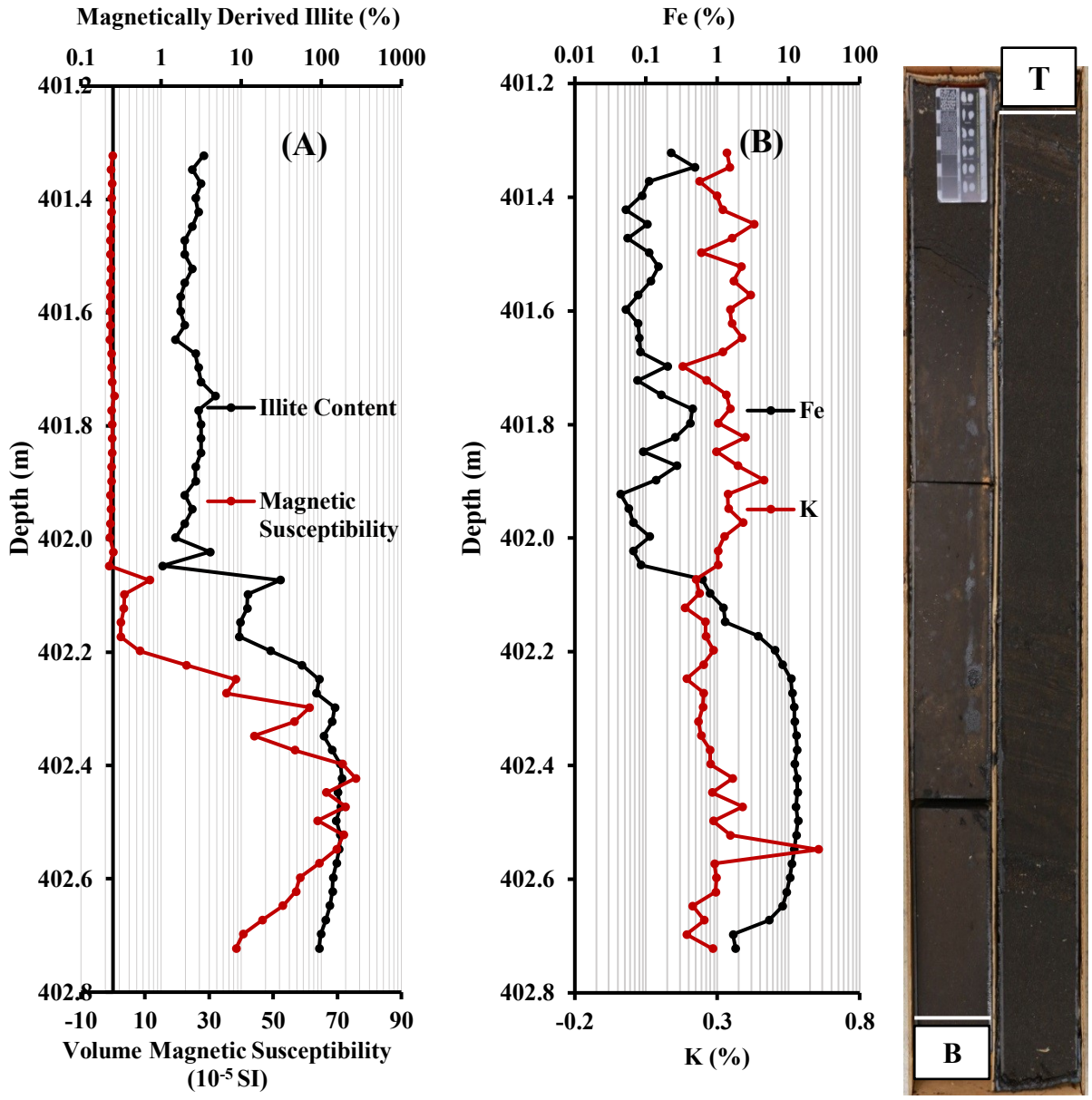


**Figure 4.4**: Test profiles from Well 02 on a section of slabbed core.**(A)** magnetic susceptibility and magnetically derived illite contents, and **(B)** Fe and K contents measured by the XRF technique and a comparison with the core images. On the image, T is the top of the core section and B is the bottom of the core section.

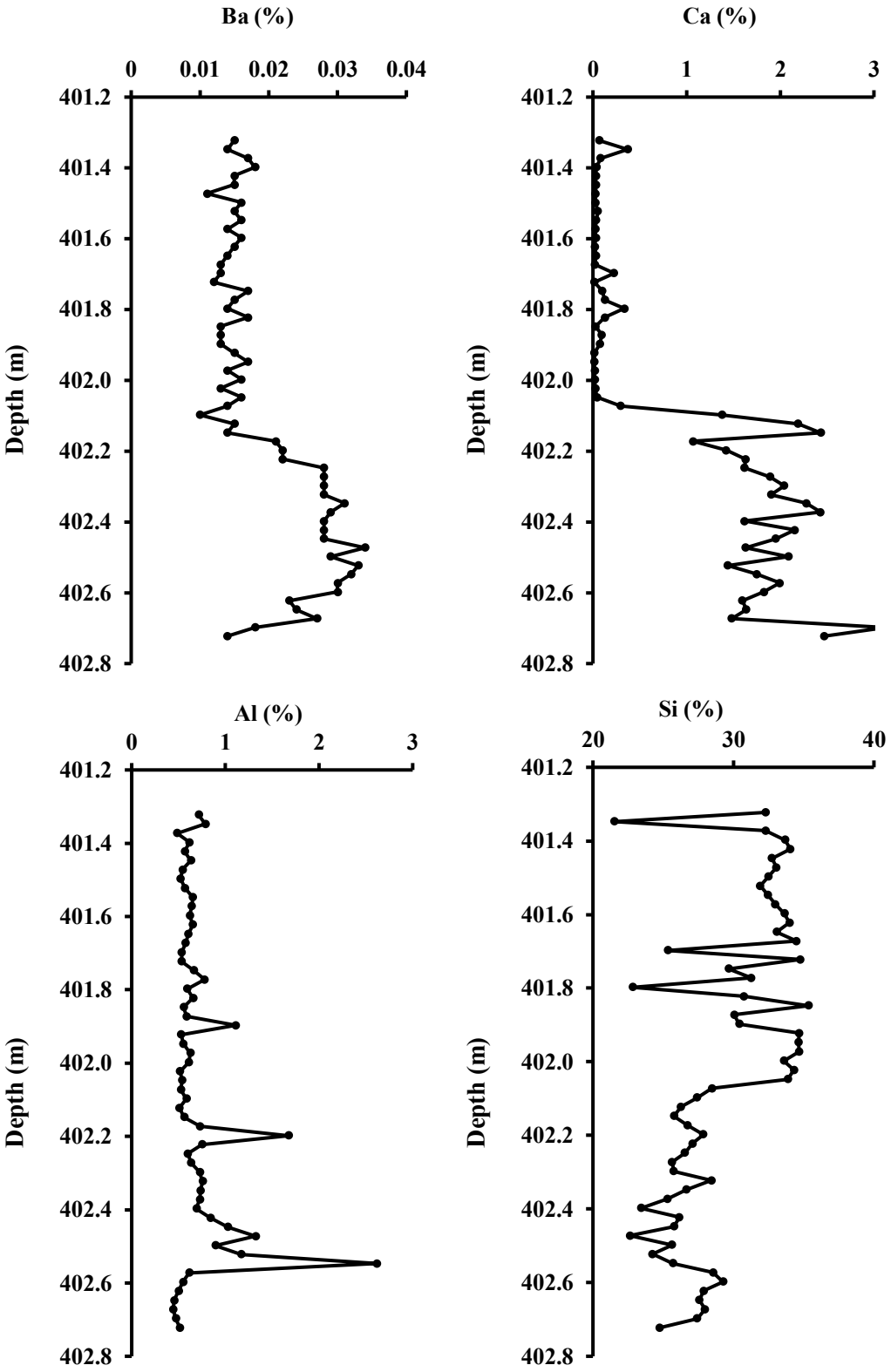


**Figure 4.5**: Ba, Ca, Al and Si elemental contents measured by the XRF technique for the example in **Figure 4.4** from Well 02.

## 4.5. Application of X-ray fluorescence on the slabbed cores of the 3 oil sands wells

This section will present the results of XRF measurements adapted for use as a non-destructive core technique for quantifying elemental contents on the slabbed cores of the 3 oil sands wells that had probe magnetic susceptibility measurements in **Chapter 3**. The raw XRF measurements were averaged over vertical intervals of 30 cm for Wells 01 02, and 1 ft for Well 03, for direct comparison with the vertical averaging of the magnetic susceptibility and the downhole log data. The profiles of major elemental contents (primarily Fe, K, Al, Ca and Si) with depth are compared with the profiles of the magnetic results and the downhole log data to evaluate the XRF technique as well as to provide further insights into the differences between the magnetic results and the downhole log data.

### 4.5.1. XRF results and comparisons of Well 01

#### a) Profile comparisons with depth

The results of XRF measurements on the slabbed cores of Well 01 and their comparisons with the magnetic results and downhole gamma ray log data are shown in **Figures 4.6** and **4.7**. The elements Fe, K and Al show correspondences with the magnetic and gamma ray profiles. At the clay / shale interval identified by magnetic susceptibility and the gamma ray log, these elemental contents increase significantly compared to other intervals. The Fe contents at the clay / shale interval are about 2% while those in the clean sands are generally around 0.1% (**Figure 4.6**). Moreover, the percentage of other common elements in illite, such as K and Al, are highest at the clay / shale interval, with values of more than 1.5% and 5% respectively. In contrast, the K and Al contents are lowest in the sands intervals with around 0.3% and 1%, respectively in most cases, although there are some higher values (**Figure 4.7**).

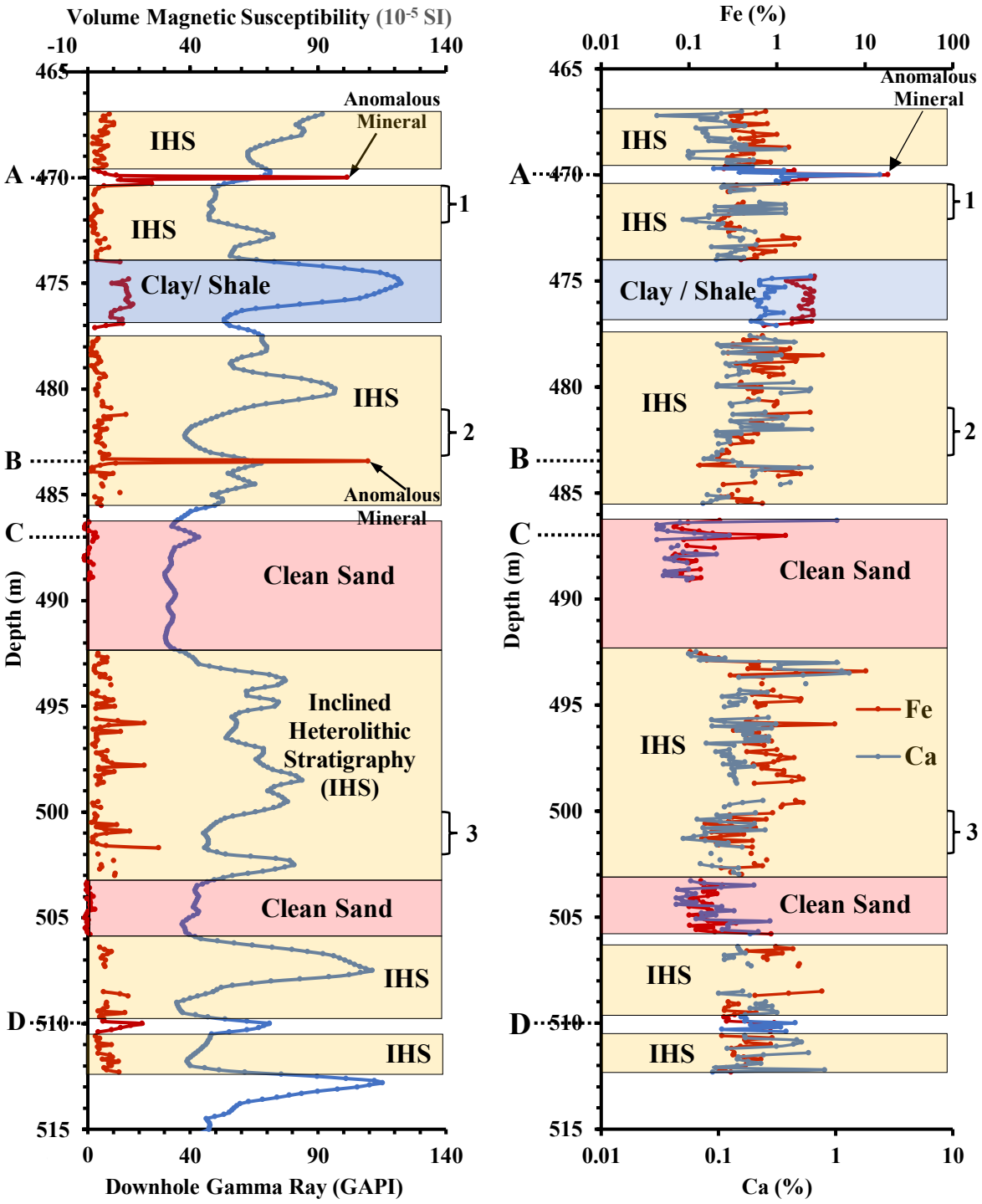


**Figure 4.6**: Well 01 profiles with depth. The left hand plot shows the average probe volume magnetic susceptibility (red curve) on the slabbed core and downhole total GR log (blue curve), and the right hand plot shows the results of the Fe (red curve) and Ca (blue curve) contents measured on the slabbed cores by the XRF technique.

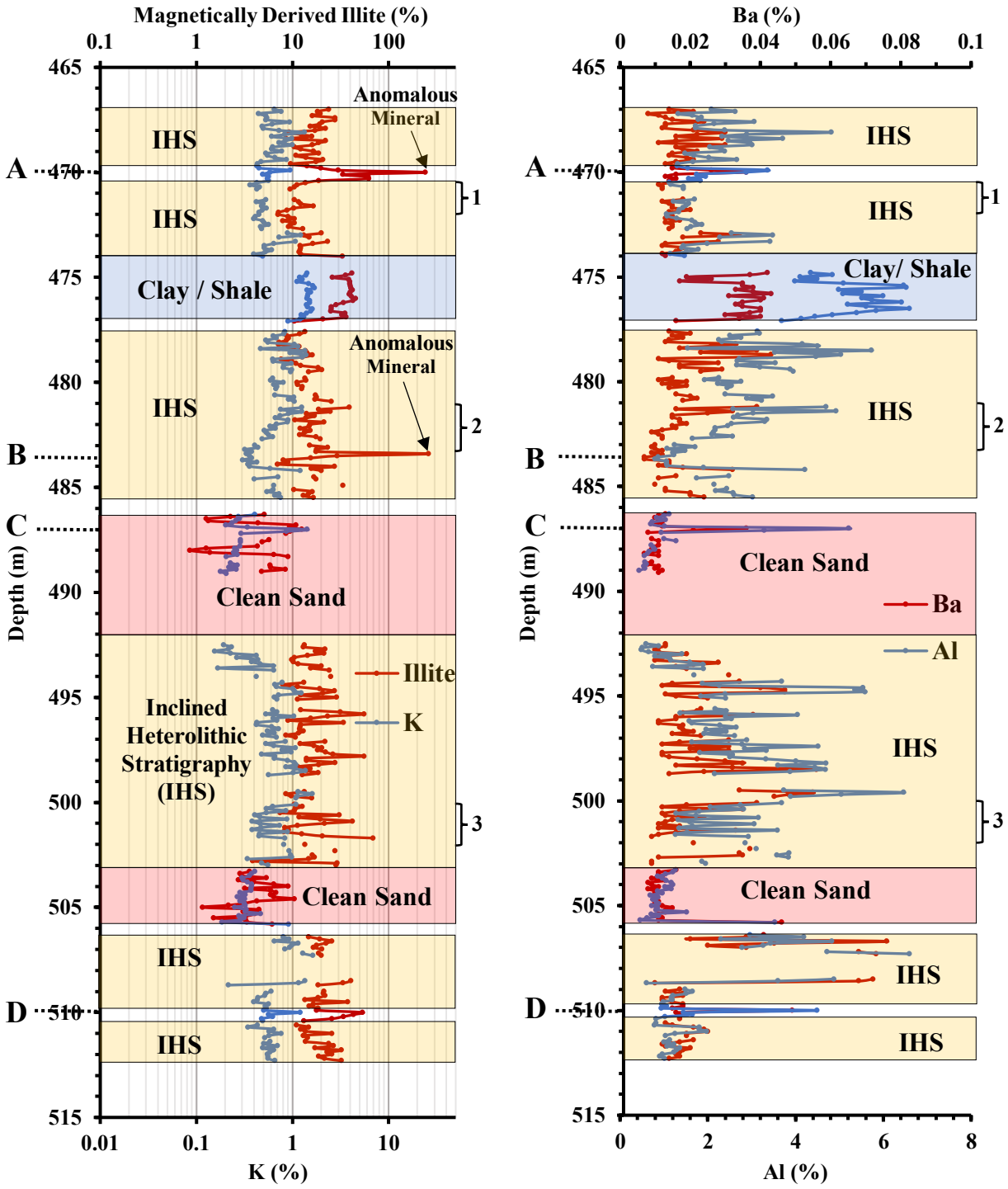


**Figure 4.7**: Well 01 profiles with depth. The left profile shows the K contents (blue curve) measured by XRF and the magnetically derived illite content (red curve) on the slabbed core, and the right profile shows the Al (blue curve) and Ba (red curve) contents measured by XRF.

In detailed comparisons, there are good correspondences between magnetic susceptibility and the elemental contents at specific depths. For example, at depth A where the magnetically derived illite content is more than 100% thus indicating an "anomalous mineral" in **Chapter 3** (**Figure 3.3**), there are also distinct increases in the XRF derived Fe and Ca contents (**Figure 4.6**). The Fe content increases to more than 18%, which is about 9 times higher than the average value in the clay / shale interval. In contrast, the contents of K and Al at this depth are lower (suggesting a lower clay mineral content) than their values in the clay /shale interval (**Figure 4.7**). The elemental contents (particularly increasing Fe and Ca) and the higher magnetic susceptibility results strongly suggest that the primary mineral at this depth could be an iron bearing carbonate mineral. This mineral could be siderite ($FeCO_3$), since pure siderite contains up to 48.3% iron (Muwanguzi et al., 2012), and its volume magnetic susceptibility (478 x $10^{-5}$ SI, Ivakhnenko, 2006) is about 12 times higher than that of illite clay (41 x $10^{-5}$ SI, Hunt et al, 1995). The total GR signal did not pick out the "anomalous mineral" at this depth.

At depth B the magnetic susceptibilities are similar to those at depth A, again indicating the presence of an "anomalous mineral" (**Figure 4.6**) which could be siderite. The XRF results at depth B, however, do not clearly indicate the mineralogy in this case. The reason could partly be because the XRF measurements interrogate a slightly smaller area of 3 mm diameter compared to the magnetic measurements. Each magnetic susceptibility measurement interrogates an area of 3.8 x 10.5 mm and one of the data points at depth B was very high at 379.9 x $10^{-5}$ SI.

The results of the elemental contents further support the correlations between the magnetic susceptibility and downhole total GR log at some specific depths, and thus the XRF

measurements help to confirm the actual core depths at intervals where the cores were not fully recovered. For example, at depth C small positive magnetic susceptibilities correlate with an increased total GR signal and increased Fe content (**Figure 4.6**) and increased K, Al and Ba contents (**Figure 4.7**). At depth D, there is also a correlation between the magnetic results and the total GR (**Figure 4.6**) together with the K, Al, and Ba contents (**Figure 4.7**).

The XRF results also support the illite clay contents derived from the magnetic results. For example, in intervals 1, 2, and 3 (**Figures 4.6** and **4.7**) the low GR signal might be misinterpreted as due to clean sand intervals, whereas the small positive magnetic susceptibility results suggest that the lithologies are in fact muddy sands or IHS beds containing a certain amount of paramagnetic clay minerals. The elemental profiles of Fe, K, and Al from the XRF measurements are consistent with the magnetic results by giving higher percentages of these typical elements in illite clay compared to the contents of these elements in the clean sand intervals.

### 4.5.2. XRF results and comparisons of Well 02

The following section presents the results of the elemental contents by the XRF technique on the slabbed cores of Well 02 and the comparisons with the magnetic results and the downhole log data.

**a) Profile comparisons with depth**

The results of XRF measurements on the oil sands slabbed cores of Well 02 and the comparisons with the magnetic results and the downhole total GR log data are shown in **Figures 4.8** and **4.9**. The profiles of elemental contents measured by XRF correspond well with the magnetic results and the total GR log data. In the shale / clay intervals from depths 355– 364 m and 368.5–378 m,

the significicant positive magnetic susceptibilities and high total GR signals correspond with high percentages of the elements Fe, K and Al. In contrast, in the lower clean sand interval, from 389.6–425.4 m, negative magnetic susceptibilities and low total GR signals correspond with low Fe, K and Al contents indicating low paramagnetic clay content. The correlations indicate that the elemental content profiles are able to distinguish the different lithologies. The results show that the elemental contents of Fe, K, and Al are generally 1–10%, 1–2%, and 4–8%, respectively in the shale / clay interval, and generally about 0.01–0.1%, <1%, and <1% respectively in the clean sand interval (**Figures 4.8** and **4.9**) although there are some exceptions. The XRF results also show that the contents of Ca and Ba in the shale / clay interval are generally higher than in the clean sand interval (**Figures 4.8** and **4.9**).

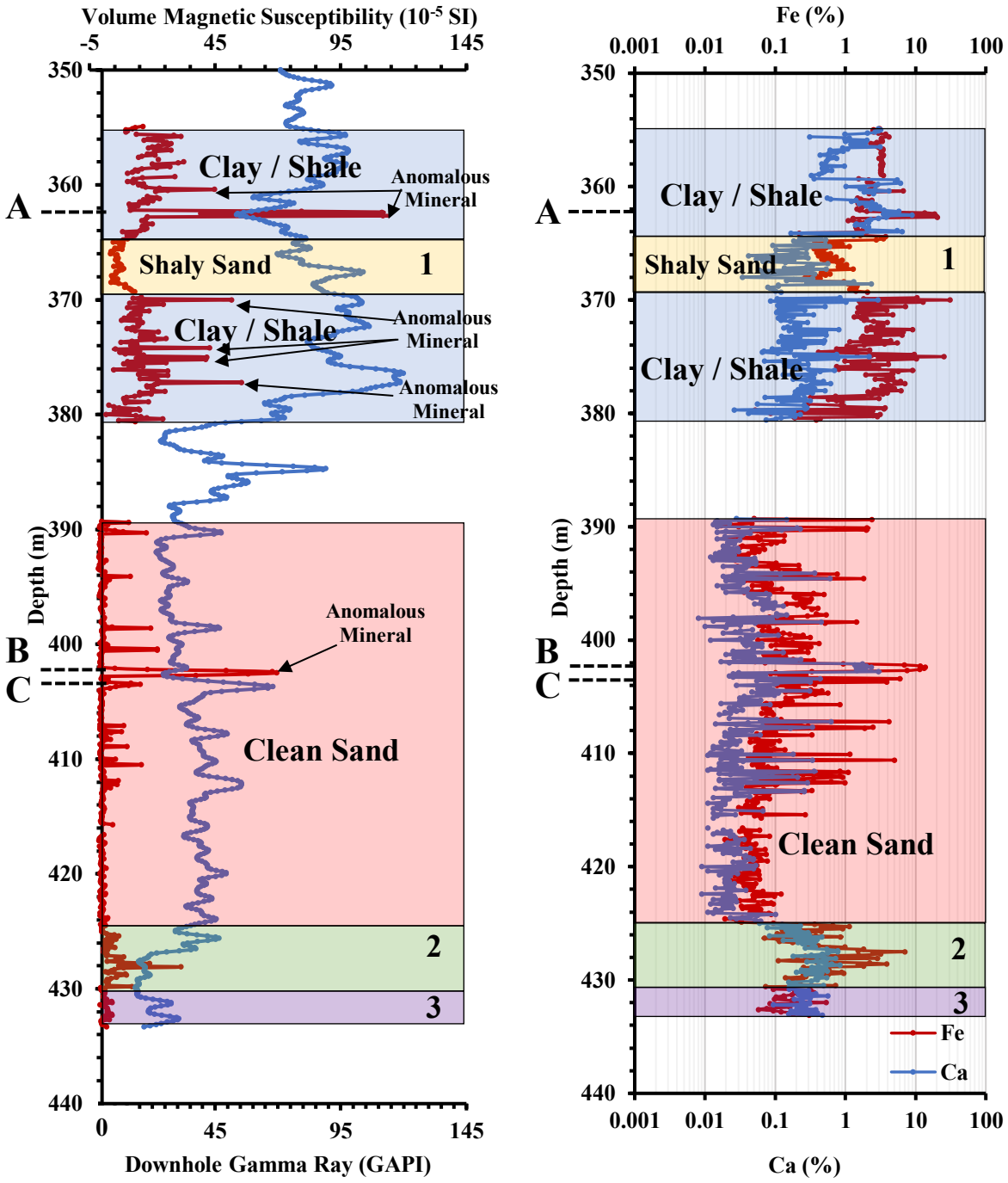


**Figure 4.8**: Well 02 profiles with depth. The left plot shows the average probe volume magnetic susceptibility (red curve) on the slabbed core and downhole total GR log (blue curve), and the right plot shows the results of the Fe (red curve) and Ca (blue curve) contents measured on the slabbed cores by the XRF technique.

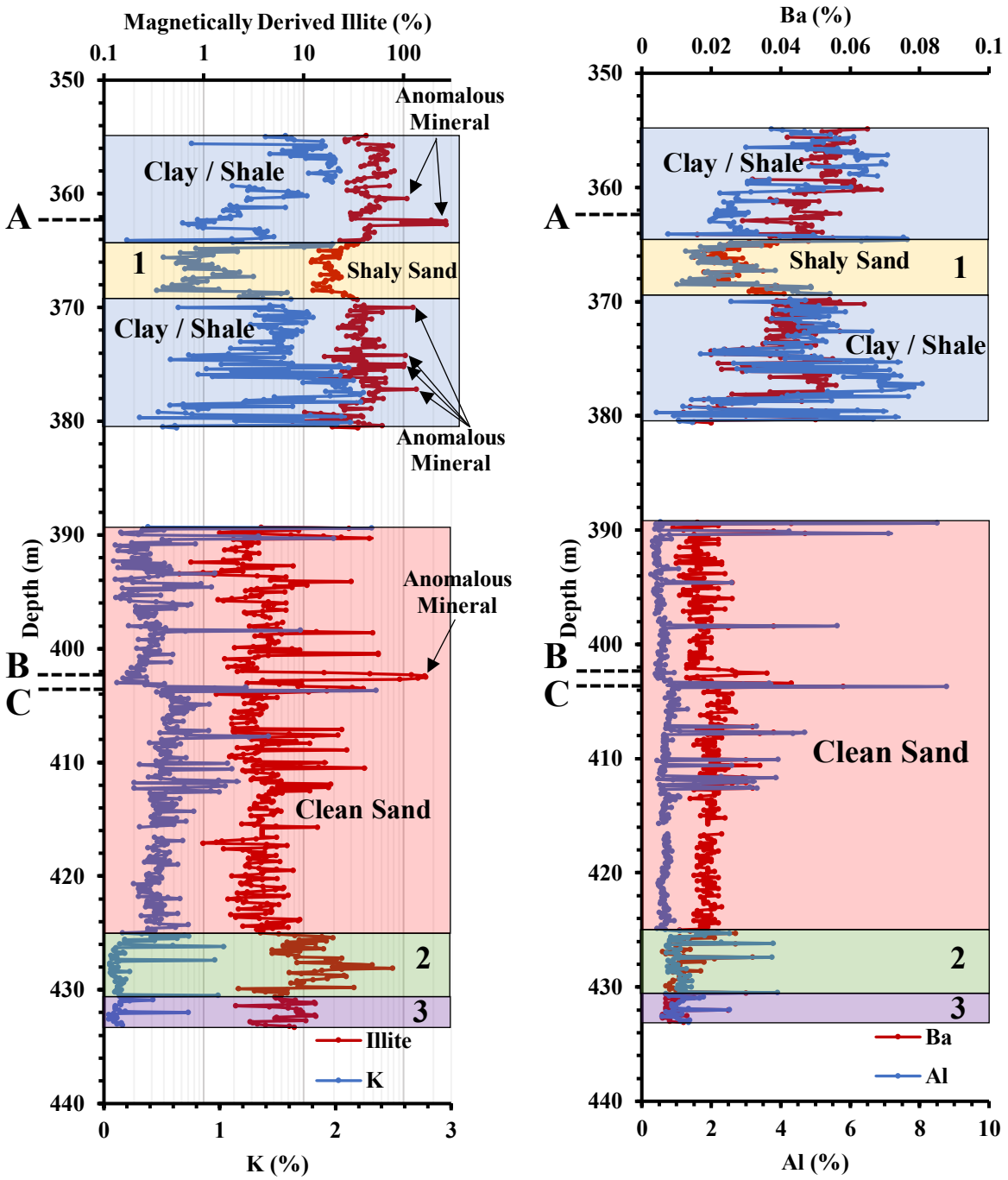


**Figure 4.9**: Well 02 profiles with depth. The left profile shows the K contents (blue curve) measured by XRF and the magnetically derived illite content (red curve), and the right profile shows the Al (blue curve) and Ba (red curve) contents measured by XRF on the slabbed core.

The results from the XRF measurements are also useful in helping to resolve differences between the magnetic and total GR log results. For example, in interval 1 from 364–369 m, the magnetic profile clearly indicates a difference in lithology from the clay intervals above and below, which the total GR log does not (**Figure 4.8**). Smaller positive magnetic susceptibility values suggest that the lithology contains less paramagnetic clay suggesting muddy or shaly sand rather than shale, while the increasing total GR suggests increasing clay mineral content. However, the contents of Fe, K, and Al from the XRF decrease significantly at this interval (**Figures 4.8** and **4.9**), which supports the smaller magnetic susceptibility and thus lower magnetically derived illite contents. In addition, the increase of Si content combined with the more negative deflection of the SP log (**Figure 4.10**) also suggest that the interval is more sand rich and permeable. The spectral K component of the GR logs decreases in this interval (**Figure 4.10**), which is also consistent with lower illite clay. In contrast, the Th and U spectral GR signals (**Figure 4.10**) generally increase in this interval (especially the Th component), and these seem to influence the total GR signal. The results from the XRF measurements, SP log, and spectral K component of the GR all support the interpretation of the lithology (muddy or shaly sand) from the magnetic susceptibility.

In interval 2, the XRF measurements also help to explain the magnetic results and the total GR log data. **Figure 4.8** shows that the total GR in this interval decreases compared to the above clean sands, while the magnetic susceptibilities increase to positive values compared to negative values in the above clean sands. The lower total GR signals suggest clean sands in interval 2, whereas the positive magnetic susceptibility suggests either a muddy sands interval or the presence of another mineral with higher magnetic susceptibility. The XRF results help to resolve

this issue. The Fe and Ca contents from the XRF measurements also increase significantly in interval 2 (**Figure 4.8)**, while the K content decreases (**Figure 4.9**). The significant increased Ca and Fe contents suggest the presence of calcite ($CaCO_3$) with an iron-bearing carbonate mineral (potentially siderite, $FeCO_3$), with the latter causing the increase in magnetic susceptibility rather than there being an increase in illite content in interval 2. The magnetically derived illite content profile of **Figure 4.8** merely assumed that all of the positive part of the magnetic susceptibility signal throughout the well was due to illite, whereas in interval 2 this does not appear to be the case. The lower total GR signal is due to decreased K, Th and U contents in interval 2 (**Figure 4.10**), which is also consistent with a lower illite content rather than an increased illite content. The combination of XRF, probe magnetic results and total GR log data appears to improve the lithology interpretation compared to using traditional GR log data alone.

In interval 3 the magnetic susceptibility decreases compared to interval 2, whereas the total GR increases slightly compared to interval 2. If we were dealing with a simple sand and clay mixture these results would be contradictory (the magnetic susceptibility would suggest clean sand, whereas the total GR would suggest more clay rich sand). However, the mineralogy is not likely to be simply sand and clay in interval 3. The XRF results of **Figure 4.8** indicate (in general) increased Fe and Ca compared with much of the large clean sand interval above. One possibility is that the lithology in interval 3 is a mixture of carbonates (calcite with some siderite, though less siderite than in interval 2 since the magnetic susceptibility is a bit lower in interval 3 compared to interval 2) together with small amounts of heavy minerals and / or organic matter that might account for the slightly increased the GR signal compared to interval 2.

The elemental contents measured by the XRF also support the results of the “anomalous minerals" identified by the magnetic susceptibility, and help to potentially identify its mineralogy. Points exhibiting greater than 100% magnetically equivalent illite content (**Figure 4.9**) correlate with increased elemental Fe content (**Figure 4.8**) suggesting the presence of an iron-bearing mineral. For example, at depths A and B (**Figure 4.8**) both Fe and Ca contents increase dramatically along with the high values of magnetic susceptibility, whereas the total GR signal does not indicate any significant difference. The XRF and magnetic susceptibility results suggest that the “anomalous mineral” at depths A and B could again be siderite.

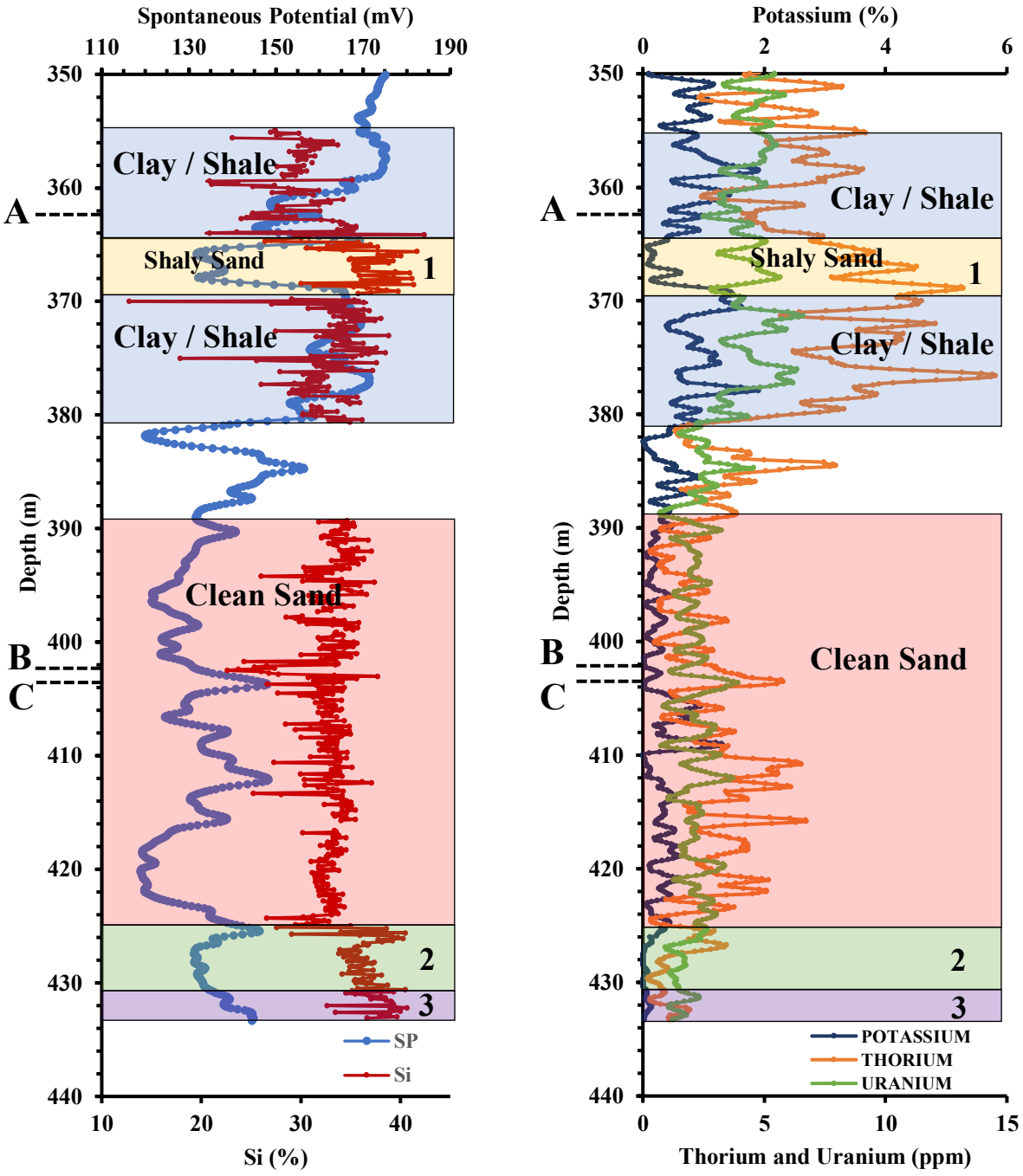


**Figure 4.10**: Well 02 profiles with depth. The left plot shows the downhole SP log (blue curve) and the Si elemental contents measured by the XRF technique (red curve) on the slabbed core. The right plot shows the downhole spectral gamma ray logs.

In contrast, at depth C the XRF results show increases in the Fe (**Figure 4.8**), K and Al elemental contents (**Figure 4.9**), which is consistent with increasing illite clay content. In this case the magnetically derived illite content is estimated to be around 40%, and the total GR increases (**Figure 4.8**), and so all these results suggest an increased illite content at depth C.

### b) Crossplots of XRF and magnetic results

The key elemental contents measured by the XRF technique were plotted against the depth-matched magnetically derived illite contents. Each relationship is plotted in two different cases: (A) includes all the data points from the cored intervals, and (B) includes all data points in the clean sand and shale / clay intervals above a depth of 425 m. Below 425 m (i.e., below intervals 2 and 3) the combined magnetic and XRF results suggested different lithologies containing minerals such as the iron carbonate siderite as detailed in section **4.5.2 (a)** above.

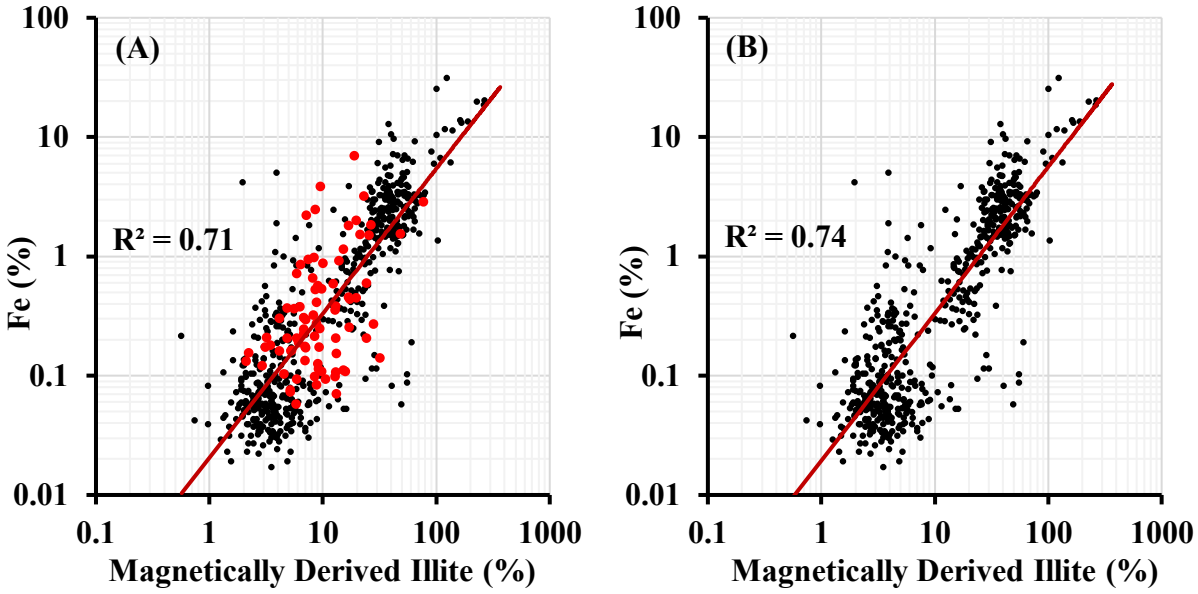


**Figure 4.11**: Well 02 crossplots of Fe contents measured by the XRF technique and magnetically derived illite contents. **(A)** includes all the data points from the cored intervals in the well, and the red points are the data in the proposed different lithology intervals 2 and 3 below a depth of 425 m. **(B)** only includes the data points in the sand and shale / clay intervals above 425 m.

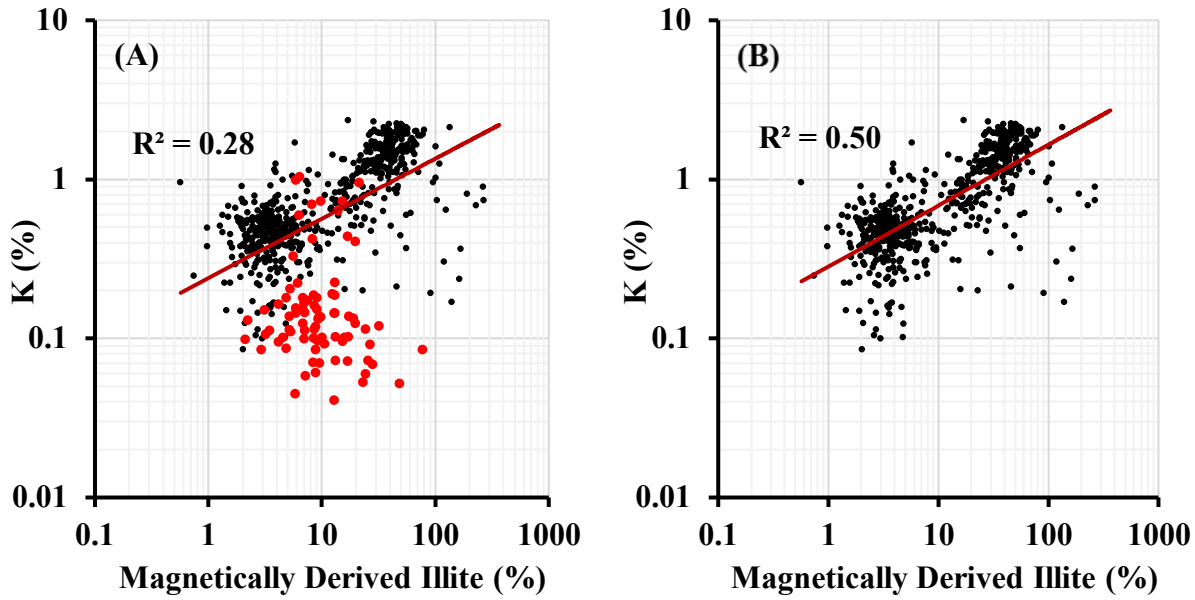


**Figure 4.12**: Well 02 crossplots of K contents measured by the XRF technique and magnetically derived illite contents. **(A)** includes all the data points from the cored intervals in the well, and the red points are the data in the proposed different lithology intervals 2 and 3 below a depth of 425 m. **(B)** only includes the data points in the sand and shale / clay intervals above 425 m.

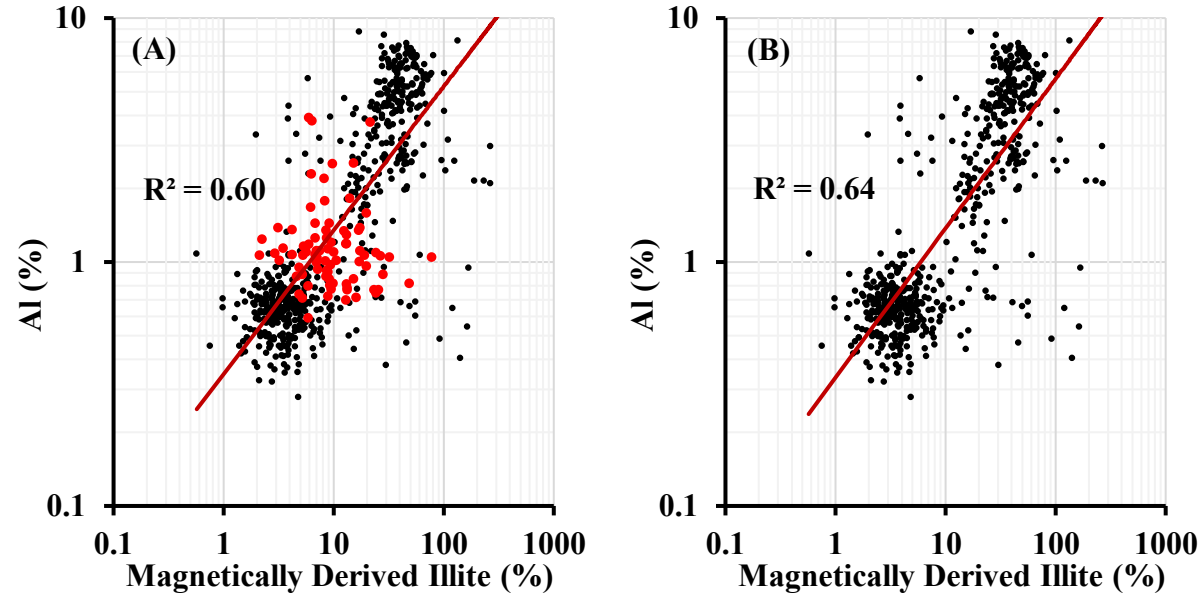


**Figure 4.13**: Well 02 crossplots of Al contents measured by the XRF technique and magnetically derived illite contents. **(A)** includes all the data points from the cored intervals in the well, and the red points are the data in the proposed different lithology intervals 2 and 3 below a depth of 425 m **(B)** only includes the data points in the sand and shale / clay intervals above 425 m.

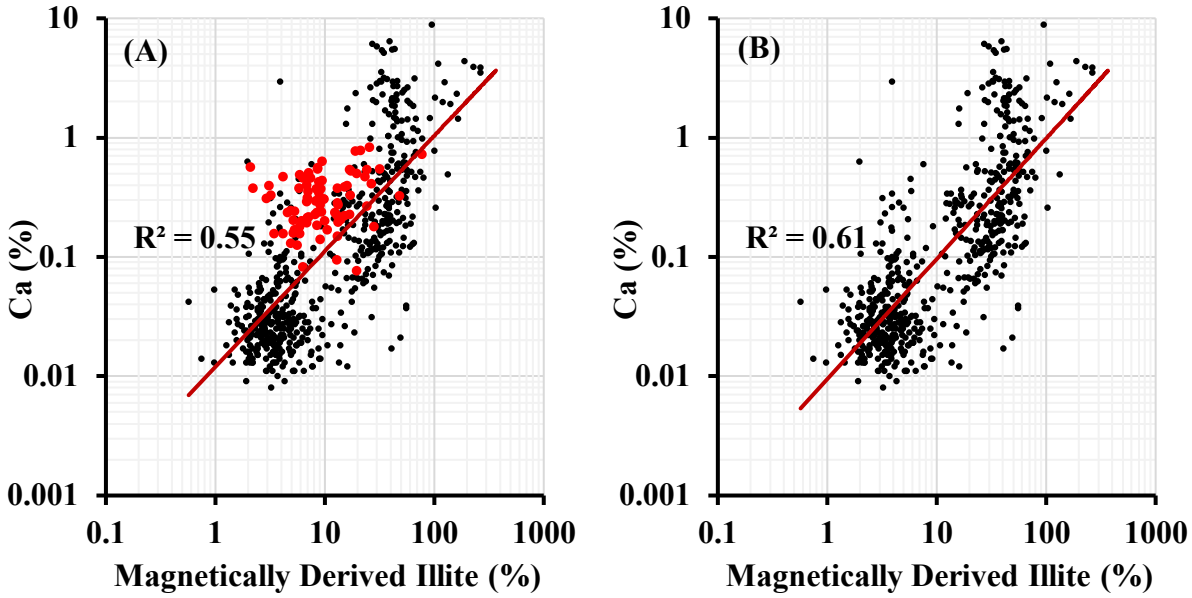


**Figure 4.14**: Well 02 crossplots of Ca contents measured by the XRF technique and magnetically derived illite contents. **(A)** includes all the data points from the cored intervals in the well, and the red points are the data in the proposed different lithology intervals 2 and 3 below a depth of 425 m. **(B)** only includes the data points in the sand and clay intervals above 425 m.

All the crossplots (**Figures 4.11**–**4.14**) show a general correspondence between the elemental contents of Fe, K, Al and Ca from the XRF measurements and the magnetically derived illite contents. Increasing elemental contents correspond with increasing illite contents, which would be expected for illite which contains the elements Fe, K and Al. The plots for Fe, K, and Al clearly distinguish the data points into two different clusters in the **(B)** cases for clean sand and shale / clay when the points (red points) for the proposed different lithologies in intervals 2 and 3 below 425 m have been removed. The lower cluster in each of the **(B)** cases represents the clean sand interval with less than 10% of magnetically derived illite and the percentages of Fe, K, and Al being less than about 0.4%, 1%, and 1%, respectively. The upper cluster represents the shale / clay interval with more than 10% of magnetically derived illite and the Fe, K, and Al contents being generally more than 1%, 1% , and 2%, respectively. The $R^2$ regression coefficient values of all the plots increase with the removal of the data points (red points) from the proposed different

lithologies in intervals 2 and 3 below 425 m. The $R^2$ value increases from 0.71 to 0.74 for the Fe content crossplots (**Figure 4.11**), increases from 0.28 to 0.5 for the K content crossplots (**Figure 4.12**), and increases from 0.60 to 0.64 for the Al content crossplots (**Figure 4.13**). The dramatic difference in the $R^2$ values between **Figures 4.12 (A)** and **(B)** is due mainly to the removal of the lower K content points in the proposed different lithologies in intervals 2 and 3 below depth 425 m. **Figure 4.12 (A)** shows that the data points (highlighted in red) belonging to these proposed different lithologies below 425 m are located in a distinct region with the lowest K contents, thus indicating the usefulness of this plot in particular for identifying and isolating these proposed different lithologies.

**c) Crossplots of the XRF results and GR log data**

The elemental contents measured by the XRF technique were crossplotted with the depth-matched GR log data. These semi-log plots generally show good relationships between the total GR signals and the elemental contents of Fe, K, and Al (**Figures 4.15**–**4.17**). The $R^2$ values are again improved if the data points (red points in the **(A)** plots) from the proposed different lithology intervals 2 and 3 below 425 m are removed (in the **(B)** plots). The $R^2$ regression coefficients in these **(B)** plots are reasonably high in all 3 cases, particularly for Al and K. This would be expected if much of the core from this well contains varying amounts of illite clay, since all 3 of these elements are components of illite. The $R^2$ value for the Fe plot is a bit lower, which may partly be due to high Fe content in the thin "anomalous mineral" layers identified by the magnetic technique. In contrast, the relationship between total GR and Ca content is weak (**Figure 4.18**).

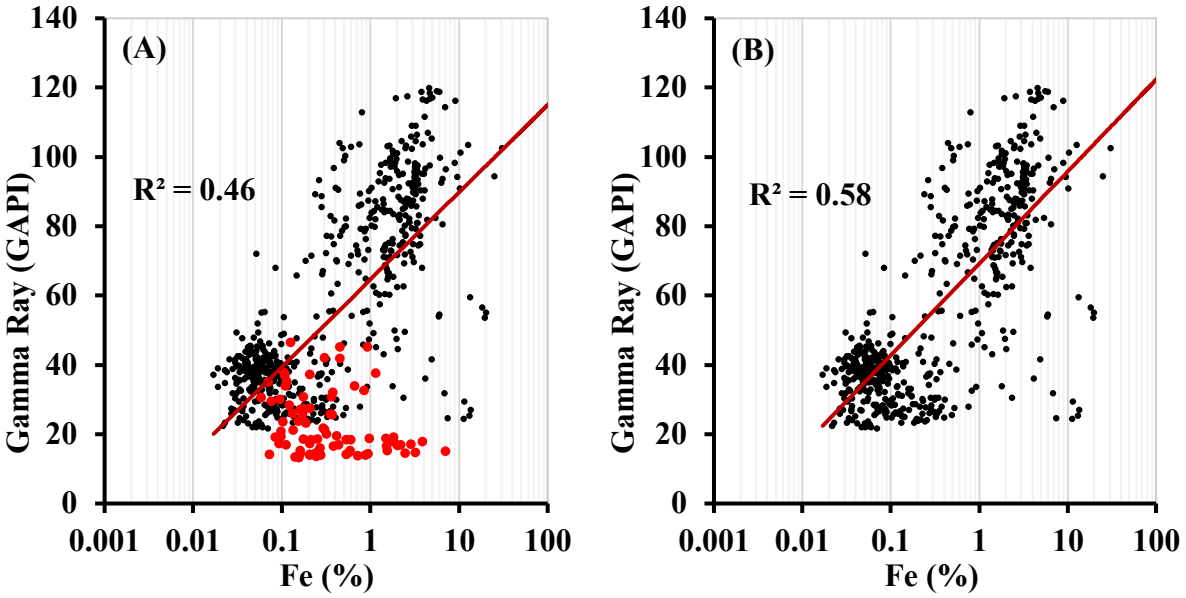


**Figure 4.15**: Well 02 crossplots of Fe contents from XRF and depth-matched total GR log data. **(A)** includes all data points from the cored intervals, and the red points are from the proposed different lithology intervals 2 and 3 below 425 m. **(B)** only includes data points in the sand and shale / clay intervals above 425 m.

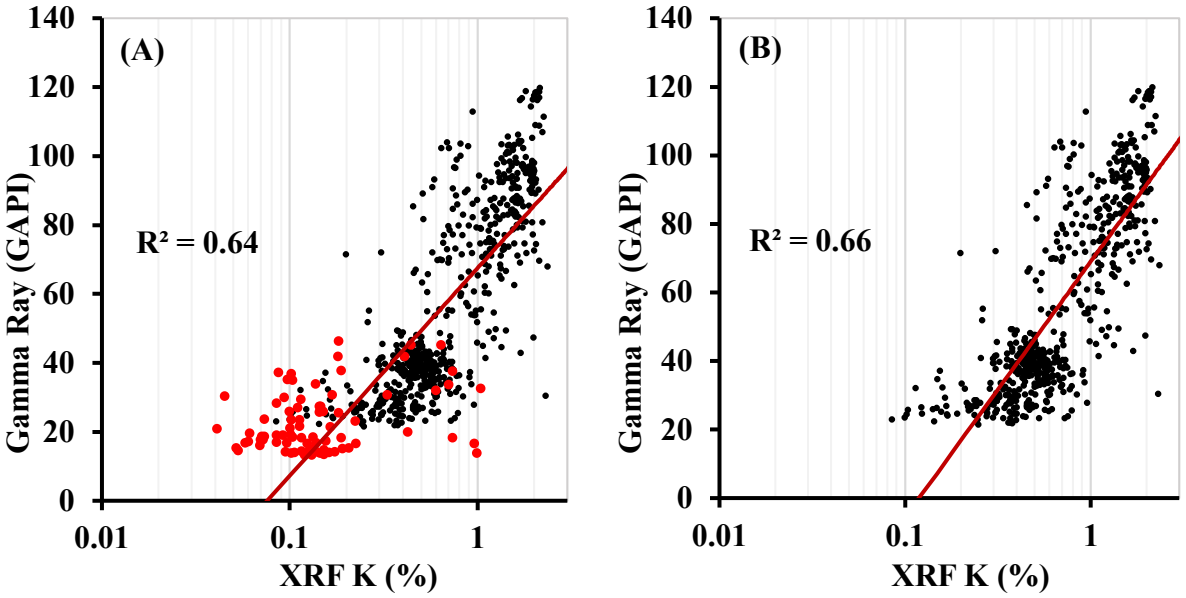


**Figure 4.16**: Well 02 crossplots of K contents from XRF and depth-matched total GR log data. **(A)** includes all data points from the cored intervals, and the red points are from the proposed different lithology intervals 2 and 3 below 425 m. **(B)** only includes data points in sand and shale / clay intervals above 425 m.

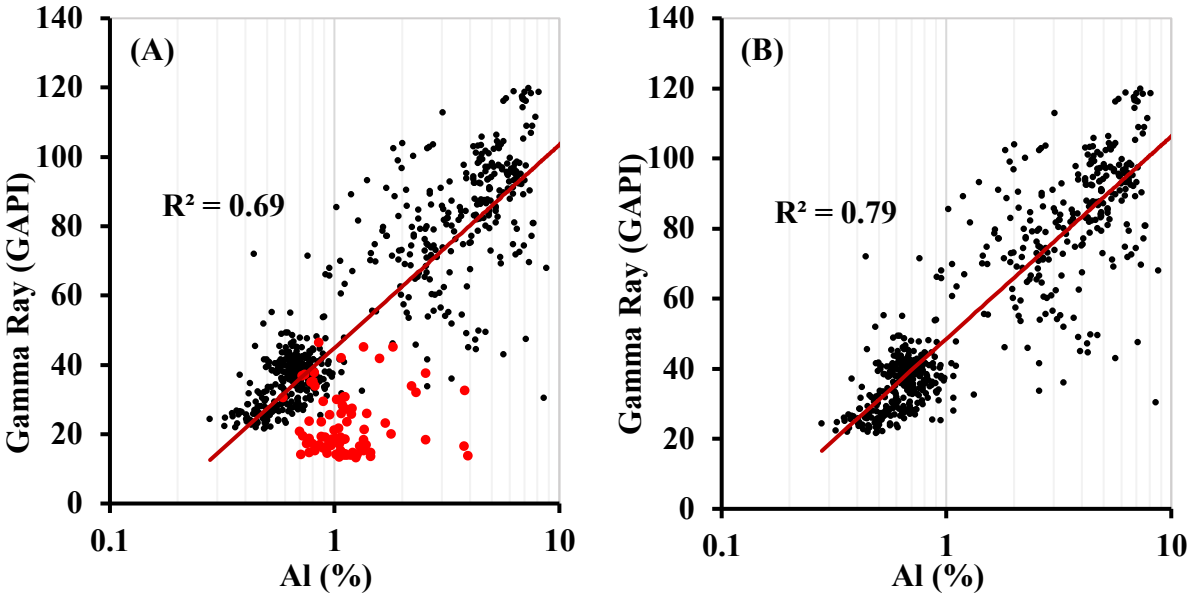


**Figure 4.17**: Well 02 crossplots of Al contents from XRF and depth-matched total GR log data. **(A)** includes all data points from the cored intervals, and the red points are from the proposed different lithology intervals 2 and 3 below 425m. **(B)** only includes data points in the sand and shale / clay intervals above 425 m.

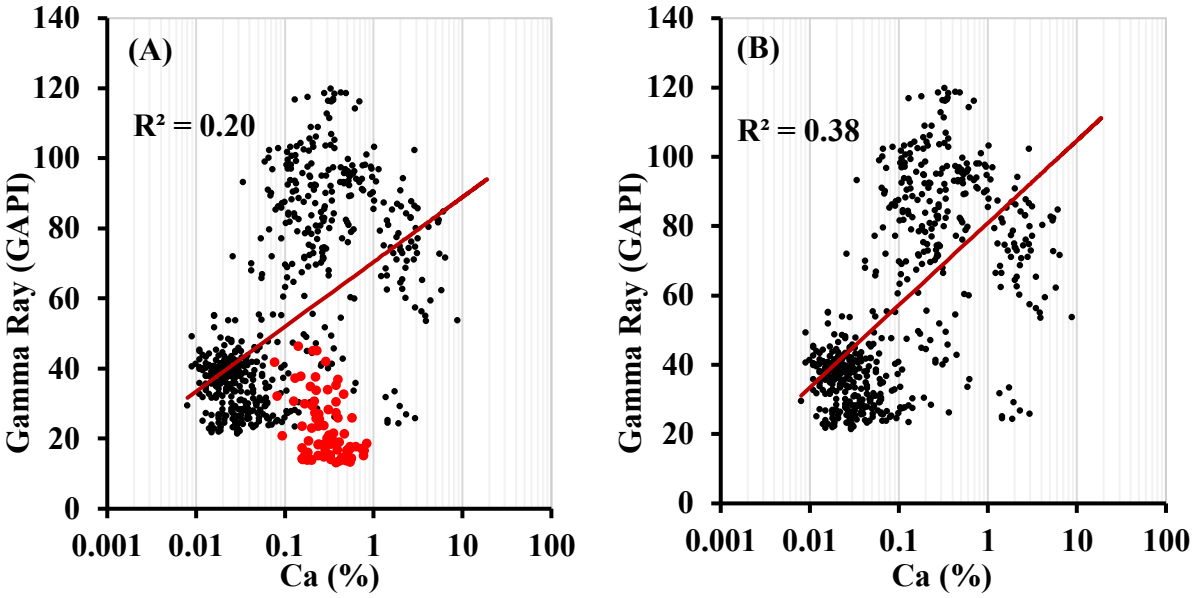


**Figure 4.18**: Well 02 crossplots of Ca contents from XRF and depth-matched total GR log data. **(A)** includes all data points from the cored intervals, and the red points are from the proposed different lithology intervals 2 and 3 below 425 m. **(B)** only includes data points in sand and shale / clay intervals above 425 m.

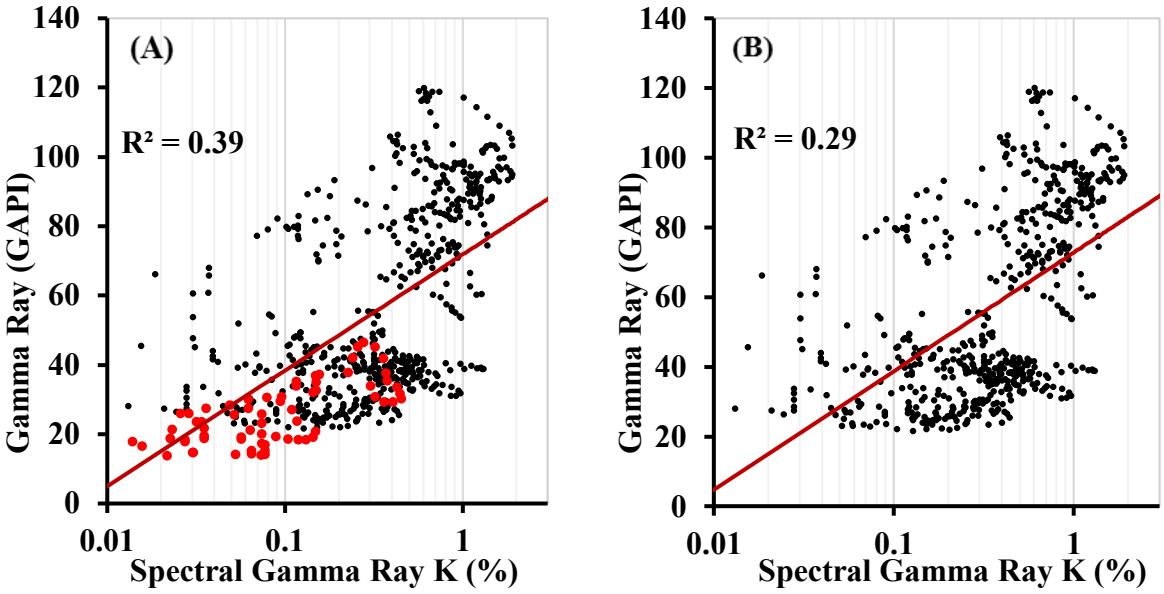


**Figure 4.19**: Well 02 crossplots of K contents from the spectral GR log (horizontal axis) and depth-matched total GR log data (vertical axis). **(A)** includes all data points from the cored intervals, and the red points are from the proposed different lithology intervals 2 and 3 below 425 m. **(B)** only includes data points in the sand and shale / clay intervals above 425 m.

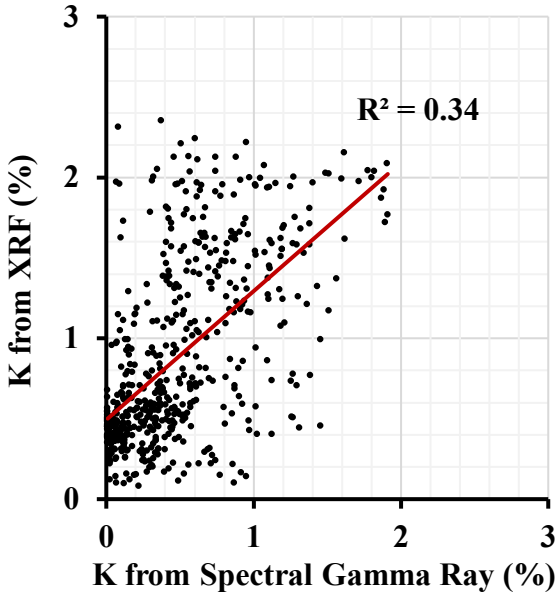


**Figure 4.20**: Well 02 crossplots of K contents from the spectral GR log (horizontal axis) and depth-matched K from XRF measurements (vertical axis).

The $R^2$ values of the crossplots between the downhole total GR and downhole spectral gamma ray K (**Figure 4.19**) are surprisingly lower than those between the downhole total GR and K

measured by XRF (**Figure 4.16**). **Figure 4.20** shows the crossplot between the K contents measured by the XRF technique and the depth-matched K contents from the downhole spectral gamma ray log. Although the K content from XRF generally increases as the K content from the downhole spectral GR increases, the $R^2$ value is quite low. This may be partly due to each technique measuring the K content at a different scale. Each XRF measurement represents the K content from a 3mm diameter spot on the slabbed core, whilst each K content from the downhole spectral GR represents an average value from around 1 foot vertically and about 1 foot into the formation rock (i.e., about a cubic foot of rock).

The crossplots in **Figures 4.15**–**4.17** clearly show two different clusters of the data points that could be potentially used for mineralogy / lithology discrimination. The lower cluster represents the clean sand interval with a total GR signal less than about 50 API and less than about 0.4%, 1%, and 1% of Fe, K, and Al respectively. In contrast, the upper cluster represents the shale / clay interval data points with higher total GR values and higher percentages of the elements. The crossplots in **Figures 4.15**–**4.18** also distinguish the data points (red points) of the proposed different lithology intervals 2 and 3 below 425 m.

**d) Crossplots between XRF derived elemental contents**

In this section the elemental contents of Fe, Ca, Al, and K from XRF measurements are cross-plotted against each other (**Figures 4.21**–**4.26**). Again the crossplots show two different cases: **(A)** includes all the data points from the cored intervals, and **(B)** excludes the data points (red points in **(A)**) from the proposed different lithology intervals 2 and 3 below 425 m. By excluding these points the $R^2$ values increase in all cases.

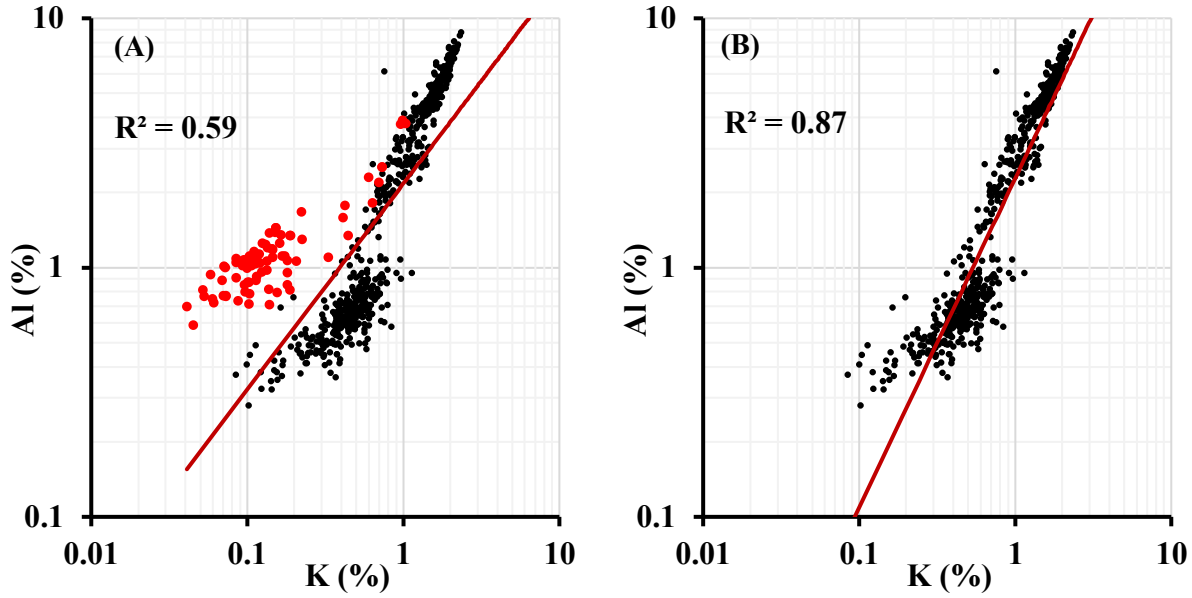


**Figure 4.21**: Well 02 crossplots between K and Al contents measured by the XRF technique. **(A)** includes all data points from the cored intervals, and the red points are from the proposed different lithology intervals 2 and 3 below 425 m. **(B)** only includes data points in the sand and shale / clay intervals above 425 m.

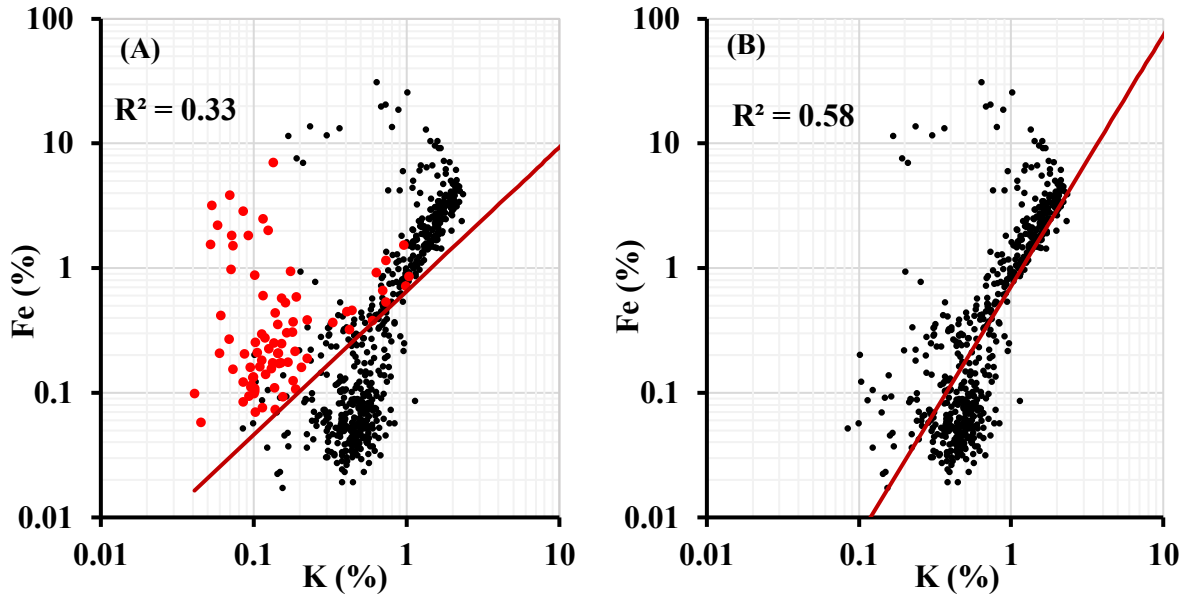


**Figure 4.22**: Well 02 crossplots between K and Fe contents measured by the XRF technique. **(A)** includes all data points in the cored intervals, and the red points are data in the proposed different lithology intervals 2 and 3 below 425 m. **(B)** only includes data points in the sand and shale / clay intervals above 425 m.

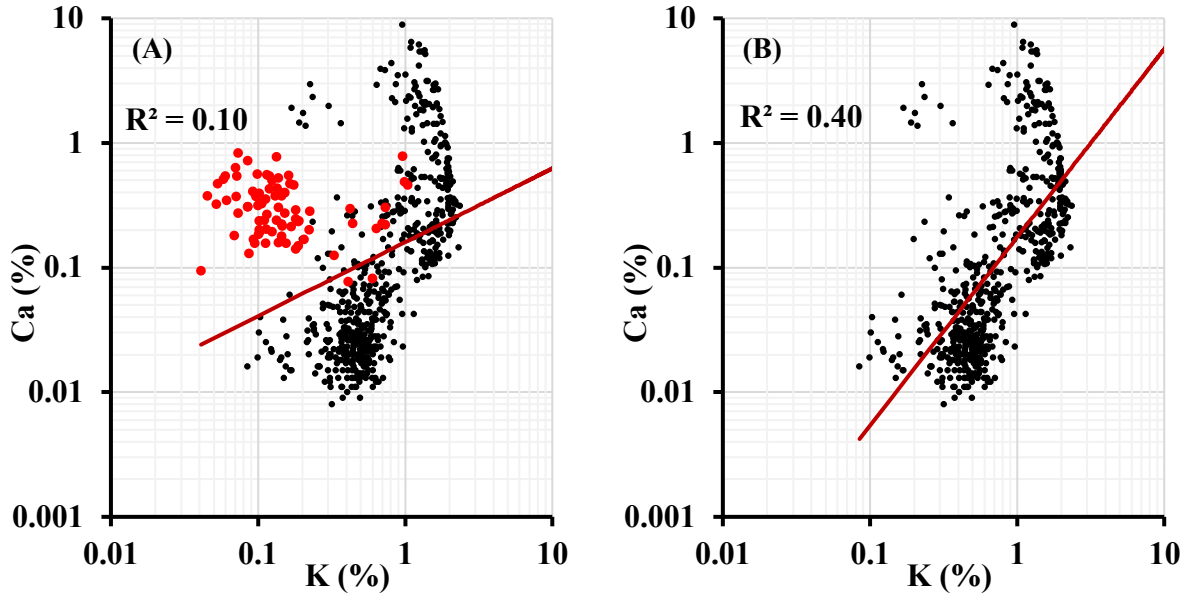


**Figure 4.23**: Well 02 crossplots between K and Ca contents measured by the XRF technique. **(A)** includes all data points in the cored intervals, and the red points are from the proposed different lithology interval 2 and 3 below 425 m. **(B)** only includes data points in the sand and shale / clay intervals above 425 m.

The crossplots indicate strong relationships between the elements K, Al, and Fe in the sand and shale / clay intervals. The $R^2$ values of Al with K and Fe are 0.87 and 0.76 (**(B)** plots of **Figures 4.21** and **4.24**) respectively, and the $R^2$ value of K and Fe is 0.58 (**(B)** plot of **Figure 4.22**). In contrast, the $R^2$ values indicate poorer relationships between Ca with K and Al (**Figures 4.23** and **4.25**). The strong relationships between the elements Fe, K, and Al suggest that the primary clay mineral is illite, which includes these 3 elements in its chemical composition.

The plots between K and Al (**Figure 4.21**), K and Fe (**Figure 4.22**), and K and Ca (**Figure 4.23**) all appear to be capable of differentiating the lower proposed different lithology points of intervals 2 and 3 (red points in the **(A)** plots of these figures). This is mainly due to the lower K contents of these intervals (as shown in the right hand plot of **Figure 4.10**).

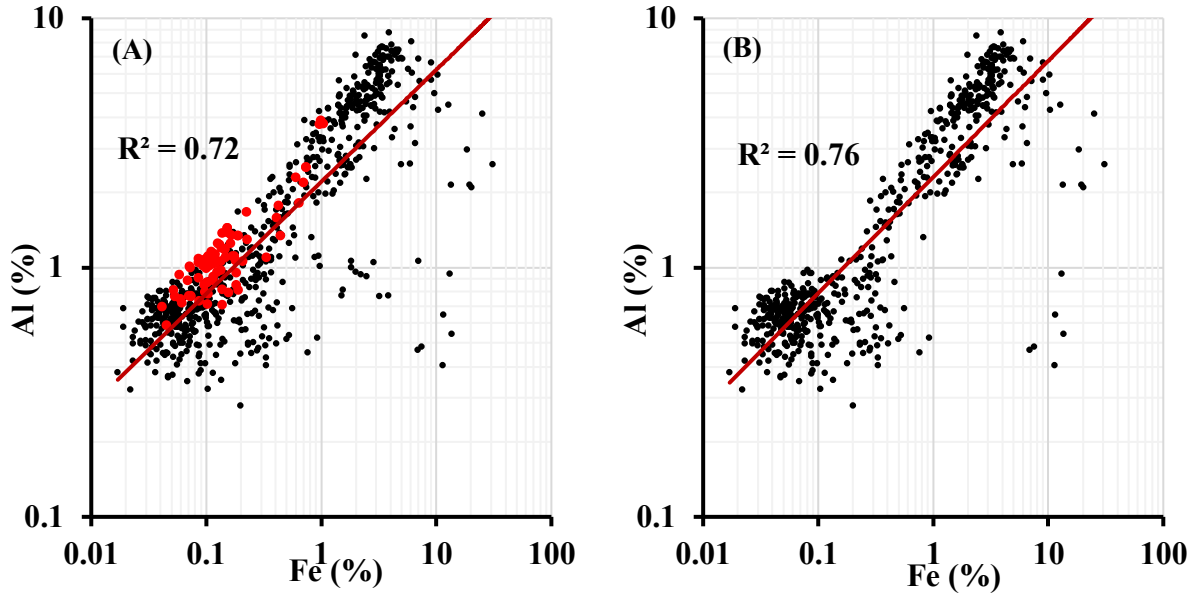


**Figure 4.24**: Well 02 crossplots between Fe and Al contents measured by the XRF technique. **(A)** includes all data points in the cored intervals, and the red points are from the proposed different lithology intervals 2 and 3 below 425 m. **(B)** only includes data points in the sand and shale / clay intervals above 425 m.

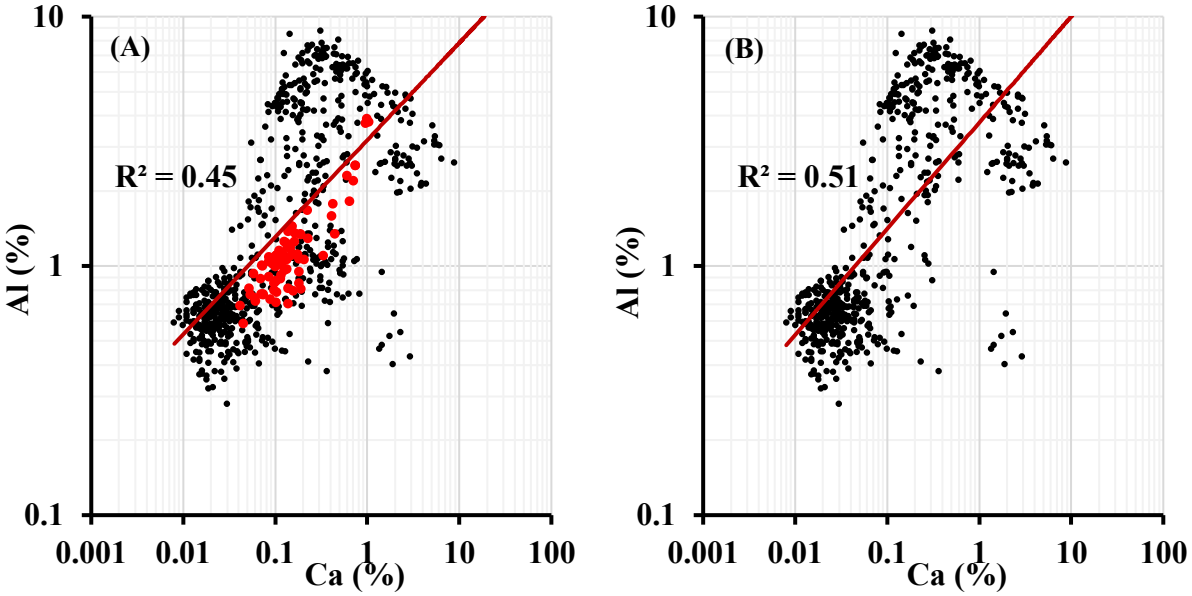


**Figure 4.25**: Well 02 crossplots between Ca and Al contents measured by the XRF technique. **(A)** includes all data points in the cored intervals, and the red points are from the proposed different lithology intervals 2 and 3 below 425 m. **(B)** only includes data points in the sand and shale / clay intervals above 425 m.

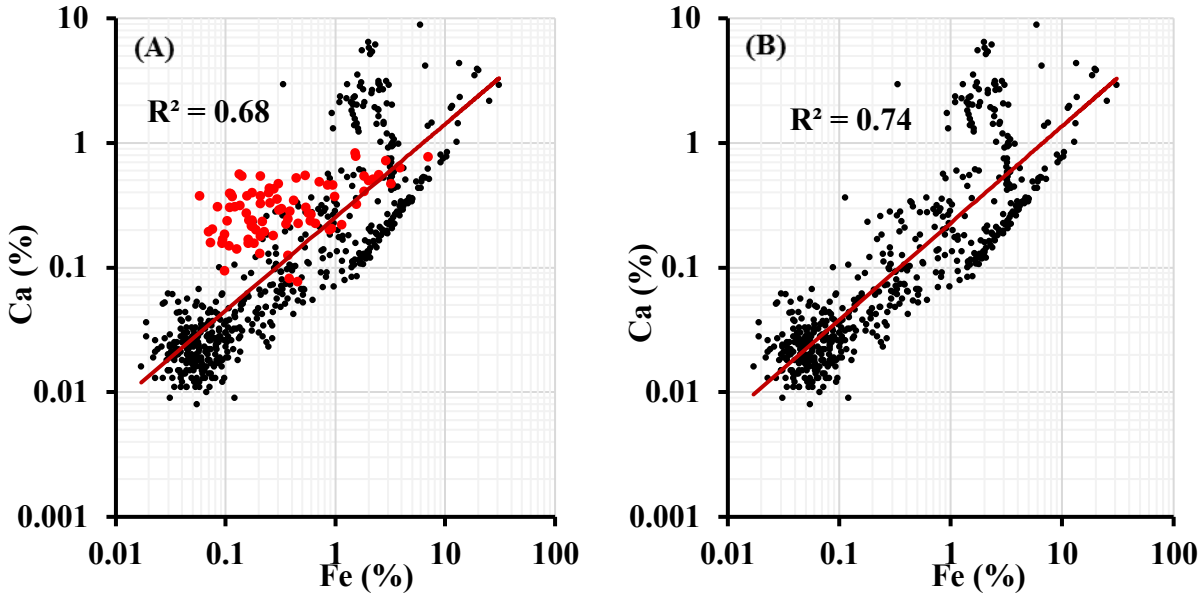


**Figure 4.26**: Well 02 crossplots between Fe and Ca contents measured by the XRF technique. **(A)** includes all data points in the cored intervals, and the red points are from the proposed different lithology intervals 2 and 3 below 425 m. **(B)** only includes data points in the sand and shale / clay intervals above 425 m.

### 4.5.3. XRF results and comparisons of Well 03

#### a) Profile comparisons with depth

The magnetic susceptibility profile characterized the slabbed cores of Well 03 into three different lithology intervals: clay / shale, IHS beds, and clean sands (left profile of **Figure 4.27**). The profiles of the Fe, K and Al elemental contents from the XRF measurements show correspondences with the magnetic results (**Figures 4.27** and **4.28**). The percentages of Fe, K, and Al are higher in the clay / shale interval and lower in the clean sands interval, being generally 2–7%, 1–2% and 3–7% respectively in the clay / shale interval, and generally <0.5%, <1% (most <0.6%) and <1% respectively in the clean sand interval, although there are some exceptions. In the IHS beds the values are intermediate between the clay / shale and clean sand intervals, with Fe, K and Al having contents of 0.1–1%, 0.2–1% and 0.5–3% respectively. The values vary within these ranges in the IHS beds due to the interbeded layers of sand and clay.

The profiles of the elemental contents of Fe (**Figure 4.27**), K and Al (**Figure 4.28**) show clear correspondences with the magnetically derived illite content (**Figure 4.28**). This is consistent with these 3 elements all being components of illite.

The profiles show a poor correspondence of the Fe, K and Al elemental contents as measured by XRF with the total downhole GR signals in the IHS beds between depths of 162–168 m. The low total GR in this interval could misinterpret the lithology as clean sand. However, as discussed in **Chapter 3**, and shown again in **Figure 4.28**, the total GR signals are affected by the Th and U signals in this interval. In contrast, the magnetic susceptibility profile with small positive susceptibilties (**Figure 4.27**) which translated to about 3–13% magnetically derived illite content (**Figure 4.28**) clearly indicated IHS beds within this interval of 162–168 m. The XRF profiles of Fe, K and Al showed a correspondence with the magnetic susceptibility and magnetically derived illite profiles and thus supported the lithological characterization of IHS beds by the magnetic susceptibility. This example also indicates the usefulness of magnetic susceptibility and XRF to improve the reservoir characterization, instead of relying on interpretations based solely on the total GR log (especially if the spectral gamma ray logs are not available).

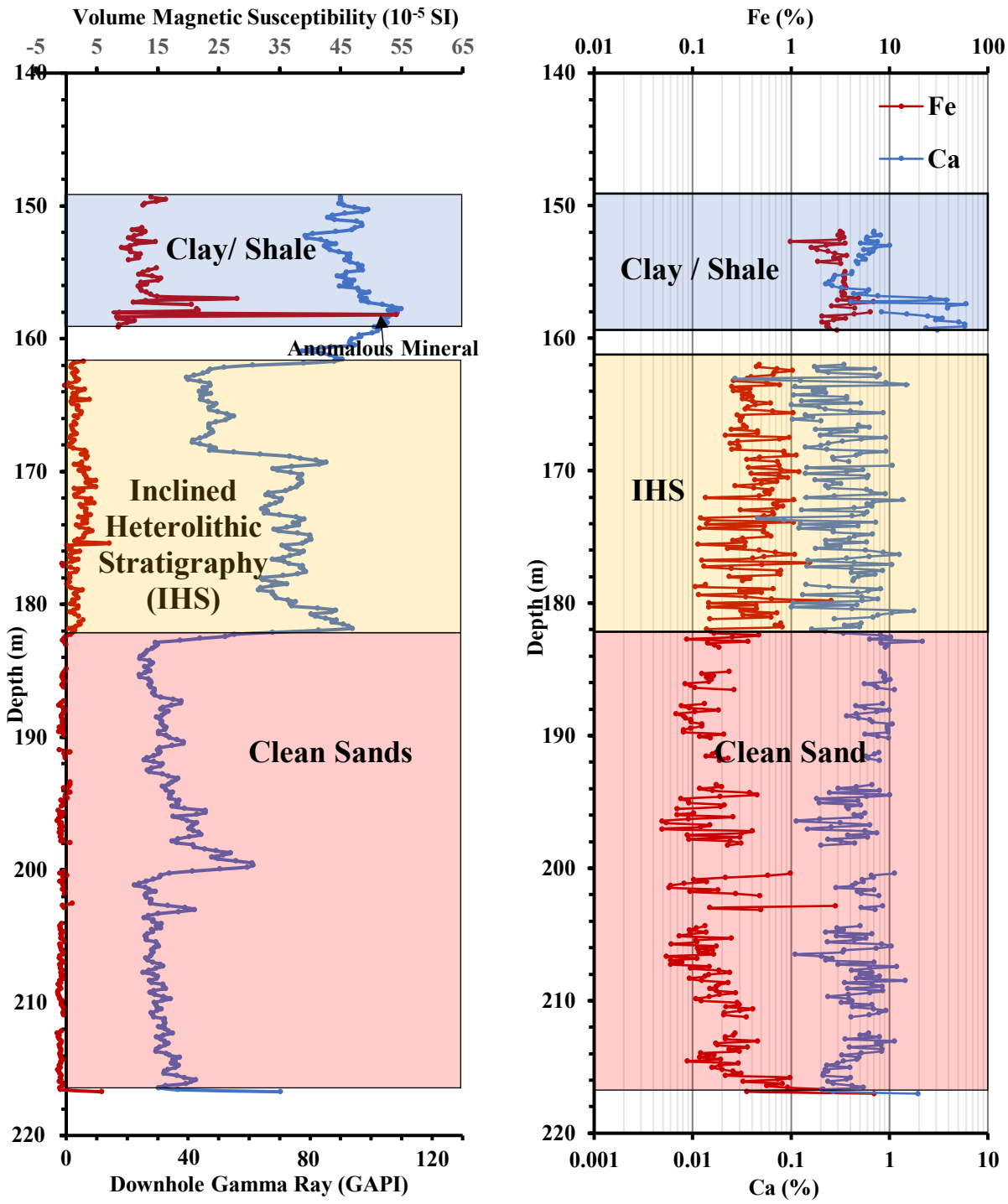


**Figure 4.27**: Well 03 profiles with depth. The left plot shows the probe volume magnetic susceptibility profile (red curve) on the slabbed core and the depth-matched downhole total GR log (blue curve). The right plot shows the Fe (red curve) and Ca (blue curve) elemental contents measured on the slabbed cores by the XRF technique.

The Ca XRF profile (**Figure 4.27**) does not show a good correspondence with the magnetic susceptibility or downhole total GR, and this may be expected in Well 03 since the 3 main lithologies are related to varying amounts of sand and paramagnetic clay (illite). The Ba XRF profile (**Figure 4.28**) shows higher values in the clay / shale compared to the IHS beds and the clean sand, although all the values are very low. The Si XRF profile (**Figure 4.29**) shows lower values in the clay / shale interval and higher values in the more sand rich IHS beds and clean sand intervals as expected.

The XRF measurements also supported the identification of a thin layer of an "anomalous mineral" from the magnetic results at a depth of 158 m as detailed in **Chapter 3**. At this depth the magnetic susceptibility results (**Figure 4.27**) indicated a thin layer of an "anomalous mineral" with over 100% estimated illite content (**Figure 4.28**), and the XRF results show significant increases of Fe, K and Al contents (**Figures 4.27 - 4.28**). The Ca content from XRF is also higher at this depth. These combined results suggest increased illite content with some iron carbonate (such as siderite).

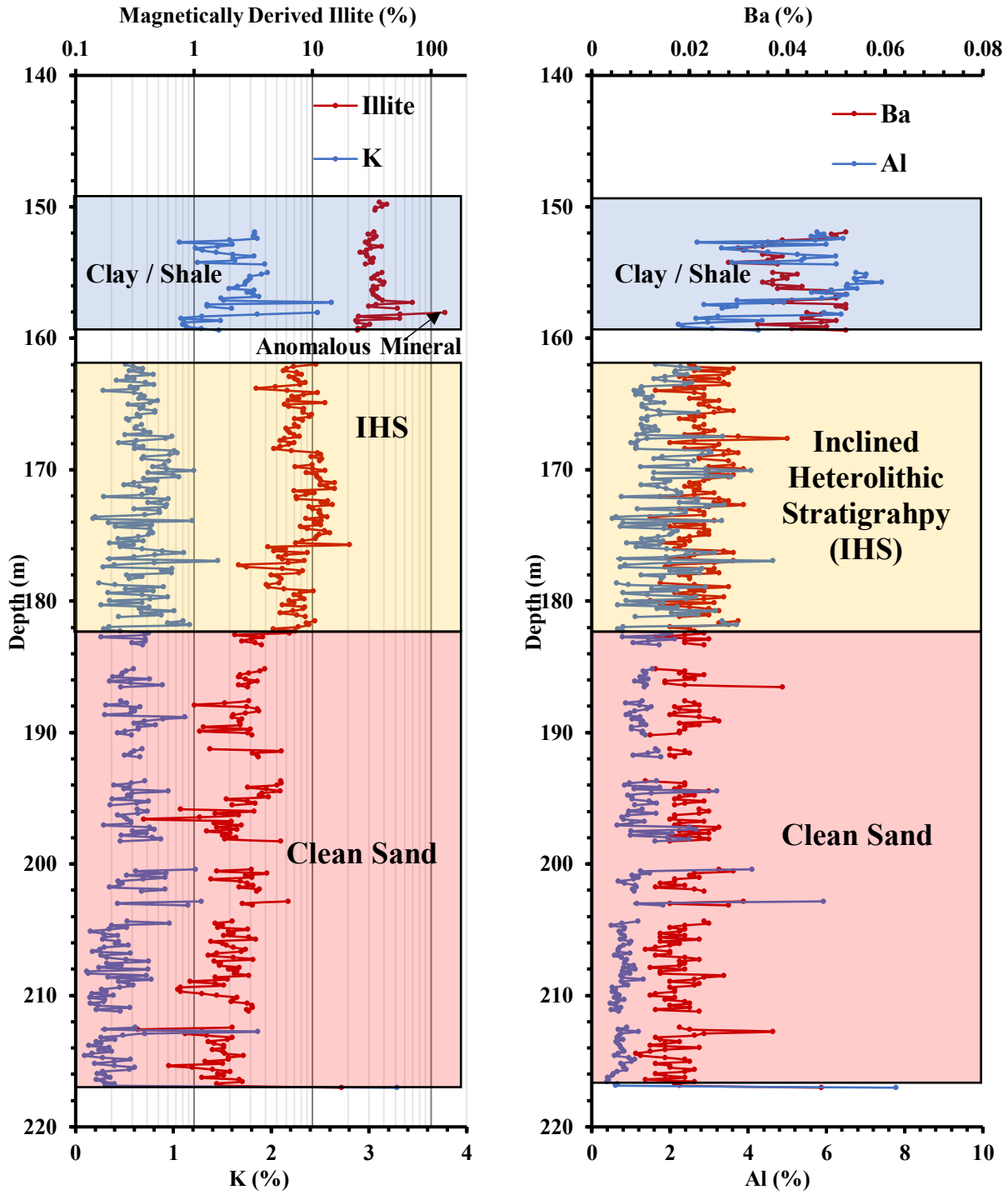


**Figure 4.28**: Well 03 profiles with depth. The left plot shows the magnetically derived illite content (red curve) and the depth-matched K elemental content from XRF (blue curve) on the slabbed cores. The right plot shows the Ba (red curve) and Al (blue curve) elemental contents measured on the slabbed cores by the XRF technique.

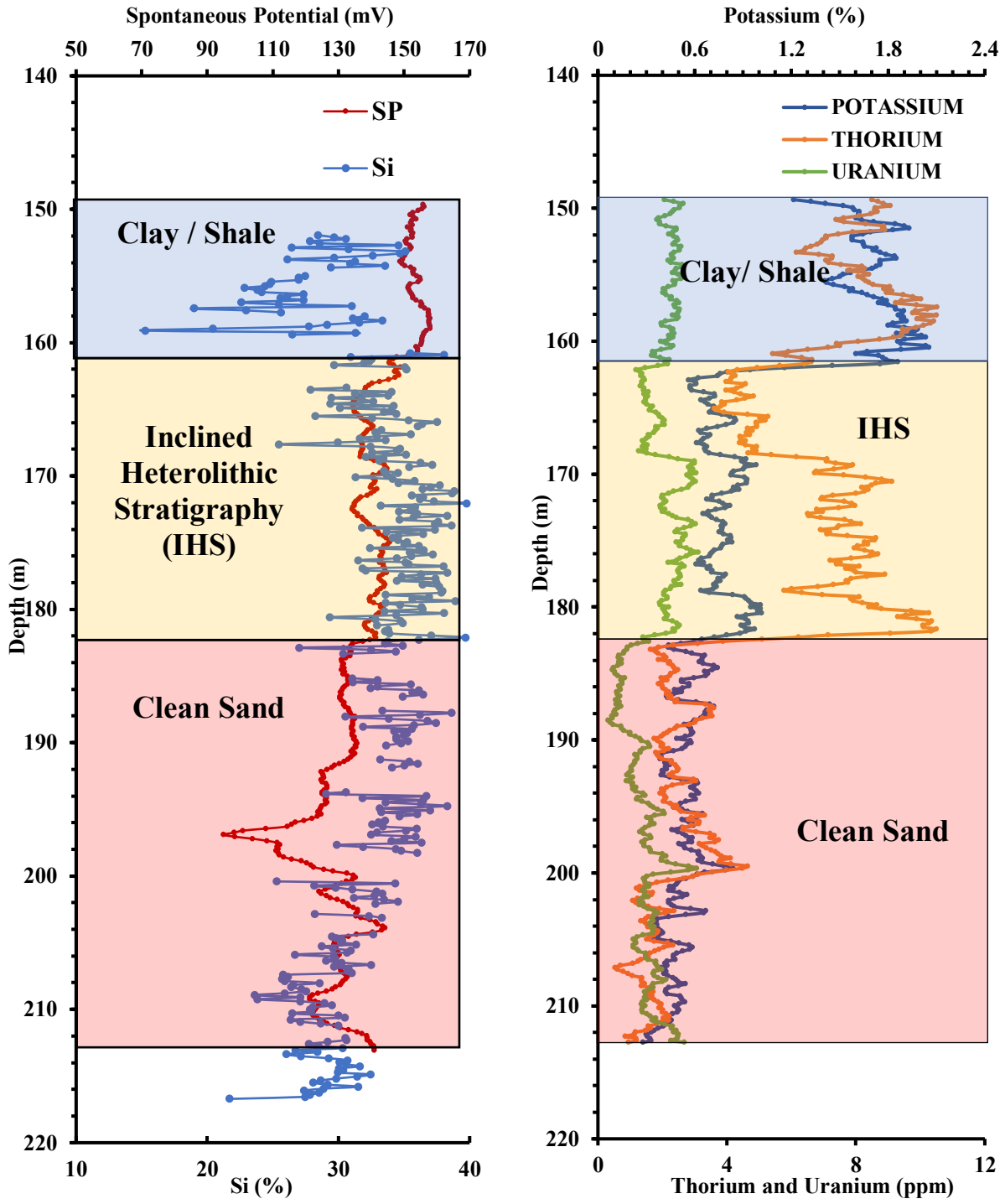


**Figure 4.29**: Well 03 profiles with depth. The left plot shows the SP log (red curve) and the Si elemental content from XRF (blue curve) on the slabbed cores. The right plot shows the potassium (blue curve), thorium (orange curve) and uranium (green curve) contents from the spectral GR logs.

**b) Crossplots of XRF results and magnetically derived illite content**

The elemental contents measured by the XRF technique were crossplotted against the depth-matched magnetically derived illite contents to quantify the relationships between them (**Figure 4.30**).

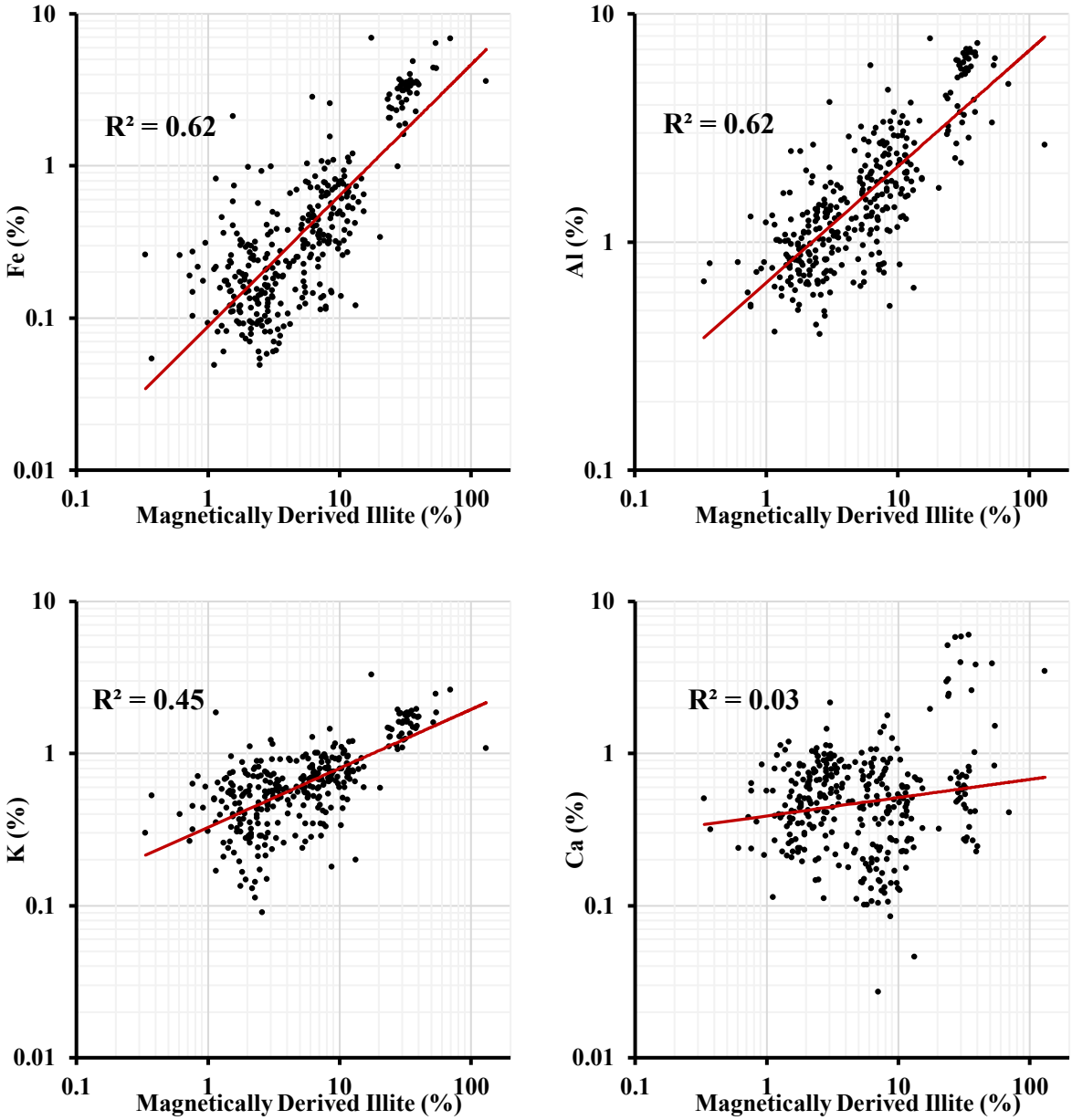


**Figure 4.30**: Well 03 crossplots of the magnetically derived illite contents against the Fe, Al, K, and Ca contents measured by the XRF technique on the slabbed cores.

The crossplots of **Figure 4.30** clearly show increasing Fe, Al, and K contents with higher magnetically derived illite content, consistent with these elements being components of illite. The $R^2$ regression coefficient is 0.62 between the magnetically derived illite content and both Fe and Al elemental contents, but a bit lower at 0.45 between the magnetic results and K content. In contrast, there is no correspondence between Ca contents and the magnetic results.

The crossplots also show clusters of data points which represent different lithologies. The clay / shale region is distinguished from the other lithologies with generally more than 20% magnetically derived illite content and more than 2%, 1%, and 3% of Fe, K and Al respectively. In this well the clean sand and IHS bed data tends to merge into one large cluster, although in general the clean sand has <4% magnetically derived illite content and <0.5%, <1% and <1% of Fe, K and Al respectively, whereas the IHS beds generally have around 4-15% magnetically derived illite content and 0.1–1% (mainly above 0.2%) Fe, 0.2–1% K and 0.5–3% Al.

**c) Crossplots of XRF results and downhole gamma ray log data**

**Figure 4.31** shows that the elemental contents of Fe, K and Al generally increase with a higher total GR signal. The relationships appear not to be as strong as those between these elements and the magnetically derived illite content (**Figure 4.30**), however the crossplots in **Figure 4.31** are on a semi-log plot rather than the log-log plots of **Figure 4.30**. Also the GR log data averages over a larger volume scale than the averaging of the discrete probe magnetic and XRF core measurements, despite averaging the core measurements over the same vertical interval as the log data. The crossplots for Fe, K and Al in **Figure 4.31** appear to show 3 clusters of points (which would be expected to represent clean sands, IHS beds and clay / shale), however as

discussed earlier the total GR did not pick out the IHS beds in the interval 162–168 m and points in this interval have low total GR values which could be misinterpreted as clean sand. **Figure 4.31** also shows a poor correlation between the total GR signals and the elemental content of Ca, suggesting carbonates are less important in Well 03 and that Ca is not so useful for characterizing the reservoir properties in this well.

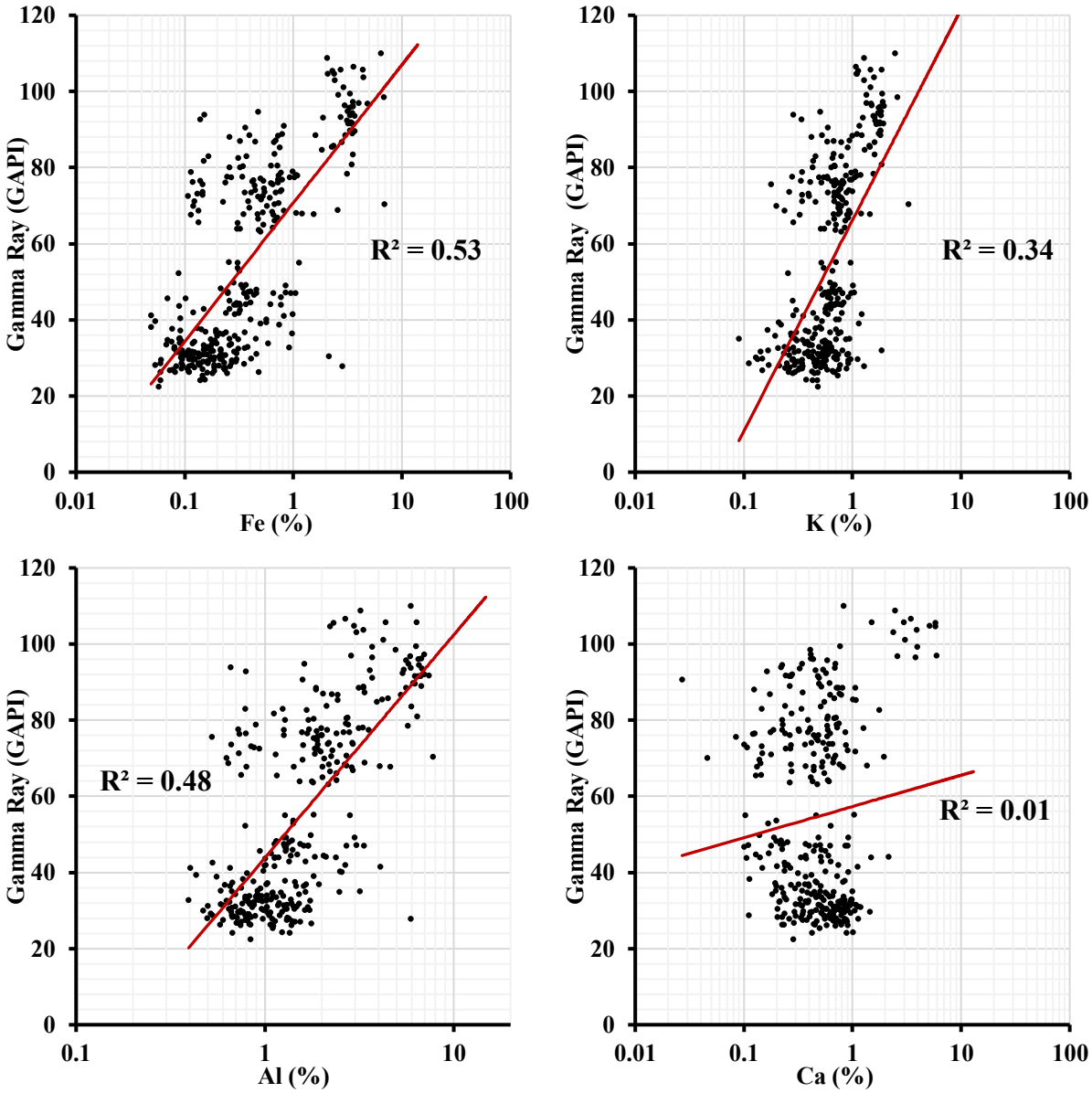


**Figure 4.31**: Well 03 crossplots of Fe, Al, K, and Ca contents measured by the XRF technique on the slabbed cores and the depth-matched downhole total GR log data.

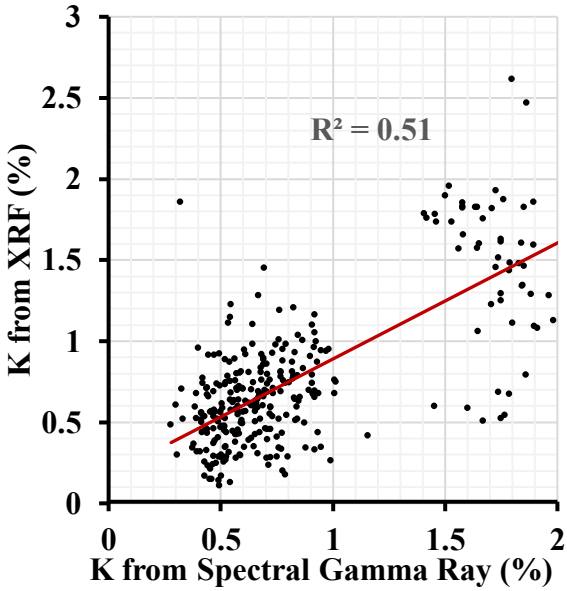


**Figure 4.32**: Well 03 crossplots of K contents from the spectral GR log (horizontal axis) and depth-matched K from XRF measurements (vertical axis).

**Figure 4.32** shows the crossplot between the K contents measured by the XRF technique and the depth-matched K contents from the downhole spectral gamma ray log for Well 03. Whilst the K content from XRF generally increases as the K content from the downhole spectral GR increases, the $R^2$ value is relatively low, but higher than for Well 02. The low $R^2$ value may partly be due to each technique measuring the K content at a different scale. Each XRF measurement represents the K content from a 3mm diameter spot on the slabbed core, whilst each K content from the downhole spectral GR represents an average value from around 1 cubic foot of formation rock.

### d) Crossplots between XRF derived elemental contents

The elemental contents of Fe, K and Al from the XRF measurements are crossplotted against each other in **Figure 4.33**. There are generally strong correlations between these elements in the slabbed cores of Well 03 as expected. The $R^2$ regression coefficient between K and Al is the highest at 0.77 and those between Fe and K and between Fe and Al are 0.53 and 0.67

respectively. These results again suggest that the primary clay mineral in this oil sands reservoir is illite, whose chemical composition contains these 3 elements.

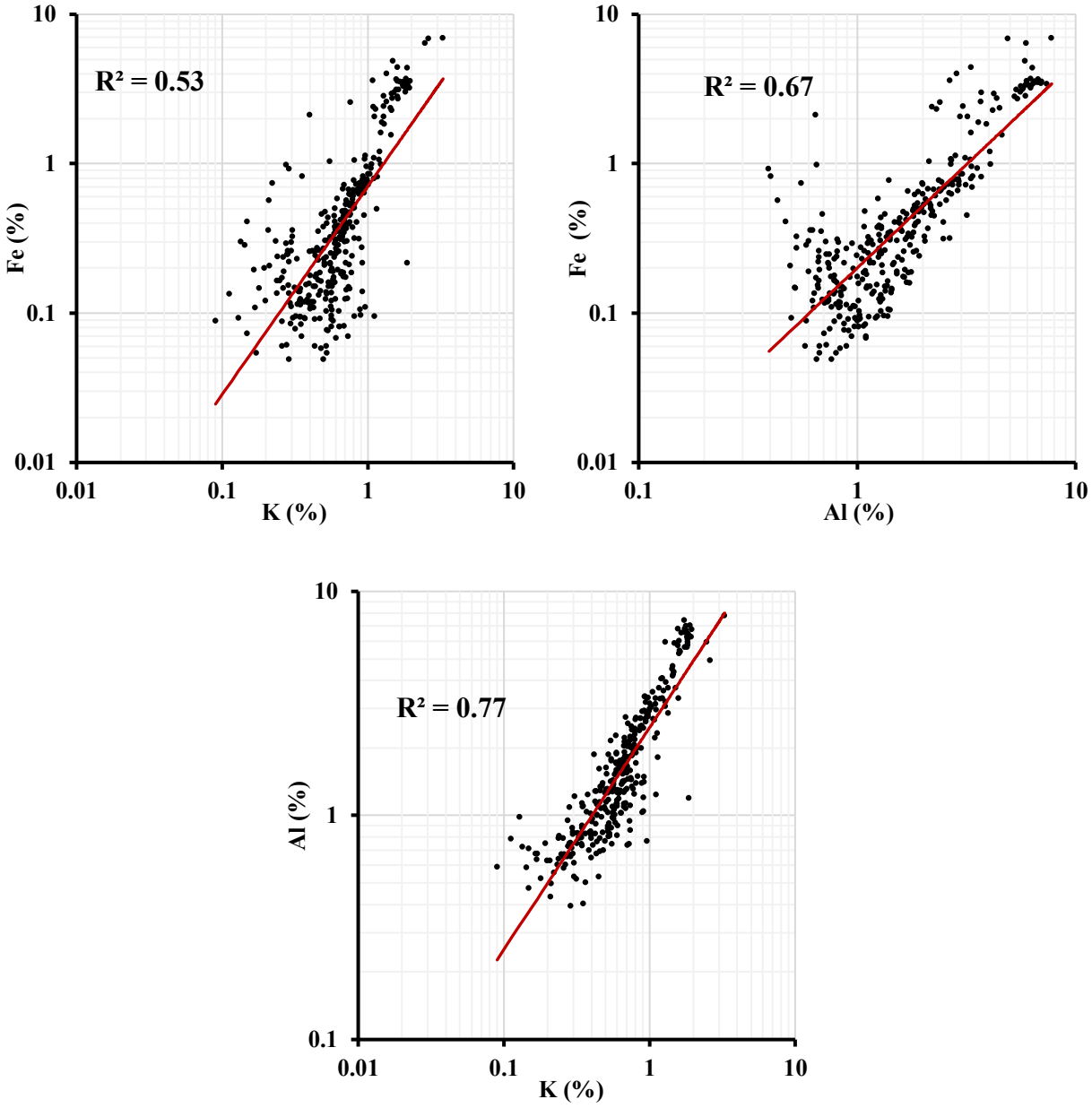


**Figure 4.33**: Well 03 crossplots between the elemental contents of Fe, K, and Al measured by the XRF technique on the slabbed cores.

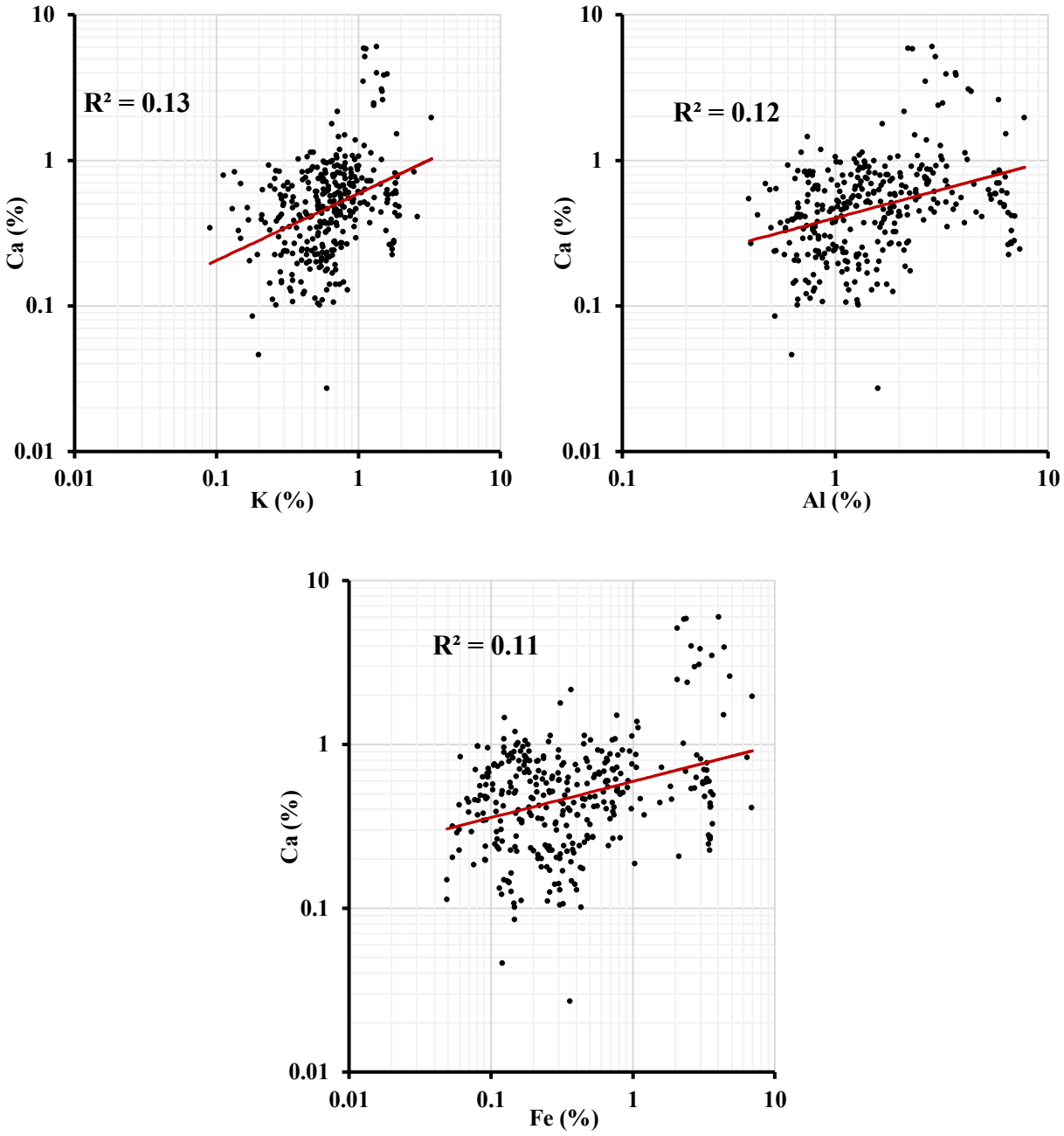


**Figure 4.34**: Well 03 crossplots of Ca with the Fe, K, and Al contents measured by the XRF technique on the slabbed cores.

In contrast, crossplots of Ca with the elemental contents of Fe, K and Al show no correlation, with the $R^2$ values being little more than 0.1 (**Figure 4.34**). The relationship between Ca and Fe in this case is much weaker than the relationship between those elements in Well 02. The results

suggest that the contribution of an iron carbonate mineral (such as siderite) in the lithologies of Well 03 is not as significant as for Well 02.

## 4.6. Conclusions

From the results of the elemental contents measured by the XRF technique and the comparisons with magnetic susceptibility and the downhole gamma ray logs of all three oil sands wells the following conclusions can be drawn:

1. Clear correspondences were observed between the magnetic profiles with depth (magnetic susceptibility and magnetically derived illite content) and the elemental content profiles of Fe, K, and Al measured by the XRF technique. This supported the assumption that illite is a major control on the varying magnetic susceptibility in these oil sands wells, since Fe, K and Al are all components of illite.
2. Magnetic susceptibility and XRF elemental contents of Fe, K and Al can be used to distinguish the 3 main lithologies (shale / clay, IHS beds and clean sand) in these oil sands wells. Low, negative magnetic susceptibilities and low concentrations of Fe, K and Al characterize the clean sands, whereas the highest values of magnetic susceptibility and elemental contents encountered here characterize the shale / clay intervals. The IHS beds are characterized by intermediate values of magnetic susceptibility and elemental contents of Fe, K and Al.
3. The XRF data for Fe, K and Al in the interval 162–168 m in Well 03 supported the interpretation from the magnetic susceptibility data which suggested (in **Chapter 3**) that this interval was part of the IHS beds. The XRF data did not support an interpretation of clean

sands from the low reading of the total GR signal. If one had merely used the total GR data one would have likely misinterpreted this interval as clean sand.

4. The elemental content profiles from XRF also supported the presence of thin layers of "anomalous minerals" identified by the magnetic susceptibility results of **Chapter 3**. In contrast, the downhole GR logs did not identify most of these "anomalous mineral" layers.
5. The combination of the magnetic susceptibility results, the XRF elemental contents of Fe, Ca and K and the total GR log data strongly suggested lithologies that were different to simple sand and clay mixtures in intervals 2 and 3 below 425 m in Well 02. The combined data strongly suggested the presence of an iron carbonate mineral (such as siderite) in interval 2.
6. The crossplots between magnetically derived illite and the contents of the elements Fe, K, and Al from XRF measurements showed strong correlations. This added further quantitative evidence suggesting illite was a major component in the cores controlling the magnetic susceptibility values. Data points from these crossplots formed different clusters depending upon the lithology (for example, 2 clusters of shale / clay and clean sand in Well 02, and 3 clusters of shale / clay, IHS beds and clean sand in Well 03, although the clean sand and IHS data in Well 03 tended to merge into 1 large cluster). These crossplots could therefore potentially be used for lithology identification and discrimination in these oil sands wells.
7. The high $R^2$ values between the crossplots of Fe, K, and Al from the XRF results again suggested that the major clay mineral in these oil sands reservoirs was likely to be illite.
8. Other crossplots from the XRF data alone (such as K against Fe, Al and Ca) or XRF in combination with the total GR data (such as total GR against Ca, Al, K and Fe) all showed a distinct cluster of data points (red points on all these crossplots) for the proposed different lithology intervals 2 and 3 below 425 m in Well 02, and thus could potentially be used to

readily identify such intervals as containing mineralogies that are different to the normal sand and clay mixtures.

## 4.7. References


Backman, B., Lindqvist, K. and Hyvönen, E., 2016. Manual for measuring soil samples with the Niton XL3 GOLDD+ XRF-instrument. Geologian Tutkimuskeskus, pp. 14.

Fajber, R. and Simandi, G. J., 2012. Evaluation of rare earth element-enriched sedimentary phosphate deposits using portable X-ray fluorescence (XRF) instruments. *British Columbia Geological Survey, Geological Field Work 2011*, Volume **2012-1**, 199-209.

Hunt, C. P., Moskowitz, B. M. and Banerjee, S.K., 1995. Magnetic properties of rocks and minerals, In: *Rock Physics and Phase Relations: A Handbook of Physical Constants*, T. J. Ahrens, (Ed.): American Geophysical Union Reference Shelf 3, 189-204.

Ivakhnenko, O. P., 2006. Magnetic Analysis of Petroleum Reservoir Fluids, Matrix Mineral Assemblages and Fluid-Rock Interactions. Ph.D. thesis, Heriot Watt University, Institute of Petroleum Engineering, Edinburgh, UK, pp. 210.

Muwanguzi, A. J. B., Karasev, A. V., Byaruhanga, J. K. and Jönsson, P. G., 2012. Characterization of chemical composition and microstructure of natural iron ore from Muko deposits. *International Scholarly Research Network, ISRN Material Science*, Volume **2012**, Article ID **174803**, 9 pages.

Potter, D. K., AlGhamdi, T. M. and Ivakhnenko, O. P., 2011. Sensitive carbonate reservoir rock characterization from magnetic hysteresis curves and correlation with petrophysical properties. *Petrophysics*, **52** (issue 1), 50-57.

# Chapter 5

# Special core analysis on selected extracted samples: (i) volume and mass magnetic susceptibilities versus X-ray fluorescence, (ii) isothermal remanent magnetization, (iii) low field versus high field magnetic susceptibility, and (iv) temperature dependent magnetic susceptibility

## 5.1. Introduction

This chapter presents results of special core analysis (SCAL) on representative core samples collected from the slabbed cores of the three oil sands wells studied by probe volume magnetic susceptibility and X-ray fluorescence (XRF) in **Chapters 3** and **4**. These laboratory SCAL measurements include low field volume and mass magnetic susceptibility, high field mass magnetic susceptibility, isothermal remanent magnetization (IRM), temperature dependent magnetic susceptibility, and XRF measurements. The purpose of these SCAL measurements was as follows:

1. The low field volume and mass magnetic susceptibility measurements on the small extracted samples, together with XRF, will be compared to the low field probe volume magnetic susceptibility and XRF measurements in **Chapters 3** and **4** to help to evaluate the effects of porosity and fluid in the pore space on the previous probe volume magnetic susceptibility measurements. Mass magnetic susceptibility is less dependent upon porosity than volume magnetic susceptibility, as will be discussed in **Section 5.2** below.
2. The further XRF measurements on the small extracted samples will also enable elemental contents to be obtained on exactly the same samples used for all the other SCAL measurements, and help to constrain the mineralogical compositions.

3. IRM measurements identify the presence of remanence carrying particles (e.g., ferrimagnetic magnetite, canted anti-ferromagnetic hematite etc) in the core samples. Only the remanence carrying particles will acquire an IRM. Moreover, the shape of the IRM acquisition curve helps one to identify the mineral type, and enables one to estimate the particle size for the particular remanence carrying mineral. The magnitude of the IRM also allows one to estimate the amount of that mineral in the sample, and this can be compared with the estimate generated from the comparison between low and high field magnetic susceptibility in purpose 4 below.
4. A comparison of low field and high field magnetic susceptibility also provides an independent method to determine the amount of remanence carrying particles (especially of ferrimagnetic minerals such as magnetite) in the core samples. These particles saturate in high fields and don't contribute to the high field magnetic susceptibility. Therefore if such particles are present the high field magnetic susceptibility will be lower than the low field magnetic susceptibility. The difference in the two values represents the magnetic susceptibility signal of such remanence carrying particles in the sample.
5. Temperature dependent magnetic susceptibility measurements enable one to identify the presence of paramagnetic minerals (e.g., illite) and to quantify their content.. Paramagnetic minerals exhibit temperature dependent magnetic susceptibility, whereas diamagnetic minerals (e.g., quartz, calcite etc) do not. In addition, temperature dependent magnetic susceptibility is important for borehole applications of magnetic susceptibility. Temperature varies with depth in boreholes and so modelling the temperature dependent magnetic susceptibility behaviour of paramagnetic minerals is important in order to accurately estimate paramagnetic mineral contents from borehole magnetic susceptibility data.

## 5.2. Low field volume and mass magnetic susceptibility and X-ray fluorescence measurements on extracted core samples

### 5.2.1. Samples and methods

In **Chapters 3** and **4** the estimated illite contents were derived from the results of low field probe volume magnetic susceptibility on the slabbed cores. Each probe volume magnetic susceptibility reading was assumed to be the result of a quartz + illite mixture, and the contribution of the pore space (porosity), and any fluids it contained, to the susceptibility signal was neglected. Each probe reading examines a specific (similar) volume, and if the porosity or fluid type changes the magnetic susceptibility may vary slightly even if the mineralogy stays the same. Usually small variations in porosity and fluid content have little effect on the volume magnetic susceptibility of sediments, since most fluids are diamagnetic. However, to minimize these effects it is useful to measure mass magnetic susceptibility (as defined in **Chapters 1** and **2**). For example, samples with similar high illite to quartz ratios and variable porosity will show small variations in volume magnetic susceptibility, but less variation in mass magnetic susceptibility. This is because the samples with lower porosity will have higher volume magnetic susceptibility and higher mass (and likewise samples with higher porosity will have lower volume magnetic susceptibility and lower mass) so that the mass magnetic susceptibilities will likely be very similar in all such cases. Therefore, this section will compare the relationships of volume and mass magnetic susceptibilities with the elemental contents measured by XRF on powdered core samples, and compare the results with the probe volume magnetic susceptibility on the slabbed core with the XRF elemental contents. These comparisons will help to evaluate the impact of porosity and fluid in the pore space on the results of the probe volume susceptibility measurements on the slabbed cores given in **Chapter 3**.

A total of 24 samples were collected from the slabbed cores of the three oil sands wells in this study for the magnetic and XRF analysis in this section (**Tables 5.1** and **5.2**). Each sample was ground into powdered form, and placed into cylindrical plastic holders about 1 inch in diameter and 1 inch in height for the magnetic susceptibility and XRF elemental contents measurements. The grinding is meant to help improve the XRF results by effectively increasing the mineral content to porosity ratio of each sample (finer ground lightly packed particles usually produce less pore space). The collected samples covered a range of different lithologies including clean sands, muddy sands, and clay/shale. The mass magnetic susceptibility was measured using a Bartington MS2W sensor connected to an MS2 susceptibility meter, as described in **Chapter 2**. The volume magnetic susceptibility was measured by using a probe MS2E sensor connected to an MS2 meter, as described in **Chapter 2.** The elemental contents of the powdered samples were measured with the XRF system. This system used the same Niton XL3t XRF analyzer as for the measurements in **Chapter 4**, but for the new measurements on the powdered samples it was connected to a portable stand specifically for laboratory measurements on small samples (**Figure 5.1 (A)**). The stand was attached to a shielded box in which the sample was placed on top of a window during the measurement (**Figure 5.1 (B)**). The shielded box is made of lead, which is able to stop scattered X-rays, thus reducing the radiation absorbed by the operator. The volume and mass susceptibilities of the powdered samples were then plotted against the XRF derived elemental contents to quantify the relationships between them. Any significant differences between the correlations of volume magnetic susceptibility versus XRF compared to mass magnetic susceptibility versus XRF will likely be due to the effect of varying porosity on the volume magnetic susceptibility of the extracted powdered core samples. Further comparisons with the probe volume magnetic susceptibility on the slabbed cores versus XRF would help to

evaluate whether porosity (and fluid content) may have had any significant impact on the slabbed core probe volume magnetic susceptibility results of **Chapter 3**.

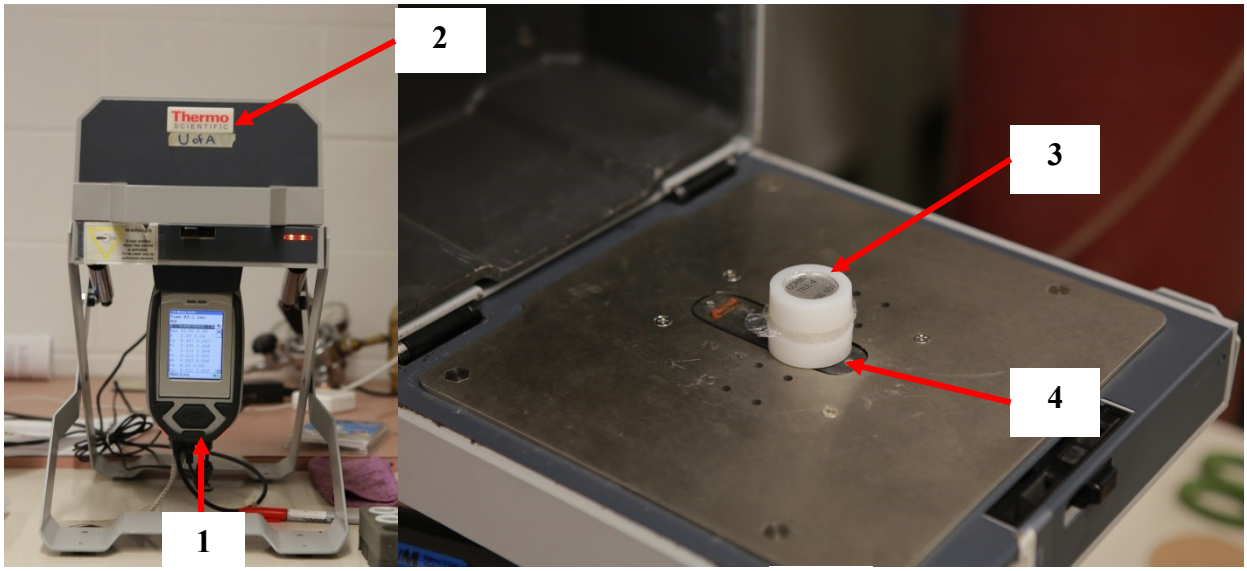


**Figure 5.1**: **(A)** shows the system for laboratory elemental contents measurements that includes (**1**) a Niton XL3t XRF analyzer connected to (**2**) a portable stand with a shielded box. **(B)** shows the interior of the shielded box with (**3**) an example of a sample placed on top of (**4**) the measurement window.

### 5.2.2. Results and discussion

**Tables 5.1** and **5.2** show the results of volume and mass magnetic susceptibility and XRF elemental contents measured on the 24 selected powdered samples, along with the relevant probe volume magnetic susceptibility and XRF measurements on the slabbed cores at the same depth. Overall, the signs of the volume and mass susceptibility results are similar with negative signs for clean sands samples and positive signs for clay/shale and muddy sands samples. There are samples whose volume susceptibilities are less negative than other samples, but their mass susceptibilities are more negative than those other samples. These differences are likely due to the different fluid contents of these samples. The theoretical volume magnetic susceptibility of quartz is -1.64 x $10^{-5}$ SI (which I converted from the mass susceptibility value given in Ivakhnenko, 2006), which is more negative than that of the heavy oil sample measured in

**Chapter 2** at -1.0025 x $10^{-5}$ SI (the value was converted from the mass magnetic susceptibility). However, the theoretical mass magnetic susceptibility of quartz is -0.62 x $10^{-8}$ $m^3kg^{-1}$ (Ivakhnenko, 2006; Potter et al, 2011), which is less negative than that of the measured heavy oil at -0.9524 x $10^{-8}$ $m^3kg^{-1}$ (**Chapter 2**).

Among the clean sand samples (i.e., those with little or no clay content) W01.07 has positive volume magnetic susceptibility (0.7 x $10^{-5}$ SI) but negative mass magnetic susceptibility (-0.62 x $10^{-8}$ $m^3kg^{-1}$). This could be the result of a very small amount of a paramagnetic and/or ferrimagnetic mineral in the sample. If the paramagnetic mineral is illite, for example, the volume magnetic susceptibility of illite is 41 x $10^{-5}$ SI (Hunt et al., 1995), and the mass susceptibility is 15 x $10^{-8}$ $m^3kg^{-1}$ (Hunt et al., 1995). A small amount of illite in an otherwise quartz rich sand sample can result in a positive volume magnetic susceptibility, but a negative mass magnetic susceptibility. Note also that among samples of sand that are saturated with heavy oil or bitumen, their differences in mineralogy are often not apparent from core observation alone due to the black nature of the hydrocarbons. This is an advantage of the magnetic technique, which can distinguish between such samples and help to quantify the mineralogy.

The probe volume magnetic susceptibilities from the extracted samples were plotted against the probe volume magnetic susceptibilities from the original intact slabbed cores at the same depths (the results for both are shown in **Tables 5.1** and **5.2**) and are shown in **Figure A.4.1** in **Appendix 4**. The crossplots for each of the 3 wells in this figure show that the results from the original intact slabbed core are comparable to those from the subsequent extracted samples.

**Table 5.1**: Results of volume and mass magnetic susceptibility on representative powdered samples that were collected from the slabbed core of the three oil sands wells. The values in brackets in the volume magnetic susceptibility column are the probe results measured on the original intact slabbed cores at the same depths.

| Well | Samples | Depth (m) | Lithology | Volume Susceptibility ($10^{-5}$ SI) | Mass Susceptibility ($10^{-8}$ $m^3kg^{-1}$) |
|---|---|---|---|---|---|
| Well 01 | W01.01 | 488.9 | Sand with heavy oil | -1.6 (-1.6) | -0.53 |
| | W01.03 | 504.8 | Sand with heavy oil | -1.2 (-1.3) | -0.84 |
| | W01.04 | 505.5 | Sand with heavy oil | -0.4 (-1.0) | -0.67 |
| | W01.05 | 486.6 | Sand with heavy oil | -0.1 (-0.9) | -0.96 |
| | W01.06 | 499.5 | Sand with heavy oil | -0.2 (-0.6) | -0.58 |
| | W01.07 | 471.3 | Sand with heavy oil | 0.7 (0.6) | -0.62 |
| | W01.08 | 510.8 | Sand with heavy oil | 0.5 (2.8) | 0.61 |
| | W01.09 | 494.0 | Muddy sand with oil | 1.9 (3.5) | 1.03 |
| | W01.10 | 511.4 | Muddy sand | 3.3 (3.6) | 2.22 |
| | W01.11 | 493.6 | Muddy sand | 4.6 (5.9) | 3.00 |
| | W01.12 | 508.5 | Muddy sand | 4.9 (7.8) | 2.96 |
| Well 02 | W02.01 | 389.6 | Sand with heavy oil | -0.3 (-1.4) | -0.92 |
| | W02.02 | 429.5 | Muddy Sand | 2.6 (2.3) | 1.16 |
| | W02.03 | 368.5 | Muddy Sand | 2.9 (2.9) | 1.22 |
| | W02.04 | 380.1 | Muddy Sand | 9.1 (10.5) | 5.79 |
| | W02.05 | 355.4 | Clay/ Shale | 15.0 (20.4) | 8.61 |
| | W02.06 | 362.3 | Clay/ Shale | 20.9 (25.5) | 11.89 |
| | W02.07 | 360.4 | Clay/ Shale | 25.1 (28.2) | 14.56 |
| Well 03 | W03.01 | 194.3 | Sand with bitumen | 0.0 (-0.5) | -0.28 |
| | W03.02 | 167.1 | Sand with bitumen | -0.1 (-0.1) | -0.81 |
| | W03.03 | 174.0 | Muddy Sand | 2.8 (4.7) | 1.79 |
| | W03.04 | 217.9 | Muddy Sand | 8.3 (12.4) | 4.53 |
| | W03.05 | 155.5 | Clay/ Shale | 10.2 (16.3) | 7.61 |
| | W03.06 | 157.1 | Clay/ Shale | 10.5 (18.4) | 7.97 |

**Table 5.2:** Results of volume and mass magnetic susceptibility and key XRF elemental contents (for Fe, K and Al) measured on powdered samples that were collected from the slabbed cores of the three oil sands wells. The values in brackets in the volume magnetic susceptibility and XRF key elements contents columns are the results measured on the original intact slabbed cores at the same depths.

| Well | Samples | Volume Susceptibility ($10^{-5}$ SI) | Mass Susceptibility ($10^{-8}$ $m^3kg^{-1}$) | Fe (%) | K (%) | Al (%) |
|---|---|---|---|---|---|---|
| Well 01 | W01.01 | -1.6 (-1.6) | -0.53 | 0.056 (0.064) | 0.162 (0.260) | 0.275 (0.571) |
| | W01.03 | -1.2 (-1.3) | -0.84 | 0.069 (0.167) | 0.273 (0.324) | 0.432 (0.819) |
| | W01.04 | -0.4 (-1.0) | -0.67 | 0.046 (0.187) | 0.230 (0.317) | 0.388 (0.882) |
| | W01.05 | -0.1 (-0.9) | -0.96 | 0.042 (0.087) | 0.098 (0.293) | 0.241 (0.942) |
| | W01.06 | -0.2 (-0.6) | -0.58 | 0.094 (0.555) | 0.193 (0.564) | 0.417 (0.144) |
| | W01.07 | 0.7 (0.6) | -0.62 | 0.153 (0.413) | 0.381 (0.531) | 0.772 (1.702) |
| | W01.08 | 0.5 (2.8) | 0.61 | 0.444 (0.432) | 0.556 (0.640) | 0.819 (1.806) |
| | W01.09 | 1.9 (3.5) | 1.03 | 0.781 (0.678) | 0.713 (0.423) | 2.148 (1.691) |
| | W01.10 | 3.3 (3.6) | 2.22 | 0.623 (0.325) | 0.724 (0.589) | 2.927 (1.129) |
| | W01.11 | 4.6 (5.9) | 3.00 | 1.905 (1.662) | 0.863 (0.633) | 3.135 (1.892) |
| | W01.12 | 4.9 (7.8) | 2.96 | 1.196 (1.365) | 1.592 (1.156) | 6.656 (3.698) |
| Well 02 | W02.01 | -0.3 (-1.4) | -0.92 | 0.036 (0.043) | 0.267 (0.518) | 0.347 (0.596) |
| | W02.02 | 2.6 (2.3) | 1.16 | 1.218 (0.569) | 0.215 (0.152) | 1.142 (1.443) |
| | W02.03 | 2.9 (2.9) | 1.22 | 0.264 (0.284) | 0.416 (0.456) | 0.775 (1.020) |
| | W02.04 | 9.1 (10.5) | 5.79 | 2.31 (2.461) | 1.608 (1.144) | 4.065 (6.042) |
| | W02.05 | 15.0 (20.4) | 8.61 | 4.265 (3.279) | 1.338 (1.653) | 5.896 (5.437) |
| | W02.06 | 20.9 (25.5) | 11.89 | 3.257 (5.943) | 1.450 (1.097) | 3.914 (6.337) |
| | W02.07 | 25.1 (28.2) | 14.56 | 6.193 (6.598) | 3.121 (1.715) | 4.779 (4.138) |
| Well 03 | W03.01 | 0.0 (-0.5) | -0.28 | 0.384 (0.379) | 0.136 (0.494) | 1.083 (1.083) |
| | W03.02 | -0.1 (-0.1) | -0.81 | 0.246 (0.333) | 0.280 (0.672) | 0.786 (1.268) |
| | W03.03 | 2.8 (4.7) | 1.79 | 0.838 (1.067) | 1.089 (1.191) | 3.292 (3.317) |
| | W03.04 | 8.3 (12.4) | 4.53 | 2.310 (3.251) | 1.608 (1.398) | 5.533 (6.624) |
| | W03.05 | 10.2 (16.3) | 7.61 | 3.474 (3.520) | 1.836 (1.787) | 5.967 (6.72) |
| | W03.06 | 10.5 (18.4) | 7.97 | 3.684 (2.982) | 1.888 (1.515) | 5.932 (6.711) |

**Figures 5.2** to **5.10** show crossplots of magnetic susceptibility against elemental contents of the key elements iron (Fe), potassium (K) and aluminium (Al) from XRF. **Figures 5.2-5.4** are for Well 01, **Figures 5.5-5.7** are for Well 02, and **Figures 5.8-5.10** are for Well 03. Each figure relates to one element and has 3 crossplots as follows: **(A)** gives the probe volume magnetic susceptibility results of the extracted core samples against the elemental contents, **(B)** gives the mass magnetic susceptibility results of the extracted core samples against the elemental contents, and **(C)** gives the probe volume magnetic susceptibility results of the original intact slabbed core samples against the elemental contents from **Chapters 3** and **4** (at the same depths as for the extracted core samples), The **(B)** crossplots might be expected to give the best regression coefficient ($R^2$) values in each figure, since mass magnetic susceptibility is less affected by porosity than volume magnetic susceptibility as detailed in **section 5.2.1**. This is indeed the case for 5 out of the 9 figures, however the $R^2$ values are quite high in almost every crossplot. This would suggest that porosity (and the fluid type within the pore space) is not having a significant effect on the volume magnetic susceptibility results, since the $R^2$ values for crossplots **(A)** and **(C)** are generally comparable to that for **(B)**. Note also that the **(A)** crossplots might be expected to give slightly better $R^2$ values than the **(C)** crossplots, since the extracted samples in **(A)** were ground into powdered form to improve the XRF results (by reducing the porosity). This is indeed the case for 8 out of the 9 figures. However, the $R^2$ values are still quite close in most cases between the **(A)** and **(C)** plots, further suggesting that the intrinsic porosity of the slabbed cores (and the fluid type within the pore space) is not having a substantial effect on the volume magnetic susceptibility and XRF results of the **(C)** crossplots. The fact that the $R^2$ values are quite high in all the crossplots also gives further support for illite as the major paramagnetic clay mineral, since Fe, K and Al are all components of illite.

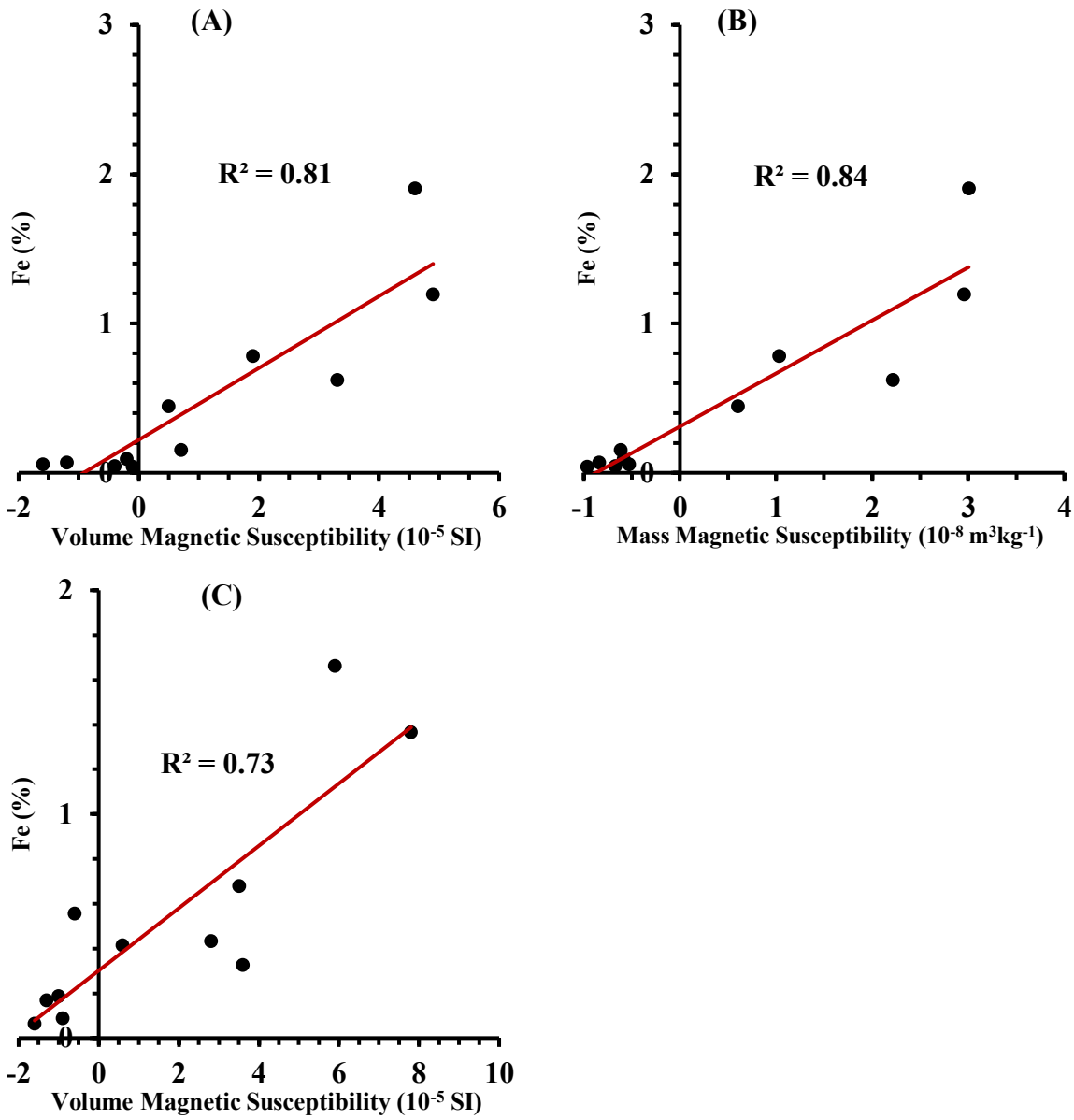


**Figure 5.2:** Well 01 crossplots of **(A)** XRF Fe contents with probe volume magnetic susceptibility of extracted samples, **(B)** XRF Fe contents and mass magnetic susceptibility measured on extracted samples and **(C)** XRF Fe contents and probe volume magnetic susceptibility measured on the original intact slabbed cores.

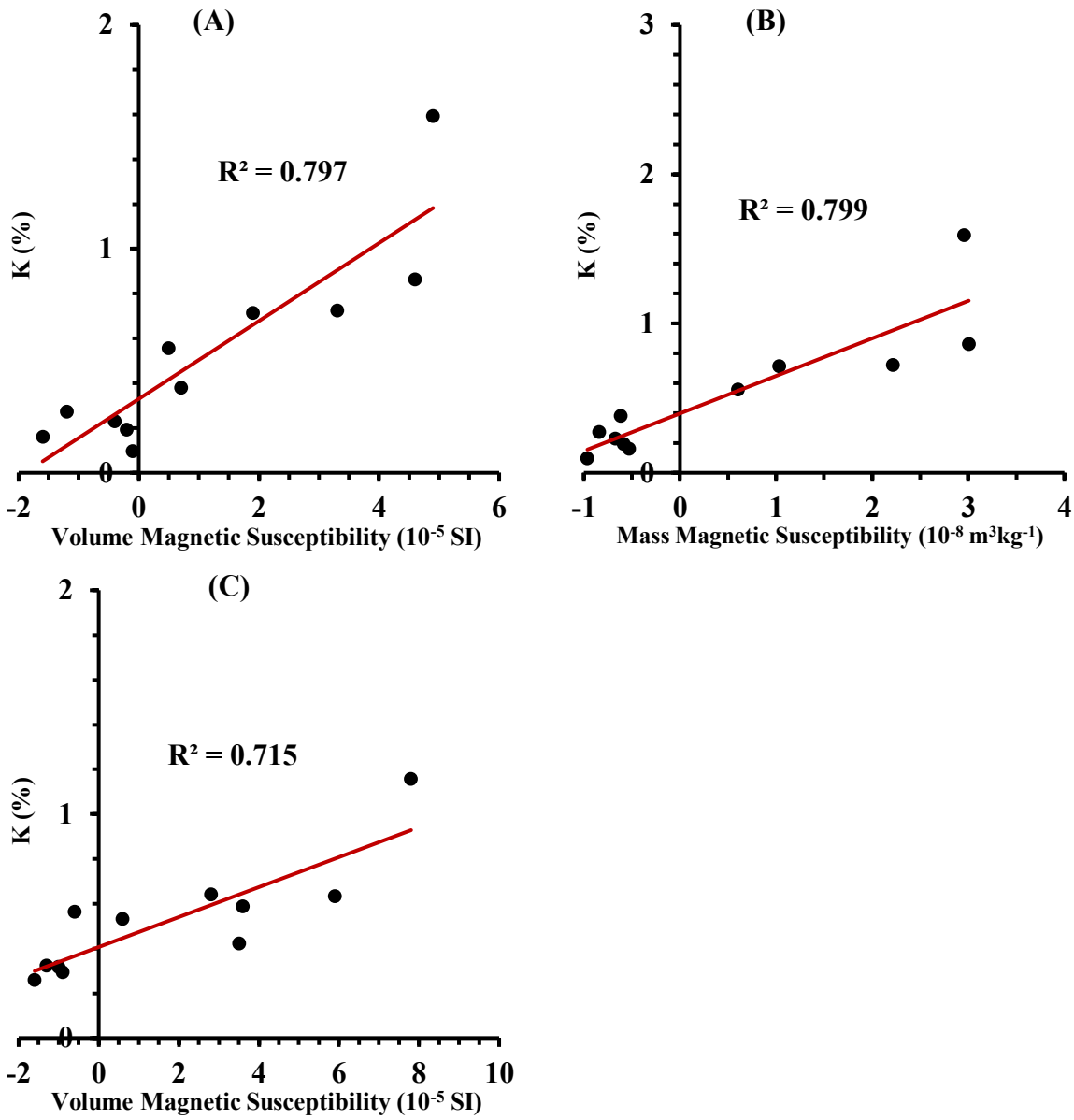


**Figure 5.3:** Well 01 crossplots of **(A)** XRF K contents with probe volume magnetic susceptibility of extracted samples, **(B)** XRF K contents and mass magnetic susceptibility measured on extracted samples and **(C)** XRF K contents and probe volume magnetic susceptibility measured on the original intact slabbed cores.

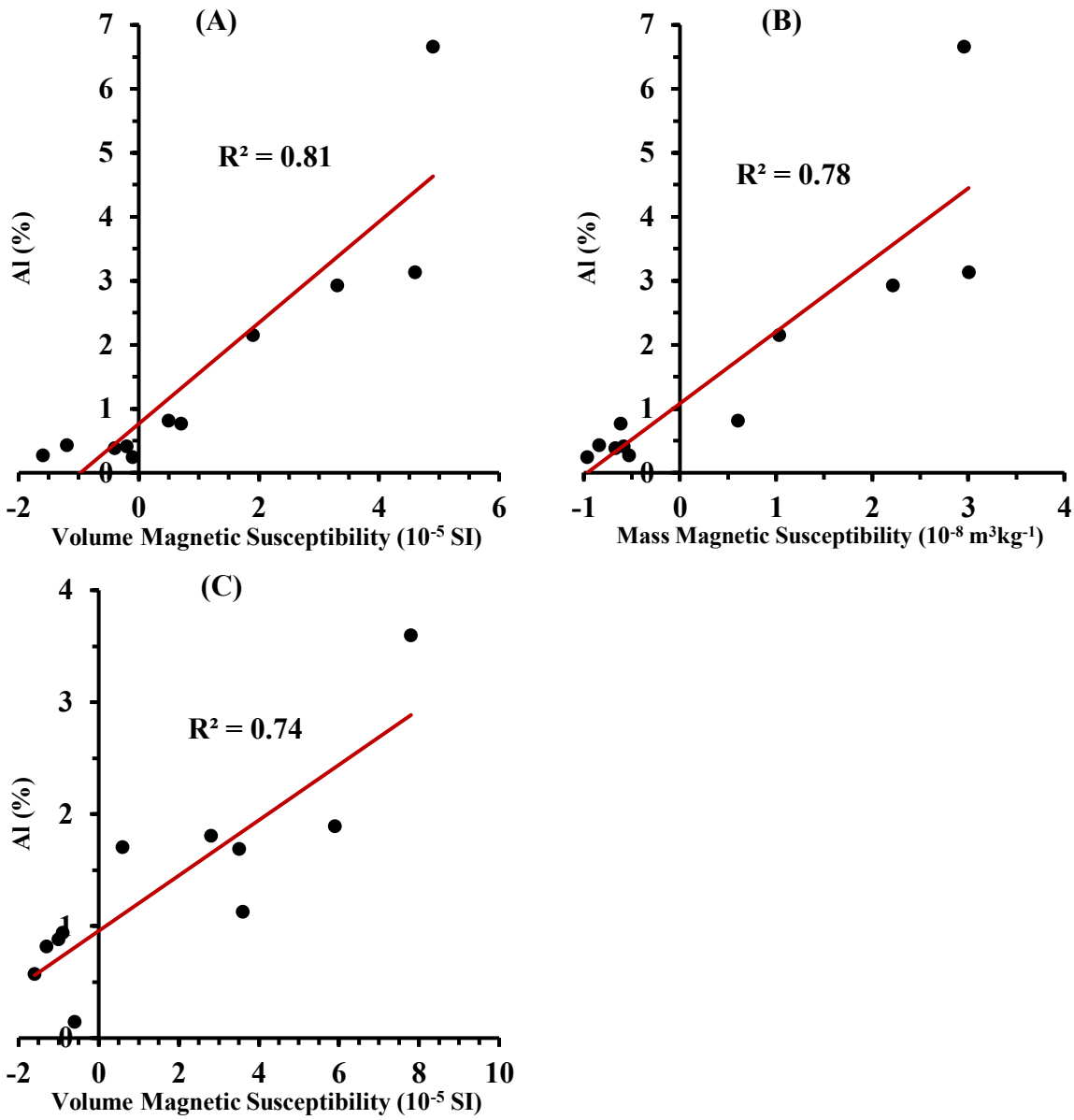


**Figure 5.4:** Well 01 crossplots of **(A)** Al contents with probe volume magnetic susceptibility of extracted samples, **(B)** Al contents and mass magnetic susceptibility measured on extracted samples and **(C)** Al contents and probe volume magnetic susceptibility measured on the original intact slabbed cores.

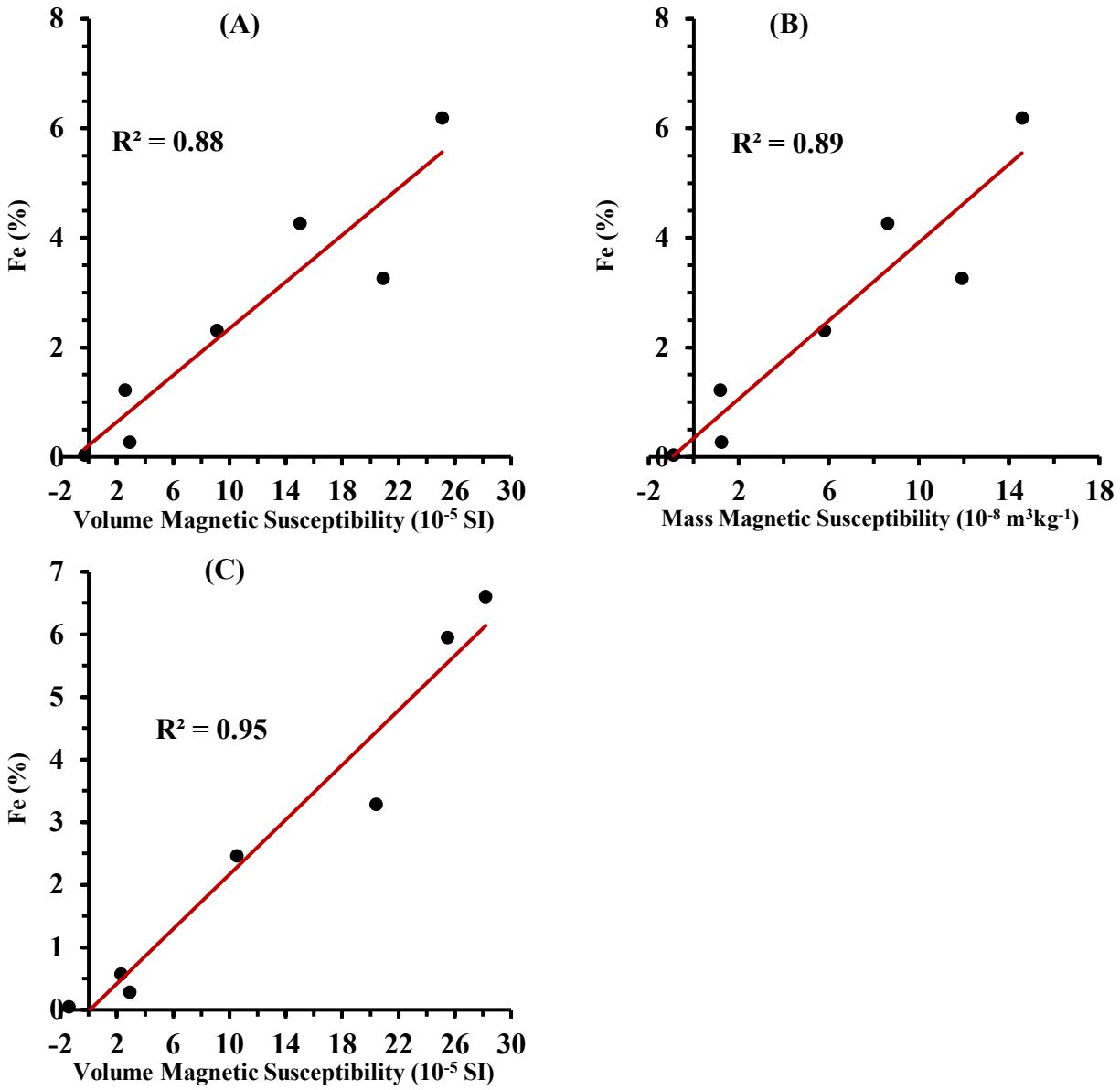


**Figure 5.5:** Well 02 crossplots of **(A)** Fe contents with probe volume magnetic susceptibility of extracted samples, **(B)** Fe contents and mass magnetic susceptibility measured on extracted samples and **(C)** Fe contents and probe volume magnetic susceptibility measured on the original intact slabbed cores.

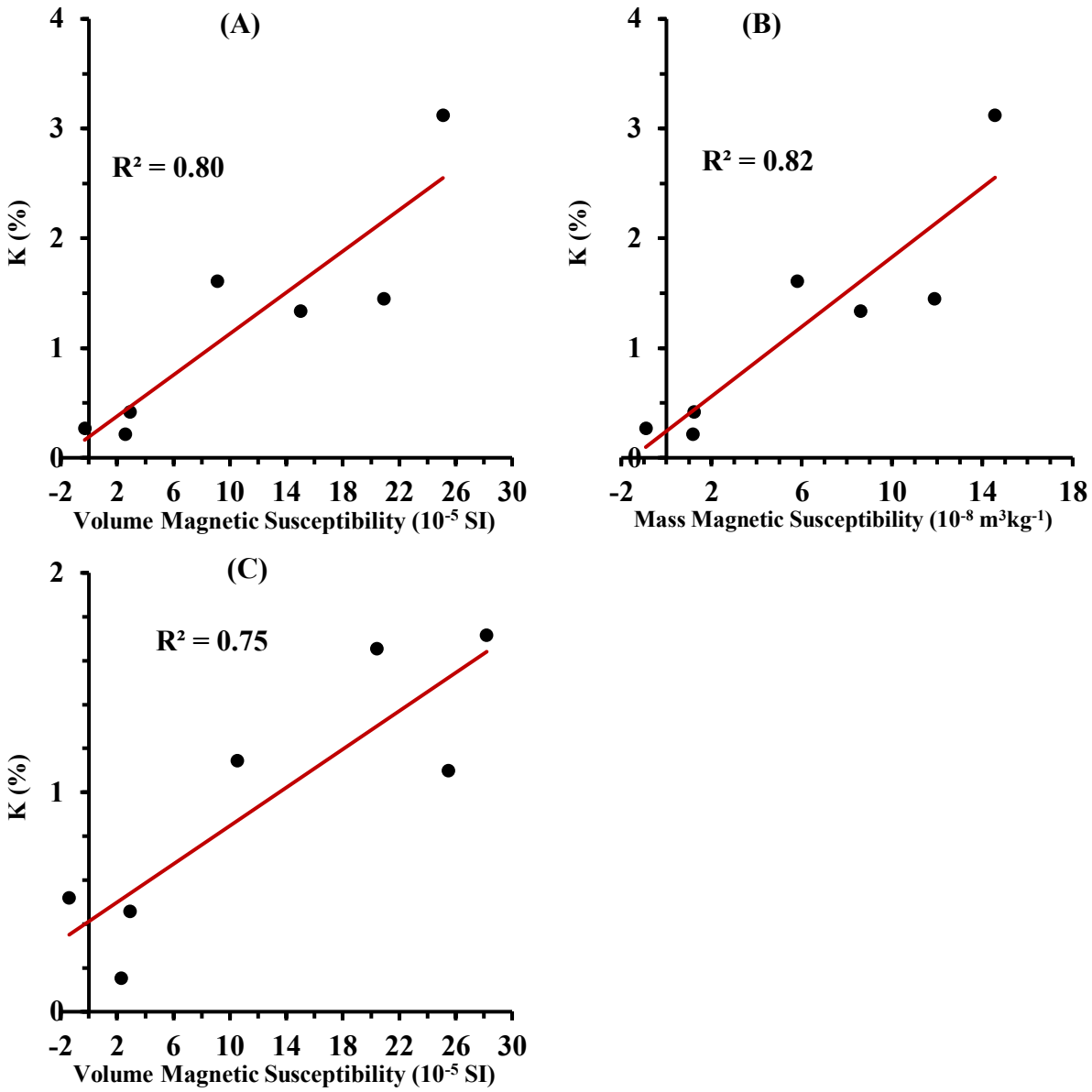


**Figure 5.6:** Well 02 crossplots of **(A)** K contents with probe volume magnetic susceptibility of extracted samples, **(B)** K contents and mass magnetic susceptibility measured on extracted samples and **(C)** K contents and probe volume magnetic susceptibility measured on the original intact slabbed cores.

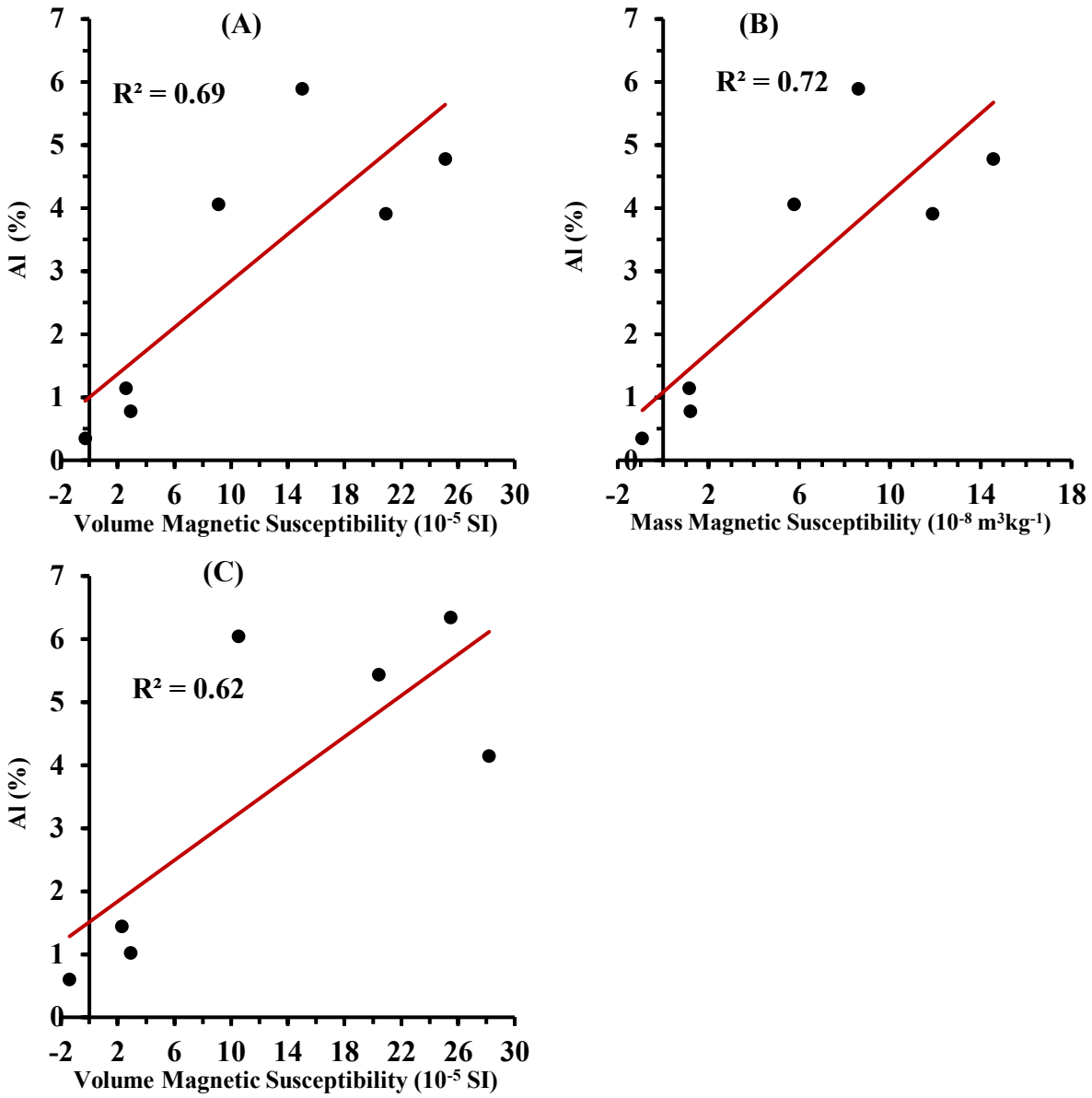


**Figure 5.7:** Well 02 crossplots of **(A)** Al contents with probe volume magnetic susceptibility of extracted samples, **(B)** Al contents and mass magnetic susceptibility measured on extracted samples and **(C)** Al contents and probe volume magnetic susceptibility measured on the original intact slabbed cores.

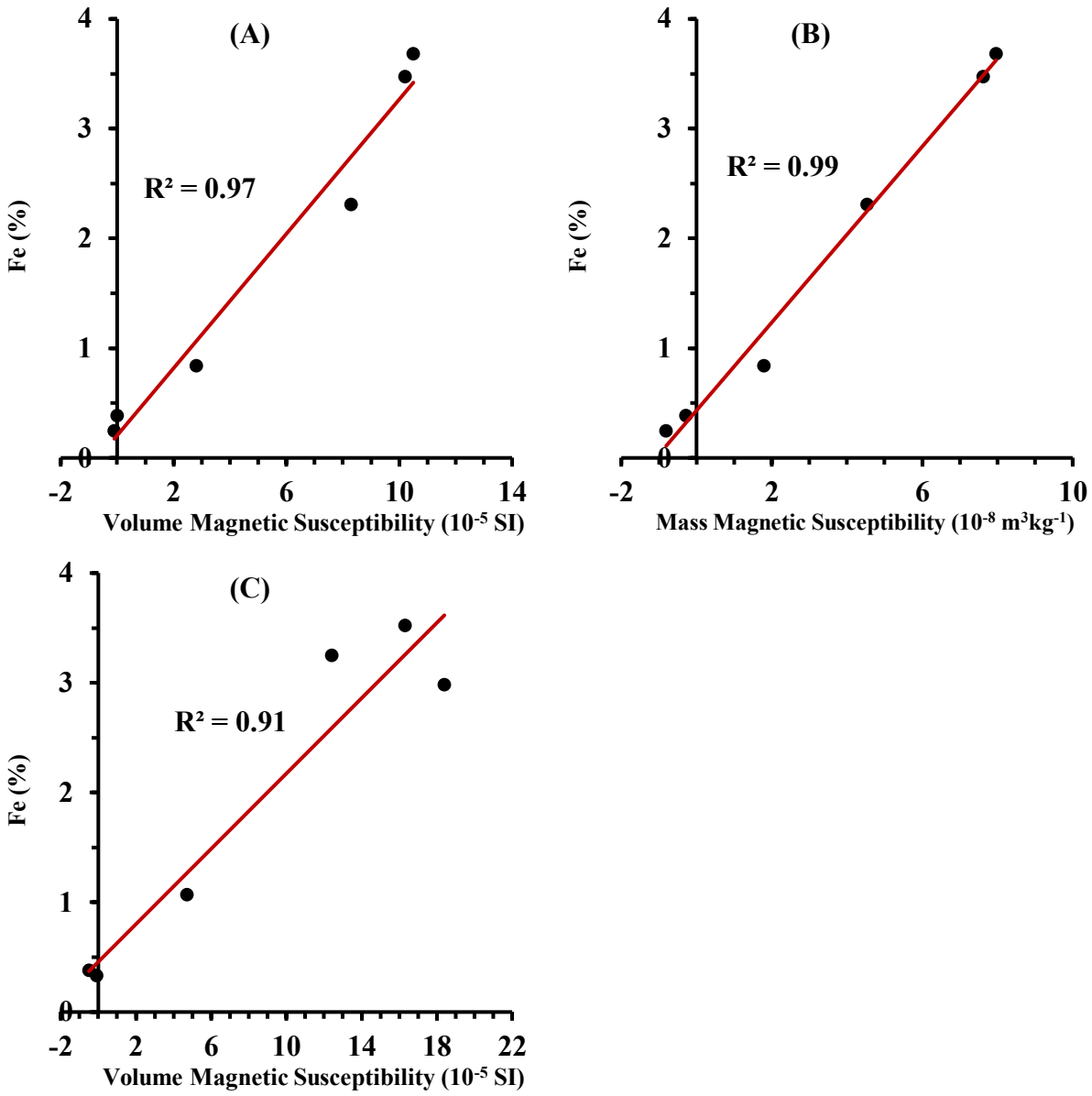


**Figure 5.8:** Well 03 crossplots of **(A)** Fe contents with probe volume magnetic susceptibility of extracted samples, **(B)** Fe contents and mass magnetic susceptibility measured on extracted samples and **(C)** Fe contents and probe volume magnetic susceptibility measured on the original intact slabbed cores.

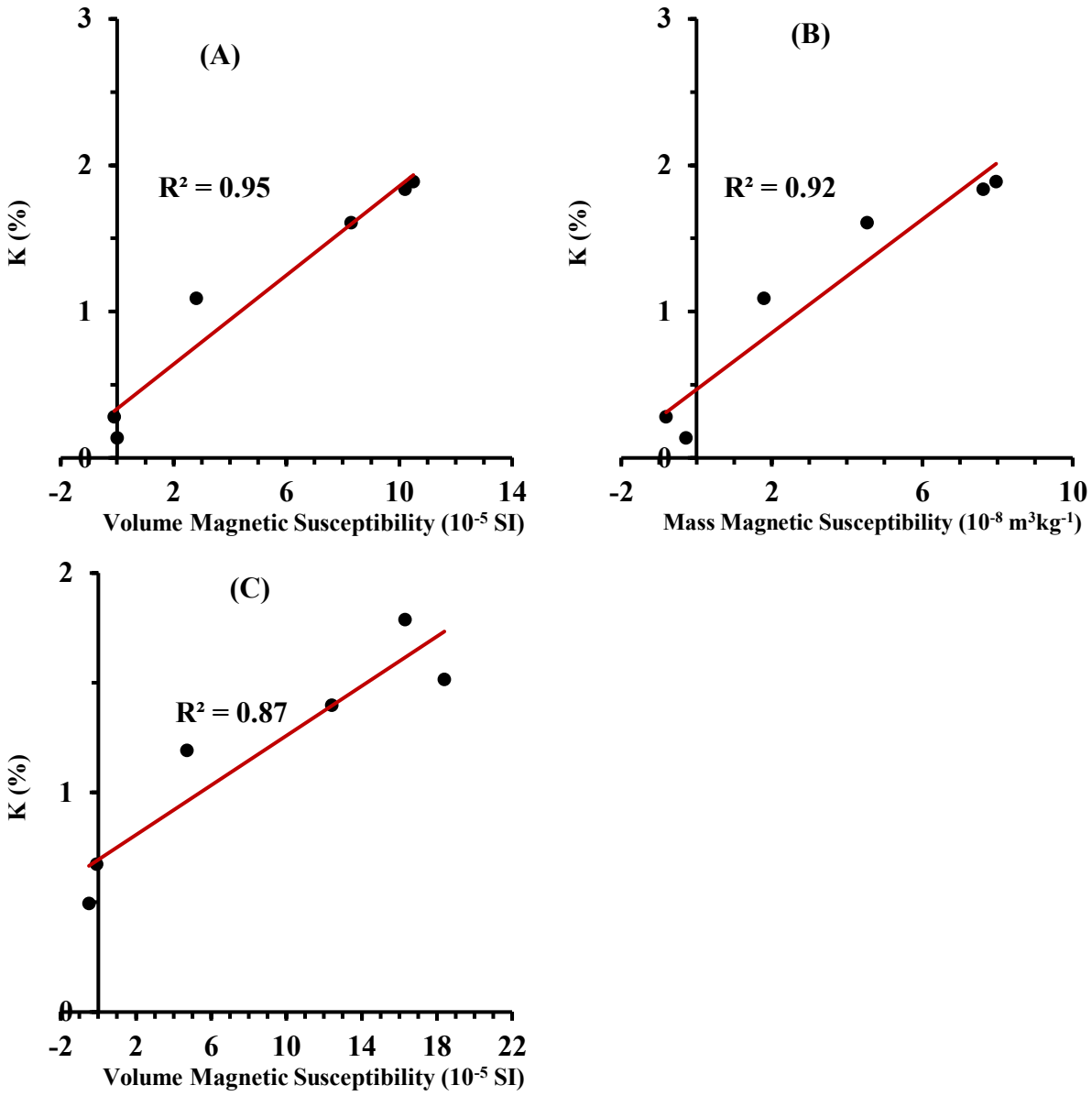


**Figure 5.9:** Well 03 crossplots of **(A)** K contents with probe volume magnetic susceptibility of extracted samples, **(B)** K contents and mass magnetic susceptibility measured on extracted samples and **(C)** K contents and probe volume magnetic susceptibility measured on the original intact slabbed cores.

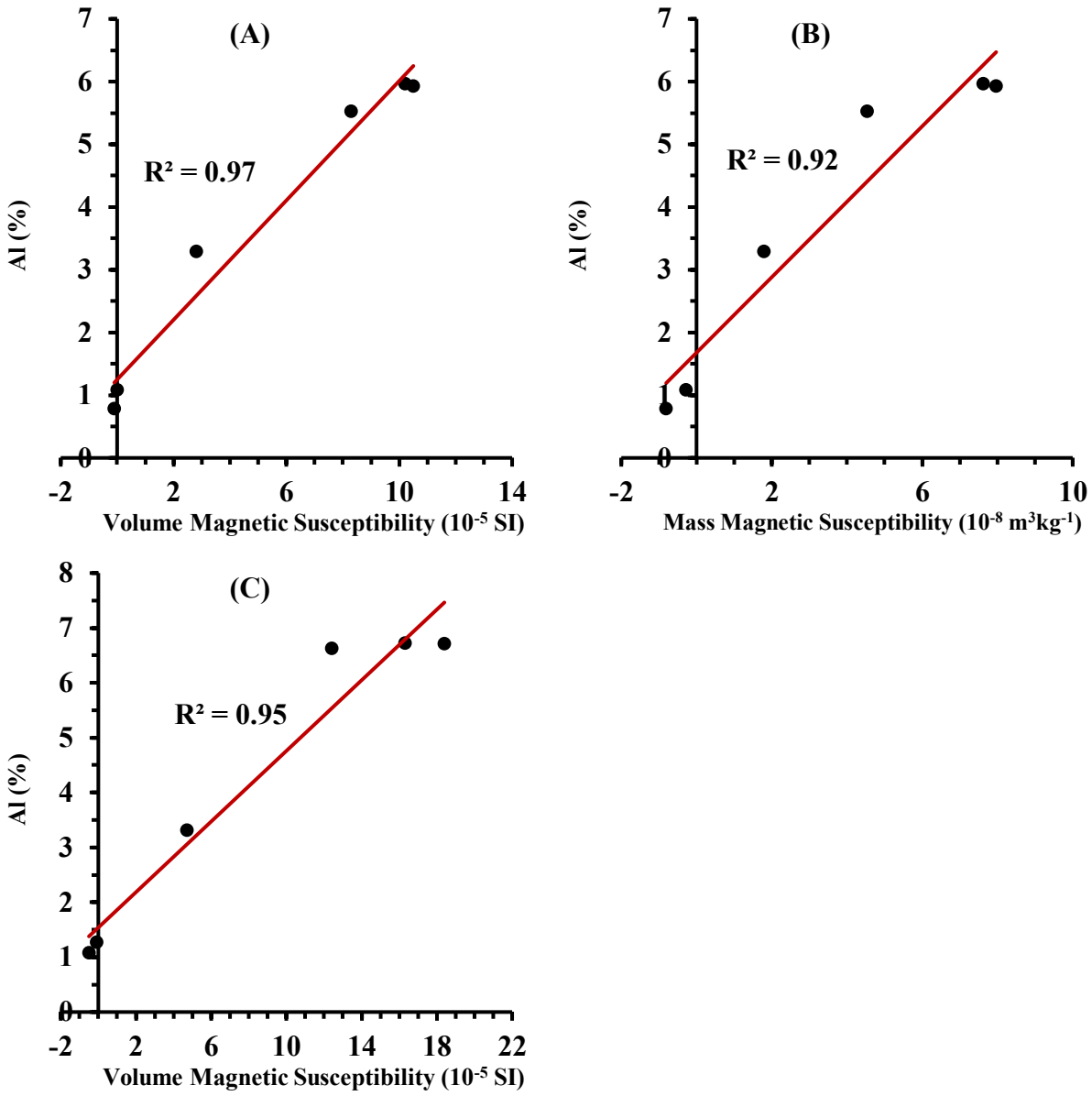


**Figure 5.10:** Well 03 crossplots of **(A)** Al contents with probe volume magnetic susceptibility of extracted samples, **(B)** Al contents and mass magnetic susceptibility measured on extracted samples and **(C)** Al contents and probe volume magnetic susceptibility measured on the original intact slabbed cores.

## 5.3. Isothermal remanent magnetization measurements

### 5.3.1. Introduction

Reservoir samples often contain small particles of remanence carrying minerals, such as the ferrimagnetic iron oxide magnetite, $Fe_3O_4$ (Ali and Potter, 2012), or the canted antiferromagnetic mineral hematite, $\alpha$-$Fe_2O_3$. These minerals have high magnetic susceptibility compared to paramagnetic minerals, and thus a small amount of them can sometimes dominate the total susceptibility signal and cause an overestimate of the paramagnetic (e.g., illite) clay content if they are not accounted for. The presence of these remanence carrying particles can be identified from magnetic hysteresis curves by exhibiting loops or kinks at low fields (Ivakhnenko and Potter, 2008). However, this section will introduce a more sensitive method that is able to identify and quantify these remanence carrying particles more accurately. This method involves the measurement of isothermal remanent magnetization (IRM). The fundamentals of this method are based on the different magnetic behaviours between diamagnetic, paramagnetic, and remanence carrying substances (the latter include ferromagnetic, ferrimagnetic and canted antiferromagnetic substances) after the removal of an externally applied field as described in **Chapter 2**. Remanence carrying particles retain magnetization (called remanent magnetization) after the removal of an applied field, whereas diamagnetic and paramagnetic substances do not. Remanent magnetization increases with increasing applied field strength until it reaches a maximum called the saturation magnetization. Therefore, one can identify the presence of remanence carrying particles by seeing whether the sample acquires a remanent magnetization, and the shape of the acquisition curve with applied field strength can give some idea of the particle size (particularly if one has additional information regarding the mineralogy of these remanence carrying particles). Since temperature can affect the magnetic susceptibility and

remanent magnetization of remanence carrying particles (generally at high temperatures close to the Curie temperature, and if some samples are heated in air which can cause oxidation) measurements are ideally taken at room temperature. IRM measurements are ideal because they are usually taken at constant room temperature, and generally give the highest signal of any form of magnetic remanence. Therefore they are able to detect extremely small amounts of remanence carrying particles.

### 5.3.2. Samples and methods

Representative samples were collected from the slabbed cores in this study for the IRM measurements. The samples covered a range of different lithologies including clean sands, muddy sands (IHS beds), and clays/shales. Each sample was placed in a cylindrical plastic cup one inch in diameter and about 1 inch in height (**Figure 5.11**). The material comprising the cup did not affect the IRM results. Each sample was subjected to a series of direct field (DF) applications up to 130 mT generated by a Molspin pulse magnetizer. Each DF application consisted of a pulse lasting about 100 ms along the z (vertical) axis. The acquired IRM magnitude after each DF application was then measured on a Molspin magnetometer. Since the samples were ground into powders (to improve the XRF results) the grains were essentially isotropically distributed and so the IRM measurements could have been performed along any of the arbitrary (x, y or z) axes and would be expected to give similar results.

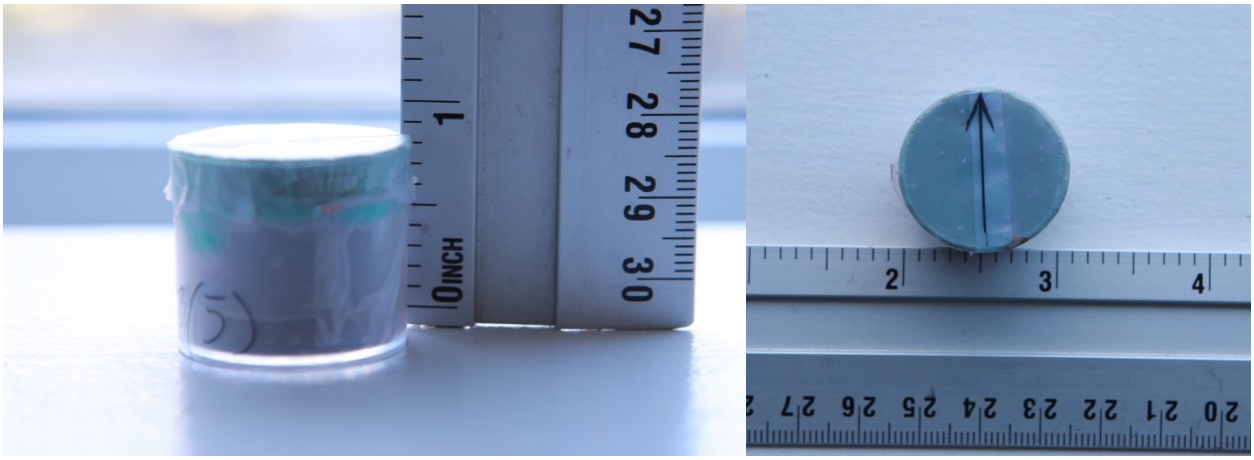

**Figure 5.11**: A typical sample used for the isothermal remanent magnetization (IRM) measurements. The direct field (DF) was applied along the positive z direction (vertically downward in the left hand image). The right hand image shows the top of the sample (the arrow represents the positive x direction, and the positive y direction is 90º clockwise from the positive x direction).

### 5.3.3. Results and discussion

The IRM acquisition curves (plotted in terms of mass magnetization) for the various samples are shown in **Figures 5.12** and **5.13**. Most curves are starting to saturate at the maximum applied field of 130 mT. This provides some insights into the type of remanence carrying particle. It cannot be hematite, since hematite needs much higher fields before it saturates. The curves are, however, similar to the types of curves acquired by magnetite (Potter and Stephenson, 1990).

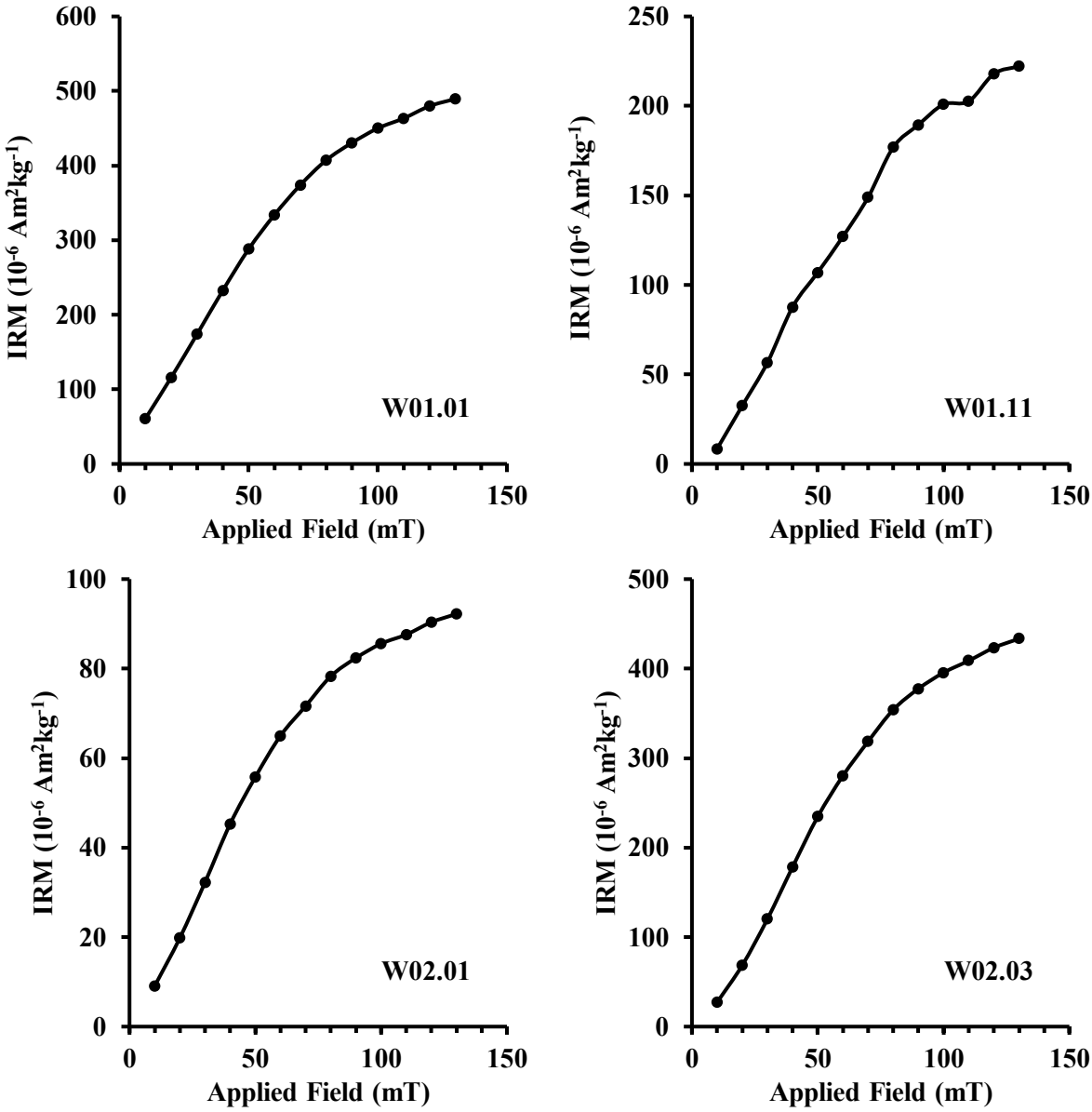


**Figure 5.12**: IRM acquisition curves as a function of applied direct field (DF) produced by a pulse magnetizer for various powdered core samples. The lithologies of the samples and other details (magnetic susceptibilities and XRF elemental contents) are given in **Tables 5.1** and **5.2**.

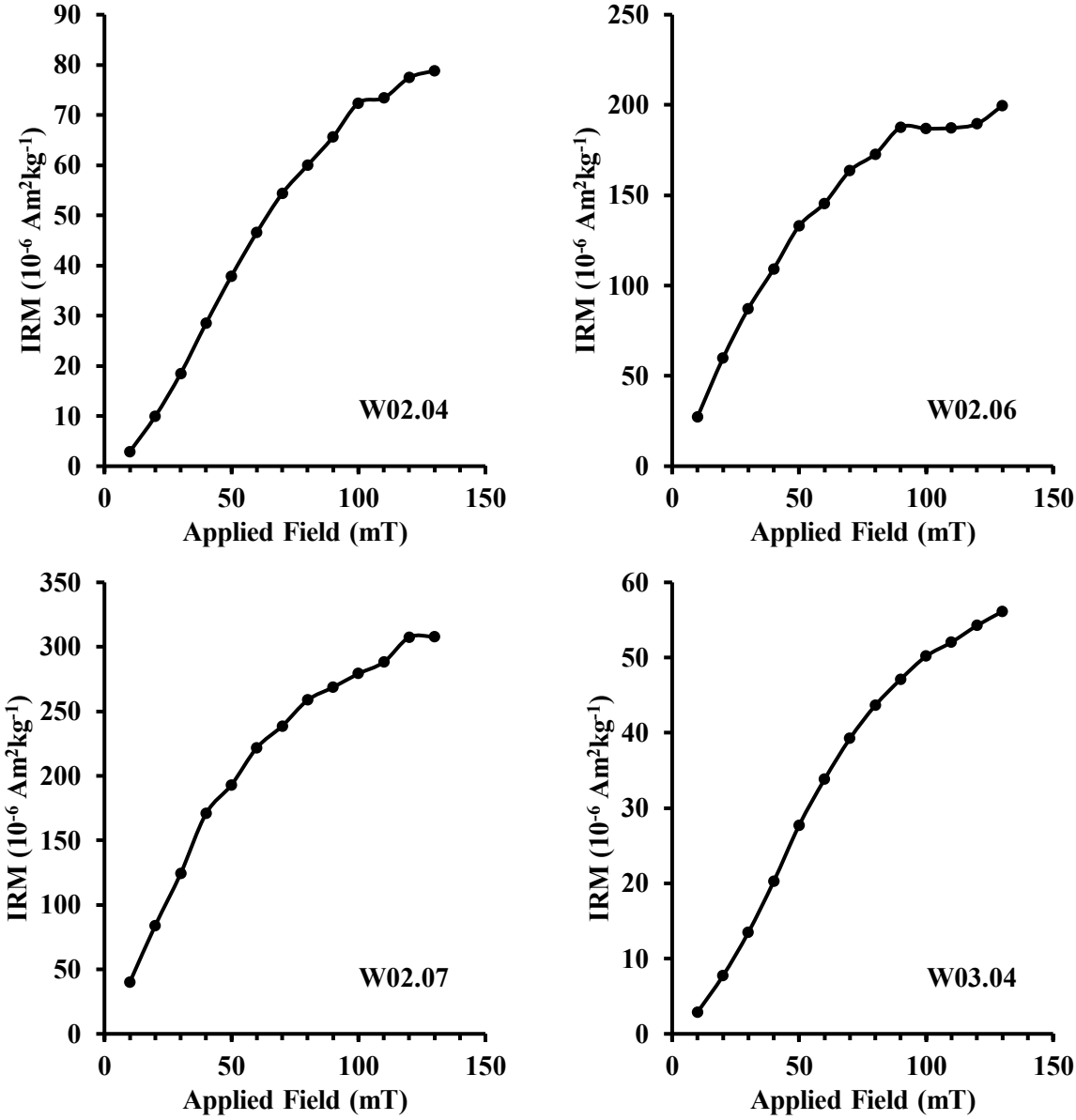


**Figure 5.13**: IRM acquisition curves as a function of applied direct field (DF) produced by a pulse magnetizer for more powdered core samples. The lithologies of the samples and other details (magnetic susceptibilities and XRF elemental contents) are given in **Tables 5.1** and **5.2**.

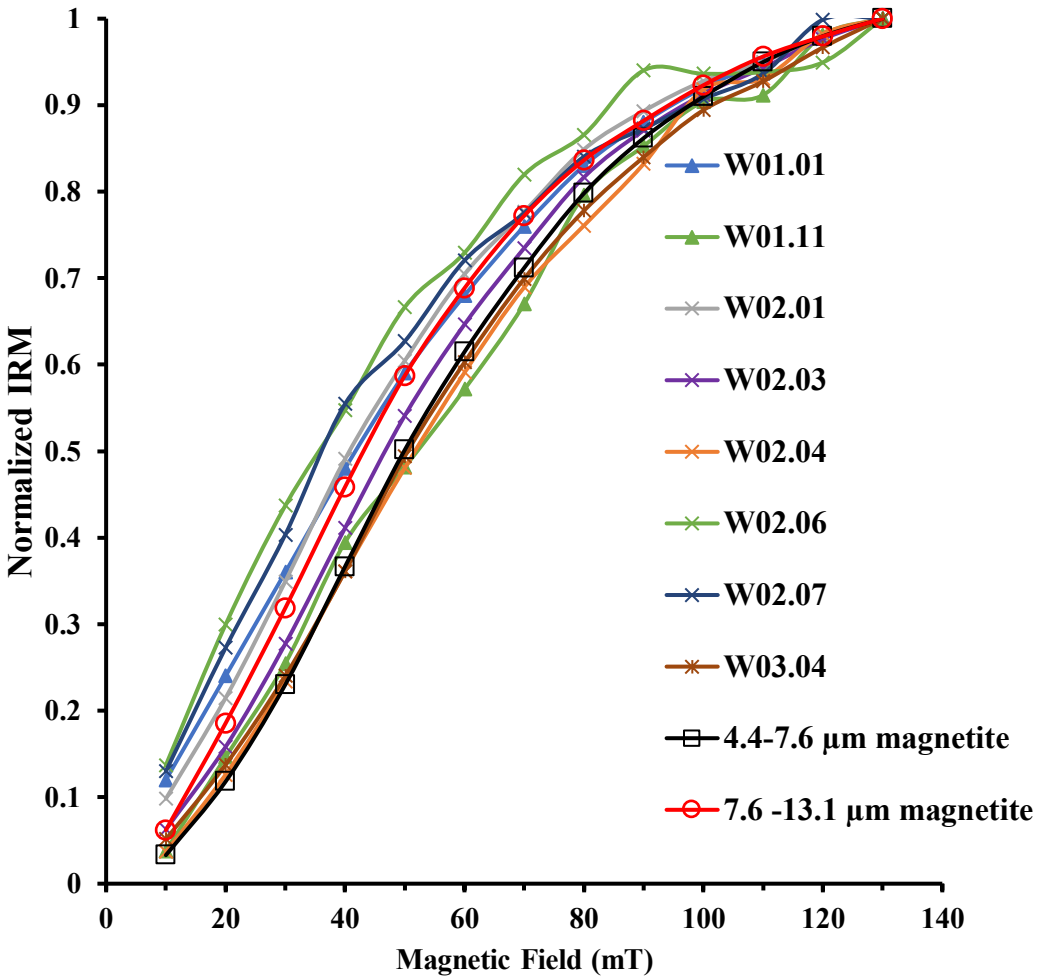


**Figure 5.14**: This shows the IRM results from **Figures 5.12** and **5.13** plotted on a normalized scale. Most of the curves follow a fairly closely related trend. Also plotted for comparison are curves for two magnetite particle size fractions (Potter, personal communication) which extend the results for magnetite shown in Potter and Stephenson (1990) up to 130 mT. Some of the normalized core samples follow the trend of the 4.4-7.6 µm magnetite sample, whilst others follow the trend of the 7.6-13.1 µm magnetite sample.

**Figure 5.14** shows the IRM results from **Figures 5.12** and **5.13** plotted on a normalized scale, and indicates that all the curves are quite similar. This suggests that the mineralogy and particle size is fairly similar for these core samples, with some minor differences. The normalized curves for core samples W01.11, W02.03, W02.04 and W03.04 show a close correspondence to the 4.4–7.6 µm magnetite sample, whereas core samples W01.01, W02.01, W02.06 and W02.07 are

closer to the 7.6-13.1 μm magnetite sample. These sizes of magnetite are regarded as small multidomain. Using this information, and assuming the IRM results for the core samples are due to magnetite, one can estimate the mass of magnetite in the core samples. The two particle size fractions of magnetite each had 10 mg of magnetite, and the mass of magnetite in the core samples could be estimated from the following equation:

Mass of magnetite in mg = [(IRM of core sample) / (IRM of 10 mg magnetite)] x 10 mg **(5.1)**

where the IRM of the core samples was taken from the IRM per unit volume values at 130 mT (**Table 5.3**), and the IRM per unit volume of the 10 mg magnetite samples was 6,802 $mAm^{-1}$ for the 4.4-7.6 μm magnetite and 3,857 $mAm^{-1}$ at 130 mT for the 7.6–13.1 μm magnetite (Potter, personal communication). The IRM per unit volume values (i.e., volume magnetization) were used since these compared similarly derived raw IRM values for the core samples and magnetite particle size fractions. Whilst **Figures 5.12** and **5.13** show IRM per unit total sample mass (mass magnetization, which is generally plotted in rock and palaeomagnetism) for the core samples, the mass magnetization IRM results for the two magnetite fractions were recorded in terms of the mass of magnetite (Potter, personal communication, and in Potter and Stephenson, 1990), so these results would not have compared like with like. The most relevant magnetite particle size fraction for each core sample, as indicated above, was used in **Equation (5.1)**. The multiplier of 10 mg in **Equation (5.1)** relates to the 10 mg mass of the magnetite particle size samples. **Table 5.3** shows the IRM values at 130 mT given both in terms of IRM per unit mass and IRM per unit volume for the core samples, together with the calculated masses of magnetite using **Equation (5.1)**, and the percentage magnetite mass in the sample. The results show that the masses of magnetite are extremely small, particularly as a percentage of the total mass of the samples (the sample masses ranged from 12.60–16.38 g). Nevertheless, the high magnetic susceptibility of

magnetite means that the contribution of this magnetite to the total magnetic susceptibility of the sample may still be significant.

The mass magnetic susceptibility, $\chi_m$, of the magnetite amounts for the core samples given in **Table 5.3** can be determined from the following equation:

$\chi_m$ = [(mass of magnetite in mg/10 mg) x $k_{sm}$ x $4\pi$ x $10^{-9}$ x 12.8] / mass of core sample in g **(5.2)**

where $k_{sm}$ is the volume magnetic susceptibility of the most relevant magnetite particle size fraction for each core sample (4.4–7.6 μm or 7.6-13.1 μm), $4\pi$ x $10^{-9}$ x 12.8 is a conversion factor from volume to mass magnetic susceptibility (and also accounts for the 1 inch cylindrical sample volume to SI units), and the 10 mg relates to the 10 mg mass of the magnetite samples. **Table 5.4** shows the mass magnetic susceptibilities of magnetite calculated via **Equation (5.2)**, as well as the total mass magnetic susceptibilities of the samples. For the clay/shale samples the magnetite mass magnetic susceptibilities represent a relatively small fraction of the total sample susceptibilities, whereas for the clean sands (which comprise predominantly diamagnetic, negative susceptibility, quartz) the magnetite signal is a significant part of the total signal.

**Table 5.3**: IRM results for an applied field of 130 mT for various samples and the corresponding masses of magnetite in those samples calculated using **Equation (5.1)**. Also shown is the magnetite mass as a percentage of the total sample mass.

| Well | Sample and lithology | IRM per unit mass at 130 mT ($10^{-6}$ $Am^2kg^{-1}$) | IRM per unit volume at 130 mT ($mAm^{-1}$) | Magnetite mass (mg) | Percent magnetite mass in sample (%) |
|---|---|---|---|---|---|
| **Well 01** | W01.01 (clean sand + heavy oil) | 489.4 | 626.0 | 1.62 | 0.0099 |
| | W01.11 (muddy sand, IHS) | 222.2 | 217.0 | 0.32 | 0.0025 |
| **Well 02** | W02.01 (clean sand + heavy oil) | 92.2 | 100.5 | 0.26 | 0.0018 |
| | W02.03 (clean sand) | 433.4 | 427.8 | 0.63 | 0.0049 |
| | W02.04 (muddy sand, IHS) | 78.9 | 95.3 | 0.14 | 0.0009 |
| | W02.06 (clay/shale) | 199.6 | 205.4 | 0.53 | 0.0040 |
| | W02.07 (clay/shale) | 307.8 | 331.6 | 0.86 | 0.0062 |
| **Well 03** | W03.04 (muddy sand, IHS) | 56.1 | 65.4 | 0.10 | 0.0007 |

**Table 5.4**: Low field mass magnetic susceptibility results for various samples (same samples as for **Table 5.3**), and the corresponding values for the magnetite component in the samples calculated using **Equation (5.2)**.

| Well | Sample and lithology | Mass magnetic susceptibility of sample ($10^{-8}$ $m^3kg^{-1}$) | Mass magnetic susceptibility of magnetite in sample ($10^{-8}$ $m^3kg^{-1}$) |
|---|---|---|---|
| **Well 01** | W01.01 (clean sand + heavy oil) | -0.53 | 6.17 |
| | W01.11 (muddy sand, IHS) | 3.00 | 1.40 |
| **Well 02** | W02.01 (clean sand + heavy oil) | -0.92 | 1.13 |
| | W02.03 (clean sand) | 1.22 | 2.72 |
| | W02.04 (muddy sand, IHS) | 5.79 | 0.50 |
| | W02.06 (clay/shale) | 11.89 | 2.51 |
| | W02.07 (clay/shale) | 14.56 | 3.89 |
| **Well 03** | W03.04 (muddy sand, IHS) | 4.53 | 0.36 |

In the previous chapters the illite content was estimated from a simple model that merely assumed a mixture of quartz + illite. This simple model assumed illite was the only positive component of the magnetic susceptibility, and will therefore overestimate the illite content to some extent if there are other positive magnetic susceptibility minerals (such as magnetite) in the sample. Knowing the contribution of the magnetite to the total magnetic susceptibility signal one can use the results in **Table 5.4** to give more accurate estimates of the illite contents. **Table 5.5** shows the initial estimated illite contents for the samples from the simple quartz + illite model, as well as the corresponding improved illite estimates taking into account the magnetic susceptibility of the magnetite. The fraction of illite, $F_I$, from the initial simple quartz + illite model is given by the following equation:

$$F_I = (\chi_T - \chi_Q) / (\chi_I - \chi_Q) \qquad \textbf{(5.3)}$$

where $\chi_T$ is the total mass magnetic susceptibility of the sample, and $\chi_I$ and $\chi_Q$ are the mass magnetic susceptibilities of illite (15 x $10^{-8}$ $m^3kg^{-1}$) and quartz (-0.62 x $10^{-8}$ $m^3kg^{-1}$), respectively. Note that this is similar to **Equation (3.2)** in **Chapter 3** except that equation was written in terms of volume magnetic susceptibilities, whereas **Equation (5.3)** is written in terms of mass magnetic susceptibilities. The improved estimation of the fraction of illite, $F_I$, that takes into account the mass magnetic susceptibility of the magnetite (and assumes a mixture of quartz + illite + magnetite) is given by the following equation, which merely replaces $\chi_T$ by $\chi_T - \chi_m$ :

$$F_I = \{(\chi_T - \chi_m) - \chi_Q\} / (\chi_I - \chi_Q) \qquad \textbf{(5.4)}$$

where $\chi_m$ is the mass magnetic susceptibility of the magnetite in the sample as before as given in **Table 5.4**. The results in **Table 5.5** show that the corrected illite contents, which account for the magnetite in the samples, are lower than the initial estimates from the simple quartz + illite model. The corrected illite estimates improve the interpretations of the lithologies. For example,

0% illite is now indicated in all the clean sand samples W01.01, W02.01 and W02.03 ("clean" sand meaning sand with little or no clay). Temperature dependent magnetic susceptibility measurements on clean sand samples in **section 5.5** will also support this by showing no temperature dependence (if illite was present there would be a drop in magnetic susceptibility with increasing temperature). It is also important to note that the improved illite estimates do not invalidate the determinations of lithology based on the initial probe magnetic susceptibility measurements. Those probe measurements indicated the 3 main lithologies (clean sands, IHS beds - muddy sand or interbedded clay and sand, and clay/shale), and the lithology designations for the samples in **Table 5.5** did not change based on the improved estimated illite contents. The trends of the initially estimated illite contents (using the probe results and the simple quartz + illite model) with depth, and the correlations with XRF and other parameters shown in **Chapters 3** and **4**, are not likely to be substantially affected if one ignores the effect of the minute amounts of magnetite particles in the core, even though the improved illite contents are lower than the initial estimates. In practical terms the initial probe magnetic susceptibility measurements on slabbed core provide a rapid, non-destructive means of estimating an "illite" content, which was demonstrated in **Chapters 3** and **4** to be a useful parameter by correlating with other downhole logs, permeability, and XRF. It would not be time- and cost-effective in an industrial petrophysical analysis context to undertake IRM measurements on several thousand samples, merely to obtain improved illite estimates, when one can rapidly screen the slabbed core using the probe magnetic technique and obtain reasonable estimates that can be correlated to other petrophysical parameters. However, one can perform some selected IRM measurements on representative samples, as in the present study, to get an idea of the improved illite estimates by accounting for the magnetite amounts.

**Table 5.5**: Illite contents for various samples (same samples as for **Tables 5.3** and **5.4**) estimated from the initial simple quartz + illite model and the sample mass magnetic susceptibilities from column 3 of **Table 5.4** and using **Equation (5.3),** together with the corrected illite estimates taking into account the mass magnetic susceptibility values of the magnetite in the samples (given in column 4 of **Table 5.4**) and using **Equation (5.4)**.

| Well | Sample and lithology | Illite estimated from simple quartz + illite model (%) | Illite estimate corrected for magnetite content (%) |
|---|---|---|---|
| **Well 01** | W01.01 (clean sand + heavy oil) | 0.58 | 0.00* |
| | W01.11 (muddy sand, IHS) | 23.18 | 14.21 |
| **Well 02** | W02.01 (clean sand + heavy oil) | 0.00* | 0.00* |
| | W02.03 (clean sand + heavy oil) | 11.78 | 0.00* |
| | W02.04 (muddy sand, IHS) | 41.04 | 37.84 |
| | W02.06 (clay/shale) | 80.09 | 64.02 |
| | W02.07 (clay/shale) | 97.18 | 72.30 |
| **Well 03** | W03.04 (muddy sand, IHS) | 32.97 | 30.67 |

*__Equations (5.3)__ and __(5.4)__ actually gave negative values for the illite content for these 3 results, and since this is not possible in reality the values have been given as zero per cent illite, which will be very close to the true values. The negative values from the equations merely arise from assuming simple model mixtures of quartz + illite for **Equation (5.3)** and quartz + illite + magnetite for **Equation (5.4)**. If the sample contains other diamagnetic components (minerals and/or fluids) that have more negative magnetic susceptibility than quartz then negative values for the "illite" content can occur.

## 5.4. Low field versus high field magnetic susceptibility measurements

### 5.4.1. Introduction

Another independent method to identify and quantify the effect of remanence carrying particles is to compare the low field and high field magnetic susceptibility signals. All minerals will contribute to the low field magnetic susceptibility signal, but most remanence carrying particles (such as ferrimagnetic magnetite) saturate in high fields (generally no higher than about 300 mT, though hematite is an exception that requires higher fields) and so do not contribute to the high field magnetic susceptibility. Therefore the difference between the low field and high field magnetic susceptibility represents the magnetic susceptibility signal of the remanence carrying particles in the sample. This, in conjunction with additional information or assumptions regarding the mineralogy and particle size of these remanence carrying particles, can be used to independently estimate the amount of these particles in the sample.

### 5.4.2. Samples and equipment

Two key samples were taken from the slabbed cores. They were a muddy sand sample and one of the anomalous mineral samples (both samples were from Well 02). Low and high field mass magnetic susceptibility measurements at room temperature were made on each of the samples. The low field measurements were undertaken using a Bartington MS2W sensor (as described in **Chapter 2**). The applied low field was 80 $Am^{-1}$, which corresponded to about 0.10 mT. The high field magnetic susceptibility measurements were undertaken using a Sherwood magnetic susceptibility balance (AUTO version). The Sherwood balance applies a field of 450 mT to the sample. The high field measurements were made for us by the company Advanced Downhole Petrophysics (ADP) in the UK, to whom we had previously lent our Sherwood balance

equipment. They had needed the equipment for other purposes, and rather than get them to send us this sensitive equipment back temporarily, we sent them the key samples for measurement in their laboratory.

### 5.4.3. Results and discussion

**Table 5.6** shows low and high field mass magnetic susceptibility results for a muddy sand sample. The high field mass magnetic susceptibility is lower than the low field mass magnetic susceptibility because the remanence carrying particles saturate in the high field, and don't contribute to the high field magnetic susceptibility. The difference between the two values should relate to the magnetic susceptibility of the remanence carrying particles, in this case the mass magnetic susceptibility of the magnetite in the sample. **Table 5.6** shows that the difference between the low and high field mass magnetic susceptibilities ($0.43 \times 10^{-8}$ $m^3kg^{-1}$**)** is indeed very close to the mass magnetic susceptibility of the magnetite in this sample ($0.50 \times 10^{-8}$ $m^3kg^{-1}$) shown in **Table 5.4** that was determined independently from the IRM method. The fact that the IRM method is consistent with the low field versus high field magnetic susceptibility method gives us confidence that the results are meaningful, and that magnetite is likely to be the remanence carrying mineral. Compared to the low field versus high field magnetic susceptibility method, the IRM method is intrinsically more accurate because it only targets the remanence carrying minerals, its signal is large, and it doesn't depend on measurements using two different pieces of equipment.

**Table 5.6**: Low field (using a Bartington MS2W sensor) and high field (using a Sherwood AUTO balance) magnetic susceptibility values for a muddy sand sample. The difference between the low and high field values (column 4) is consistent with the mass magnetic susceptibility of magnetite in the sample that was independently determined from the IRM results (column 5) given previously in **Table 5.4**.

| **Sample** | **Low field mass magnetic susceptibility ($10^{-8}$ $m^3kg^{-1}$)** | **High field mass magnetic susceptibility ($10^{-8}$ $m^3kg^{-1}$)** | **Difference between the low and high field mass magnetic susceptibilities ($10^{-8}$ $m^3kg^{-1}$)** | **Mass magnetic susceptibility of magnetite in the sample from IRM results of Table 5.3 ($10^{-8}$ $m^3kg^{-1}$)** |
|---|---|---|---|---|
| W02.04 (muddy sand, IHS) | 5.79 | 5.36 | 0.43 | 0.50 |

**Table 5.7** shows low and high field mass magnetic susceptibility results for one of the anomalous mineral samples from Well 02 (depth 374.2 m). The difference between the two values, 8.87 x $10^{-8}$ $m^3kg^{-1}$, represents the contribution of the remanence carrying particles to the low field mass magnetic susceptibility. The remaining value (35.77 x $10^{-8}$ $m^3kg^{-1}$ according to the high field mass magnetic susceptibility) must be due to the combined signal of the diamagnetic + paramagnetic components. This signal is too large to be from illite alone (100% illite would only give 15 x $10^{-8}$ $m^3kg^{-1}$). Therefore there must be another mineral (with or without illite) comprising the sample that has a higher paramagnetic susceptibility than illite. A prime candidate is the paramagnetic carbonate siderite ($FeCO_3$). This is also consistent with the relatively high iron content of this sample (24.7% from XRF). A siderite content of about 29% would give the required mass magnetic susceptibility of 35.77 x $10^{-8}$ $m^3kg^{-1}$ (100% siderite would give 122.57 x $10^{-8}$ $m^3kg^{-1}$, see **Table 4.2** in **Chapter 4**). Alternatively, less siderite is required if there is some illite in the sample. The results of **Table 5.7** provide further independent

support for the suggestion made in **Chapters 3** and **4** that this anomalous mineral is (at least in part) comprised of siderite.

**Table 5.7**: Low field (using a Bartington MS2W sensor) and high field (using a Sherwood AUTO balance) magnetic susceptibility values for an "anomalous mineral" sample from Well 02. The difference between the two values, 8.87 x $10^{-8}$ $m^3kg^{-1}$, represents the contribution of the remanence carrying particles (assumed to be magnetite) to the low field mass magnetic susceptibility. The remaining signal that is left at high field (35.77 x $10^{-8}$ $m^3kg^{-1}$) must be due to the combined signal of the diamagnetic + paramagnetic components. Since this value is too high to be due to illite alone (100% illite would give 15 x $10^{-8}$ $m^3kg^{-1}$) then the results suggest that a paramagnetic mineral with higher magnetic susceptibility than illite, such as siderite, comprises at least part of this sample.

| **Sample** | **Low field mass magnetic susceptibility ($10^{-8}$ $m^3kg^{-1}$)** | **High field mass magnetic susceptibility ($10^{-8}$ $m^3kg^{-1}$)** | **Difference between the low and high field mass magnetic susceptibilities ($10^{-8}$ $m^3kg^{-1}$)** |
|---|---|---|---|
| W02.99 (anomalous mineral) | 44.64 | 35.77 | 8.87 |

## 5.5. Temperature dependent magnetic susceptibility measurements

### 5.5.1. Introduction

All the magnetic susceptibility measurements so far (in the previous chapters and this chapter) were made at ambient (room temperature) conditions on core samples. The applications of magnetic susceptibility (for estimating illite content, fluid permeability trends etc) can also be potentially extended to in-situ borehole magnetic susceptibility logging. However, for borehole measurements the temperature dependence of magnetic susceptibility for certain minerals needs to be taken into consideration. Temperature generally increases with increasing depth within boreholes, and so it is important to determine how this affects the magnetic susceptibility of reservoir minerals and fluids. The magnetic susceptibility of diamagnetic minerals (such as quartz, calcite, kaolinite) and most reservoir fluids do not theoretically vary with changes in temperature. In contrast, the magnetic susceptibility of paramagnetic minerals (e.g., illite) decreases with increasing temperature according to the Curie law (quantified by **Equation (5.5)** in **section 5.5.2** below).

In addition, the measurement of temperature dependent magnetic susceptibility is potentially useful as a further laboratory method for identifying and quantifying the content of paramagnetic minerals (such as illite) in a rock sample. Any paramagnetic components can be identified and quantified from decreases in magnetic susceptibility with increasing temperature. Samples which are comprised entirely of diamagnetic components will not exhibit any change in magnetic susceptibility with variations in temperature.

This section will present temperature dependent magnetic susceptibility results on representative extracted samples from the slabbed cores of the three oil sands wells in this study. The temperature dependent results are plotted on model template curves for mass magnetic susceptibility (introduced by Ali and Potter, 2011) as a further independent method of quantifying illite content, and are compared with the illite contents estimated from the room temperature probe volume magnetic susceptibility measurements on the intact slabbed core. The temperature dependent template curves are also extended for use with volume magnetic susceptibility, and with depth (by converting the temperature scale to a depth scale using a relevant local geothermal gradient for the Albertan oil sands), in order to demonstrate how the volume magnetic susceptibility and illite content would vary with depth for in-situ borehole volume magnetic susceptibility applications.

### 5.5.2. Methods

Ali and Potter (2011) generated a series of model template curves of temperature dependent mass magnetic susceptibility for mixtures of illite and quartz using the Curie law equation below:

$$\chi = C/T \qquad \textbf{(5.5)}$$

where M is the mass magnetization, H is the applied field, M/H is then the mass magnetic susceptibility, C is a mineral-specific Curie constant, and T is the absolute temperature in Kelvin. Note that a similar equation can be written in terms of the magnetization per unit volume, J, which would replace M, so that J/H would then be the volume magnetic susceptibility. This is potentially important for borehole magnetic susceptibility measurements, since borehole sensors will measure the volume magnetic susceptibility as the mass will not be measured during normal borehole logging operations. The model template curves of Ali and Potter (2011) are reproduced

here in **Figure 5.15** and used ambient (room temperature) mass magnetic susceptibility values of -0.62 x $10^{-8}$ $m^3kg^{-1}$ for quartz (theoretical value from Ivakhnenko, 2006), and 15 x $10^{-8}$ $m^3kg^{-1}$ for illite (Hunt et al., 1995).

Measuring the variation of magnetic susceptibility with temperature potentially allows for more accurate determinations of the paramagnetic versus diamagnetic contents in a reservoir sample, compared to a single room temperature magnetic susceptibility measurement. For example, a single room temperature negative magnetic susceptibility measurement could mean a pure diamagnetic mineral or a diamagnetic mineral with a small amount of a paramagnetic mineral. However, any changes of magnetic susceptibility with temperature would identify the presence of a paramagnetic mineral. Furthermore, a single room temperature positive magnetic susceptibility measurement does not indicate whether there are just one or multiple positive magnetic susceptibility minerals in the sample. However, a temperature dependent magnetic susceptibility curve can help to distinguish these different possibilities. For example, if the curve follows the trend of an illite + quartz curve (**Figure 5.15**) then one can be fairly confident that illite is the only positive magnetic susceptibility mineral present. If the curve does not follow the trend of an illite + quartz curve then there may be other positive magnetic susceptibility minerals (paramagnetic, ferrimagnetic or canted antiferromagnetic) present either in addition to or without illite.

Measurements of temperature dependent mass magnetic susceptibility were undertaken using a Bartington system that included a MS2 susceptibility meter, a MS2WF furnace, and an MS2W sensor (described in **Chapter 2**), which for these experiments was cooled by a water jacket to

avoid damage to the sensor from the furnace coils surrounding the sample (**Figure 5.16**). The sensor has a 30 mm internal diameter sample cavity. The furnace coils were comprised of non-inductively wound platinum wire. The furnace was specially designed for use with the water jacketed MS2W sensor to facilitate temperature dependent magnetic susceptibility measurements up to 850 °C. A MS2WFP power supply unit was connected to the MS2WF furnace via an 8-way cable for the transmission of data and power. The unit supplies power to the furnace and provides either direct control of the temperature, or a slowly varying linear increase or decrease of temperature. During operation of the furnace, the flow of water needs to be steady to avoid any thermal damage to the sensor. Therefore, a submersible water pump was used to circulate the water around the sensor during the measurements. A flowmeter was connected to the water pipe to ensure the water was flowing at the required rate.

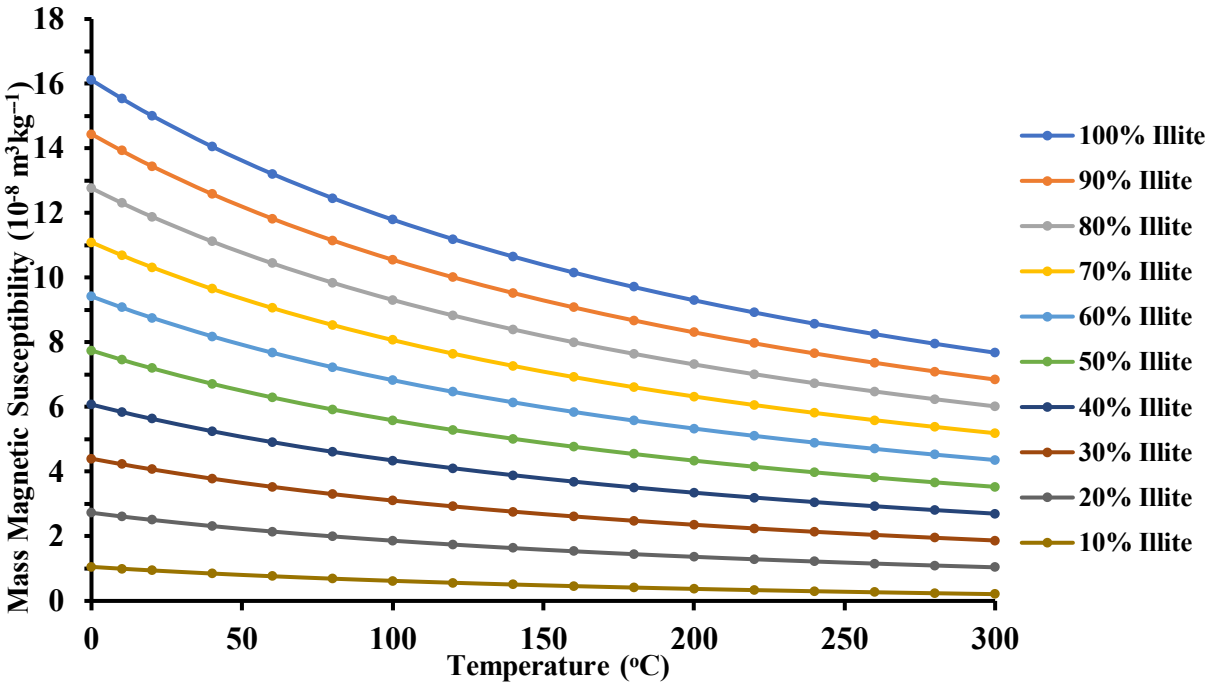


**Figure 5.15**: Theoretical mass magnetic susceptibility curves as a function of temperature for various mixtures of quartz and illite (edited from Ali and Potter, 2011).

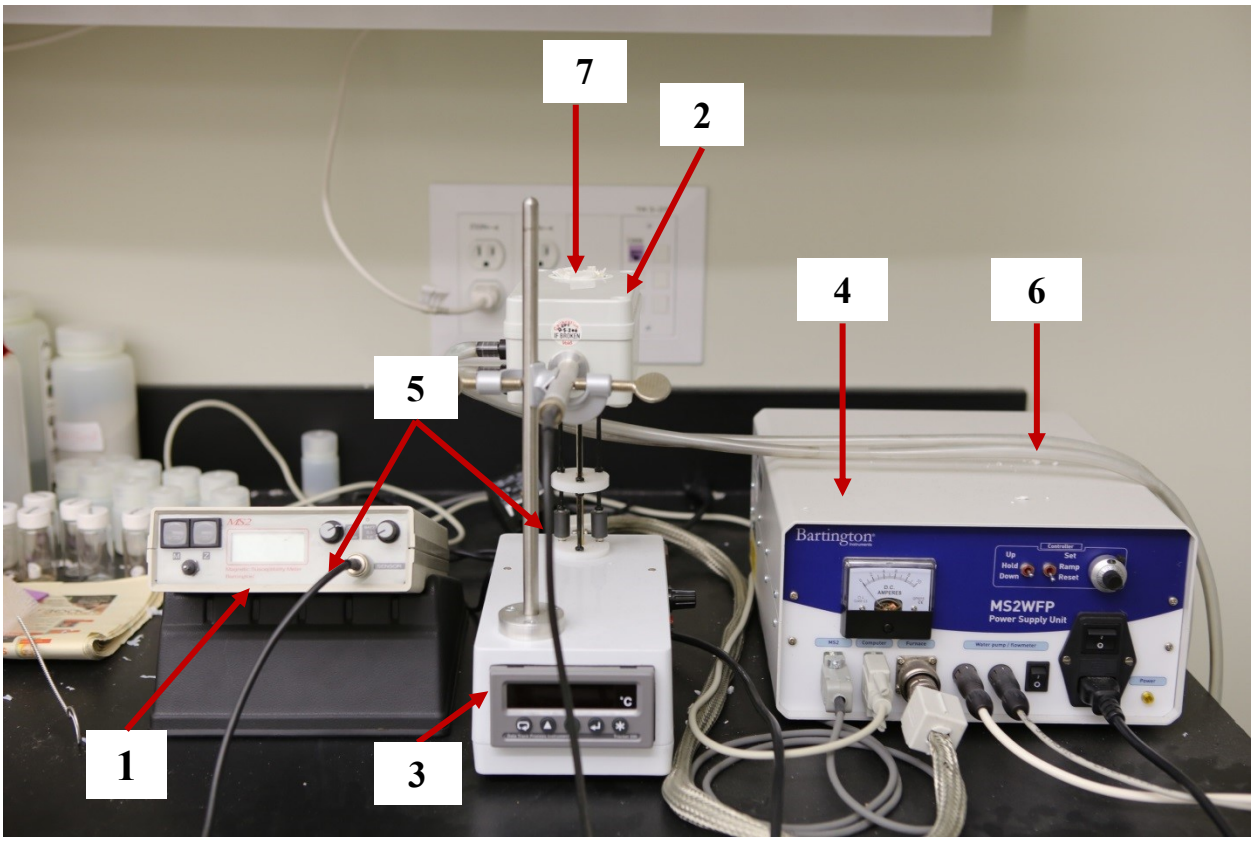


**Figure 5.16:** Bartington temperature dependent magnetic susceptibility measurement system. **1** is the MS2 magnetic susceptibility meter, **2** is the MS2W sensor, which is water cooled and surrounds the furnace coils, **3** is the MS2WF furnace and heating coils that surround the sample, **4** is the MS2WFP power supply unit for the furnace, **5** is cable connecting the meter and sensor, **6** is a water pipe circulating water between the supply tank and the sensor, and **7** is the sample cavity.

### 5.5.3. Samples and results

Eight powdered samples from the slabbed cores of the three oil sands wells were selected for temperature dependent magnetic susceptibility measurements. The samples covered a range of different lithologies, which included clean sands, muddy sands, and clay/shale. **Table 5.8** summarizes the samples with their depths, room temperature probe volume magnetic susceptibilities on the slabbed cores, the estimated illite contents from the room temperature probe volume magnetic susceptibilities on the slabbed cores, and estimated illite contents from the temperature dependent mass magnetic susceptibility measurements on the extracted samples

in conjunction with the model template curves for quartz + illite mixtures from Ali and Potter (2011).

**Table 5.8:** A list of powdered samples that were selected for temperature dependent magnetic susceptibility measurements. The table includes the results of room temperature volume magnetic susceptibility measured on the slabbed cores using the MS2E probe sensor (fourth column), illite contents derived from the room temperature probe volume magnetic susceptibility, and not corrected for magnetite content (fifth column), and illite contents quantified from the results of temperature dependent mass magnetic susceptibility on extracted samples using the MS2W sensor and furnace set-up (**Figure 5.16**) in conjunction with the model template curves of Ali and Potter (2011) again not corrected for magnetite content (sixth column).

| Well | Sample | Depth (m) | Room Temperature Probe Volume Magnetic Susceptibility ($10^{-5}$ SI) | Illite Content from the Room Temperature Probe Volume Magnetic Susceptibility Results (%) | Illite Content from Temperature Dependent Mass Magnetic Susceptibility Results and the Model Template Curves (%) |
|---|---|---|---|---|---|
| **Well 01** | W01.01 | 488.9 | -1.6 | 0.1 | 0.4 - 0.6 |
| | W01.12 | 508.9 | 7.8 | 22.1 | 22 - 23 |
| | W01.15 | 320.1 | 19.8 | 50.3 | 50 - 71 |
| **Well 02** | W02.01 | 388.9 | -1.4 | 0.6 | 0.0 |
| | W02.05 | 355.5 | 20.4 | 51.7 | 50 - 59 |
| **Well 03** | W03.01 | 192.4 | -0.5 | 2.7 | 2.1 - 3.8 |
| | W03.03 | 174.0 | 4.7 | 14.9 | 14 - 16 |
| | W03.06 | 157.1 | 18.4 | 47.0 | 40 - 57 |

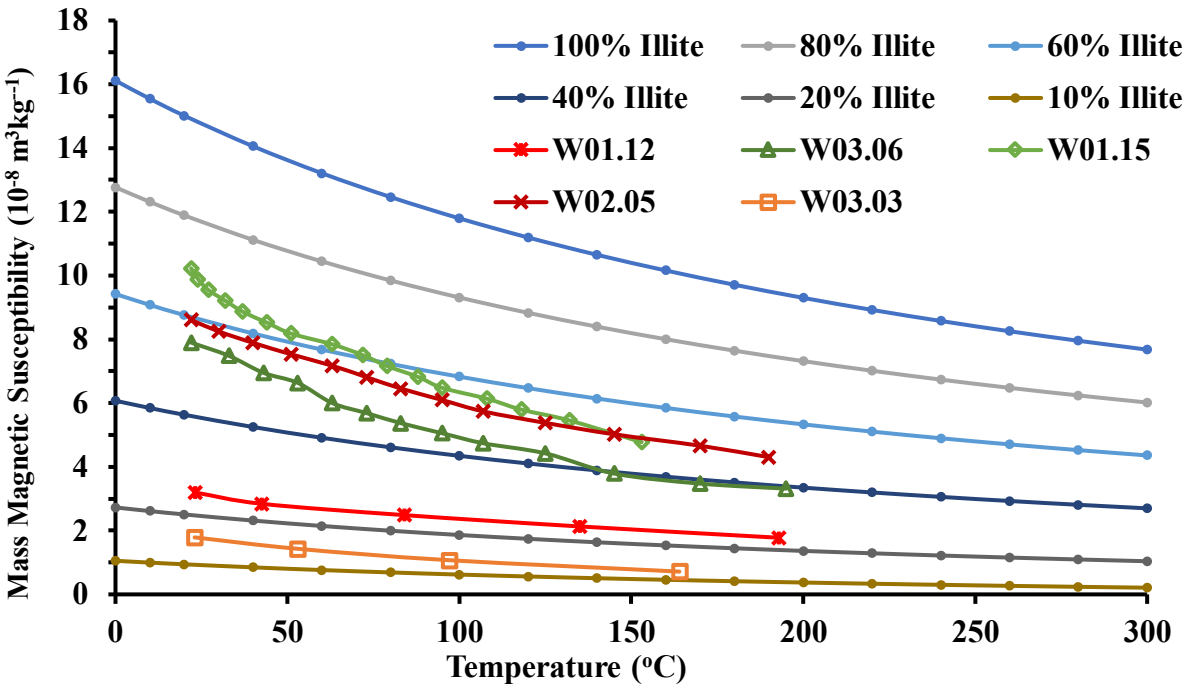


**Figure 5.17:** Results of temperature dependent magnetic susceptibility measured on 5 muddy sand and clay/shale samples from the three oil sands wells. The results are plotted on the model template curves of Ali and Potter (2011) for various mixtures of illite + quartz. The susceptibilities of all these samples decrease with increasing temperature, indicating that the samples contain a paramagnetic mineral or minerals. For samples W01.12, W02.05 and W03.03 the curves largely follow the trend of the template curves (especially for W01.12), strongly suggesting that illite is the main (and possibly only) paramagnetic mineral in these samples (the estimated illite contents from these curves are given in column six of **Table 5.8**). In contrast, the curves of samples W01.15 and W03.06 do not follow the trend of the illite + quartz curves exactly. These samples could contain small amounts of another paramagnetic mineral in addition to illite, or a different paramagnetic mineral without illite.

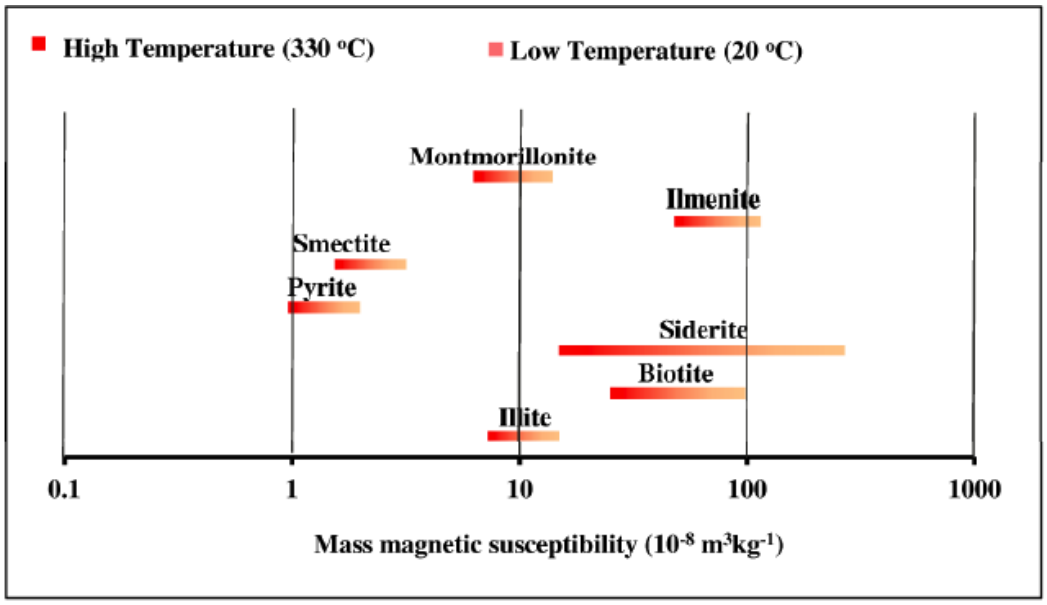


**Figure 5.18:** Theoretical variation of mass magnetic susceptibility values for various paramagnetic reservoir minerals at temperatures ranging from 20 °C to 330 °C using the Curie law (Ali and Potter, 2012).

The variation of magnetic susceptibility with temperature for the 5 muddy sand or clay/shale samples is shown in **Figure 5.17**. The susceptibilities of all these samples decrease with increasing temperature, indicating that the samples contain a paramagnetic mineral or minerals. For samples W01.12, W02.05 and W03.03 the curves largely follow the trend of the template curves (especially for W01.12), strongly suggesting that illite is the main (and potentially only) paramagnetic mineral in these samples. The estimated illite contents from these curves are given in column six of **Table 5.8.** These illite contents are close to those estimated independently from the room temperature probe volume magnetic susceptibility results on the slabbed core (fifth column of **Table 5.8**). In contrast, the curves of samples W01.15 and W03.06 are slightly steeper than the trends of the illite + quartz curves. These samples could contain small amounts of another paramagnetic mineral in addition to illite, or a different paramagnetic mineral without illite. To account for the slightly steeper trends this paramagnetic mineral should have a larger variation of magnetic susceptibility with temperature than illite. From **Figure 5.18** (taken from

Ali and Potter, 2012) one such mineral that has a larger variation than illite is the iron carbonate siderite. Sample W03.06 was collected close to the depth where the magnetic susceptibility profile also indicated a thin layer of an anomalous mineral with more than 100% magnetically estimated equivalent illite. The magnetic and XRF results described in **Chapter 4** suggested that this anomalous mineral could be siderite. Therefore, the temperature dependent results for sample W03.06 are consistent with this sample containing a certain amount of siderite (with or without illite).

The mass magnetic susceptibilities of samples W01.01, W02.01 and W03.01 do not show any variation with increasing temperature up to around 190 ºC (**Figure 5.19**). These samples are clean sands saturated with heavy oil (for samples W01.01 and W02.01) or with bitumen (sample W03.01). This means there are no paramagnetic minerals (e.g., illite) in these samples, otherwise there would have been decreases in magnetic susceptibility with increasing temperature. The results are consistent with the values of 0% illite for all the clean sand samples corrected for the magnetite content given in previous **Table 5.5** (samples W01.01 and W02.01 in **Figure 5.19** are the same samples as in **Table 5.5**). Samples W01.01 and W03.01 have slightly less negative magnetic susceptibility than pure quartz that has a theoretical value of -0.62 x $10^{-8}$ $m^3$ $kg^{-1}$ (Ivakhnenko, 2006). This is due to a very small amount of ferrimagnetic magnetite (1.62 mg or 0.0099% of the sample mass) for sample W01.01 (**Table 5.3**), whose magnetic susceptibility also doesn't change within the temperature range 20 ºC to 190 ºC. A similar explanation is likely for sample W03.01. Sample W02.01 has a slightly more negative value than pure quartz. This may be due to the higher heavy oil saturation in this sample (**Chapter 2** showed that the mass magnetic susceptibility of the heavy oil sample is more negative than for pure quartz). Heavy oil is diamagnetic and so its magnetic susceptibility is also independent of temperature.

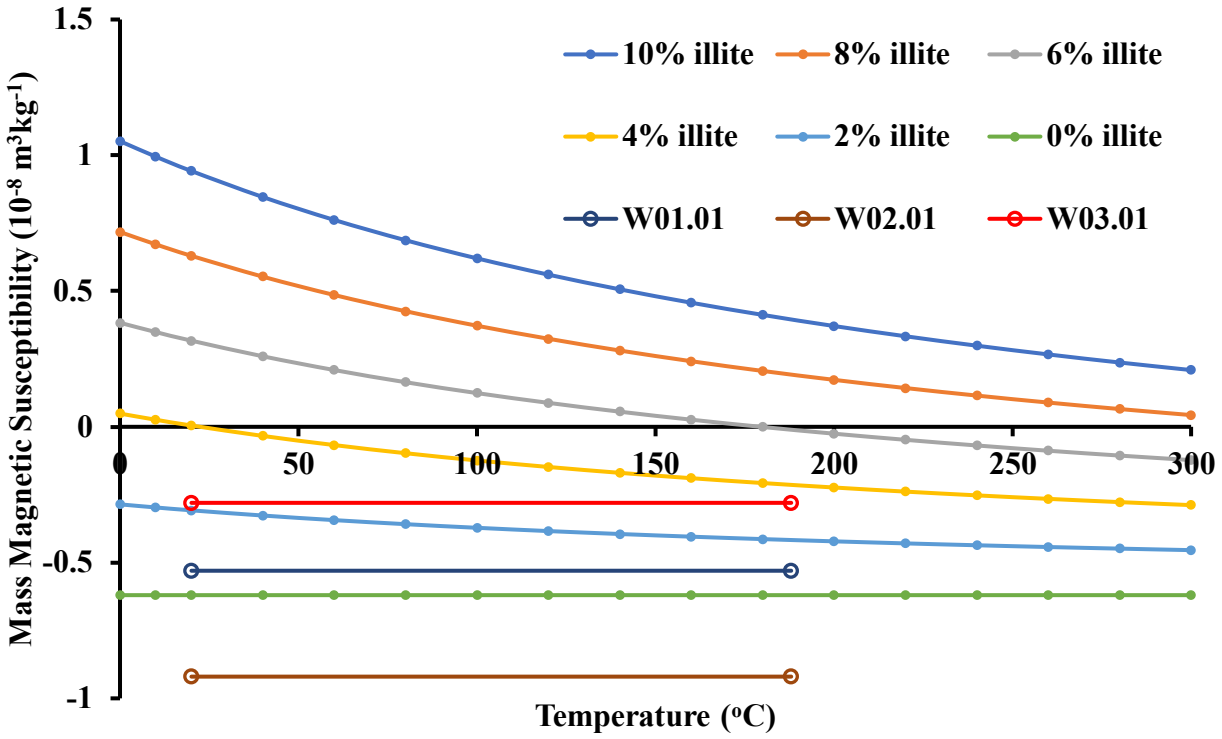


**Figure 5.19:** Results of temperature dependent magnetic susceptibility measurements on 3 selected clean sand samples (W01.01, W02.01 and W03.01) from the three oil sands wells. The results are plotted on the model template curves of Ali and Potter (2011) for various mixtures of illite + quartz. Since the samples are clean sands they contain predominantly diamagnetic quartz, which has negative magnetic susceptibility and is independent of temperature. The variations between the samples may be due to small amounts of other components, as detailed in the text, that are also temperature independent.

### 5.5.4. Model templates of volume magnetic susceptibility with temperature and depth for mixtures of quartz and illite for oil sands reservoir applications (core analysis and in-situ borehole applications)

Ali and Potter (2011) introduced theoretical model template curves of mass magnetic susceptibility with temperature for various mixtures of illite and quartz. However, the present thesis study has focused mainly on the application of probe volume magnetic susceptibility measurements to characterize oil sands reservoirs in Northern Alberta. Moreover, borehole magnetic susceptibility sensors measure the volume magnetic susceptibility (not the mass magnetic susceptibility). Therefore model template curves for the temperature dependence of

volume magnetic susceptibility for mixtures of illite + quartz would be potentially useful for applications in oil sands wells. **Figures 5.20** and **5.21** show temperature dependent model template curves for volume magnetic susceptibility for various mixtures of illite + quartz. **Figure 5.20** is for high illite contents and **Figure 5.21** is for low illite contents. The curves used theoretical room temperature volume magnetic susceptibility values of -1.643 x $10^{-5}$ SI for quartz (Ivakhnenko, 2006) and 41 x $10^{-5}$ SI for illite (Hunt et al., 1995). The decrease in absolute volume magnetic susceptibility is more significant at temperatures less than 80 °C, which is more relevant for the reservoir conditions of Albertan oil sands.

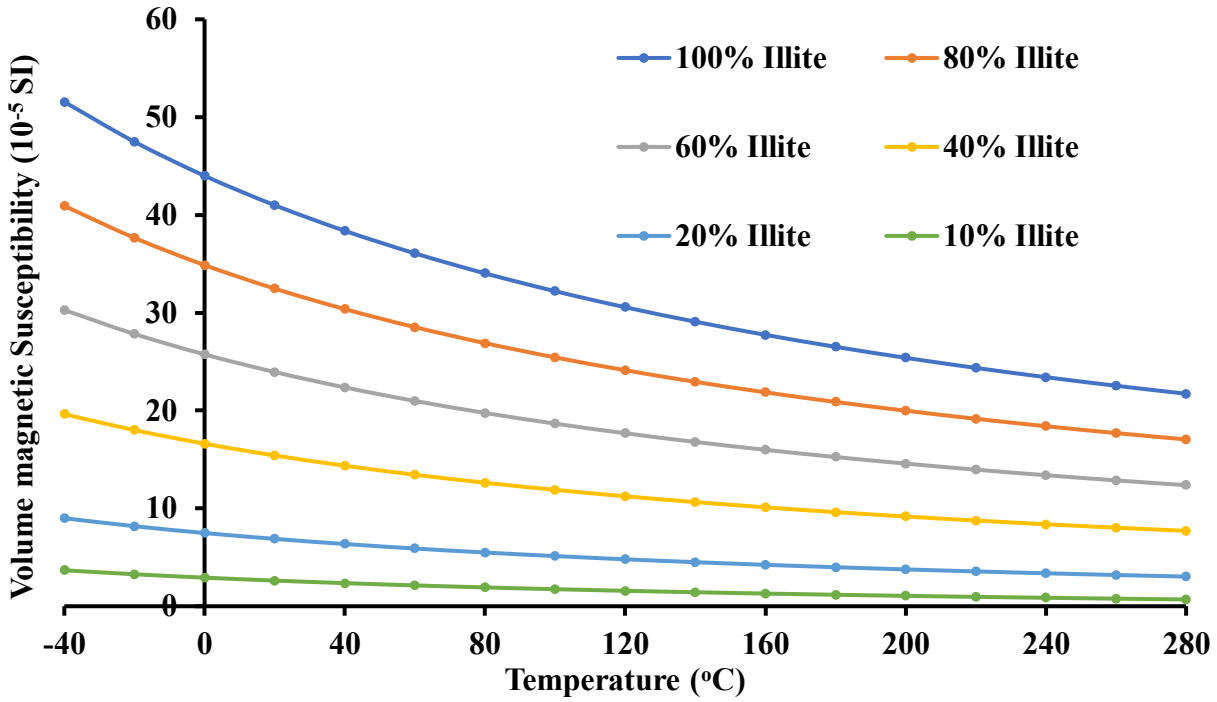


**Figure 5.20:** Theoretical volume magnetic susceptibility curves as a function of temperature for various mixtures of illite and quartz using the Curie law **Equation (5.5)**, but using the magnetization per unit volume (J) instead of the magnetization per unit mass (M). The curves show illite contents varying from 10% to 100%.

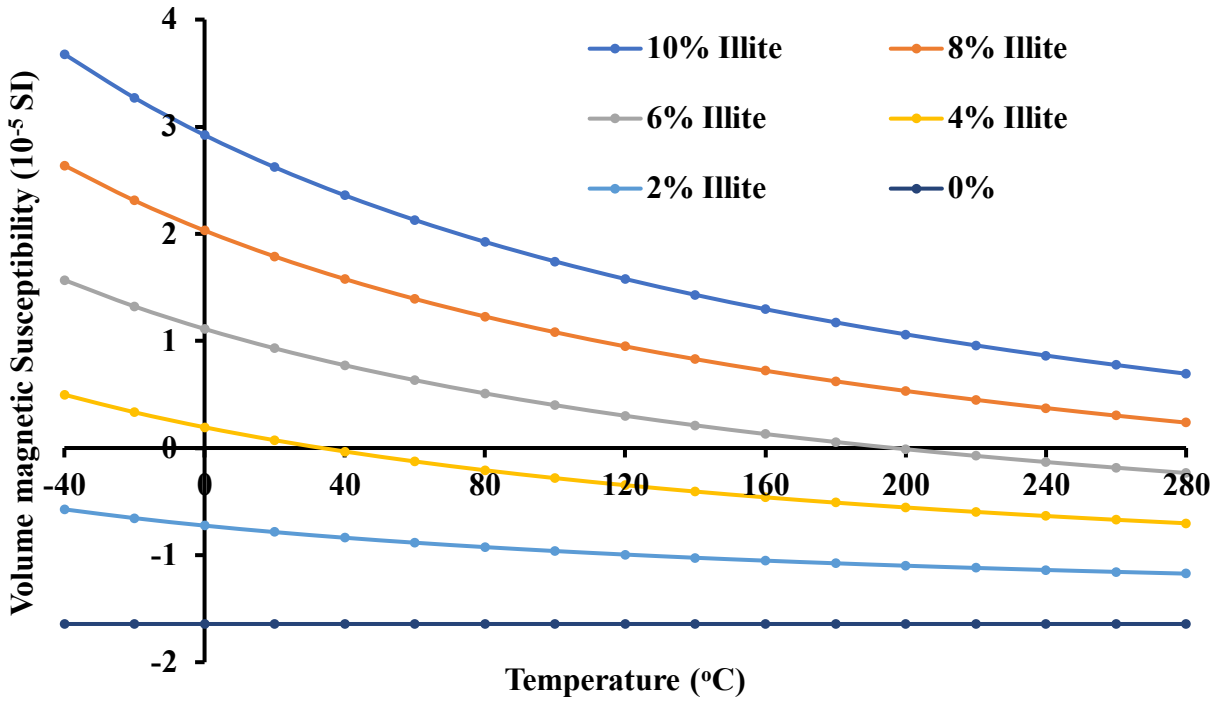


**Figure 5.21:** Theoretical volume magnetic susceptibility curves as a function of temperature for various mixtures of illite and quartz using the Curie law **Equation (5.5)**, but using the magnetization per unit volume (J) instead of the magnetization per unit mass (M). The curves show illite contents varying from 0% to 10%.

Borehole measurements of temperature dependent volume magnetic susceptibility would be potentially useful in distinguishing lithology (clay/shale, muddy sands and clean sands) and quantifying permeability controlling paramagnetic clay minerals in-situ in oil sands reservoirs. For example, smooth decreases of volume magnetic susceptibility with depth would likely indicate the presence of paramagnetic mineral(s) whose content does not change significantly (Ali and Potter, 2011). In contrast, temperature independent negative volume magnetic susceptibility would indicate clean sand intervals. Note that the volume magnetic susceptibility of a mixture of 6% illite and 94% of quartz becomes negative at around 200 ºC (**Figure 5.21**). Since the temperature at a depth of 1000 m at different locations in the Western Canada Sedimentary Basin is less than 50 ºC, and the surface temperature is around 0 ºC (Majorowicz et

al., 2013b), then any negative volume magnetic susceptibility signal measured in a borehole should indicate a clean sand interval.

**Figure 5.22** shows the model template curves of volume magnetic susceptibility with depth for various mixtures of illite + quartz for a typical Athabasca oil sands reservoir (the reservoir fluids are ignored, but are unlikely to make any significant difference to the results). In this figure the depth scale is converted from the temperature based on a geothermal gradient of 20 $^{o}$C/km in Fort McMurray area (Majorowicz et al., 2013a), and it is assumed that the surface temperature is 0 $^{o}$C. The variation of the volume magnetic susceptibility from the surface to a depth of 1000 m is less with lower illite contents (right hand plot of **Figure 5.22**). The template curves also show that the volume magnetic susceptibility varies more from the surface to a depth of 700 m, than between 700 m and 1,000 m. The variation is less than 1 x $10^{-5}$ SI from 700 – 1,000 m for the curve having 100% illite (seen in the left hand plot of **Figure 5.22**). The left hand plot of **Figure 5.22** shows that the variation of volume magnetic susceptibility from the surface to a depth of 1000 m is about 1 x $10^{-5}$ SI or less for the mixtures containing less than 20% illite. The right hand plot of **Figure 5.22** shows that the variation of volume magnetic susceptibility with depth is about 0.1 x $10^{-5}$ SI or less for the mixtures containing less than 4% illite. Note that the magnetic results measured on the slabbed cores of the three oil sand wells in this study have shown that the magnetically derived illite contents in a clay or shale interval are more than 20% and in a clean sand interval are generally less than 4% (**Chapter 3**). Therefore, the borehole volume magnetic susceptibility signals should show a significant decrease with depth in a clay or shale interval, while the signals should be consistently negative or close to zero at a clean sand interval.

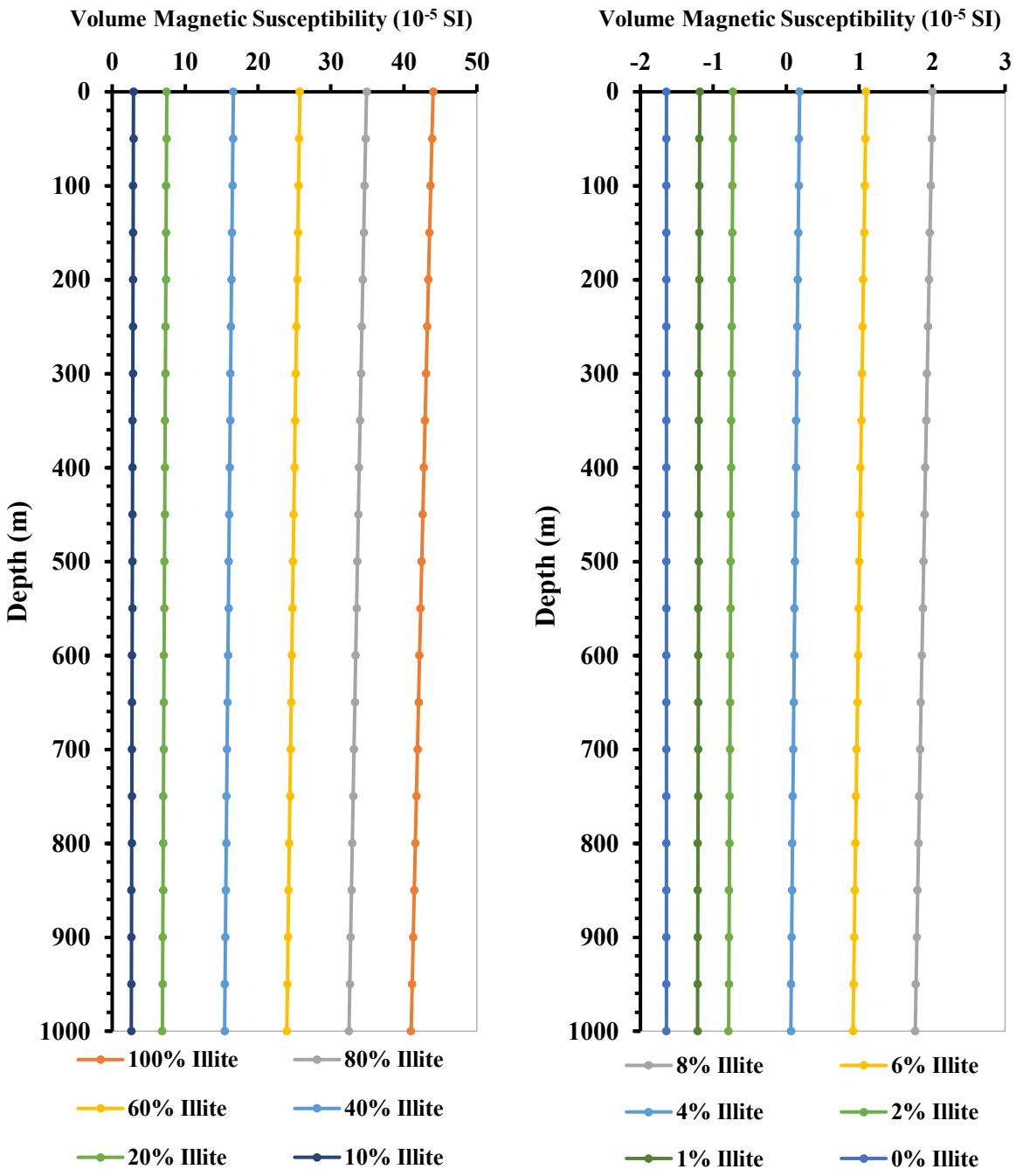


**Figure 5.22:** Theoretical volume magnetic susceptibility template curves with depth for various mixtures of illite and quartz for a typical Athabasca oil sands well where the geothermal gradient is 20 °C/km and the surface temperature is assumed to be 0 °C. The curves show illite contents from 10% to 100% (left hand plot) and from 0% to 8% (right hand plot).

## 5.6. Conclusions

From the results of the special core analysis in this chapter the following conclusions can be drawn:

1. Crossplots of volume and mass magnetic susceptibilities versus elemental contents of Fe, K and Al from XRF on small extracted samples from the slabbed cores showed generally high correlation coefficients, further supporting illite as the major paramagnetic clay in these samples.
2. The correlation coefficients between the respective volume and mass magnetic susceptibilities and the elemental contents of Fe, K and Al for the small extracted samples were similar, and were also quite similar to the respective coefficients for the probe volume magnetic susceptibilities and the elemental contents for the original intact slabbed cores. This suggested that the effects of porosity and fluid type in the pore space of the slabbed cores did not significantly affect the original results of probe volume magnetic susceptibility measurements on the slabbed cores. The small extracted samples were ground (in order to minimize porosity and give a better XRF signal due to the mineralogy), whereas the slabbed cores were expected to have generally slightly higher porosity (especially in the sands), and so any effect due to the porosity or fluid type in the pores would likely manifest itself in lower correlation coefficients between the slabbed core probe volume magnetic susceptibilities and the XRF elemental contents. The correlation coefficients were indeed generally slightly lower between the probe volume magnetic susceptibilities of the slabbed core and the XRF elemental contents, compared to those between the probe volume magnetic susceptibilities of the extracted samples and the XRF elemental contents, however all the

respective coefficients were close and quite high suggesting minimal effect of porosity and fluid type in the pore space for the slabbed core results.

3. The IRM measurements allowed small amounts of remanence carrying particles to be detected and quantified. The IRM acquisition curves suggested that these particles were magnetite of particular size ranges. This allowed estimates of the amount of magnetite to be determined, and the contribution of this magnetite to the low field magnetic susceptibility signal. This in turn enabled one to make corrected estimates of the illite content taking into account the effect of the magnetite on the total low field magnetic susceptibility signal. The improved illite content estimates did not change the lithology categories of the samples that were initially assigned, nor invalidate the main correlations and conclusions, from the probe magnetic susceptibility measurements on the slabbed cores without any corrections. In a practical industrial context the initial rapid probe magnetic susceptibility measurements, without correcting for magnetite by performing IRM experiments, give reasonable results rapidly for several thousand measurements. Some representative corrected illite content estimates could be made using the IRM technique, though it wouldn't be time- or cost-effective to do this for large numbers of samples.
4. A comparison of low field and high field magnetic susceptibility demonstrated that the difference in the two susceptibilities for a muddy oil sand (IHS) sample was consistent with the magnitude of the mass magnetic susceptibility of the remanence carrying mineral component identified by the independent IRM method. The correspondence of both methods strongly supported the suggestion that this remanence carrying mineral was magnetite. The low field magnetic susceptibility includes the component due to the magnetite, whereas the high field magnetic susceptibility does not since the magnetite saturates at high field.

5. A comparison of low field and high field magnetic susceptibility for one of the anomalous mineral samples also provided further support that the mineral siderite was (at least in part) a component of this sample, as suggested from previous results in **Chapters 3** and **4**.
6. Temperature dependent magnetic susceptibility measurements enabled one to identify the presence of a paramagnetic mineral or minerals in the extracted core samples from the decrease of magnetic susceptibility with increasing temperature. The clean sand samples exhibited no temperature dependence, indicating no paramagnetic minerals (e.g., illite) were present in those samples. This was consistent with the 0% illite estimates for clean sand samples corrected for the magnetite content in **Table 5.5**.
7. Comparisons between the temperature dependent magnetic susceptibility measurements and a set of theoretical template curves for mixtures of quartz + illite provided an independent method to estimate the illite content, and also to identify samples that likely contained other minerals (with or without illite). The results gave estimates of illite content comparable to those obtained from the room temperature probe volume magnetic susceptibility measurements. The comparisons between the temperature dependent measurements and the template curves provide an improved means of identifying and quantifying the mineralogy over single room temperature magnetic susceptibility measurements. For example, a single measurement at room temperature could be the result of different possibilities (e.g., one mineral or a mixture of minerals), whereas a temperature dependent curve would follow the trend of a specific mineral or mixture of minerals.
8. The theoretical template curves of volume magnetic susceptibility with depth for relevant mineral mixtures (quartz + illite in the studied case), constructed using an appropriate geothermal gradient in the Albertan oil sands, allows one to provide improved interpretations

of mineralogy (that take into account the temperature dependence of paramagnetic minerals) from in-situ borehole volume magnetic susceptibility measurements.

## 5.7. References


Ali, A. and Potter, D. K., 2011. Model templates for quantifying permeability controlling paramagnetic clay minerals at in situ reservoir temperatures. In *Proceedings of the 2011 International Symposium of the Society of Core Analysts***,** *18-21 September 2011,* Austin, Texas, USA. Paper SCA2011-047 (6 pages).

Ali, A., and D. K. Potter, 2012. Temperature dependence of the magnetic properties of reservoir rocks and minerals and implications for in situ borehole predictions of petrophysical parameters. *Geophysics*, **77** (no.3), 211-221.

Hunt, C. P., Moskowitz, B. M. and Banerjee, S.K., 1995. Magnetic properties of rocks and minerals, In: *Rock Physics and Phase Relations: A Handbook of Physical Constants*, T. J. Ahrens, (Ed.): American Geophysical Union Reference Shelf 3, 189-204.

Ivakhnenko, O. P., 2006. Magnetic analysis of petroleum reservoir fluids, matrix mineral assemblages and fluid-rock interactions. Ph.D. thesis, Heriot-Watt University, UK, pp. 210.

Ivakhnenko, O. P. and Potter, D. K., 2008. The use of magnetic hysteresis and remanence measurements for rapidly and non-destructively characterizing reservoir rocks and fluids. *Petrophysics,* **49**, (issue 1), 47-56.

Majorowicz, J., Hofmann, H., and Babadagli, T., 2013a. Deep geothermal heat storage under oil sands – can we use it to help oil sands industry? New EGS concept proposed. Geothermal Research Council Conference, Las Vegas, GEC Transactions, **37**, 173-178.

Majorowicz, J., Unsworth, M., Chacko, T., Gray, A., Heaman, L., Potter, D. K., Schmitt, D. R., and Babadagli, T., 2013b. Geothermal energy as a source of heat for oil sands processing in

Northern Alberta, Canada, in Hein, F. J., Leckie, D., Larter, S., and Suter, J. R., eds., Heavy-oil and oil-sand petroleum systems in Alberta and beyond: *AAPG Studies in Geology*, **64**, 725-746.

Potter, D. K., AlGhamdi, T. M. and Ivakhnenko, O. P., 2011. Sensitive carbonate reservoir rock characterization from magnetic hysteresis curves and correlation with petrophysical properties. *Petrophysics*, **52** (issue 1), 50-57.

Potter, D. K. and Stephenson, A., 1990. Field-impressed anisotropies of magnetic susceptibility and remanence in minerals. *Journal of Geophysical Research - Solid Earth*, **95**, 15573-15588.

# Chapter 6

# Conclusions and Recommendations for further work

## 6.1. Conclusions

The following overall conclusions can be drawn from this study:

1. Low field probe volume magnetic susceptilibility profiles, which can be generated rapidly and non-destructively on this unconsolidated slabbed core, could clearly distinguish the 3 main lithologies in these oil sands wells. Negative and near-zero volume magnetic susceptibility values indicated clean sand intervals, small positive values (generally up to about 5 x $10^{-5}$ SI) corresponded to inclined heterolithic stratification (IHS) beds or muddy sands, and higher positive values (generally greater than 10 x $10^{-5}$ SI) corresponded to shale. Whilst there were general correspondences between the magnetic results and the downhole log data for total gamma ray (GR) and spontaneous potential (SP), the magnetic results were better at distinguishing the 3 main lithologies. In particular, the total GR did not clearly show a clean sand interval in Well 02, and incorrectly suggested clean sand instead of IHS beds in the interval 162–168 m in Well 03. In both these cases the magnetic results indicated the correct lithology, which was supported by visual observations, and/or XRF results, and/or the quantitative grain size profiles.
2. The probe magnetic technique was particularly useful for distinguishing different lithologies, and quantifying variations in mineralogy, in bitumen and heavy oil saturated cores. This was often not possible from visual observations alone, since the black reservoir hydrocarbons obscured the details. This is a major advantage of the probe magnetic technique in oil sands core.

3. The novel sensors (the probe MS2E sensor and the MS2W sensor) performed successfully on a suite of standard reservoir mineral samples, giving magnetic susceptibility values very close to previously published data. Also, magnetic susceptibility measurements on a heavy oil sample from the Albertan oil sands were consistent with previously published trends of crude oils. The diamagnetic signal of the heavy oil sample meant that it was unlikely to affect the ability of the probe magnetic sensor to distinguish between quartz rich oil sands and the increased amounts of paramagnetic clays in the IHS beds and shales.
4. The probe raw magnetic susceptibility results were processed using a simple model mineral mixture of quartz + illite to derive illite contents. The magnetically derived illite content was a useful parameter since it could readily distinguish the main lithologies, and exhibited good correlations with the following:
    a. Total downhole gamma ray (GR). There was also a strong correlation between the magnetically derived illite content and the spectral K gamma ray in Well 03.
    b. Downhole spontaneous potential (SP). Permeable zones were indicated by low values of magnetically derived illite and large deflections to the left by the SP tool. However, the magnitude and direction of the deflection of the SP log depends on the difference in salinity between the formation water and drilling mud filtrate, and would not show a deflection at a permeable zone if the salinities of the two fluids are equal. In contrast, the magnetic technique has the advantage that it can potentially identify a permeable zone in this situation regardless of the salinities.
    c. Fluid permeability. A strong correlation was observed between the magnetically derived illite content and core permeability in the one well (Well 03) where

permeability data was available. The results were marginally better than the correlation between the core permeability and the total downhole GR signal, and substantially better than the correlations between the core permeability and either the SP log data or the spectral GR potassium data.

d. X-ray fluorescence (XRF). Strong correlations between the magnetically derived illite content and elemental contents of Fe, K and Al (all components of illite) supported the suggestion that illite was a major paramagnetic clay in the 3 wells.

5. The magnetically derived illite contents enabled one to identify thin layers of anomalous minerals, where "illite" contents were greater than 100% from the simple model. The total GR, spectral GR and SP logs did not generally identify these thin layers of anomalous minerals.
6. Crossplots of magnetic susceptibility or magnetically derived illite content against XRF (elemental contents of Fe, K and Al), or crossplots of magnetically derived illite against total GR, all showed promise for distinguishing the main lithologies.
7. The combination of the magnetic susceptibility results, the XRF elemental contents of Fe, Ca and K, and the total GR log data, strongly suggested lithologies that were different to simple sand and clay mixtures in intervals 2 and 3 below 425 m in Well 02. The combined data strongly suggested the presence of an iron carbonate mineral (such as siderite) in interval 2.
8. Crossplots of volume and mass magnetic susceptibilities versus elemental contents of Fe, K and Al from XRF on small extracted samples from the slabbed cores showed generally high correlation coefficients, further supporting illite as a major paramagnetic clay in these samples.

9. The correlation coefficients between the respective volume and mass magnetic susceptibilities and the elemental contents of Fe, K and Al for the small extracted samples were similar, and were also quite similar to the respective coefficients for the probe volume magnetic susceptibilities and the elemental contents for the original intact slabbed cores. This suggested that the effects of porosity and fluid type in the pore space of the slabbed cores did not significantly affect the original results of the low field probe volume magnetic susceptibility measurements on the slabbed cores.
10. Isothermal remanent magnetization (IRM) measurements allowed small amounts of remanence carrying particles to be detected and quantified. The IRM acquisition curves suggested that these particles were magnetite of particular size ranges. This allowed estimates of the amounts of magnetite to be determined, and the contribution of this magnetite to the low field magnetic susceptibility signals. This in turn enabled one to make corrected estimates of the illite contents taking into account the effect of the magnetite on the total low field magnetic susceptibility signals. These improved illite content estimates did not alter the lithology categories of the samples that were initially assigned, nor invalidate the main correlations and conclusions, from the probe magnetic susceptibility measurements on the slabbed cores without correcting for the magnetite content. In a practical industrial context the initial rapid probe magnetic susceptibility measurements, without correcting for magnetite by performing IRM experiments, give reasonable results rapidly for several thousand measurements. In this context corrected illite content estimates could be made on a few representative samples using the IRM technique, to check for the effect of magnetite, though it would be unlikely to be time- or cost-effective to do this for large numbers of samples.

11. A comparison of low field and high field mass magnetic susceptibility demonstrated that the difference in the two susceptibilities for a muddy oil sand (IHS) sample was consistent with the magnitude of the mass magnetic susceptibility of the remanence carrying mineral component identified by the independent IRM method. The correspondence of both methods strongly supported the suggestion that this remanence carrying mineral was magnetite.
12. A comparison of low field and high field mass magnetic susceptibility in **Chapter 5** for one of the anomalous mineral samples provided further support that the mineral siderite was (at least in part) a component of this sample, as suggested earlier from the initial low field probe volume magnetic susceptibility and XRF results in **Chapters 3** and **4**.
13. Temperature dependent mass magnetic susceptibility measurements enabled one to identify the presence of a paramagnetic mineral or minerals in the extracted rock samples from the decrease of magnetic susceptibility with increasing temperature. Moreover, comparisons between the temperature dependent mass magnetic susceptibility values and a set of theoretical template curves for mixtures of quartz + illite provided an independent method to estimate the illite content, and also to identify samples that likely contained other minerals (with or without illite). The results gave estimates of illite content comparable to those obtained from the room temperature probe volume magnetic susceptibility measurements. The clean sand samples exhibited no temperature dependence, indicating no paramagnetic minerals such as illite were present in those samples. This was consistent with the 0% illite estimates for clean sand samples corrected for the magnetite content in **Table 5.5**. Note that the temperature dependent measurements potentially provide an improved means of identifying and quantifying the mineralogy over single room temperature magnetic susceptibility measurements, since a single measurement at room temperature could be the

result of different possibilities (e.g., one mineral or a mixture of minerals), whereas a temperature dependent curve would follow the trend of a specific mineral or mixture of minerals.

14. The probe volume magnetic susceptibility results acquired from slabbed core in this study indicated the potential for a magnetic susceptibility borehole tool for improved in-situ identification of oil sands lithologies. Theoretical template curves of volume magnetic susceptibility with depth for relevant mineral mixtures (quartz + illite in this case) were therefore constructed, using an appropriate geothermal gradient in the Albertan oil sands. These template curves allow one to provide improved interpretations of mineralogy (that take into account the temperature dependence of paramagnetic minerals) from in-situ borehole volume magnetic susceptibility measurements.

### 6.2. Recommendations for future work

The recommendations for future studies are as follows:

1. X-ray diffraction (XRD) measurements would be useful on selected core samples to confirm our suggestions of the mineralogy. We selected samples for this, but the Covid-19 pandemic meant that the samples have not yet been measured. We sent the samples to Glasgow University, UK, and they were in a queue to be measured when shortly afterwards the Covid-19 pandemic started. We particularly want to confirm illite as a major paramagnetic mineral in the samples, and compare our magnetically derived illite contents with XRD derived contents in some selected samples. Plots of potassium against thorium from the spectral gamma ray provide evidence for illite (particularly for Well 03) as shown in **Figures A5.1** and **A5.2** of **Appendix 5**. Note that our "illite" content is essentially a total clay parameter

since our simple model assumes illite is the only positive magnetic susceptibility component (so our "illite" is effectively a lump sum term for the total illite, mixed clay, montmorillonite, smectite and mica contents). We also want to test some of the "anomalous mineral" samples to see if XRD identifies siderite, since the magnetics and XRF data in **Chapters 3**, **4** and **5** produced strong evidence for this mineral. Note, however, that whilst XRD is generally good at identifying the minerals present, it has certain disadvantages as follows: (i) it is only semi-quantitative, (ii) it requires crystalline samples, and won't identify fine-grained amorphous material (less than about 2μm), (iii) it is unlikely to be able to identify or quantify the minute amounts of ferrimagnetic magnetite that we believe many of the samples contain, (iv) it uses small sample volumes, and (iv) commercial measurements are very expensive per sample.

2. Curie point determinations would be useful to confirm whether magnetite is the ferrimagnetic mineral in the core samples. Magnetite would give a Curie temperature of 575 $^{o}$C. The amounts of magnetite are extremely small, so we cannot use the temperature dependence of magnetic susceptibility equipment as the signal will be too low. One possible method would be to thermally demagnetize an IRM. Ideally we would need to put the sample in a small evacuated capsule (essentially a vacuum) to prevent oxidation through heating in air, though we don't currently have access to the glass blowing facilities in the chemistry department due to the Covid-19 pandemic.
3. Ideally we would want to measure the magnetic susceptibility of a high viscosity bitumen sample from the Athabasca oil sands, since this is the fluid in Well 03. As mentioned in **Chapter 2** we only had access to a heavy oil sample, relevant to Wells 01 and 02.
4. Future borehole magnetic susceptibility measurements, in conjunction with the model template curves that account for the temperature dependence of magnetic susceptibility of

paramagnetic minerals, should be conducted to test the effectiveness of the magnetic technique as an in-situ downhole method to characterize oil sands reservoirs. Comparisons between downhole magnetic susceptibility results and other traditional downhole logs such as gamma ray and spontaneous potential log should be useful to evaluate the results of borehole magnetic susceptibility measurements.

5. Low temperature magnetic susceptibility measurements on selected core samples would be useful to compare with borehole magnetic susceptibility signals at depths representing the same temperatures, in order to ground truth cases where logging temperatures may be relatively low as in the oil sands, particularly during winter. Note that the model template curves for volume magnetic susceptibility shown in **Figures 5.20** and **5.21** give a range of values down to -40 $^{o}$C. Low temperature measurements are also useful to identify the presence of small amounts of paramagnetic minerals in relatively clean sand samples, since the Curie law **Equation (5.5)** and **Figures 5.20** and **5.21** show that the magnetic susceptibility signal of a paramagnetic mineral increases with decreasing temperature.

# BIBLIOGRAPHY

Adams, J. J., Rostron, B. J., Mendoza, C. A, 2004. Coupled fluid flow, heat and mass transport, and erosion in the Alberta basin: implications for the origin of the Athabasca oil sands. *Canadian Journal of Earth Sciences*, **41**, 1077-1095.

Ali, A. and Potter, D. K., 2011. Model templates for quantifying permeability controlling paramagnetic clay minerals at in situ reservoir temperatures. In *Proceedings of the 2011 International Symposium of the Society of Core Analysts**,** 18-21 September 2011,* Austin, Texas, USA. Paper SCA2011-047 (6 pages).

Ali, A., and D. K. Potter, 2012. Temperature dependence of the magnetic properties of reservoir rocks and minerals and implications for in situ borehole predictions of petrophysical parameters. *Geophysics*, **77** (no.3), 211-221.

Ali, A., Potter, D. K. and Tugwell, A., 2014. Correlation between magnetic properties and permeability: results from a new case study in the North Sea. In *Proceedings of the 2014 International Symposium of the Society of Core Analysts*, 8-11 September 2014, Avignon, France. Paper SCA2014-077 (6 pages).

Anfort, S. J., Bachu, S., Bentley, L. R., 2001. Regional-scale hydrogeology of the Upper Devonian-Lower Cretaceous sedimentary succession, south-central Alberta basin, Canada. AAPG Bulletin, **85**, 637-660.

Backman, B., Lindqvist, K. and Hyvönen, E., 2016. Manual for measuring soil samples with the Niton XL3 GOLDD+ XRF-instrument. Geologian Tutkimuskeskus, pp. 14.

Borradaile, G. J., MacKenzie, A. and Jensen E., 1990. Silicate versus trace mineral susceptibility in metamorphic rocks. *Journal of Geophysical Research - Solid Earth*, **95**, 8447-8451.

Brubacher, L., Stafford, F, 1962. Magnetic susceptibility: A physical chemistry laboratory experiment. *Journal of Chemical Education*, **39**, 574-584.

Bruckshaw, J. M., Robertson, E. I., 1948. The measurement of the magnetic properties of rocks. *J. Sci. Instrument*., **25**, 444-449.

Carlin, R. L., 1986. *Magnetochemistry*. Springer 312 pp.

Dunlop, D. J. and Özdemir, Ö, 1997. *Rock Magnetism: Fundamentals and Frontiers*. Cambridge University Press, Cambridge, 573 pp.

Ebufegha, V. T and Potter, D. K., 2015. Low temperature magnetic anisotropy in shales and mudstones: application in modelling mineralogy and fabric in the Horn River Basin, British Columbia. *2015 GeoConvention: New Horizons*, Calgary, Alberta, Canada.

Ergin, Y. V., & Yarulin, K. S. (1979). *Magnetic Properties Of Oils*. Nauka., Moscow, USSR, 200 pp.

Evans, D. F., 1974. A new type of magnetic balance. *Journal of Physics E: Scientific Instruments*, **7**, 247-249.

Fajber, R. and Simandi, G. J., 2012. Evaluation of rare earth element-enriched sedimentary phosphate deposits using portable X-ray fluorescence (XRF) instruments. *British Columbia Geological Survey, Geological Field Work 2011*, Volume **2012-1**, 199-209.

Fowler, M. G., Stasiuk, L. D., Hearn M., et al, 2001. Devonian hydrocarbon source rocks and their derived oils in the Western Canada Sedimentary Basin. *Bulletin of Canadian Petroleum Geology*, **49**, 117-148.

Gingras, M. K. and Korosh, D., 2004. A brief overview of the geology of heavy oil, bitumen and oil sand deposits. 2004 *CSEG National Convention*, Calgary, Alberta, Canada.

Hay, P. W., 1994. Oil and Gas Resources of the Western Canada Sedimentary Basin. In: *Geological Atlas of the Western Canada Sedimentary Basin*, G. D. Mossop and I. Shetsen (comp.). Calgary, Canadian Society of Petroleum Geologists and Alberta Research Council, Chapter 32, 469-470.

Hayes, B. J. R., Christopher, J. E., Rosental, L., Los, G., Mc Kercher, B., Minken, D. F., Tremblay, Y. M., and Fennell, J. W., 1994. Cretaceous Mannville Group of the Western Canada Sedimentary Basin. In: *Geological Atlas of the Western Canada Sedimentary Basin*, G. D. Mossop and I. Shetsen (comp.). Calgary, Canadian Society of Petroleum Geologists and Alberta Research Council, Chapter 19, 317-335.

Hubbard S. M., Pemberton S. G., and Howard E. A., 1999. Regional geology and sedimentology of the basal Cretaceous Peace River Oil Sands deposit, north-central Alberta. *Bulletin of Canadian Petroleum Geology*, **47**, 270-297.

Hunt, C. P., Moskowitz, B. M. and Banerjee, S.K., 1995. Magnetic properties of rocks and minerals, In: *Rock Physics and Phase Relations: A Handbook of Physical Constants*, T. J. Ahrens, (Ed.): American Geophysical Union Reference Shelf 3, 189-204.

Hunt, J. M., 1996. *Petroleum Geology and Geochemistry (2nd)*. W. H. Freeman and Co., New York. 743 pp.

Ivakhnenko, O. P., 2006. Magnetic analysis of petroleum reservoir fluids, matrix mineral assemblages and fluid-rock interactions. PhD Thesis, Heriot-Watt University, Edinburgh, UK, 210 pp.

Ivakhnenko. O. P., 2012. Magnetic susceptibility of petroleum reservoir crude oils in petroleum engineering. In: *Crude Oil Exploration in the World*, Prof. Mohamed Younes (Ed.), Chapter 4, 71-88, InTech.

Ivakhnenko, O. P. and Potter, D. K., 2004. Magnetic susceptibility of petroleum reservoir fluids. *Physics and Chemistry of the Earth*, **29**, 899-907.

Ivakhnenko, O. P. and Potter, D. K., 2008. The use of magnetic hysteresis and remanence measurements for rapidly and non-destructively characterizing reservoir rocks and fluids. *Petrophysics,* **49**, (issue 1), 47-56.

Lancaster, D. E., 1966. Electronic metal detection. *Electronic World*, (Dec.), 39-63.

Likhite, S. D., Radhakhrishnamurty, C. and Sahasrabudhe, P. W., 1965. Alternating current electromagnet-type hysteresis loop tracer for minerals and rocks. *Rev. Sci. Instrum*, **36**, 1558-1621.

Lucia, F. J., Kerans, C., Jenning, J. W., 2003. Carbonate reservoir characterization. *Journal of Petroleum Technology, Society of Petroleum Engineering*, **55**, (no. 6), 70-72. SPE-82071-PA. DOI: 10.2118/82071-MS.

Majorowicz, J., Hofmann, H., and Babadagli, T., 2013a. Deep geothermal heat storage under oil sands – can we use it to help oil sands industry? New EGS concept proposed. Geothermal Research Council Conference, Las Vegas, GEC Transactions, **37**, 173-178.

Majorowicz, J., Unsworth, M., Chacko, T., Gray, A., Heaman, L., Potter, D. K., Schmitt, D. R., and Babadagli, T., 2013b. Geothermal energy as a source of heat for oil sands processing in Northern Alberta, Canada, in Hein, F. J., Leckie, D., Larter, S., and Suter, J. R., eds., Heavy-oil and oil-sand petroleum systems in Alberta and beyond: *AAPG Studies in Geology*, **64**, 725-746.

Monger, J. and Price, R., 2002. The Canadian Cordillera: Geology and Tectonic Evolution. *Recorder of Canadian Society of Exploration Geophysics*, **27**, 17-36.

Mooney, H. M., 1952. *Geophysics*, **27**, (no. 3), 531-543.

Mossop, G. D. and Shetsen, I., 1994. Introduction to the Geological Atlas of the Western Canada Sedimentary Basin. In: *Geological Atlas of the Western Canada Sedimentary Basin*, G. D. Mossop and I. Shetsen (comp.). Calgary, Canadian Society of Petroleum Geologists and Alberta Research Council, Chapter 1, 1-12.

Muwanguzi, A. J. B., Karasev, A. V., Byaruhanga, J. K. and Jönsson, P. G., 2012. Characterization of chemical composition and microstructure of natural iron ore from Muko deposits. *International Scholarly Research Network, ISRN Material Science*, Volume **2012**, Article ID **174803**, 9 pages.

Nagata, T., 1953. *Rock Magnetism*. Maruzen Co, Tokyo, 225 pp.

Potter, D. K., 2007. Magnetic susceptibility as a rapid, non-destructive technique for improved petrophysical parameter prediction. *Petrophysics*, **48** issue 3), 191-201.

Potter, D. K., Al-Ghamdi, T. M., Ivakhnenko, O. P., 2011. Sensitive carbonate reservoir rock characterization from magnetic hysteresis curves and correlations with petrophysical properties. *Petrophysics*, **52** (issue 1), 50-57.

Potter, D. K., Corbett, P. W. M., Barclay, S. A., and Haszeldine, R. S., 2004. Quantification of illite content in sedimentary rocks using magnetic susceptibility—a rapid complement or alternative to X-ray diffraction. *Journal of Sedimentary Research*, *Research Methods Papers Section*, **74** (no. 5), 730-735.

Potter, D. K. and Ivakhnenko, O. P., 2008. Clay typing - sensitive quantification and anisotropy in synthetic and natural reservoir samples using low- and high-field magnetic susceptibility for improved petrophysical appraisals. *Petrophysics*, **49** (issue 1), 57-66.

Potter, D. K. and Stephenson, A., 1990. Field-impressed anisotropies of magnetic susceptibility and remanence in minerals. *Journal of Geophysical Research - Solid Earth*, **95**, 15573-15588.

Price, R.A., 1973. Large-scale gravitational flow of supracrustal rocks, southern Canadian Rockies. In: *Gravity and Tectonics*. K. A. De Jong and R. Scholten (eds.). New York, Wiley and Sons, 491-502.

Radhakrishnamurty, C., Likhite, S. D., Admin, B. S. and Somayajulu B. L. K., 1968. Magnetic susceptibility stratigraphy in ocean sediment cores. Earth Planet. Sci. Letters, **4**, 464-471.

Ranger, M. J., and Gingras, M. K., 2003. Geology of the Athabasca Oil Sands – Field guide and overview. *Canadian Society of Petroleum Geologists*, Calgary, 123 pp.

Ricketts, B. D, 1989. *Western Canada Sedimentary Basin – A Case History*. Calgary, Canadian Society of Petroleum Geologists, 320 pp.

Riediger, C. L, Fowler, M. G., Snowdon L. R. et al, 1999. Origin and alteration of Lower Cretaceous Mannville Group oils from the Provost oil field, east central Alberta, Canada. *Bulletin of Canadian Petroleum Geology*, **47**, 43-62.

Riediger, C. L., Ness S., Fowler M. G., Akpulat, T., 2000. Timing of oil migration, Palaeozoic and Cretaceous bitumen and heavy oil deposits, eastern Alberta. *Proceedings of GeoCanada 2000*, Calgary, Alberta, Paper 419, 4pp.

Selwood, P.W., 1956. Magnetochemistry, Second edition. Interscience Publishers, New York, 435 pp.

Sharpe, E., 2019. Canada's Oil Sands – Familiar trouble. *Energy Ink Magazine*. July 2019.

Shuquing, Z., Haiping, H., and Yuming, L., 2008. Biodegradation and origin of oil sands in the Western Canada Sedimentary Basin. *Petroleum Science*, **5** (no. 2), 87-94.

Smith, D. G., 1994. Paleogeographic Evolution of the Western Canada Foreland Basin. In: *Geological Atlas of the Western Canada Sedimentary Basin*, G. D. Mossop and I. Shetsen

(comp.). Calgary, Canadian Society of Petroleum Geologists and Alberta Research Council, Chapter 17, 277-296.

Stewart, G.A., MacCallum, G.T., 1978. Athabasca Oil Sands Guide Book. *C.S.P.G. international conference, facts and principles of world oil occurrence*. Canadian Society of Petroleum Geologists, Calgary, Alberta, 33 pp.

Thompson, R., and Oldfield, F., 1986. *Environmental Magnetism*. Allen and Unwin, London, 243 pp.

Tissot, B. P. and Welte, D. H., 1984. *Petroleum Formation and Occurrence (2nd Ed.)*. Springer-Verlag Berlin Heidelberg, New York, 160-198.

West, G. F. and Dunlop, D. J., 1971. An improved ballistic magnetometer for rock magnetic experiments. *J. Phys. E: Sci*. Instrum., **4**, 37-40.

# APPENDICES

**Appendix 1:** Crossplots for Well 01.

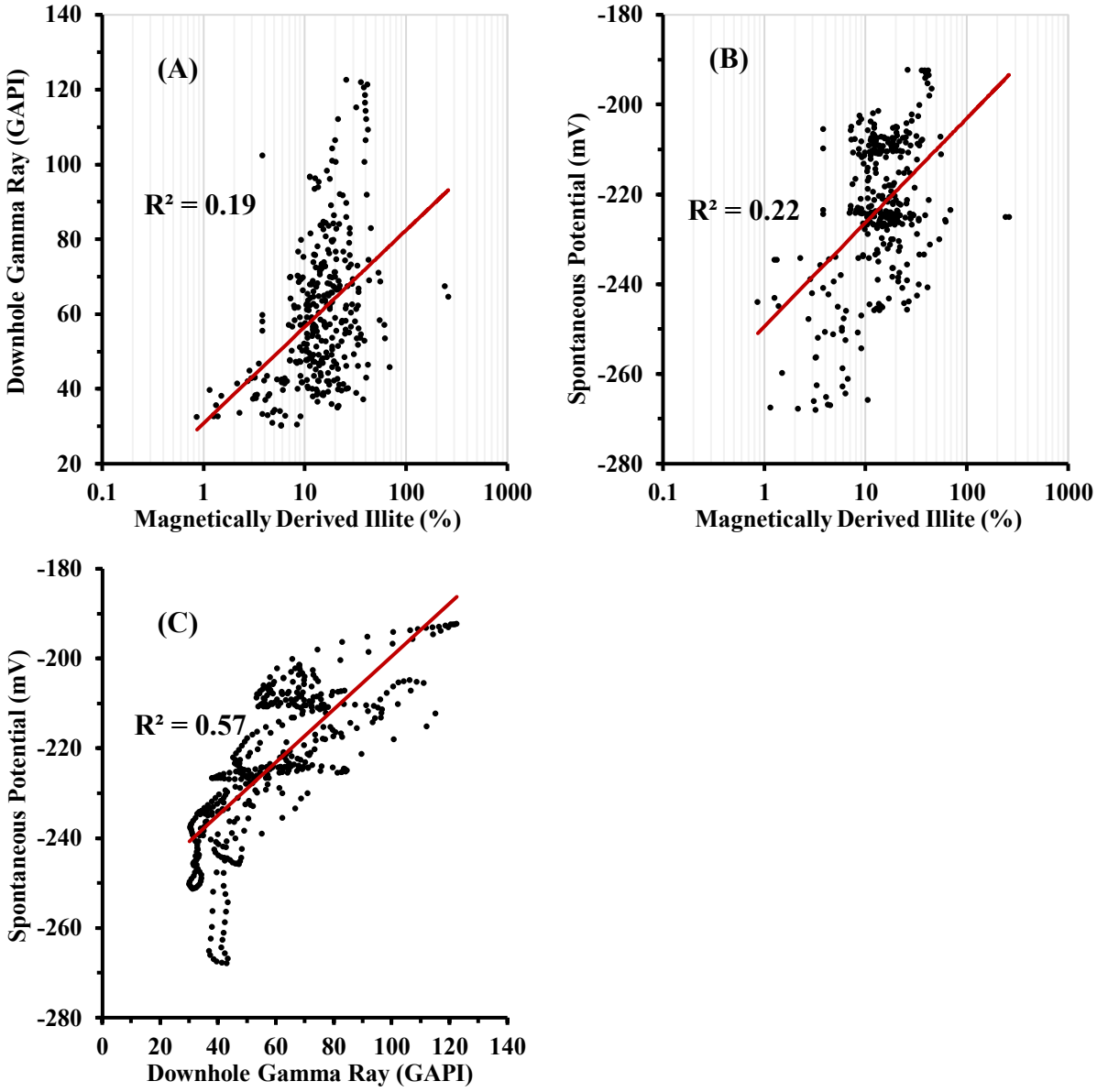


**Figure A1.1: (A)** and **(B)** are crossplots of the averaged (30 cm vertically) magnetically derived illite contents and depth-matched downhole GR and SP log data and **(C)** is a crossplot of the downhole GR and SP log data.

**Appendix 2:** Additional crossplots for Well 02.

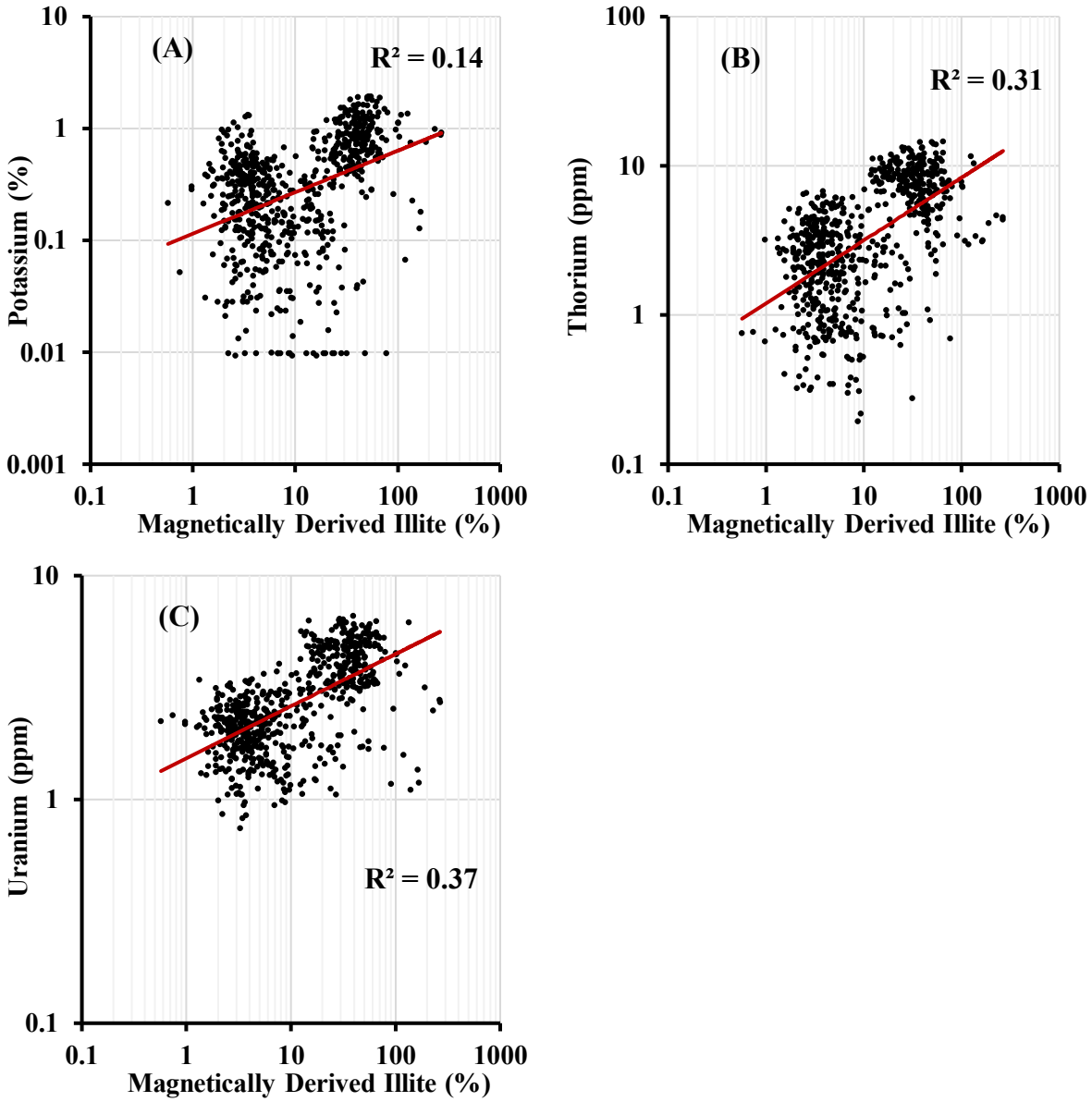


**Figure A2.1: (A), (B)** and **(C)** are crossplots of the averaged (30 cm vertically) magnetically derived illite contents with the depth-matched spectral GR downhole log data for potassium, thorium and uranium.

**Appendix 3:** Additional crossplots for Well 02.

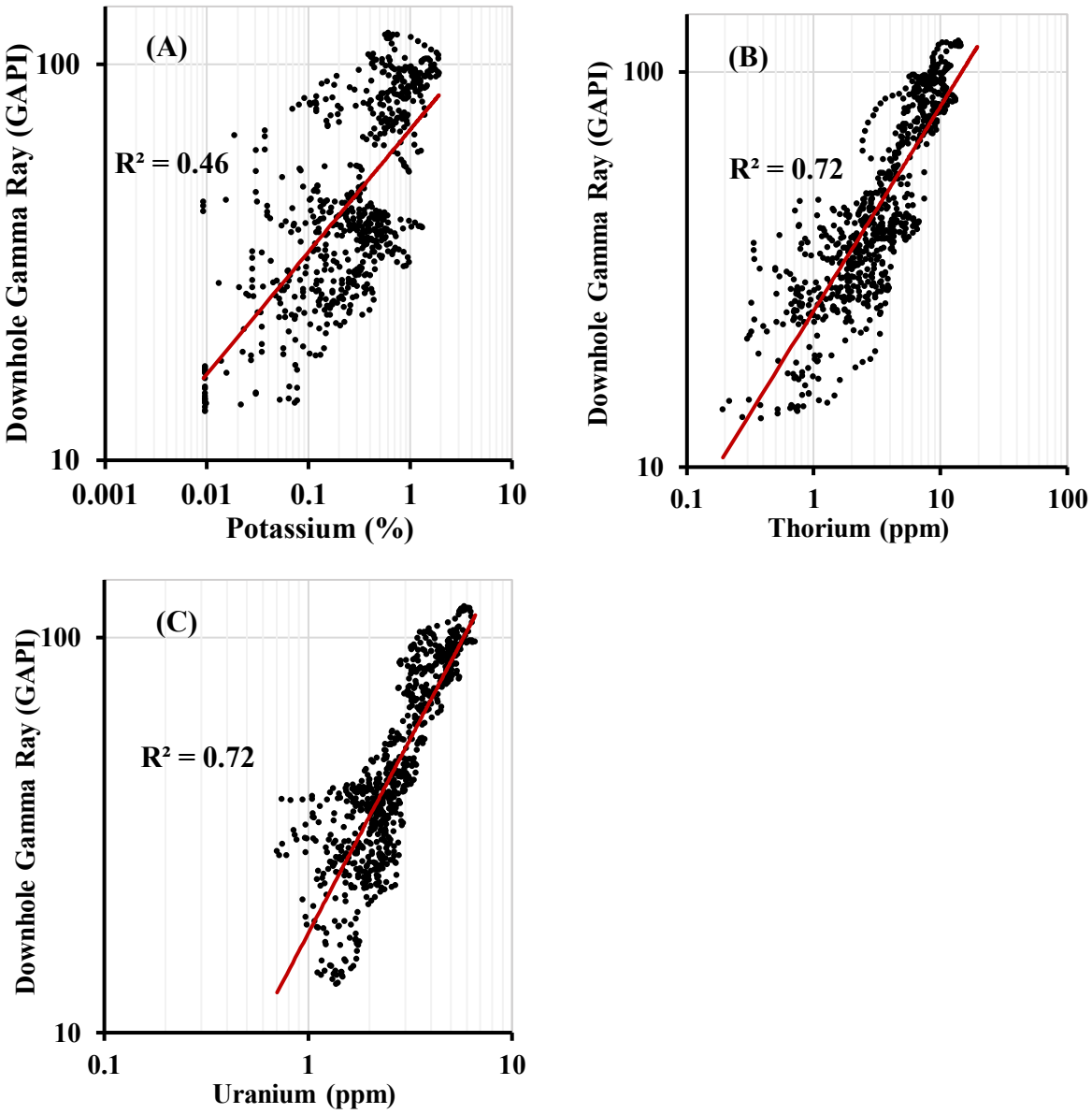


**Figure A3.1: (A), (B)** and **(C)** are crossplots of the total downhole GR log data with the depth-matched spectral downhole log data of potassium, thorium and uranium.

**Appendix 4:** Probe volume magnetic susceptibility crossplots for extracted samples and slabbed core.

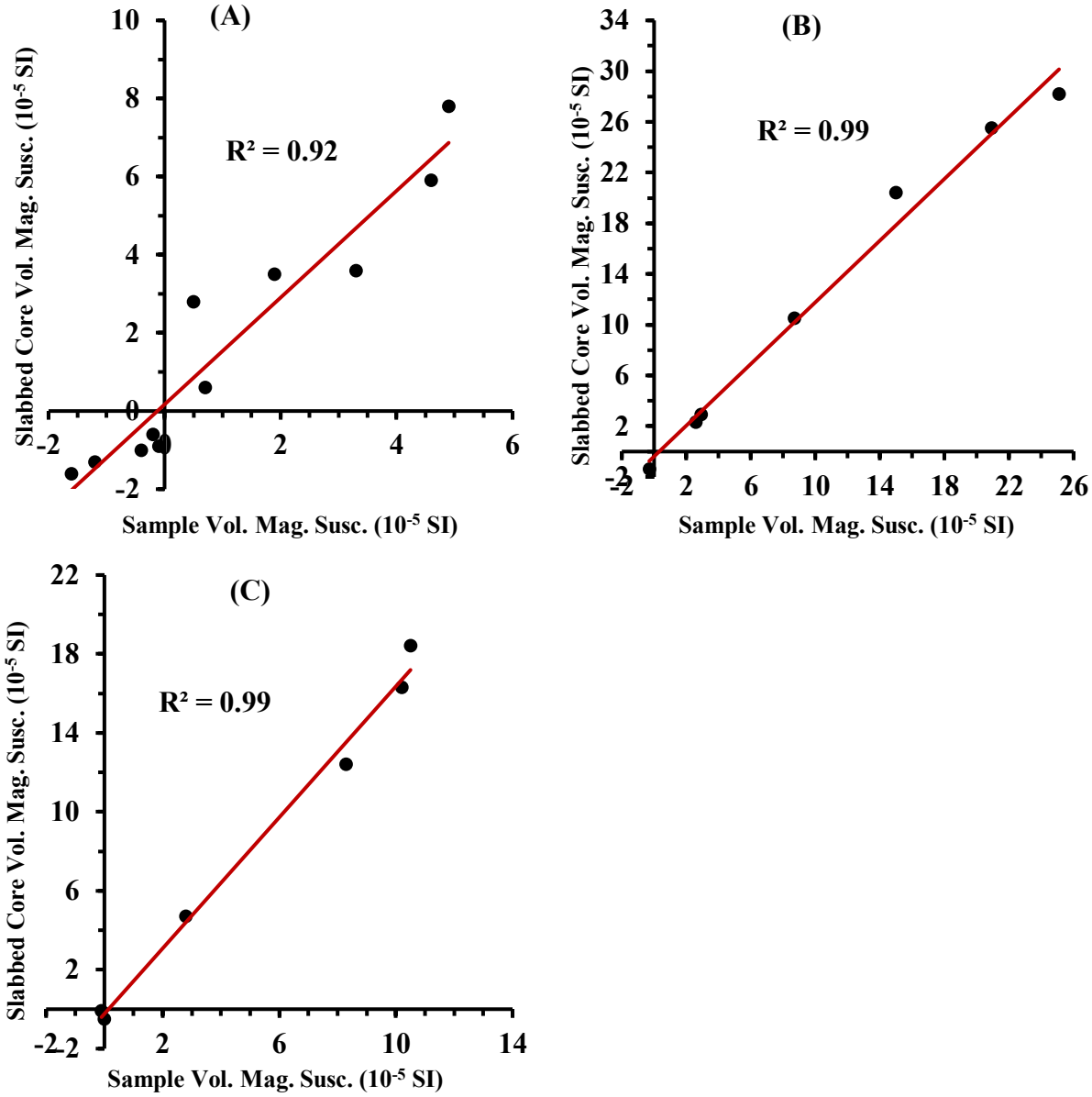


**Figure A4.1:** Crossplots of probe volume magnetic susceptibility measured on the extracted samples (horizontal axis) and probe volume magnetic susceptibility measured on the slabbed cores at the same depths (vertical axis) for **(A)** Well 01, **(B)** Well 02 and **(C)** Well 03.

**Appendix 5:** Thorium-Potassium crossplots (Schlumberger Chart CP-19) for Wells 02 and 03 (there was no spectral gamma ray data for Well 01).

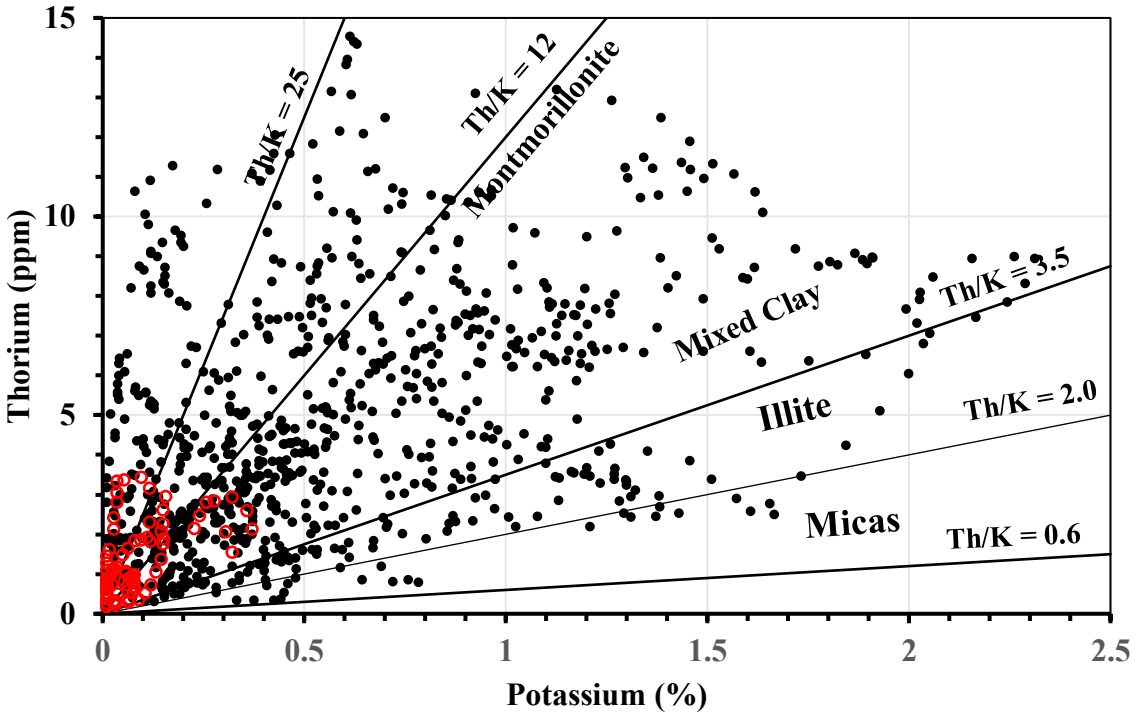


**Figure A5.1:** Th/K crossplot for Well 02. Red points are from the carbonate interval below 425 m.

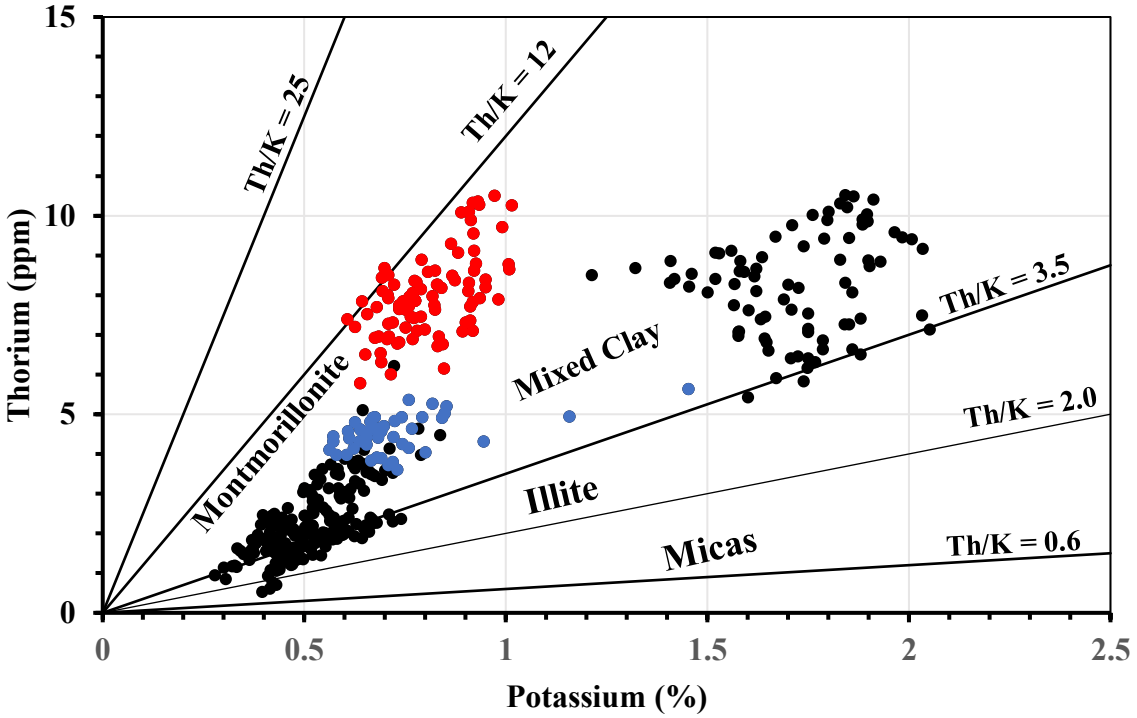


**Figure A5.2:** Th/K crossplot for Well 03. Blue data points in the IHS beds are from the depth interval 161.7 -168.4 m. Red data points in the IHS beds are from the depth interval 168.4 -182.2 m.